Schweizerische Eidgenossenschaft
Confédération suisse
Confederazione Svizzera
Confederaziun svizra

Swiss Confederation

Federal Department of Home Affairs FDHA
Federal Office of Meteorology and Climatology MeteoSwiss

Scientific Report MeteoSwiss No. 97

Seasonal Variation of Daily Extreme Precipitation in Switzerland

Alexander Umbricht, Sophie Fukutome, Mark A. Liniger, Christoph Frei, Christof Appenzeller

ISSN: 1422-1381

Scientific Report MeteoSwiss No. 97

Seasonal Variation of Daily Extreme Precipitation in Switzerland

Alexander Umbricht, Sophie Fukutome, Mark A. Liniger, Christoph Frei, Christof Appenzeller

Recommended citation:
Umbricht A, Fukutome S, Liniger M A, Frei C, Appenzeller C: 2013, Seasonal variation of daily extreme precipitation in Switzerland, *Scientific Report MeteoSwiss,* **97,** 122 pp.

Editor:
Federal Office of Meteorology and Climatology, MeteoSwiss, © 2013

MeteoSwiss
Krähbühlstrasse 58
CH-8044 Zürich
T +41 44 256 91 11
www.meteoschweiz.ch

Abstract

Extreme weather events, such as the flood episode in Switzerland in August 2005, deeply affect our society through their adverse impact on human life, infrastructure and economy. The assessment of their return periods and values is crucial for accurate planning of infrastructure and prevention measures. It is done by means of the statistical tools of Extreme Value Theory, which assumes stationarity of the precipitation process. So far, only yearly return levels are computed operationally, yet monthly values are desirable for many applications but still not as reliable as necessary.

The stationarity requirement is not met in reality since, in Switzerland, precipitation generally undergoes a seasonal cycle. The purpose of the present thesis is to explicitly model these non-stationarities in an attempt to evaluate their influence on return period estimates. In addition, the analysis is expected to shed light on the seasonal behaviour of extreme precipitation.

Non-stationarity is taken into account by considering monthly maxima of daily precipitation, and introducing a time covariate in the parameters of the generalized extreme value (GEV) distribution. The location and scale parameter are modelled with a truncated Fourier Series, such that the time dependent GEV distribution follows the seasonal cycle. The number of terms of the series is determined separately at each station by means of the Akaike Information Criterion, supported in the case of nested models by a Likelihood Ratio Test. Yearly return level estimates are derived from the non-stationary monthly GEV distributions with an iterative numerical procedure.

The data used are monthly maxima of daily precipitation at 97 stations of the Swiss observational network. Stations are chosen according to their representativeness of precipitation variability in Switzerland, and to the length of their time series, which is required to cover the period 1901 to 2010.

Results show that monthly return levels computed with the selected models adequately reproduce the seasonal cycle at most stations, both in amplitude and phase. Yearly return levels derived from the non-stationary analysis differ from those estimated with the stationary analysis of yearly maxima, but are generally well within their confidence intervals. The derived analysis mostly results in a reduction in return level uncertainty, except for a number of stations in the southeastern part of Switzerland. A tentative experiment to include a simple trend term in the model selection process gives evidence that in 48~percent of the cases the long-term non-stationarity should not be neglected.

From the climatological point of view, the seasonal analysis shows that the probability that, say, a 100-year event occurs in winter is 8.6 percent on average, but is 51 percent in summer. In summer, the probability is highest in the Swiss Plateau and especially northeastern Switzerland, while in fall, the Ticino and Southeastern Switzerland are most likely to exhibit extreme precipitation. Overall, largest return levels are found in Ticino.

Contents

List of Figures

List of Tables

1 Introduction

1.1 Motivation

> "However big floods get, there will always be a bigger one coming; so says one theory of extremes, and experience suggests it is true."
> (Cooke et al., 1950, p. 141)

Extreme weather events such as heavy precipitation episodes affect our society through their adverse impact on agriculture and economy (Rosenzweig et al., 2001). For example the flood in August 2005 in Switzerland—which lasted 'only' for two days—killed several people, caused a damage of roughly CHF 3 billion, and destroyed an impressive amount of crop (Hilker et al., 2008).

The questions implied in the quote by Cooke et al. (1950) are therefore of practical relevance: what exactly is a most extreme event? How often will it return? Extreme value theory (EVT) addresses precisely such questions. It allows the analysis of the occurrence rate, termed return period, of highly unusual events, such as a 100 year flood. Extreme value theory is widely used in hydrology and climatology.

Results obtained from EVT play an important role in engineering practise e. g. in water resources design and management (Katz et al., 2002). For Switzerland, official return periods and return levels for extreme precipitation events, based on data ending in 1970, are published in (Zeller et al., 1991). On special request, the Federal Office of Meteorology and Climatology MeteoSwiss, provides most recent values for return periods and return levels for all stations of the Swiss observational network. Engineers, for example, can then use the results to design buildings, dams, etc., that are sufficiently secure, considering their life span.

One of several assumption of EVT is the stationarity of time series. At our latitudes (46° to 48° north), however, climate has a distinct seasonal cycle and precipitation data cannot be considered to be stationary with respect to the seasonal cycle. While investigating the data and the available results for Switzerland, it has become obvious that most stations show different distributions in the high quantiles, depending on seasons.

Indeed, Fig. 1.1 illustrates this point for stations La Chaux-de-Fonds, Basel/Binningen, and Locarno-Monti. The underlying data consist of time series of maximum daily precipitation for each month of the year and covers the years 1901 to 2010. The 110 measurements available for each month, are used to create boxplots (left-hand side) and pie charts of the 110 observations available for each month . The latter show how often the yearly maximum precipitation event falls into a particular month. Especially for station Locarno-Monti (Fig. 1.1e and 1.1f), a pronounced seasonal cycle is obvious, such that the stationarity assumption is violated. This indicates that results obtained with the current method, which assumes no seasonal cycle, may not be very accurate. This points to the necessity of examining the role of the seasonal non-stationarities when calculating return periods.

The seasonal evolution of extreme precipitation is in itself a subject of interest. Apart from its climatological significance, it can find practical use, for instance as input for flood models where, amongst other parameters (e. g. snow melt), the information about heavy precipitation events in a given month of the year, and within a given catchment area, is important.

The purpose of explicitly modelling the seasonal non-stationarities using monthly precipitation data is twofold: on the one hand, we expect to improve the quality of the yearly return level estimates, on the other hand, we hope to shed light on the seasonal behaviour of extreme precipitation in Switzerland.

To our knowledge this is the first attempt to model seasonal non-stationarities for extreme precipitation in Switzerland, but similar studies were conducted recently for several regions outside of Switzerland, e. g. by Rust et al. (2009) and Maraun et al. (2009).

1.2 Broader Context

The statistical theory of extremes began in the 1920s. In 1958 Gumbel published the first book entirely about this subject, covering mainly engineering topics. Ever

since, EVT became more important and still remains a subject of active research, both in theoretical and applied statistics. (Katz et al., 2005, 2002).

In the context of climatological research, the question how extremes are affected by Climate Change is of particular interest, since extreme events probably have the severest impact on human welfare. In Switzerland, for instance, Schmidli and Frei (2005) investigated trends of heavy precipitation during the 20th century and found an increasing trend for winter and autumn at a high number of rain-gauge stations. Similar work was carried out for Germany (Trömel and Schönwiese, 2007), the Carpathian Basin (Bartholy and Pongracz, 2007) and many other regions. On a larger spatial scale, Klein Tank and Können (2003) were looking for trends in daily temperature and in precipitation extremes during the years 1946 to 1999 throughout Europe. They were able to show that, on average in Europe, wet extremes increase whilst there are distinct regional differences.

Extreme value theory is also used to validate Regional Climate Models. Their predictions should be comparable to observations. Buonomo et al. (2007), for instance, could show two Regional Climate Models' ability to simulate extreme precipitation realistically, at least for return periods of two to twenty years.

In any case, the assumption of an underlying trend in extreme events, per definition, violates one of the fundamental premises of EVT: stationarity. Research on non-stationarity in the context of extreme value theory started already in the 1980s. Theoretical aspects were examined for instance by Leadbetter et al. (1983). Covariate modelling, which is now widely used, was investigated by Moore (1987), and in the context of threshold excess models by Davison and Smith (1990).

These techniques have led to many applications in the environmental sciences. Also during the last 20 years, research on extreme environmental events has extended to seasonal values by accounting for non-stationarities in the course of the year as well. This leads to more accurate representation of the seasonal behaviour of extremes.

Recent studies include assessing the seasonality's influence on wave height (Menéndez et al., 2009) or for modelling of seasonality for extreme precipitation in the United Kingdom (Maraun et al., 2009; Rust et al., 2009).

Such information has practical relevance. Corn seedlings, for instance, are more vulnerable to heavy precipitation than their mature stages. Depending on the changes in the occurrence rate of heavy precipitation events during these stages, different effects on agriculture and economy have to be expected (Rosenzweig et al., 2001).

To assess the impact of future changes it is consequently necessary to study the seasonal cycle of heavy precipitation. Maraun et al. (2009) developed a model to analyse the annual cycle of precipitation extremes, considering monthly maxima. Their work is based on on more general methods described by Coles (2001) and Katz et al. (2003), who extended their analyses by incorporating external influences such as covariates.

In the present study, we use the approach proposed by Maraun et al. (2009) to account for seasonal non-stationarities and to gain understanding of the annual cycle in precipitation extremes. The detection of long-term trends is not the purpose of this thesis.

1.3 Goals of this Thesis

The main goal of this study is to take into account the fact that precipitation—and therefore extreme precipitation events—in Switzerland are not evenly distributed over the year. Until now, the information contained within the annual cycle has not been exploited to improve estimates of return levels and return periods.

The main objective is to 'harvest' the information contained in the monthly data to provide more reliable estimates of return levels with less uncertainty. Statements for return levels and return periods on a monthly basis should become more trustworthy. This might be interesting, since an extreme event in January can be smaller than an average event in say July.

1.4 Structure of this Thesis

In Chapter 1 we have presented the motivation to choose this topic and gave a brief overview over similar work

already done. In Chapter 2, we describe the underlying data and discuss their possible shortcomings. We also shortly introduce the software used for the necessary calculations. Chapter 3 presents the relevant aspects of EVT, and especially the method used to address non-stationarity. A substantial part is devoted to describing the way the optimal model is selected, i. e. how the form of seasonal time-dependence is selected automatically. Adequate representation of the seasonal cycle is verified in Chapter 4, where we also set the findings in a climatological context. Chapter 5 discusses the quality of the derived return levels. In the same chapter we give an outlook where further research might be worthwhile. In Chapter 6, finally, we draw our conclusions.

In the appendix we show additional tables and figures which further illustrate the work done.

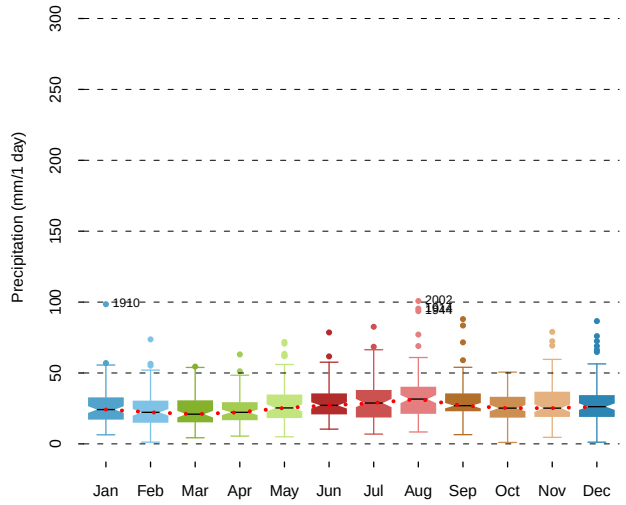

(a) La Chaux-de-Fonds, monthly maximas

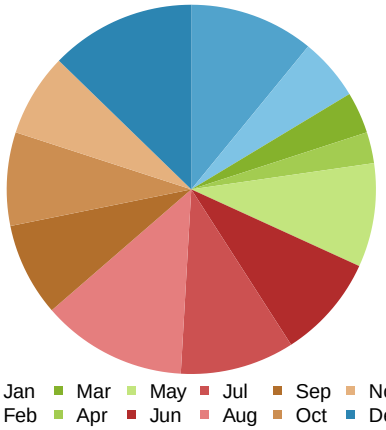

(b) La Chaux-de-Fonds, occurrence month of yearly maxima

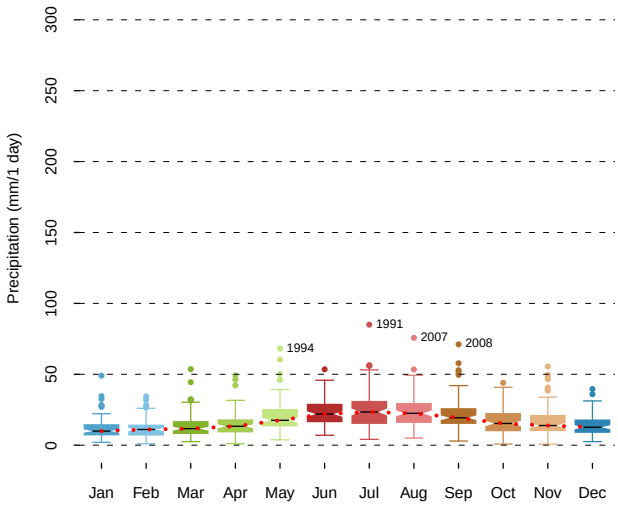

(c) Basel/Binningen, monthly maximas

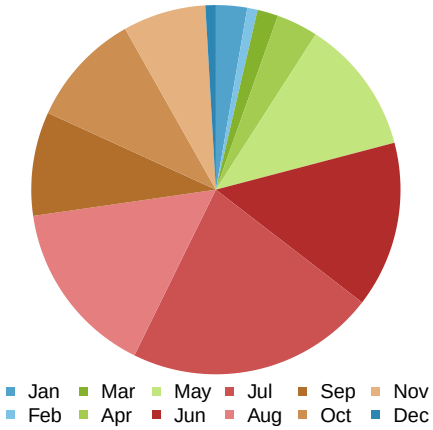

(d) Basel/Binningen, occurrence month of yearly maxima

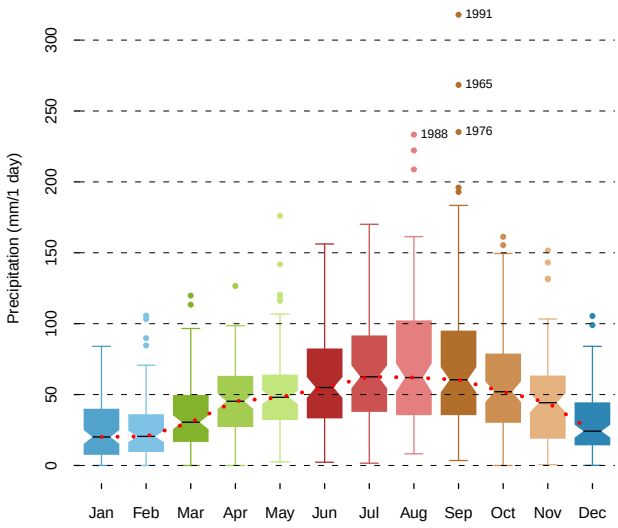

(e) Locarno-Monti, monthly maximas

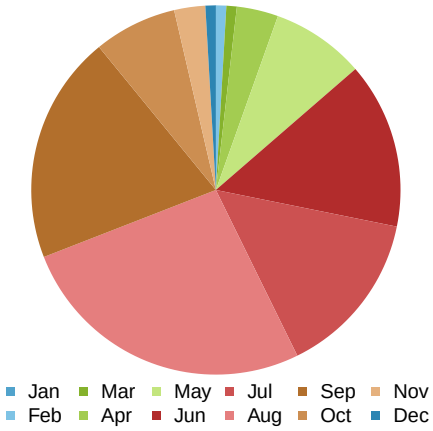

(f) Locarno-Monti, occurrence month of yearly maxima

Fig. 1.1: The panel on the left hand side shows boxplots of the monthly maxima of daily precipitation. The pie charts on the right hand side give the proportion of yearly maxima falling in each month of the year. The three stations shown are La Chaux-de-Fonds, Basel/Binningen, and Locarno-Monti and the time series used start in 1901 and end in 2010.

2 Data

The use of an accurate method to calculate return periods is crucial in order to obtain reliable results. Yet, even the most accurate method fails if the data quality is deficient. Here we describe the data chosen for the present study, and briefly present the software used for the analysis.

2.1 Swiss Precipitation Data

The Federal Office of Meteorology and Climatology MeteoSwiss has the official duty to continuously measure meteorological key variables throughout Switzerland. It fulfils this task since 1863 when operational measurement started.

We use the data from the so called SwissMetNet, which includes the "Niederschlagsmesseinheit" (NIME).

2.1.1 SwissMetNet

The SwissMetNet is the new modern meteorological network which currently is under construction. Essentially it is a state of the art network of gauging stations based on several older networks such as the Automatic Network (ANETZ) and Complementary Network (ENET), but updated with modern instruments. After its completion in 2013 it will consist of 134 stations which transmit the measured data every ten minutes to MeteoSwiss's database. It also meets the World Meteorological Organization (WMO) specifications for weather stations. (MeteoSwiss, 2010)

2.1.2 NIME

The NIME network has measured precipitation since December 1863. The measurements are taken manually at 7:30 am local time on a daily basis. The corresponding data sheet is sent to MeteoSwiss at the end of each month. Since the spatial variability of precipitation is larger compared to other parameters, the NIME network consists nowadays of 350 stations. (Gyarmati, 2004; MeteoSchweiz, 2009)

2.2 Selected Data

In order to model the seasonal non-stationarities explicitly, we first need precipitation data with a temporal resolution small enough to aggregate it to monthly maxima. Since the seasonal variation can strongly vary from year to year, we need long time series to capture a station's climatology. Therefore we use stations with records of daily precipitation starting at least in 1901. This criterion is met at 97 different stations, distributed all over Switzerland (s. Fig. 2.1). All extreme values have undergone a review process at MeteoSwiss, and should therefore also be reliable.

In Müller (1980), twelve large climate regions were defined to represent the Swiss climate and its variability. Each region is represented with at least one station of the MeteoSwiss observational network. These stations constitute the Swiss National Basic Climatological Network (Swiss NBCN) (Begert et al., 2007).

In an effort to verify whether the density and distribution of the Swiss NBCN stations accurately represent the Swiss climate and its variability, a cluster analysis of monthly mean temperature and precipitation data was carried out at all stations of the MeteoSwiss observational network. The cluster analysis revealed that the selected stations are representative for temperature, but not for precipitation. The number of regions necessary to represent the precipitation climate accurately was much larger. A further set of stations was defined, the Swiss Swiss National Basic Climatological Network for Precipitation (Swiss NBCN-P), to accommodate the more complex variability of precipitation (Begert, 2008).

The stations chosen for the present study include all the Swiss NBCN and Swiss NBCN-P stations with sufficiently long time series. Twenty-three are part of the Swiss NBCN-P and another sixteen of the Swiss NBCN. Fig. 2.1 shows the location of the 97 stations chosen for this study. The Swiss NBCN and Swiss NBCN-P stations are distinguished by their colour. They cover 30 out of 32 precipitation regions. Only the two regions

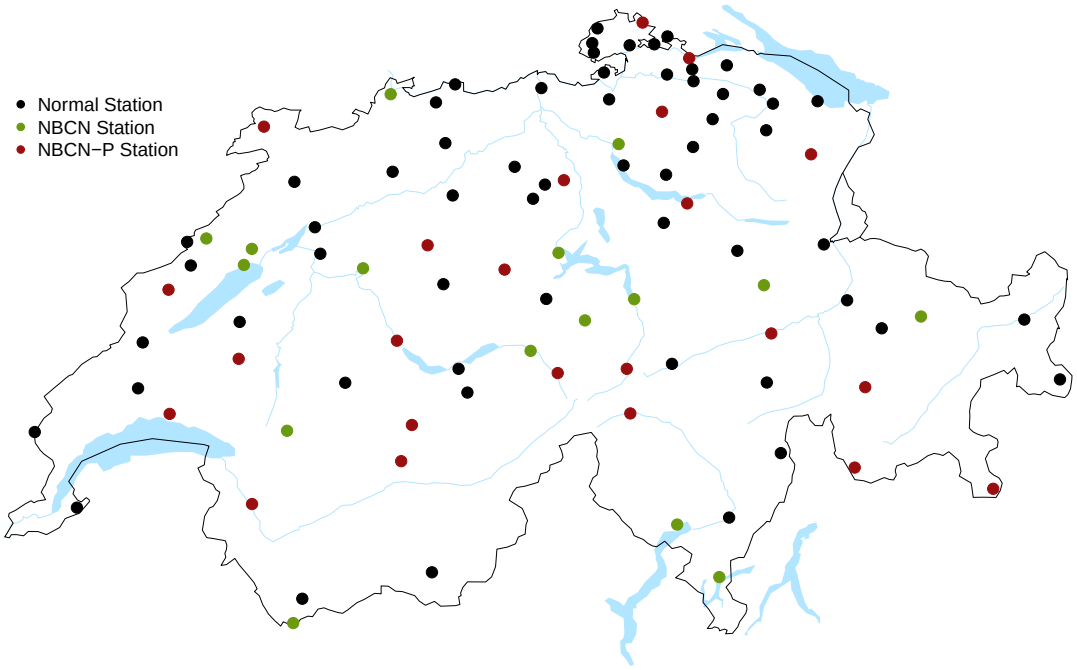

Fig. 2.1: Location of the 97 stations chosen for this study. Green coloured points indicate Swiss NBCN stations, red ones stations of the Swiss NBCN-P. A map with the station's abbreviation can be found in the Appendix (s. Fig. B.1).

defined by station sets 'Binn, Simplon Dorf, Saas Fee' and 'Susch, Zernez, Buffalora' cannot be represented with our stations. Thus, although it is uncertain whether the Swiss NBCN-P classification is appropriate for extreme precipitation, we believe the stations selected to be sufficiently representative of the Swiss precipitation climate for the purposes of our study.

As mentioned before, in this thesis we present mostly results using the yearly or monthly maxima of daily precipitation. Maxima of 1 hour, 2 day, 3 day, 4 day, 5 day, and 10 day precipitation were also briefly examined. Time series for these maxima are available at least from 1901 to 2010, except for 1 hour maxima. The time series of the latter start in 1981, when MeteoSwiss began the recording of meteorological variables with a temporal resolution of 10 minutes. For stations La Chaux-de-Fonds, Basel/Binningen, and Locarno-Monti the results using all mentioned maxima are presented in section D.2 of the Appendix.

2.3 Representative Key Stations

For the most part, methods, results, and conclusions will be shown and discussed for the three stations La Chaux-de-Fonds, Basel/Binningen, and Locarno-Monti (s. Fig. 2.2). These stations represent the spectrum of possible seasonal behaviour that can be expected in Switzerland. Stations with little seasonal variability can be compared to La Chaux-de-Fonds, while Basel/Binningen is a proxy for most stations with a moderate seasonality in precipitation. Finally Locarno-Monti, in contrast to La Chaux-de-Fonds, stands for stations with a very marked yearly cycle.

If necessary and instructive, seasonal results from other stations are shown as well.

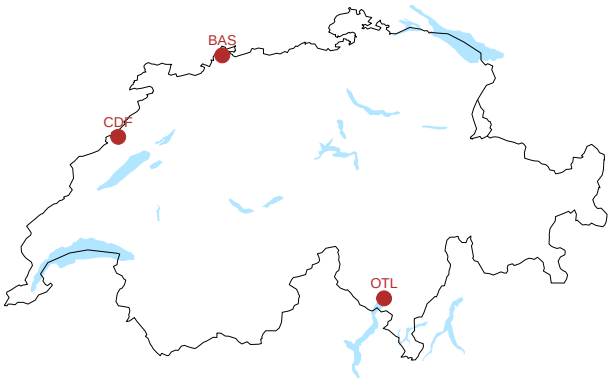

Fig. 2.2: Location of the three stations La Chaux-de-Fonds (CDF), Basel/Binningen (BAS), and Locarno-Monti (OTL).

The relevant characteristics of the stations La Chaux-de-Fonds, Basel/Binningen, and Locarno-Monti are briefly introduced in the following.

La Chaux-de-Fonds

La Chaux-de-Fonds is located in the Jura mountains in the northern part of Switzerland at an altitude of roughly 1000 m a. s. l. In August 2002 a precipitation amount of 101 mm within one day was measured—a record for the years 1901 to 2010.

Fig. 1.1a illustrates the weak seasonality of precipitation in La Chaux-de-Fonds. The median of the 110 monthly maxima ranges only between 21 mm (March) and 32 mm (August).

The almost uniform distribution of the yearly maxima throughout the seasons (s. Fig. 1.1b) is rather unusual for Switzerland: yearly maxima occur as many times in December as in August.

Basel/Binningen

Basel/Binningen is located in northwestern Switzerland at an altitude of 320 m a. s. l. The record for precipitation within one day is 85 mm and occurred in July 1991.

Compared to La Chaux-de-Fonds, the seasonality is larger. The median of the monthly extremes (s. Fig. 1.1c) varies between 10 mm (January) and 23 mm (July).

The yearly maxima are not uniformly distributed amongst the months (s. Fig. 1.1d). Roughly in half of the years, the severest precipitation event occurs in summer, most often in July.

Locarno-Monti

Locarno-Monti is situated in the southern and more Mediterranean part of Switzerland. With its 367 m a. s. l. it is one of the stations with the lowest altitude. The heaviest precipitation amount recorded since 1910, occurred in September 1991: 318 mm of rain within one day. Amongst all studied stations this is the one with the highest record.

Only few of the stations we investigate display such a strong seasonal cycle in precipitation. February, for instance (median: 20 mm), has similar characteristics as March in La Chaux-de-Fonds. In July, however, a completely different picture is found (s. Fig. 1.1e): The extreme events are distributed over a wide range of values and the median assumes a value of 63 mm.

The pie chart (s. Fig. 1.1f) reveals that approximately 25 % of the yearly maxima occur in August. In the last 110 years the annual maximum never was measured in January and only rarely in December and February. In some years, these two months were completely dry, i. e. no precipitation was measured at all.

Summary

All three stations show a seasonal cycle, weak in La Chaux-de-Fonds, pronounced in Locarno-Monti. Looking at the medians of the monthly maximum precipitation events, we see that they do not behave randomly, but rather follow some kind of oscillation, not unlike a sine function.

2.4 Software

The statistical analyses performed in this thesis were carried out with the *R* software (R Development Core Team, 2009). *R* is an open source and free software with a programming language rooted in the programming language *S*.

It can to organise data, run calculations on the information, and create graphics representing the data sets. Since it allows any scientist, engineer, and statistician to improve the software's code or to compile packages, it is widely used not only within the scientific community but also e. g. by financial services. Packages can be contributed by any user. They add for example advanced algorithms, graphical devices, or import and export capabilities to different data formats. These packages make *R* highly extensible and a "de facto standard among statisticians for the development of statistical software" (Fox and Andersen, 2005).

For this thesis we used the *extRemes* (Gilleland et al., 2009) and the *gevXgpd* (Frei, 2010) packages.

The *extRemes*-package appends some further functionality to the often used *ismev*-package (Coles and

Stephenson, 2009) and therefore is designed to enable the statistical modelling of non-stationary extreme events to *R*. It basically supports the exemplary computations in Coles's book *An Introduction to Statistical Modelling of Extreme Values* (2001).

MeteoSwiss operates its own package to perform block maxima and peak over threshold extreme value analysis with *R* (Frei, 2009).

We use the gevXgpd package mostly to compare our results with the return levels and return periods calculated operationally at MeteoSwiss (Fukutome et al., 2009; North et al., 2007, p. 35).

3 Theory and Methods

Extreme value theory (EVT) is concerned with the statistical properties of the tails of distributions. By providing the necessary methods to estimate the distribution of the extremes of a time series, it offers the possibility to quantify the return values and return periods of extreme events.

Only a relatively short overview of the essential features of the statistical theory of extreme values will be provided here. Since the present thesis is about extreme precipitation events, the focus lies on maxima i. e. the distributions' upper tails.

Extreme value theory provides several routes to the probabilistic description of extremes. In the work presented here, we focus on the block maxima approach.

3.1 Extreme Value Theory–An Overview

Let us consider a sequence of n random variables $X_1, X_2, \ldots, X_n$ which are, following the assumptions of EVT, independent and identically distributed (i. i. d.), and have a common distribution function F. Then let $M_n = \max(X_1, \ldots, X_n)$ denote the maximum of the process over n time units. In our particular case, the X_i represent daily precipitation. If n is the number of observations in a year, then M_n is the annual maximum.

3.1.1 Generalised Extreme Value Distribution

For sufficiently large n, the distribution of M_n can be approximated by the generalised extreme value (GEV) distribution:

$$G(x;\mu,\sigma,\xi) = \begin{cases} \mathrm{e}^{-\left(1+\xi\frac{x-\mu}{\sigma}\right)^{-\frac{1}{\xi}}} & \xi \neq 0 \\ \mathrm{e}^{-\mathrm{e}^{-\frac{x-\mu}{\sigma}}} & \xi = 0 \end{cases} \tag{3.1}$$

defined on

$$\left\{x : 1+\xi\frac{x-\mu}{\sigma} > 0\right\},$$

where $\mu \in \mathbb{R}$, $\sigma > 0$ and $\xi \in \mathbb{R}$.

The parameters of the GEV distribution in eq. (3.1) are named location (μ), scale ($\sigma > 0$) and shape (ξ). The location parameter specifies the position of the distribution's maximum (s. Fig. 3.1a), whereas the scale parameter characterises its spread (s. Fig. 3.1b). If the random variable M_n is GEV distributed then the standardised variable $\frac{M_n-\mu}{\sigma}$ depends neither on μ nor σ, but only on ξ.

The GEV distribution can assume three possible shape types (s. Fig. 3.1c), depending on the sign of ξ. The shape essentially governs the behaviour of the distribution's tail:

1. $\xi = 0$
   Gumbel distribution with an unbounded exponentially decreasing upper tail.
2. $\xi > 0$
   Fréchet distribution with an unbounded but slowly decreasing upper tail. Its moments are infinite for all orders greater than $\frac{1}{\xi}$, e. g. the variance is infinite if $\xi > \frac{1}{2}$.
3. $\xi < 0$
   Weibull distribution with a finite upper bound at $x = \mu - \frac{\sigma}{\xi}$.

Distributions of the GEV family are max-stable, that is, the maxima of a sequence of maxima should lead to a distribution identical in shape, with a change of scale and location. A distribution is max-stable if and only if it is a GEV distribution. (Coles, 2001)

3.2 Block Maxima

The block maxima approach aims to describe the probability distribution of the maxima of a block, e. g. annual maximum precipitation.

The full dataset is divided into equally sized subsets of data, for instance yearly blocks of 365 daily precipitation measurements (366 in leap years). The maximum for each block is determined, and subsequently the GEV distribution fitted to the obtained maxima. Finally, return levels and return periods can be calculated.

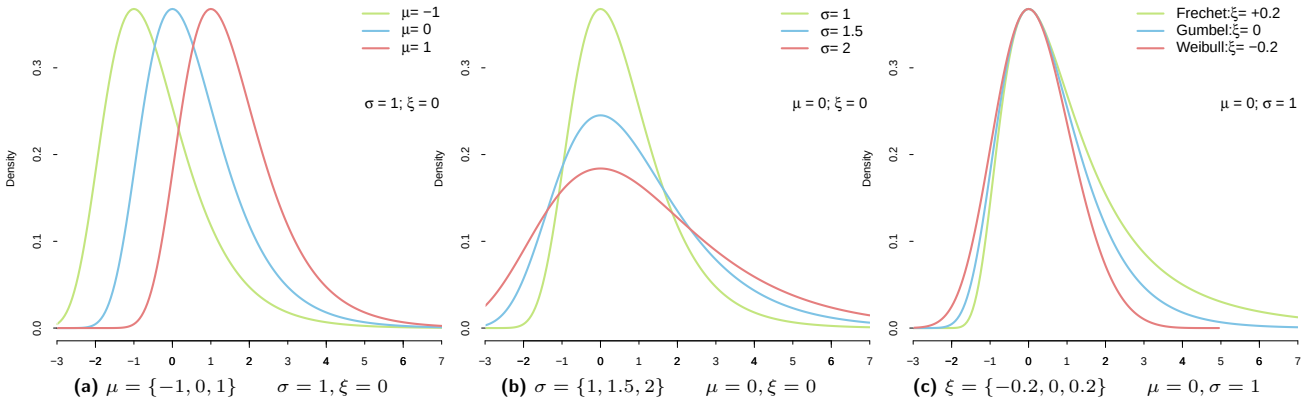

(a) $\mu = \{-1, 0, 1\}$ $\sigma = 1, \xi = 0$ **(b)** $\sigma = \{1, 1.5, 2\}$ $\mu = 0, \xi = 0$ **(c)** $\xi = \{-0.2, 0, 0.2\}$ $\mu = 0, \sigma = 1$

Fig. 3.1: Effect of the GEV distribution's parameters on the probability density function (PDF). In each figure two parameters are held constant, to the third three different values are assigned. In (a) the location parameter is varied, in (b) the scale and in (c) the shape.

An appropriate choice of the block size is important. A small number of blocks results in larger sample errors but a small block size results in biases because the distribution of the maxima of the parent distribution may not have converged toward the GEV distribution. Consequently a 'good choice' of block size is a compromise between bias and sampling errors.

As it turns out, the number of block elements necessary for the distribution of their maxima to converge, depends on the form of the generally unknown parent distribution F. For exponential (normal) parent distributions, block sizes greater than 20 (greater than 50) provide a reasonably bias free approximation for return periods equal to 5 to 100 times the length of a single block. (Frei, 2009)

3.2.1 Relaxation—Non-stationary GEV

In principle, the GEV distribution as presented above, is only valid for independent observations. This assumption is not critical, however, provided long-range dependence at extreme levels is weak. In such a case, the series is only required to be stationary. As long as extreme events are near-independent, the maxima remain GEV distributed, but with modified values for the location and the scale parameter. The shape parameter is the same as if the observations had been independent.

Yet, precipitation data can hardly be expected to be stationary. As shown in Section 1.1, the extremes display a seasonal dependence. This issue can be addressed by modelling the non-stationarity explicitly by assuming that the parameters of the GEV distribution depend on time, or on a covariate, as for instance in eq.(3.2) for the location parameter.

Our purpose is to model explicitly the seasonal dependence of extreme precipitation. We follow the method proposed by Rust et al. (2009) introducing covariates in the parameters of the GEV distribution. The form of the dependence, as well as the parameter to which it is applied, are deduced from preliminary analysis of the time series.

$$\begin{aligned} \mu = \mu(t) &= \mu_0 + \mu_1 \cdot c(t) \\ t &= \{1, 2, \ldots, n\} \end{aligned} \tag{3.2}$$

In eq. (3.2) $c(t)$ can denote a general function of time, for instance a parametric trend. Of course, $c(t)$ can be used to reflect the seasonality of the occurrence of maxima, as in eq. (3.3) for the location parameter, for instance,

$$\mu_i = \mu_0 + A_\mu \sin(\omega c_i + \phi_\mu), \quad i = \{1, 2, \ldots, n\} \tag{3.3}$$

where A_μ is the amplitude of the sinusoidal component and ϕ_μ the phase. The angular frequency is denoted by $\omega = \frac{2\pi}{T}$ where T represents the number of blocks within a year, i. e. twelve in the case of months. Counted in days starting on 1st January, c_i stands for the centre of the i^{th} block (e. g. month) each year.

Variables A_μ and ϕ_μ are considered free parameters of

the model which are to be estimated. Equation (3.3) can be rewritten in the more convenient linear form:

$$\mu_i = \mu_0 + \mu_1 \sin(\omega c_i) + \mu_2 \cos(\omega c_i), \quad i = 1, \ldots, n \tag{3.4}$$

Both the amplitude and phase of μ_i can be recovered from eq. (3.4) with

$$A_\mu = \sqrt{\mu_1^2 + \mu_2^2} \quad \text{and} \quad \phi_\mu = \arctan2\left(\frac{\mu_2}{\mu_1}\right) \tag{3.5}$$

Scale and shape parameter can be treated analogously.

In fact, this model of the seasonal cycle corresponds to a truncated *Fourier Series*

$$f(t) = \frac{a_0}{2} + \sum_{\kappa=1}^{k} (a_\kappa \cdot \sin(\kappa \cdot \omega t) + b_\kappa \cdot \cos(\kappa \cdot \omega t)) \tag{3.6}$$

With each harmonic added to the series, the number of parameters to estimate increases by 2. In addition, for each parameter, the number k of harmonics can be chosen independently: $(k_\mu, k_\sigma, k_\xi) \in \{1, 2, \ldots, \infty\}$, resulting in a large number of possible models. A more accurate representation of the seasons therefore comes at the cost of estimating more parameters. The purpose of the model selection presented in Section 3.4 below will be to strike a balance between these conflicting aspects. (Katz et al., 2005; Rust et al., 2009)

3.2.2 Return Period and Return Level

After a severe precipitation event and heavy floods, journalists, scientists, and the public are curious to know how seldom such an event occurs. Is it something that happens (statistically) once in 100 years or does it as rarely as once every 1000 years?

Extreme value theory provides some answers. In the terminology of EVT 'once in y years' means: The event has a return period of y years. Hence such an event occurs in a given year with a probability of $p = \frac{1}{y}$. For example the probability $p = 0.01$ corresponds to a 100 year return period.

The return level associated with a return period of y years is the amount of precipitation which is exceeded on average at least once in y years. Therefore the return level corresponds to the $(1-p)^{\text{th}}$ quantile of the GEV distribution.

By inverting the cumulative distribution function G in eq. (3.1), a return level can be linked to any $p \in [0, 1]$:

$$G^{-1}(1-p;\theta) = \begin{cases} \mu - \frac{\sigma}{\xi}\left(1 - [-\ln(1-p)]^{-\xi}\right) & \xi \neq 0 \\ \mu - \sigma \ln[-\ln(1-p)] & \xi = 0 \end{cases} \tag{3.7}$$

Evidently, eq. (3.7) is linear in μ and σ, but highly non-linear in the shape parameter. Thus, a reliable estimate of ξ is more critical than in cases of μ and σ, especially for return levels corresponding to long return periods. (Coles, 2001; Katz et al., 2005)

3.3 Parameter Estimation

To estimate the location, scale, and shape parameter of the GEV distribution in eq. (3.1), several methods are available. The ones most commonly used are probability weighted moments and the maximum-likelihood method (ML). The ML is computationally demanding, but can easily be extended to the non-stationary case—which for our purposes is useful.

Conceptually speaking, the ML selects the parameters $\theta = (\mu, \sigma, \xi)^T$ that maximise the probability of drawing the measurements $M_1, M_2, \ldots, M_n$ as a random sample from the GEV distribution.

Mathematically speaking, we consider m (e. g. 50) blocks of length n (e. g. 365 days for one year), thus yielding m observed maxima m_t; $t = \{1, 2, \ldots, m\}$, e. g. 50 yearly precipitation maxima. The m_t are independent realisations of a GEV-distributed random variable with probability density function (PDF) $g(m_t; \theta)$.

The likelihood $\mathcal{L}$ is defined as:

$$\mathcal{L}(\theta | m_1, m_2 \ldots, m_m) = \prod_{t=1}^{m} g(m_t; \theta) \tag{3.8}$$

It is a function of the unknown parameters μ, σ, and ξ, for the given observations m_t.

Even though the likelihood is a distribution function it is not a PDF in θ. It is a non normalised product of PDFs which is, however, proportional to the probability of observing a set of maxima $m_t;\ t = \{1, 2, \ldots, m\}$ given the parameters μ, σ, and ξ. By maximising the likelihood $\mathcal{L}(\theta|m_1, m_2, \ldots, m_m)$ we obtain the maximum-likelihood estimator (MLE) for the unknown location, scale and shape parameters:

$$\hat{\theta} = \left(\hat{\mu}, \hat{\sigma}, \hat{\xi}\right) = \arg\max_{\theta} \left[\mathcal{L}(\theta)\right] \tag{3.9}$$

In practise, it is more convenient to work with the logarithm of the likelihood function, since we can transform a product into a sum. The new distribution is called the log-likelihood ℓ.

$$\ell = \ln \mathcal{L}(\theta|m_1, \ldots, m_m) = \sum_{t=1}^{m} \ln g(m_t; \theta) \tag{3.10}$$

In general the calculations to find the MLEs are done by numerical optimisation, which is computationally demanding. (Coles, 2001)

3.4 Model selection

Even if we consider, as suggested by the preliminary analysis (s. Fig. 1.1), only models with oscillating harmonics (s. Section 3.2.1) a very large number of statistical models are possible to model the seasonal cycle i. e. the time dependence of the GEV parameters (s. Tab. 3.1). The challenge is to limit the number of possible models to a small fraction which we can handle and which includes the models reasonable to analyse the data. Then we have to determine the optimal model for each station separately.

We concentrate on models which use a truncated Fourier Series with $k \in \{0, 1, 2\}$ harmonics to model seasonality. More harmonics do not seem reasonable since the seasonal cycle mostly is not very complex and each additional harmonics introduces further parameters to estimate.

We allow each of the parameters $\mu(t)$, $\sigma(t)$, and $\xi(t)$ an independent choice of k, e. g. it is possible to model the location with $k_\mu = 2$, the scale with $k_\sigma = 1$ and the shape with $k_\xi = 0$. A value $k = 0$ means that the corresponding GEV parameter is constant i. e. not time-dependent.

Model $\mathcal{M}_{0,0}$ will denote the basic model, which assumes that the GEV parameters are independent of time, as in the case of the stationary GEV $(k_\mu = k_\sigma = k_\xi = 0)$. This means that the twelve months of the year are assumed to have the same GEV parameters. Within the spanned framework $\mathcal{M}_{0,0}$ is also the simplest model with only three parameters to estimate. For the most

Tab. 3.1: Nomenclature of the different GEV distributions used, following Mudersbach and Juergen (2011). All distributions are calculated with data starting in 1901 and ending in 2010, such that the time series have the same length.

Name	Abbreviation	Comment
Yearly Stationary GEV	S-GEV	Corresponds to the standard block maxima approach with a block length of one year. In the present study it will be referred to as *yearly S-GEV*.
Monthly Stationary GEV	S-GEV$_{\text{jan}}$	Stands also for the standard block maxima approach, but one month is treated as if it represented an entire year; values from other months are discarded. Thus we can estimate GEV parameters for each month independently. In this thesis we refer to it as *monthly Stationary GEV (S-GEV)* or as *S-GEV$_{feb}$*, for instance, if it concerns the estimation of the GEV for Februaries only.
Seasonal Non-Stationary GEV	NS-GEV	Modified block maxima approach: The seasonal time dependence of the GEV parameters is modelled as described in Tab. 3.2. In the text we refer to it as *Non-Stationary GEV* or as *seasonal time dependent GEV*.

complex model, $k_\mu = k_\sigma = k_\xi = 2$, on the other hand, fifteen parameters must be estimated:

$$\begin{aligned} G(\theta(t)) =& \mathrm{e}^{-\left(1+\xi(t)\frac{x-\mu(t)}{\sigma(t)}\right)^{-\frac{1}{\xi(t)}}} \text{ with} \\ \mu(t) =& \mu_0 + \mu_1 \sin\left(\frac{2\pi t}{T}\right) + \mu_2 \cos\left(\frac{2\pi t}{T}\right) + \\ & \mu_3 \sin\left(2\frac{2\pi t}{T}\right) + \mu_4 \cos\left(2\frac{2\pi t}{T}\right) \\ \sigma(t) =& \sigma_0 + \sigma_1 \sin\left(\frac{2\pi t}{T}\right) + \sigma_2 \cos\left(\frac{2\pi t}{T}\right) + \\ & \sigma_3 \sin\left(2\frac{2\pi t}{T}\right) + \sigma_4 \cos\left(2\frac{2\pi t}{T}\right) \\ \xi(t) =& \xi_0 + \xi_1 \sin\left(\frac{2\pi t}{T}\right) + \xi_2 \cos\left(\frac{2\pi t}{T}\right) + \\ & \xi_3 \sin\left(2\frac{2\pi t}{T}\right) + \xi_4 \cos\left(2\frac{2\pi t}{T}\right) \end{aligned} \tag{3.11}$$

Since k can take three different values for each parameter μ, σ, and ξ, in total $3^3 = 27$ models are possible. Each can be applied for all considered stations. But, at a particular station, which of them is best?

According to Coles (2001), parsimony is the guiding principle in model selection i. e. "Choose the simplest model possible that explains as much of the variation in the data as possible." This often is done by using the log-likelihood ratio test (LLR-test) and/or Akaike's information criterion (AIC), which both avoid overfitting and test for significant improvements of higher dimensional statistical models. (Sienz et al., 2010)

3.4.1 Log-Likelihood Ratio Test

If a model $\mathcal{M}_i$ is a sub-model of model $\mathcal{M}_j$, then we can perform a log-likelihood ratio test to select the better model. Let $\mathcal{M}_j$ be a model with parameter vector θ. $\mathcal{M}_i$ is a sub-model of model $\mathcal{M}_j$ if $\mathcal{M}_i$ is obtained by constraining l of θ's components to be zero. In other words, it is possible to partition $\theta = (\theta^{(1)}, \theta^{(2)})$ in such a way that the l-dimensional sub-vector $\theta^{(1)} = 0$ in $\mathcal{M}_i$. The model $\mathcal{M}_i$ and is then said to be nested in$\mathcal{M}_j$. For instance, in Tab. 3.2, $\mathcal{M}_{0,1}$is a sub-model of $\mathcal{M}_{1,1}$.

The deviance is defined as:

$$D = 2 \cdot [\ell_j(\mathcal{M}_j) - \ell_i(\mathcal{M}_i)] \tag{3.12}$$

where $\ell_i(\mathcal{M}_i)$ and $\ell_j(\mathcal{M}_j)$ denote the maximised log-likelihoods for models $\mathcal{M}_i$ and $\mathcal{M}_j$ respectively.

For large samples, D has a chi-square distribution with l degrees of freedom (χ^2_l). For a chosen level of significance α, let c_α denote the $(1-\alpha)$ quantile of the χ^2_l distribution. Model $\mathcal{M}_i$ can now be unambiguously rejected in favour of $\mathcal{M}_j$ if $D > c_\alpha$. (Coles, 2001)

Since the proposed models are not necessarily nested (see for example $\mathcal{M}_{1,0}$and $\mathcal{M}_{0,1}$in Tab. 3.2), the LLR-test is not always applicable. It is possible to overcome this restriction by using AIC as explained below. (Sienz et al., 2010)

3.4.2 Akaike's information criterion

Akaike's information criterion is a measure of the goodness of fit of a statistical model. It was developed by Hirotsugu Akaike in 1973 and estimates the expected, relative distance between the fitted model and the unknown true mechanism resulting in the observed data.

This means that we compare our description of the data generating process, i. e. our statistical model $\mathcal{M}_j$, to some unknown true process F which generated the considered data in the first place. To this end, we consider two candidate models to represent F: $\mathcal{M}_i$ and $\mathcal{M}_j$. If we knew F, there would be ways to quantify the information lost by using either $\mathcal{M}_i$ or $\mathcal{M}_j$ to represent F. We would then choose the candidate model that minimised the information loss. Since we do not know F, a reliable selection is not possible.

Akaike (1973) showed, however, that we can estimate how much more (or less) information is lost by $\mathcal{M}_i$ than by $\mathcal{M}_j$ in relation to F. This can be done by computing the AIC for each model under consideration:

$$\mathrm{AIC} = -2\ell(\hat{\theta}|\mathcal{M}_j) + 2K \tag{3.13}$$

where $\hat{\theta}$ denotes the MLE, and $\ell(\hat{\theta}|\mathcal{M}_j)$ is the log-likelihood evaluated at $\theta = \hat{\theta}$. $\mathcal{M}_j$ represents the model to be examined, and K the number of its estimable parameters (Burnham and Anderson, 2002); $K \in [3, 11]$ for the models used (s. Tab. 3.2). Note that the model selected by the AIC may still be poor in an absolute

sense. It is therefore important to ensure that the considered models are well founded.

If more parameters are added to the approximating model, the right-hand side's first term usually decreases while the second term grows. This can be interpreted as a trade-off between bias and variance as well as a trade-off between under- and overfitting (Burnham and Anderson, 2002). The effects of this balance can be observed in Tab. 4.1.

It turns out that the AIC may perform poorly when the ratio of sample size n to the number of parameters K is less than 40. We encounter this problem when investigating 1 hour maxima. In such cases, the use of a second-order AIC ($\mathrm{AIC_c}$) is advisable: it penalises additional parameters more severely than the original AIC. (Burnham and Anderson, 2002)

$$\mathrm{AIC_c} = -2\ell(\hat{\theta}|M_j) + 2K\left(\frac{n}{n-K-1}\right) \tag{3.14}$$

In a set of models $\mathcal{M}_j$, the one with the minimum $\mathrm{AIC_c}$ value ($\mathrm{AIC_{min}}$) is the best model, since its estimates are 'closest' to F. The Akaike difference ($\Delta\mathrm{AIC_c}$) can be calculated according to eq. (3.15) to rank the models (Burnham and Anderson, 2002; Sienz et al., 2010)

$$\Delta\,\mathrm{AIC_{c},}_j = \mathrm{AIC_{c},}_j - \mathrm{AIC_{min}} \tag{3.15}$$

According to Sienz et al. (2010)

$$\Delta\,\mathrm{AIC_{c},}_j \begin{cases} \in [0,2) & \text{gives strong support} \\ \in (4,7) & \text{gives considerably less support} \\ \in (10,\infty) & \text{gives no support} \end{cases}$$

to model $\mathcal{M}_j$.

Tab. 3.2: Statistical models considered in this study. The first column denotes the model name, the second to fourth columns show the modelled time dependence for the parameters $\mu(t)$, $\sigma(t)$, and $\xi(t)$. Model $\mathcal{M}_{0,0}$ is the basic model, $\mathcal{M}_{2,2}$ has the most parameters to estimate. Models $\mathcal{M}_{1,0}$, $\mathcal{M}_{0,1}$ and $\mathcal{M}_{1,1}$ only use the first harmonic of a Fourier Series whereas $\mathcal{M}_{2,0}$ to $\mathcal{M}_{2,2}$ use two harmonics for at least one parameter.

Name	$\boldsymbol{\mu(t)}$	$\boldsymbol{\sigma(t)}$	$\boldsymbol{\xi(t)}$
$\mathcal{M}_{0,0}$	μ_0	σ_0	ξ_0
$\mathcal{M}_{1,0}$	$\mu_0 + \mu_1 \sin\left(\frac{2\pi t}{T}\right) + \mu_2 \cos\left(\frac{2\pi t}{T}\right)$	σ_0	ξ_0
$\mathcal{M}_{0,1}$	μ_0	$\sigma_0 + \sigma_1 \sin\left(\frac{2\pi t}{T}\right) + \sigma_2 \cos\left(\frac{2\pi t}{T}\right)$	ξ_0
$\mathcal{M}_{1,1}$	$\mu_0 + \mu_1 \sin\left(\frac{2\pi t}{T}\right) + \mu_2 \cos\left(\frac{2\pi t}{T}\right)$	$\sigma_0 + \sigma_1 \sin\left(\frac{2\pi t}{T}\right) + \sigma_2 \cos\left(\frac{2\pi t}{T}\right)$	ξ_0
$\mathcal{M}_{2,0}$	$\mu_0 + \mu_1 \sin\left(\frac{2\pi t}{T}\right) + \mu_2 \cos\left(\frac{2\pi t}{T}\right) + \mu_3 \sin\left(2\frac{2\pi t}{T}\right) + \mu_4 \cos\left(2\frac{2\pi t}{T}\right)$	σ_0	ξ_0
$\mathcal{M}_{0,2}$	μ_0	$\sigma_0 + \sigma_1 \sin\left(\frac{2\pi t}{T}\right) + \sigma_2 \cos\left(\frac{2\pi t}{T}\right) + \sigma_3 \sin\left(2\frac{2\pi t}{T}\right) + \sigma_4 \cos\left(2\frac{2\pi t}{T}\right)$	ξ_0
$\mathcal{M}_{1,2}$	$\mu_0 + \mu_1 \sin\left(\frac{2\pi t}{T}\right) + \mu_2 \cos\left(\frac{2\pi t}{T}\right)$	$\sigma_0 + \sigma_1 \sin\left(\frac{2\pi t}{T}\right) + \sigma_2 \cos\left(\frac{2\pi t}{T}\right) + \sigma_3 \sin\left(2\frac{2\pi t}{T}\right) + \sigma_4 \cos\left(2\frac{2\pi t}{T}\right)$	ξ_0
$\mathcal{M}_{2,1}$	$\mu_0 + \mu_1 \sin\left(\frac{2\pi t}{T}\right) + \mu_2 \cos\left(\frac{2\pi t}{T}\right) + \mu_3 \sin\left(2\frac{2\pi t}{T}\right) + \mu_4 \cos\left(2\frac{2\pi t}{T}\right)$	$\sigma_0 + \sigma_1 \sin\left(\frac{2\pi t}{T}\right) + \sigma_2 \cos\left(\frac{2\pi t}{T}\right)$	ξ_0
$\mathcal{M}_{2,2}$	$\mu_0 + \mu_1 \sin\left(\frac{2\pi t}{T}\right) + \mu_2 \cos\left(\frac{2\pi t}{T}\right) + \mu_3 \sin\left(2\frac{2\pi t}{T}\right) + \mu_4 \cos\left(2\frac{2\pi t}{T}\right)$	$\sigma_0 + \sigma_1 \sin\left(\frac{2\pi t}{T}\right) + \sigma_2 \cos\left(\frac{2\pi t}{T}\right) + \sigma_3 \sin\left(2\frac{2\pi t}{T}\right) + \sigma_4 \cos\left(2\frac{2\pi t}{T}\right)$	ξ_0

With Akaike weights (AIC_w), which denote model j's probability w_j to be the best one, further interpretation is gained.

$$w_j = \frac{e^{-0.5\Delta\,AIC_{c,j}}}{\sum_{j=1}^{J} e^{-0.5\Delta\,AIC_{c,j}}} \tag{3.16}$$

AIC_w assigns a probability to a model $\mathcal{M}_j$ that denotes how likely it is that model $\mathcal{M}_j$ is the best model amongst all tested models.

3.4.3 AIC_c vs. LLR-test

The AIC_c emerges as a useful tool to select a suitable model among a collection of different non-hierarchical models, but may occasionally yield ambiguous results if the ΔAIC_cs are too small. In such a case, and if the relevant models are nested, we can resort to the LLR-test mentioned above for a more reliable verdict.

In our model selection, we therefore proceed in two steps. First we calculate the AIC_cs. If they are not conclusive and a LLR-test is possible, we then use the results of the LLR-test to select the appropriate model. In cases where a LLR-test is not possible, we rely entirely on the AIC_c.

If, by coincidence, this still is inconclusive, e. g. if $\mathcal{M}_i$ and $\mathcal{M}_j$ have the same AIC_c and a LLR-test is not possible, we choose the model with the least parameters.

3.4.4 Constant Shape Parameter

Due to a lack of information in the distribution's upper tail, it is difficult to estimate the shape parameter (Parey et al., 2007), which also tends to be strongly influenced by a few large events.

As can be seen in Fig. 3.2, the monthly S-GEV's best estimate of the shape parameter is somewhat erratic, and its confidence intervals are very large. The figure shows the values and uncertainty of ξ at Basel/Binningen if the GEV parameters are estimated for each month using the monthly S-GEV: there is no distinct seasonal cycle to account for. See also figures 4.1g and 4.1i.

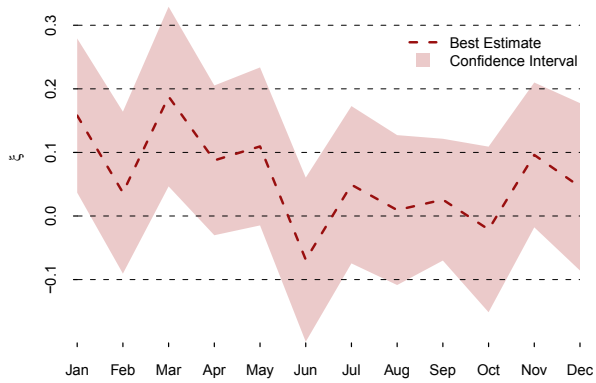

Fig. 3.2: Best estimates and 95 % confidence interval (shaded red area) for ξ as determined with parametric resampling for Basel/Binningen

Given the difficulty of estimating the shape parameter, it is therefore customary to assume that the shape parameter does not depend on time or, in this particular case, on the season. Nevertheless, a preliminary model selection analysis was performed in which the seasonal dependence of the shape parameter was tentatively modeled. It turned out that a model with $\xi(t) \neq$ const. was selected at 18 % of the stations. These stations are shown in Fig. 3.3. We do not know whether these stations have a common feature that we overlooked. It is noticeable that for most stations in Graubünden, according to model selection, a time-dependent shape parameter is required.

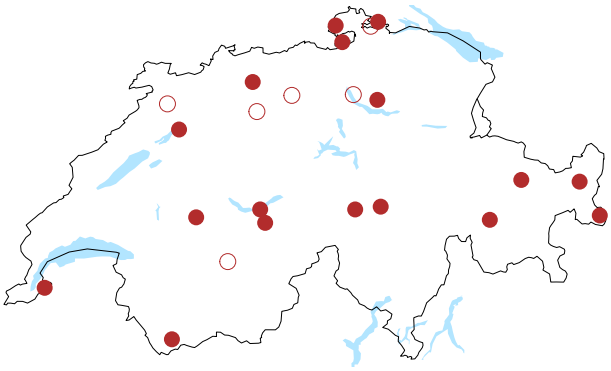

Fig. 3.3: Stations where explicit modelling of ξ is recommended by the ΔAIC_c. After a LLR-test, the stations marked with circles are considered compatible with a constant ξ.

In the remainder of this study, the shape parameter will be assumed constant throughout the seasons, and, where relevant, over the entire period under consideration. This reduces the number of models to 9. We

denote these models ($\mathcal{M}_{i,j}, i, j \in [0, 2]$). The indices i, j indicate the number of harmonics used to describe the seasonal dependence. Thus, $\mathcal{M}_{0,0}$ is the simplest and $\mathcal{M}_{2,2}$ the most complex model. The explicit formulation of all models can be found in Tab. 3.2.

3.5 Validation Strategy

The Non-Stationary GEV (NS-GEV) analysis provides us with location, scale, and shape parameter, as well as return level estimates for each month of the year. For validation we will compare them with the results of the monthly S-GEV analysis.

For the monthly S-GEV the parameters are estimated one month at a time. Parameters μ, σ, and ξ will for instance be estimated for consecutive January maxima between 1901 and 2010. Thus, only one value per year enters the calculation. Note that this generally leads to relatively large confidence intervals, since there are three parameters per month to estimate, and 110 observations. For comparison: Our most complex model for a seasonal Non-Stationary GEV, $\mathcal{M}_{2,2}$, only estimates 11 different parameters with 1320 observations. A priori, we therefore expect the seasonal Non-Stationary GEV to provide more accurate estimates.

As we shall see below, yearly return levels can be derived from the monthly non-stationary return levels. Thus, to further validate the time dependent GEV, we compare the derived yearly return levels with the results obtained from the yearly S-GEV. The yearly non-stationary best estimates and confidence intervals are gained as described in section 3.6. For comparability, all the different GEVs are calculated using the same data with time series from 1901 to 2010.

3.6 From Monthly to Yearly Values

In the present study, we explicitly model the seasonal dependence of the precipitation maxima, and obtain a different set of GEV parameters for each month. Fig. 3.4 shows the CDFs of daily precipitation for the station Basel/Binningen. Return levels can be estimated for each month separately.

To avoid confusion and have a proper nomenclature, an event which happens once every y Januaries (Februaries, Marches, ...) will, from now on, have the subscript *jan*. Thus a 100_{jan} year event denotes an amount of rainfall that is exceeded at least once in 100 Januaries. If there is no subscript, the traditional y year event is meant.

By estimating the return levels for the individual months of the year, we gain the ability to put a heavy precipitation event in January in relation with other January events, and events in other months, i. e. we can say: "Indeed, the precipitation amount z_y is extraordinary for January, even though we have the same amount of precipitation every second August." Note that this might be of particular interest in some areas such as agriculture.

For operational purposes, however, a yearly return level is often required, depending on the application. We would like to have the y year event for a year, not a month. To achieve this, we note that the probability that the yearly maximum is smaller than a given value z is equal to the probability that the maxima of each month also are smaller than z. Let $G_y(z_y)$ denote the probability that the yearly maximum is below z_y, the return level associated with the return period $y = \frac{1}{p}$. Then,

$$G_y(z_y) = \prod_{j=1}^{12} G_j(z_y; \mu_j, \sigma_j, \xi_j) = 1 - \frac{1}{y} \qquad (3.17)$$

Unfortunately this cannot be solved analytically, and we have to apply a numerical approximation procedure. In our case we use *Newton's method*. The resulting return level z_y can also be used to conclude how often the y year event will fall in a particular month (s. Fig. 3.4b). Note that a similar method was applied by Buishand and Demaré (1990) to derive the yearly return levels of 10-minute, 1-hour, and 1-day precipitation from smoothed monthly Gumbel estimates.

Newton's Method

Newton's Method is designed to find successively better approximations to equations of the form

$$f(x) = 0, \qquad (3.18)$$

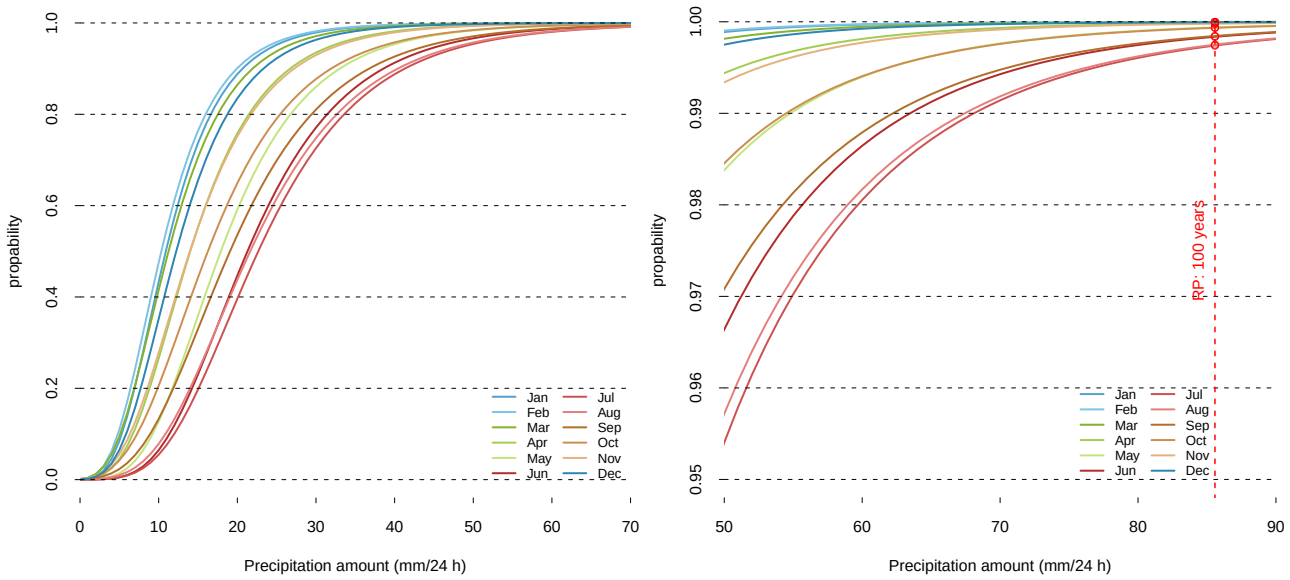

(a) The entire CDF **(b)** Zoom from $p = 0.95$ to $p = 1$

Fig. 3.4: Cumulative density functions (CDFs) of the maximum daily precipitation amount for each month at Basel/Binningen. In (a) we see the entire CDFs whereas (b) only shows the highest quantiles. Additionally, the return level of a 100 year event is marked with the dashed vertical line. Its intersection with each CDF (red points) denotes the probability that a yearly 100 year event will be exceeded in a specific month.
For instance, the chance that a precipitation event of 85.6 mm is exceeded in January is ca. $p_{\text{jan}} = 1.83 \cdot 10^{-5}$ which means this happens on average once in 54,612 years. In August, on the other hand, this amount of precipitation will be reached in average every 385 years ($p_{\text{aug}} = 2.60 \cdot 10^{-3}$). Multiplication $\prod_{j=1}^{12}(1 - p_j)$ leads to a value of 0.99—which is the quantile of a 100 year event.

which in case of eq. (3.17) only needs a little bit of rearranging:

$$\prod_{j=1}^{12} G_j(z_y; \mu(j), \sigma(j), \xi(j)) - \left(1 - \frac{1}{y}\right) = 0 \quad (3.19)$$

First we have to make an initial guess for z_y which should be as close as possible to the solution. Otherwise there is a chance that Newton's Method does not converge to the solution, i. e. in our case it results in a value of $\pm\infty$.

As initial guess we can use the direct estimate of the return levels from the yearly S-GEV. We use it to begin the following iteration process:

$$x_{n+1} = x_n - \frac{f(x_n)}{f'(x_n)} \quad (3.20)$$

where $f'(x_n)$ is the first derivative of $f(x_n)$. We terminate the iteration process after a previously defined small threshold ($Tr \geqslant x_{n+1} - x_n$) has been reached. (Sebah and Gourdon, 2001)

Unfortunately, at certain stations the confidence interval calculation occasionally produces extreme events that are much larger than the best estimates. In theses cases the application of Newton's Method leads to iteration cycles that never converge.

We are not sure whether the chosen algorithm fails by design or whether our programming is not flexible enough. In the worst case, for a return level of 300 years, around 3 ‰ of the samples S (s. Section 3.7) must be discarded, which leads to confidence intervals that are a little too narrow.

The problem becomes less acute for less pronounced and less complex seasonality patterns, and for lower return periods. Until now we were not able to find a solution to this particular problem.

3.7 Calculation of Confidence Intervals

Confidence intervals are essential for ascertaining the accuracy of our estimates. In particular, when deducing yearly return levels from the seasonal analysis, it

is interesting to know whether explicitly modelling the seasonal cycle has led to a reduction in the uncertainty. While the amount of data has increased by a factor of twelve we have to estimate between 1.33 and almost 4 times the amount of parameters used for the yearly S-GEV, depending on the model selected.

The method of our choice is parametric resampling, a type of Monte Carlo method[1] used frequently in applied statistics. This method allows us to compute confidence intervals by sampling the estimated distribution. Unfortunately, it is computationally demanding, since according to Burnham and Anderson (2002), thousands of samples are needed in complex data analysis.

The confidence intervals are estimated as follows. The estimated parameters $\hat{\theta}$ of the selected model uniquely define a GEV distribution, which can therefore be sampled. A random sample S of size n equal to that of the original sample is generated from the GEV distribution specified by $\hat{\theta}$.

The cumulative density function (CDF) assigns a probability $p \in [0,1]$ to a particular precipitation event. Sample S can be drawn by first randomly choosing a value for $p \in [0,1]$ n times. The associated precipitation events are then calculated using eq. (3.21), which is obtained by inverting eq. (3.1):

$$M_t = \mu + \frac{\sigma}{\xi} \cdot \left[(-\ln p)^{-\xi} - 1\right] \tag{3.21}$$

By repeating this procedure, say 5,000 times, enough samples $S_i;\ i = \{1, \ldots, 5000\}$ for further investigation are gained. In a second step, each sample's MLE $\hat{\theta}_i$ is estimated with the same model for seasonal dependence as was used for the original data.

The 95 % quantiles of the 5,000 $\hat{\theta}_i$ yield the confidence intervals for $\mu(t)$, $\sigma(t)$, and $\xi(t)$. To each $\hat{\theta}_i$, a return level can be calculated which in turn enables us to obtain a confidence interval for the return level. (Burnham and Anderson, 2002)

3.8 Modelling Long-Term Trends

All of the stations under consideration in the present study have data over a hundred years or more. Therefore the possibility of a long-term non-stationarity in the time-series cannot be excluded. Thus, although it is not the primary objective of this thesis to systematically investigate long-term changes in the behaviour of extreme precipitation, it appears necessary to examine the relevance of such a non-stationarity for our results.

If the effect of a long-term trend is significant, a subsequent, more thorough investigation would be worthwhile.

To this end, we assume the simplest possible form of long-term non-stationarity by adding a linear dependence on time in the GEV parameters. This translates into slightly modified models for the parameters $\mu(t)$ and $\sigma(t)$ e. g.

$$\mu(t) = \mu_{\mathcal{M}_j}(t) + \mu_T \cdot t \tag{3.22}$$

where $\mu_{\mathcal{M}_j}$ denotes any of the previously used models of $\mu(t)$ including $\mu = \text{const}$. Since the linear term $\mu_T \cdot t$ is a simple addition to the model, we can perform a log-likelihood ratio test to decide whether the long-term time dependence should be taken into account.

As mentioned above, it is not our purpose to perform a systematic study of long-term non-stationarities. For this reason, the linear time dependence will only be included whenever explicit modelling of seasonal dependence has been shown to be meaningful. Given that the shape parameter has been assumed constant, we do not allow it to have a linear time dependence. According to Zhang et al. (2004) this is plausible since in case of a GEV distribution with a modestly changing tail the variation of the scale parameter can approximate the tail's change.

Our formulation of the long-term trend, thus only affects the location and scale parameters and is the same for each month of the year.

3.9 Limitations

3.9.1 Data

The used dataset assumes that e. g. a daily maximum in precipitation always occurs, for instance, from midnight

[1] "A Monte Carlo simulation uses a computer to generate a large number of scenarios based on probabilities for inputs." (Hubbard, 2007)

to midnight. Obviously the maximum sum of 24 hours of rain, however, could also be from 4:13 pm to the same time next day. Since most of the precipitation data, especially in long time series, is collected once a day at 7:30 am local time, it is very likely that we miss the real 24 hour maxima. Nevertheless, the available data should be a close enough approximation.

With the installation of new and fully automated stations in 1981, precipitation data with a resolution of 10 minutes became available at a number of stations. With this data, it is possible to determine the 'real' maximum value of 24 hour precipitation. Unfortunately the disadvantage of a short time series (1981 to 2010 instead of 1901 to 2010) is larger than not having the real 24 hour value.

Long time series usually have systematic inhomogeneities and their use for climatological studies can lead do misinterpretations. Thus, it is better to use homogenised time series (Begert et al., 2003). For the present study, only eight homogenised time series were available over the complete time span of 110 years. Of these eight stations, two had identical series of maxima. A sensitivity analysis revealed that the results of the extreme value analysis differed only by 5 % to 6 % even for 300 year return periods. Since these small differences are not expected to have a bearing on the results of this study, we forwent the homogenised data.

3.9.2 Method

The described methods only allow us to choose the best model amongst all models under consideration. There may be much better models that we have not thought of. Therefore, the 'best' model we found might still be very poor. In either case, we are able to get an idea whether the newly developed models lead to an improvement in accuracy and certainty.

4 Results

In this section, we compare the seasonal non-stationary estimates of parameters and return levels with those provided by the Stationary GEV (S-GEV) applied to the individual months. Later on, the results of the yearly return levels derived from the seasonal non-stationary analysis are examined. Because our time series extend over 110 years, we then consider the possibility of long-term non-stationarities. We present the resulting trends' strength and their sign.

Finally, we use the monthly estimations of the Non-Stationary GEV (NS-GEV) parameters for a short investigation of the spatial and seasonal distribution of extremes.

First of all, however, we need to find the optimal NS-GEV models.

4.1 Optimal NS-GEV Models

Ranking the models for modelling the Non-Stationary GEV according to AIC_c leads to the results presented in Tab. 4.1. These results give a good indication as to which model should be used. Depending on the Akaike difference (ΔAIC_c) and the Akaike weights (AIC_w) we also have some indication whether other models have to be considered and whether a log-likelihood ratio test (LLR-test) is, if possible, advisable.

4.1.1 Optimal Models for Key Stations

La Chaux-de-Fonds

For La Chaux-de-Fonds (s. Tab. 4.2a) $\mathcal{M}_{2,1}$ seems to fit best. The AIC_c values indicates that $\mathcal{M}_{1,1}$ and especially $\mathcal{M}_{2,0}$ are close behind. Since both are submodels of $\mathcal{M}_{2,1}$ we can perform a LLR-test.

With a p-value of 0.017, $\mathcal{M}_{2,1}$ clearly performs better than $\mathcal{M}_{1,1}$. Model $\mathcal{M}_{2,0}$, while better than $\mathcal{M}_{1,1}$, is still not preferable: $\mathcal{M}_{2,1}$ is significantly better (p-value: 0.037).

Thus, at La Chaux-de-Fonds $\mathcal{M}_{2,1}$ turns out to be the optimal model. In other words, the location parameter is modelled with two harmonics $(k_\mu = 2)$ of the Fourier Series but only one is needed for the scale parameter $(k_\sigma = 1)$. Recall that the shape parameter is held constant for all stations and for all models $(k_\xi = 0)$.

Basel/Binningen

Here too, the AIC_c (s. Tab. 4.2b) suggests that $\mathcal{M}_{2,1}$ performs best. The indications for $\mathcal{M}_{2,1}$ at Basel/Binningen are, however, much stronger, since AIC_w assigns roughly a probability of 90 % to this particular model. Only 9 % are assigned to $\mathcal{M}_{2,2}$ and 1 % to $\mathcal{M}_{1,1}$.

A LLR-test is not necessary since $\mathcal{M}_{2,2}$'s ΔAIC_c is 4.5 and since it needs three additional parameters to estimate. It is therefore unlikely to be selected. Model $\mathcal{M}_{1,1}$'s AIC_w is poor. Nevertheless, to illustrate this point we performed the LLR-test: Hypothesis "$\mathcal{M}_8$ better than $\mathcal{M}_{2,1}$" has a p-value of 1, hypothesis "$\mathcal{M}_{2,1}$ better than $\mathcal{M}_3$" one of 0.00093.

Thus, we choose at Basel/Binningen the same model as at La Chaux-de-Fonds with two harmonics $(k_\mu = 2)$ of the Fourier Series for the location parameter and only one for the scale parameter $(k_\sigma = 1)$.

Locarno-Monti

The situation at Locarno-Monti (s. Tab. 4.2b) is different: Model $\mathcal{M}_{1,2}$ now performs best (AIC_w: 57 %). Unfortunately, the second best ($\mathcal{M}_{2,1}$; AIC_w: 21 %) is not nested in $\mathcal{M}_{1,2}$. Thus, a LLR-test is not possible.

Tab. 4.1: These three tables rank the models $\mathcal{M}_j$ for the stations La Chaux-de-Fonds (a), Basel/Binningen (b) and Locarno-Monti (c), according to the AIC_c. The fist column indicates the model used, the second the AIC_c-value, the third the AIC_c's difference to the 'best' model, the fourth the model's probability to be the most accurate, and the last column ranks the models. First ranks are marked in green colours.

Model	AIC_c	ΔAIC_c	AIC_w	Rank
$\mathcal{M}_{0,0}$	10349	50.8	0 %	7
$\mathcal{M}_{1,0}$	10305	7.2	2 %	6
$\mathcal{M}_{0,1}$	10351	52.5	0 %	8
$\mathcal{M}_{1,1}$	10302	4.1	8 %	3
$\mathcal{M}_{2,0}$	10301	2.5	18 %	2
$\mathcal{M}_{0,2}$	10351	53.1	0 %	9
$\mathcal{M}_{1,2}$	10305	7.1	2 %	5
$\mathcal{M}_{2,1}$	*10298*	*0*	*64 %*	*1*
$\mathcal{M}_{2,2}$	10303	4.8	6 %	4

(a) La Chaux-de-Fonds

Model	AIC_c	ΔAIC_c	AIC_w	Rank
$\mathcal{M}_{0,0}$	9612	307	0 %	9
$\mathcal{M}_{1,0}$	9417	111	0 %	6
$\mathcal{M}_{0,1}$	9591	286	0 %	8
$\mathcal{M}_{1,1}$	9315	9.9	1 %	3
$\mathcal{M}_{2,0}$	9410	105	0 %	6
$\mathcal{M}_{0,2}$	9585	279	0 %	7
$\mathcal{M}_{1,2}$	9318	12.2	0 %	4
$\mathcal{M}_{2,1}$	*9306*	*0*	*90 %*	*1*
$\mathcal{M}_{2,2}$	9310	4.5	9 %	2

(b) Basel/Binningen

Model	AIC_c	ΔAIC_c	AIC_w	Rank
$\mathcal{M}_{0,0}$	12875	326	0 %	9
$\mathcal{M}_{1,0}$	12681	132	0 %	6
$\mathcal{M}_{0,1}$	12859	310	0 %	8
$\mathcal{M}_{1,1}$	12552	2.6	15 %	3
$\mathcal{M}_{2,0}$	12678	129	0 %	5
$\mathcal{M}_{0,2}$	12841	292	0 %	7
$\mathcal{M}_{1,2}$	*12549*	*0*	*57 %*	*1*
$\mathcal{M}_{2,1}$	12551	2.0	21 %	2
$\mathcal{M}_{2,2}$	12553	4.3	7 %	4

(c) Locarno-Monti

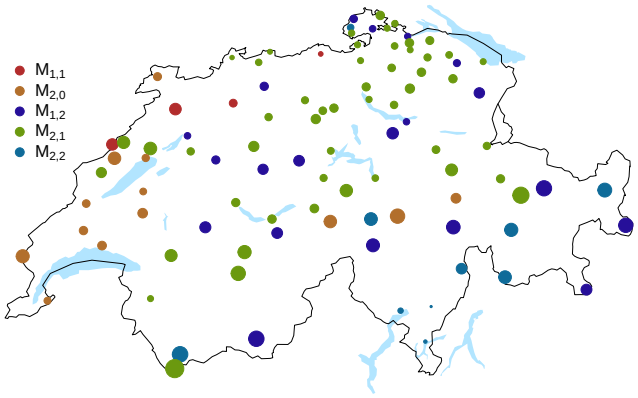

Fig. 4.2: Spatial distribution of selected models, indicated by colour. The point sizes refer to their elevation: The larger the point the higher the station's location.

Due to its relatively high AIC_w (15 %), $\mathcal{M}_{1,1}$ must also be taken into consideration. Since it is nested in $\mathcal{M}_{2,1}$ and $\mathcal{M}_{1,2}$, its relative position with respect to $\mathcal{M}_{1,2}$ and $\mathcal{M}_{2,1}$ can be tested with the LLR-test. The results are unambiguous: whereas $\mathcal{M}_{1,2}$ outperforms $\mathcal{M}_{1,1}$ (p-value: 0.036), $\mathcal{M}_{1,1}$ turns out to be better than $\mathcal{M}_{2,1}$ (p-value: 0.094).

4.1.2 Optimal Models for all Stations

If we focus on all 97 evaluated stations, we find that $\mathcal{M}_{2,1}$ is generally the most likely model (s. Fig. 4.2). It is chosen at 52 % of the stations. Nevertheless $\mathcal{M}_{2,2}$ fits the data best at 21 % of the stations. Models $\mathcal{M}_{1,1}$ (13 %), $\mathcal{M}_{1,2}$ (10 %) and $\mathcal{M}_{2,0}$ (4 %) rarely outperform the other models.

Model $\mathcal{M}_{0,0}$ is worst at four out of five stations, while models that exclusively take the scale parameter's seasonality ($\mathcal{M}_{0,1}$ and $\mathcal{M}_{0,2}$) into account are worst at 7 % and 12 % of the stations. On the other hand, $\mathcal{M}_{1,0}$ performs neither especially well, nor especially badly.

If we compare AIC_c with the LLR-test, the results of model selection differ at 18 % of the stations. The AIC_c always tends to favour the more complex model.

The spatial distribution of the selected models (s. Fig. 4.2) does not reveal very marked structures. Yet, some features can be noted tentatively: Model $\mathcal{M}_{2,1}$, while dominant in the Central Plateau, looses its importance in the southern and western parts of Switzerland. In Southern Switzerland, the seasonal variation of the scale parameter seems to become more complex, and its modelling requires two oscillations of the Fourier Series ($k_\sigma = 2$). The opposite can be observed further

to the west. Indeed, the seasonal variation for the scale parameter is no longer justified. This indicates a larger (smaller) variation of extreme precipitation events in southern (western) parts of Switzerland than in the northern parts.

4.1.3 Parameters of the Optimal Models

In order to see how well the chosen models estimate the generalised extreme value (GEV) parameters $\mu(t)$, $\sigma(t)$, and $\xi(t)$, we compare them with the estimates of the GEV parameters calculated separately for each individual monthly S-GEV. These are represented in Fig. 4.1 by a dashed red line, and their confidence intervals by the shaded red area. Values obtained with the 'best' seasonal model are coloured in green (location), blue (scale), and purple (shape). The shaded areas mark the confidence intervals and the lines the best estimates.

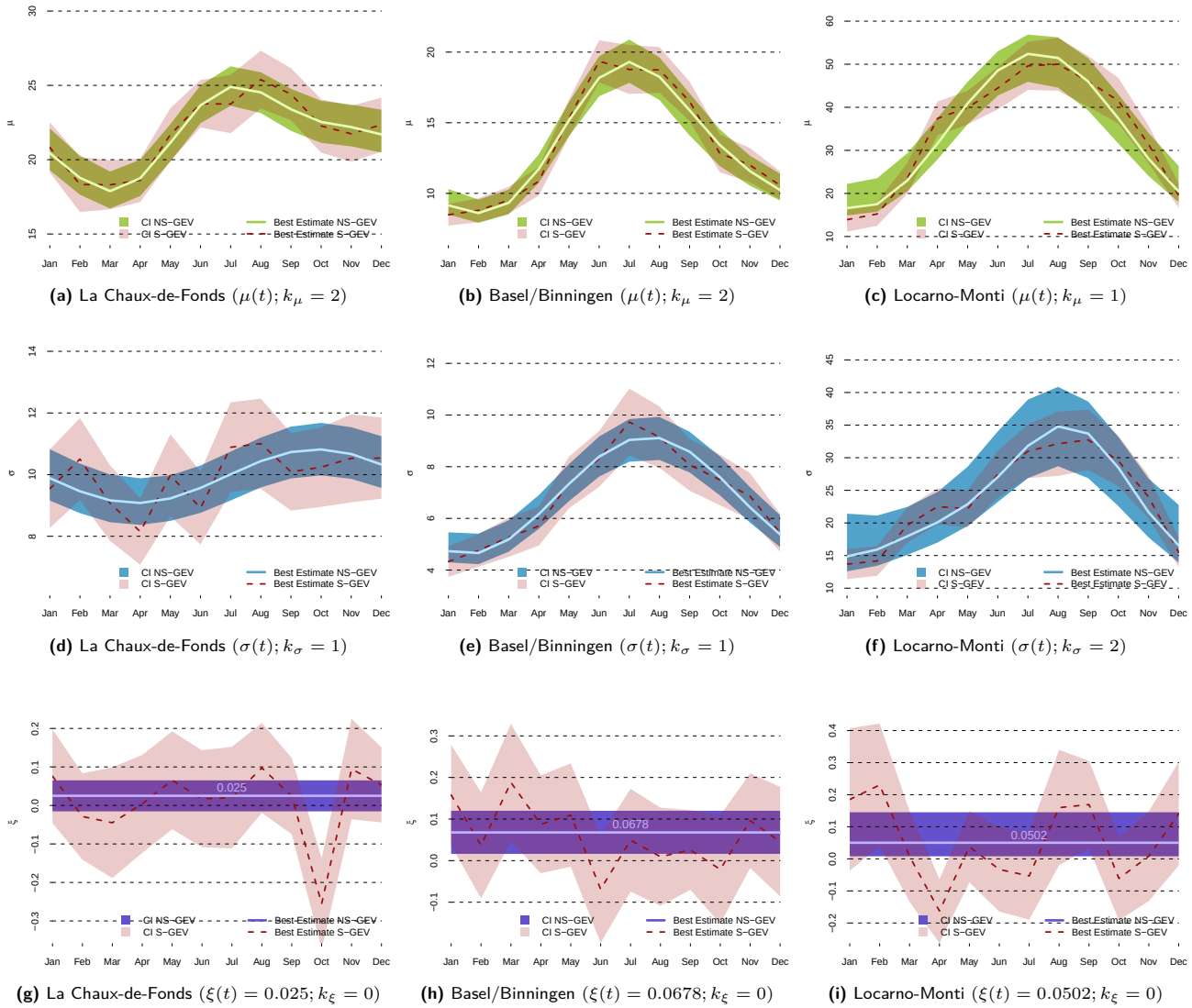

(a) La Chaux-de-Fonds $(\mu(t); k_\mu = 2)$ **(b)** Basel/Binningen $(\mu(t); k_\mu = 2)$ **(c)** Locarno-Monti $(\mu(t); k_\mu = 1)$

(d) La Chaux-de-Fonds $(\sigma(t); k_\sigma = 1)$ **(e)** Basel/Binningen $(\sigma(t); k_\sigma = 1)$ **(f)** Locarno-Monti $(\sigma(t); k_\sigma = 2)$

(g) La Chaux-de-Fonds $(\xi(t) = 0.025; k_\xi = 0)$ **(h)** Basel/Binningen $(\xi(t) = 0.0678; k_\xi = 0)$ **(i)** Locarno-Monti $(\xi(t) = 0.0502; k_\xi = 0)$

Fig. 4.1: Time dependent, i. e. NS-GEV parameters estimated with the 'best' model, and estimated independently for each month according to the monthly S-GEV (red) at stations La Chaux-de-Fonds, Basel/Binningen, and Locarno-Monti. The coloured areas mark the confidence intervals, the lines the best estimates.
The top panels show the location parameters, the middle panels the scale parameters, and the bottom panels the shape parameters. Here, the constant value for ξ is noted above the best estimate's line. Note: The y-axis is scaled differently for each station, whereas the x-axis always shows the month of the year from January to December.

Location parameter $\mu(t)$

Figures 4.1a to 4.1c show that, except for January, February, and April at Locarno-Monti, the seasonal best estimates are well within the monthly confidence intervals. Also the monthly best estimates are within the seasonal confidence intervals, except for the aforementioned months at Locarno-Monti. Due to the Fourier representation of the seasonal cycle in the GEV parameters, the seasonal curve is very smooth. Both the monthly and the seasonal confidence intervals are approximately of the same size.

Scale parameter $\sigma(t)$

Without exception, the seasonal best estimates of the scale parameter (blue line) are within the confidence intervals of the monthly S-GEV. The best estimates of the monthly S-GEV, on the other hand, are, on rare occasions, outside the seasonal confidence intervals (blue areas).

The smoothing of $\sigma(t)$ due to the seasonal analysis is most pronounced at station La Chaux-de-Fonds, where the monthly curve fluctuates strongly. The seasonal confidence intervals at La Chaux-de-Fonds and Basel/Binningen are a few percents smaller than the monthly ones. At Locarno-Monti, on the contrary, the seasonal confidence interval is up to two times larger than the monthly one. This is a surprising result for which, to date, we have no explanation. Note, however, that Locarno-Monti is among the stations in the southeastern part of Switzerland at which a model with a sophisticated seasonal dependence of the scale parameter was selected.

Shape parameter $\xi(t)$

The monthly curves are erratic with distinct extremes, e. g. for October in La Chaux-de-Fonds. In the case of Basel/Binningen, the values jump up and down and the the curve's slope changes sign each month. The shape does not show any kind of distinct seasonal cycle. This supports our decision not to vary the shape parameter (s. Section 3.4.4).

The seasonal shape parameter—which we have kept constant—is generally not entirely within the confidence intervals of the monthly analysis, except perhaps for Basel/Binningen. The monthly best estimates are often outside the seasonal's confidence intervals. The latter, on the other hand, are mostly within the monthly confidence intervals.

A further property of the NS-GEV confidence intervals is that they are much narrower than the monthly ones. Their size is around one third to one half.

Summarising, we can state that the selected models produce reasonable values for $\mu(t)$ and $\sigma(t)$. On the other hand, the shape parameter as computed with the monthly S-GEV is more difficult to model since its monthly values seem to be random. However, the modelling of non-stationarities in μ and σ while keeping ξ constant decreases the confidence intervals for the shape parameter in relation to the monthly S-GEV.

4.2 Return Levels of Extreme Precipitation Events

4.2.1 Estimate of Yearly Return Levels

A novel aspect of this study compared to Buishand and Demaré (1990) is to derive the yearly return levels from the explicitly modeled seasonal NS-GEV (s. Section 3.6), rather than from the smoothed monthly stationary GEV estimates. The additional information of the monthly maxima is expected to improve the yearly return level estimates, especially in terms of their associated uncertainties. Here, we compare the derived estimates with those of the yearly S-GEV.

The three figures in Fig. 4.3 compare the best estimates and their confidence intervals[2] between the yearly S-GEV (red colours) and those computed on the basis of the seasonal analysis (green colours). Observed yearly maxima (blue dots) are shown as well. The return levels for 10, 30, 100 and 300 years and their respective confidence interval can be found and compared in Tab. 4.2.

[2] As mentioned in Section 3.6, paragraph *Newton's Method* (p. 16) the CIs are a little too small for RPs larger than 100 years at stations with a pronounced seasonal cycle, since in up to 3 ‰ of the parametric resamples Newton's Method fails to yield a return level.

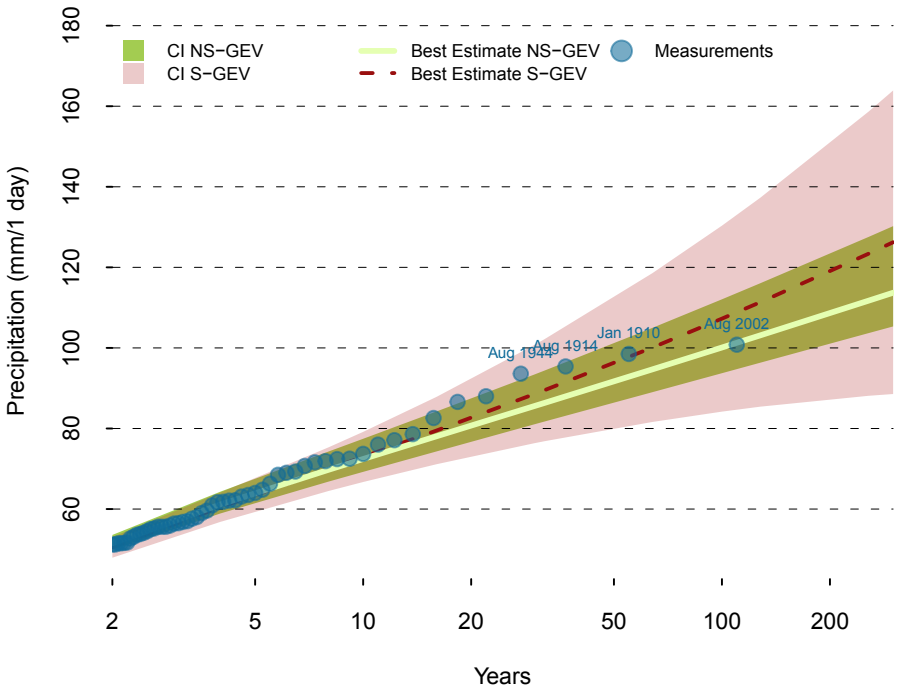

(a) La Chaux-de-Fonds

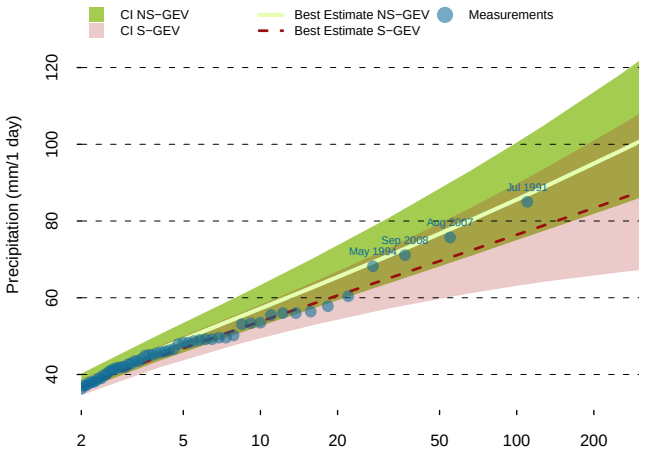

(b) Basel/Binningen

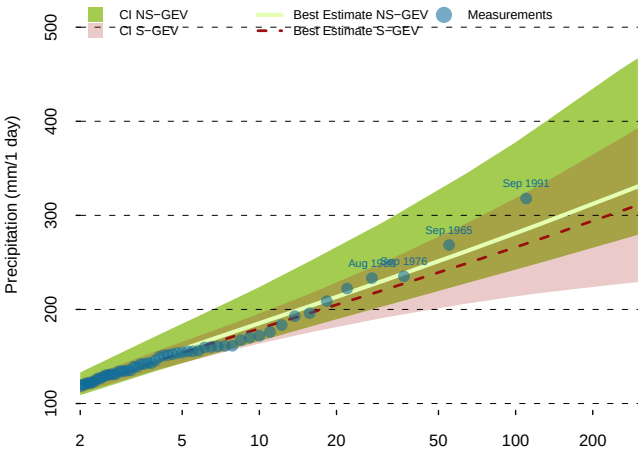

(c) Locarno-Monti

Fig. 4.3: Return levels of the yearly S-GEV (red) and the NS-GEV (green) model for the stations La Chaux-de-Fonds (a), Basel/Binningen (b) and Locarno-Monti (c). The areas mark the confidence interval's spread, the lines the best estimates. Blue dots indicate the heaviest yearly precipitation events observed.

The best estimate of the seasonal NS-GEV differs from the yearly S-GEV, but is generally within the confidence intervals of the yearly S-GEV, and therefore essentially compatible with previous results. At La Chaux-de-Fonds, the seasonal NS-GEV results in slightly higher return periods, while it leads to lower return periods at Basel/Binningen and Locarno-Monti.

The additionally introduced precipitation data leads to clearly smaller confidence intervals at stations La Chaux-de-Fonds and Basel/Binningen, especially for large return periods. Locarno-Monti behaves differently, as could be expected from the confidence intervals of its scale parameter (s. Fig. 4.1f).

A closer look at each station reveals some differences:

La Chaux-de-Fonds

According to the values obtained from the seasonal NS-GEV analysis, the August 2002 event is no longer

Tab. 4.2: Estimated return levels for return periods of 10, 30, 100 and 300 years and their 95 % confidence intervals for the yearly analysis (S-GEV) and the seasonal analysis (NS-GEV) at stations La Chaux-de-Fonds, Basel/Binningen, and Locarno-Monti. The difference between the stationary and the non-stationary GEV is denoted Δ. The 'spread' shows the confidence interval's size for a given return period.

Return period		**La Chaux-de-Fonds**			**Basel/Binningen**			**Locarno-Monti**		
		old	new	Δ	old	new	Δ	old	new	Δ
10 years	2.5 %	67 mm	69 mm		49 mm	53 mm		163 mm	166 mm	
	$\widehat{\mathrm{E}}$	73 mm	72 mm	$-1\,\%$	54 mm	57 mm	$+6\,\%$	180 mm	185 mm	$+3\,\%$
	97.5 %	79 mm	77 mm		58 mm	63 mm		196 mm	224 mm	
	spread	12 mm	8 mm	$-33\,\%$	9 mm	10 mm	$+11\,\%$	33 mm	58 mm	$+76\,\%$
30 years	2.5 %	76 mm	81 mm		57 mm	63 mm		191 mm	203 mm	
	$\widehat{\mathrm{E}}$	89 mm	86 mm	$-3\,\%$	65 mm	70 mm	$+8\,\%$	220 mm	230 mm	$+5\,\%$
	97.5 %	101 mm	93 mm		72 mm	80 mm		249 mm	292 mm	
	spread	25 mm	12 mm	$-52\,\%$	15 mm	17 mm	$+13\,\%$	58 mm	89 mm	$+53\,\%$
100 years	2.5 %	84 mm	94 mm		63 mm	75 mm		214 mm	242 mm	
	$\widehat{\mathrm{E}}$	107 mm	100 mm	$-7\,\%$	76 mm	86 mm	$+13\,\%$	266 mm	281 mm	$+6\,\%$
	97.5 %	130 mm	112 mm		90 mm	100 mm		318 mm	378 mm	
	spread	46 mm	18 mm	$-61\,\%$	27 mm	25 mm	$-7\,\%$	104 mm	136 mm	$+31\,\%$
300 years	2.5 %	89 mm	106 mm		67 mm	86 mm		229 mm	279 mm	
	$\widehat{\mathrm{E}}$	126 mm	114 mm	$-10\,\%$	88 mm	101 mm	$+15\,\%$	311 mm	331 mm	$+6\,\%$
	97.5 %	167 mm	130 mm		108 mm	119 mm		393 mm	467 mm	
	spread	78 mm	24 mm	$-65\,\%$	41 mm	33 mm	$-20\,\%$	164 mm	188 mm	$+14\,\%$

expected to occur on average every 68 years, its return period increased to 108 years (s. Fig. 4.3a).

The most apparent change at station La Chaux-de-Fonds is the amount by which the time dependent GEV's confidence interval is smaller, compared to the one from the yearly S-GEV (s. Fig. 4.3a). For a return period of 10 years it is approximately one third smaller, for a return period of 300 years the difference has increased to two thirds.

Basel/Binningen

The additional monthly data of the seasonal analysis drastically reduces the return period of the heavy precipitation events. The August 2007 event, for instance, is no longer expected to occur on average every 93 years, but every 46 years. This amounts to a change of no less than 50 %. (s. Fig. 4.3b).

Even though the Non-Stationary GEV's confidence interval is 11 % larger for a return period of 10 years the uncertainty about the best estimates increases much more slowly than the confidence intervals calculated with the yearly S-GEV. At a return period of 300 years

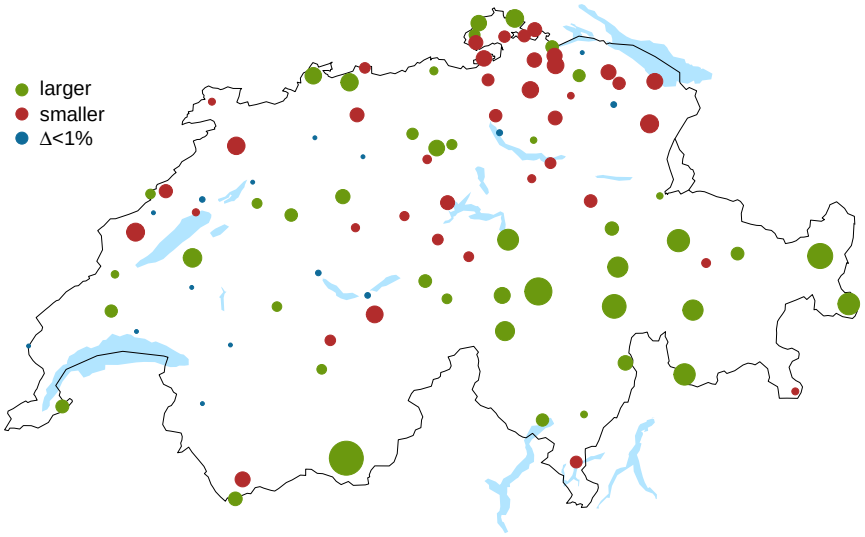

Fig. 4.4: Difference in return levels between the best estimates of yearly S-GEV and the ones obtained from the Non-Stationary GEV. Green bullets indicate smaller return levels with the S-GEV, red bullets larger ones. At stations with a blue bullet the difference in return levels is less than 1 %. The bullet's size grows with larger differences.

the NS-GEV return level's confidence interval is 20 % smaller but encompasses higher return levels for a given return period.

Locarno-Monti

At Locarno-Monti, the best estimate of the NS-GEV is closer to the stationary one. The return periods have become smaller. This means that the new estimate expects heavy precipitation events to be more frequent than previously estimated. The event of September 1965, for instance, has, when relying on the seasonal NS-GEV, to be expected once in 75 years instead of once in 106 years, as suggested by the yearly S-GEV.

Contrary to the results for La Chaux-de-Fonds, at Locarno-Monti the confidence intervals of the Non-Stationary GEV are larger than the ones calculated with the yearly S-GEV (s. Fig. 4.3c).

For a return period of 10 years the confidence interval is almost twice as large. With larger return periods, the difference becomes smaller but is still about 14 % larger for a return period of 300 years. The Non-Stationary GEV's confidence intervals tend to encompass larger return levels for a given return period. This becomes more prominent the higher the return periods.

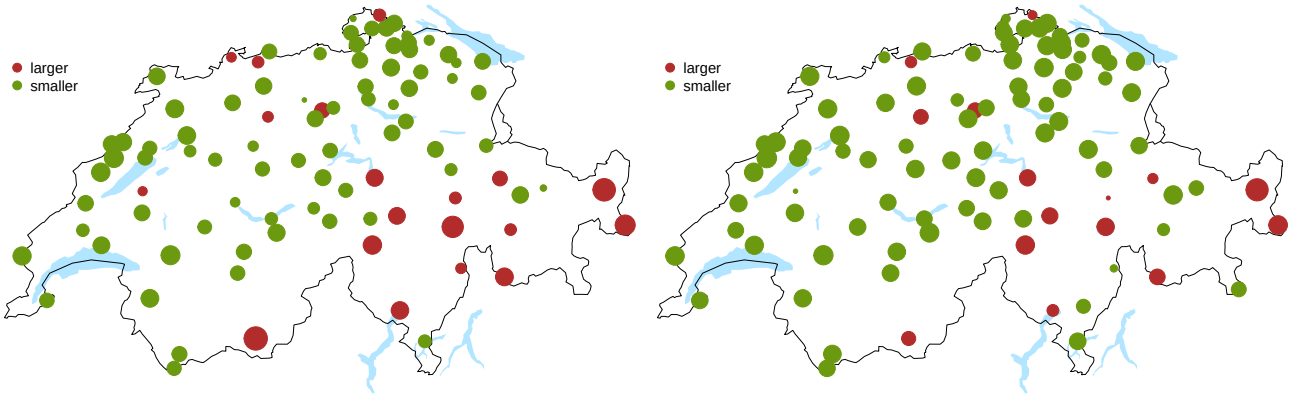

(a) CI: Difference for a RP of 10 years

(b) CI: Difference for a RP of 300 years

Fig. 4.5: Difference of the CI's width between the yearly S-GEV and NS-GEV, evaluated for return periods of 10 years (a) and of 300 years (b). Bullets are green if yearly S-GEV confidence intervals are smaller, otherwise red. The bullets' size is related to the relative difference. The larger the difference the larger the bullet.

Summary

The results presented in Fig. 4.3 and Tab. 4.2 show quite a spectrum of different outcomes. The best estimates of yearly return levels derived from the seasonal NS-GEV are generally within the confidence intervals of the yearly S-GEV estimates, and are therefore compatible with previous results. In most cases the increase in the amount of data entering the estimation has reduced the size of the confidence intervals, or at least how fast they increase with the return period. There are exceptions, such as Locarno-Monti, where we have already seen that the confidence intervals for the NS-GEVparameters are larger.

If we relate best estimates of the seasonal analysis to best estimates of the yearly S-GEV and compare return levels of a 100 year event, we find that half of the stations' best estimate is smaller when using a Non-Stationary GEV, the remaining stations obtain larger best estimates. Almost at every 6th station the difference of return level is smaller than 1 %.

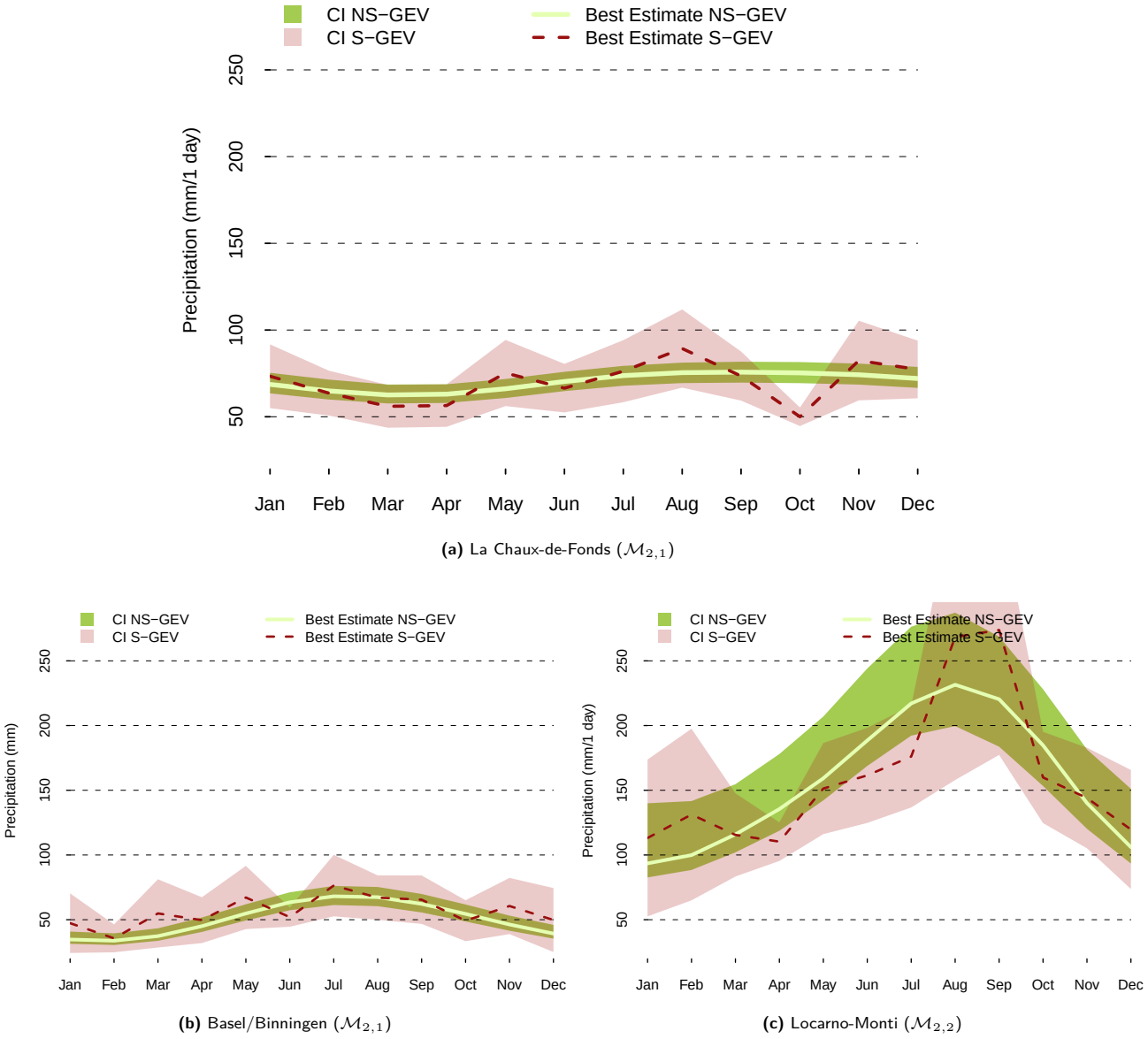

(a) La Chaux-de-Fonds ($\mathcal{M}_{2,1}$)

(b) Basel/Binningen ($\mathcal{M}_{2,1}$)

(c) Locarno-Monti ($\mathcal{M}_{2,2}$)

Fig. 4.6: Return levels for a monthly return period of 100 years. The seasonal values, modeled with the 'best' model, are shown with green colours, the independently estimated (S-GEV) in red. The coloured areas mark the confidence intervals, the lines the best estimates.

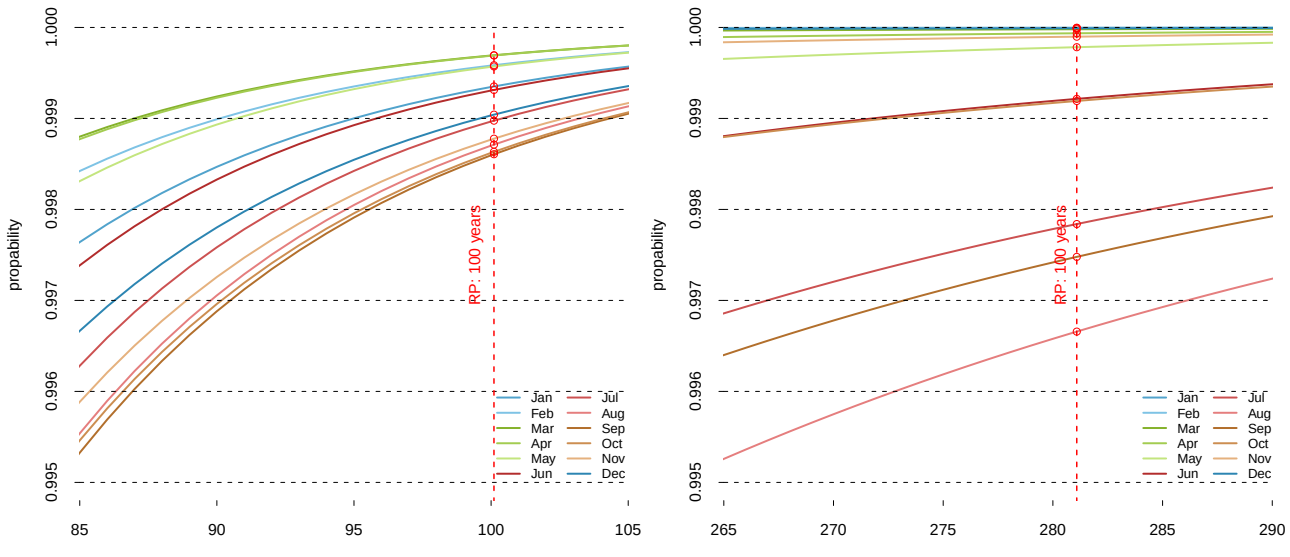

(a) La Chaux-de-Fonds **(b)** Locarno-Monti

Fig. 4.7: Cumulative density functions for each month at La Chaux-de-Fonds (a) and Locarno-Monti (b) for the highest daily precipitation amount, zoomed on the highest quantiles. Additionally the best estimate of the return level for a 100 year event is marked with the dashed vertical line. Its intersection with each CDF is marked with red circles. Be aware that the x-axis is differently scaled for each plot.

When looking at spatial patterns regional differences emerge (s. Fig. 4.4). In Northeastern Switzerland using a Non-Stationary GEV in the majority of cases leads to reduced return levels for a 100 year event. In other words, heavy precipitation is less frequent than previously estimated. In contrast, the obtained return levels in Southern and Southeastern Switzerland are often larger compared to the ones from the yearly S-GEV: heavy precipitation is more frequent than previously estimated.

At the majority of stations, the uncertainty in the estimates has been reduced, the more so for higher return periods (compare 4.5a and 4.5b). However for stations with a distinct seasonal cycle the improvements are small or none at all. Often the latter stations are the same as the stations where the NS-GEV estimates resulted in a clear increase in return levels.

4.2.2 Estimate of Monthly Return Levels

Since we use data on a monthly basis and since we also model the seasonal cycle, we are able to estimate return levels for a specific month, e. g. January, only. Again we use the monthly S-GEV to validate the results from the seasonal analysis.

For this validation we calculated the monthly return levels for a monthly return period of 100 years, as well as their respective confidence intervals. The results are shown in Fig. 4.6.

The use of a monthly S-GEV leads to rather noisy curves without a 'regular' seasonal cycle. Their evolution generally reflects that of the shape parameter (s. Fig. 4.1), modulated by the variation in location and scale. The confidence intervals are large where ξ is large. We find extreme outliers e. g. the values for October at La Chaux-de-Fonds. Even so, the time dependent GEV confidence intervals (green areas) lie mostly within the ones obtained with the monthly S-GEV (red areas), but are much smaller, except for Locarno-Monti. Section E in the Appendix illustrates that there is no other exception.

In general, the seasonal evolution appears well captured. On average, in one half of the months the best estimates derived from the seasonal analysis lie below the best estimates of the monthly S-GEV, in the other half, above.

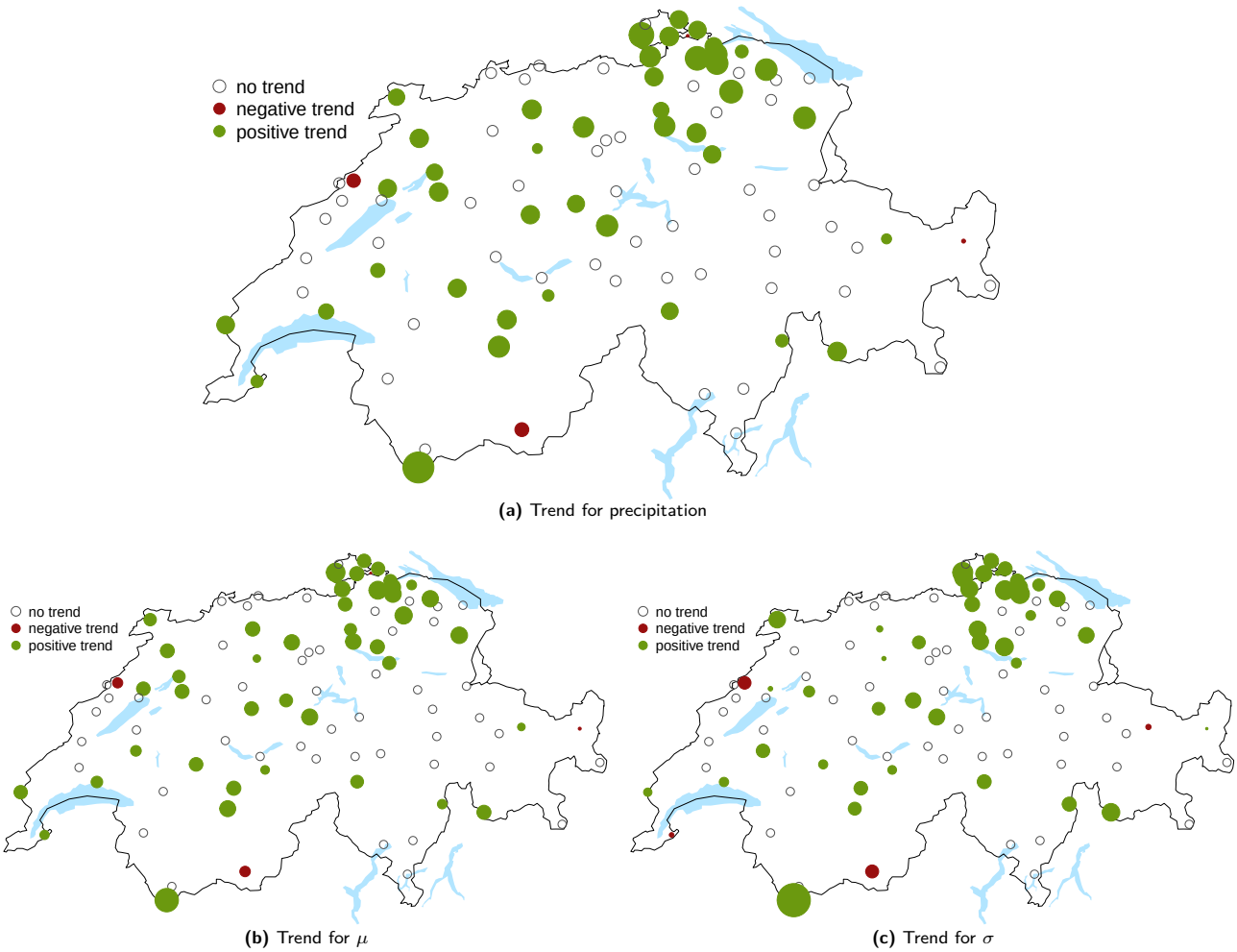

(a) Trend for precipitation

(b) Trend for μ

(c) Trend for σ

Fig. 4.8: The top map (a) shows the trend for the 100 year return levels, the left map (b) shows the trends for the location parameter and map (c) the trends for the scale parameter. Bullets (circles) show where a (no) significant linear trends in extreme precipitation events has been found. Green (red) colours are used for positive (negative) trends. The larger the bullet, the larger the trend.

We also can use the monthly CDFs to investigate how often a y year event falls, on average and not considering any uncertainty, into a particular month. For instance at La Chaux-de-Fonds (s. Fig. 4.7a) it is least (most) likely that the 100 year event falls in March (September). There, a 100 year event happens on average only every 3,275 (718) years. Therefore the probability for a 100 year event differs amongst the months only by a factor of 4.6.

At Basel/Binningen (s. Fig. 3.4b) the probabilities already differ by a factor of 169: A 100 year event is likely to happen in February (July) only every 64,901 (385) years.

The largest differences can be expected at Locarno-Monti (s. Fig. 4.7b), since its seasonality is most pronounced. The numbers verify this assumption: A 100 year event is 1114 times more likely to happen in August (299_{aug} year event) than in January ($333{,}210_{\text{jan}}$ year event).

4.2.3 Estimate of Long-Term Trends

In the present study, it is not our purpose to perform a systematic study of long-term non-stationarities. Since we consider data over more than hundred years, however, we are interested in the relevance of such a non-stationarity on our results.

Model selection, performed as before, picks in 47 cases (48 %) a linear trend. In the following, we will consider the trend as significant if the log-likelihood ratio test sig-

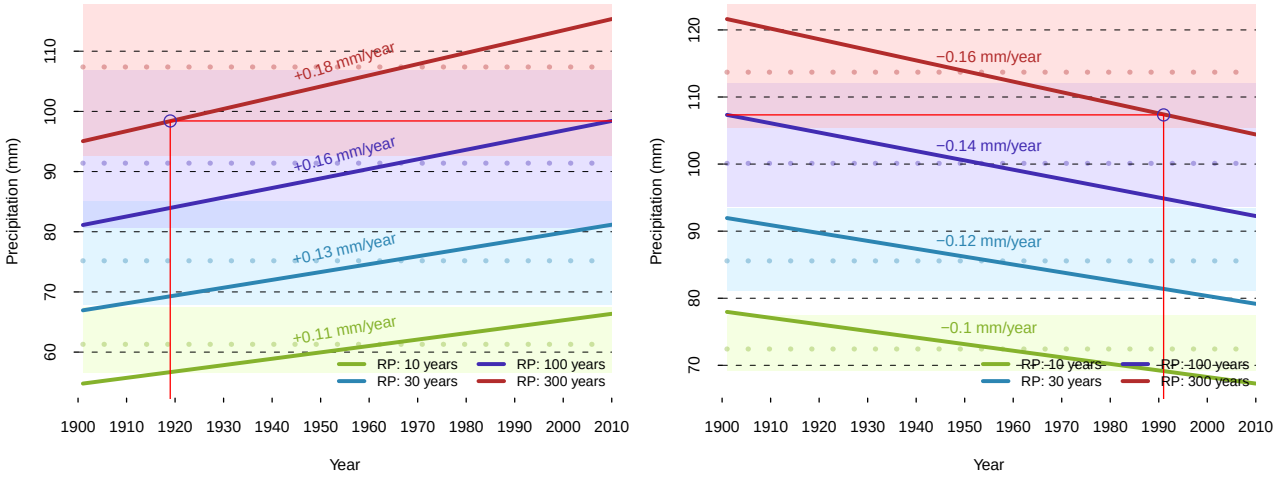

(a) Schaffhausen **(b)** La Chaux-de-Fonds

Fig. 4.9: The changing return levels for return periods of 10, 30, 100 and 300 years are drawn here with solid lines for stations Schaffhausen (a) and La Chaux-de-Fonds (b). The return levels without linear trend are indicated with dotted lines, and their confidence intervals with coloured surfaces. The blue circles show in which year the maximum 100 year return levels corresponded to a 300 year return level.

nalled better representation of the data when including dependence on the year. This means that significance is associated to the station, and not to the amount by which the return levels, for instance, may have increased or decreased. We show in Fig. 4.8a the stations at which we find a significant linear trend for a 100 year return level. In all but three cases the trend is positive (green colours). The trends for the 100 year return levels range from $-16\,\%$ to $+92\,\%$ of precipitation within one day if we compare 2010 with 1901.

Apparently we more often see a significant trend in northern parts of Switzerland, especially close to the canton Schaffhausen. The only station with a large trend in Southern Switzerland is Col du Grand St-Bernard. This particular result has to be treated carefully since the precipitation data for Col du Grand St-Bernard is known to be erroneous (Zbinden, P., MeteoSwiss, personal communication).

It is interesting to compare this result with the trend seen in the NS-GEV parameters (s. Fig. 4.8). Often the relative trends in shape and scale are of similar size. At this point, we must attract attention to the fact that the linear dependence was simply added to the existing seasonal dependence in μ or σ. Therefore, the trend in σ on Fig. 4.8c cannot be regarded as independent of that in μ (s. Fig. 4.8b).

Translating the trends into return levels gives an alternative view how measurable a trend is. For Schaffhausen (s. Fig. 4.9a), we see an increase in return levels of more than 10 mm per decade, even for a 10 year event. A precipitation event which in 1919 was considered to be a 300 year event in 2010 is three times more likely: it is now a 100 year event. Note that they remain within the confidence intervals of the stationary (with respect to the year, not to the seasons) estimate. Recall that significance is associated here to the model selection at each station, and not to the amount by which the return levels may have changed.

La Chaux-de-Fonds is one of very few stations with a significant negative trend (s. Fig. 4.9b). Here, what was considered a 100 year event in 1901 became in 1993 a 300 year event. At Basel/Binningen and Locarno-Monti, the trend was not significant. This means that the selected model does not contain a long-term trend term, an no trend could be calculated.

Note that these trends should be interpreted with caution, since the data used is not homogenised, and we do not have any idea about the models uncertainties. Nevertheless, they would justify further enquiry.

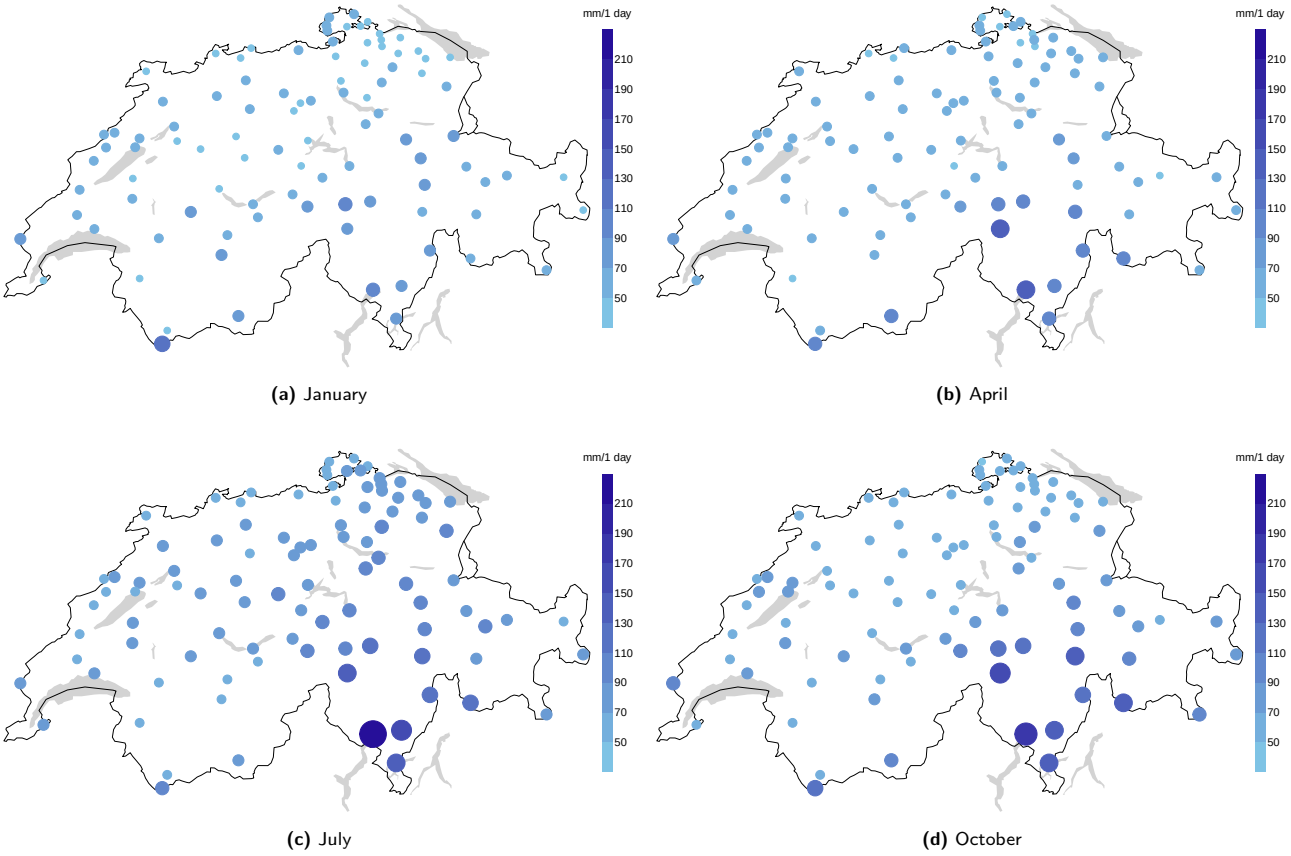

(a) January **(b)** April

(c) July **(d)** October

Fig. 4.10: Best estimates of return levels for monthly 100 year events in January (a), April (b), July (c), and October (d). The colours indicate the precipitation amount within 1 day in mm. The size of the dots is proportional to the return level. The figures for all months can be found in the Appendix, Section F.1

4.3 Spatial Distribution of Extremes

Results yielded with the monthly NS-GEV allow us, for instance, to look month by month for spatial patterns in extreme precipitation.

4.3.1 Return Levels

In Fig. 4.10 we investigate the spatial and seasonal distribution of extremes. On display are the best estimates of a monthly 100 year event in the middle month of each season, estimated for each station independently. In general, higher return levels can be found in the Central Alps and the Ticino, while the Rhone Valley remains rather dry all year round. It appears that in January (s. Fig. 4.10a), higher return levels have to be expected at stations located further south, except in Graubünden where the values are comparable to the ones in the Central Plateau.

In April (s. Fig. 4.10b) the daily values are mostly 10 to 20 mm higher. The largest difference can be found in Airolo, where a one day 100_{apr} year event is 57 mm larger than a 100_{jan} year event.

The increase in return levels from April to July (s. Fig. 4.10c) are in general similar in magnitude to those between January and April. The largest change by far can now be observed at Locarno-Monti: +82 mm.

Large parts of the Central Plateau have (s. Fig. 4.10d) similar values in October as in April. In Graubünden the values remained more or less constant.

Generally, the largest change happens from the middle of autumn to winter. Almost every station's 24 hours value drops, at Locarno-Monti by more than 90 mm.

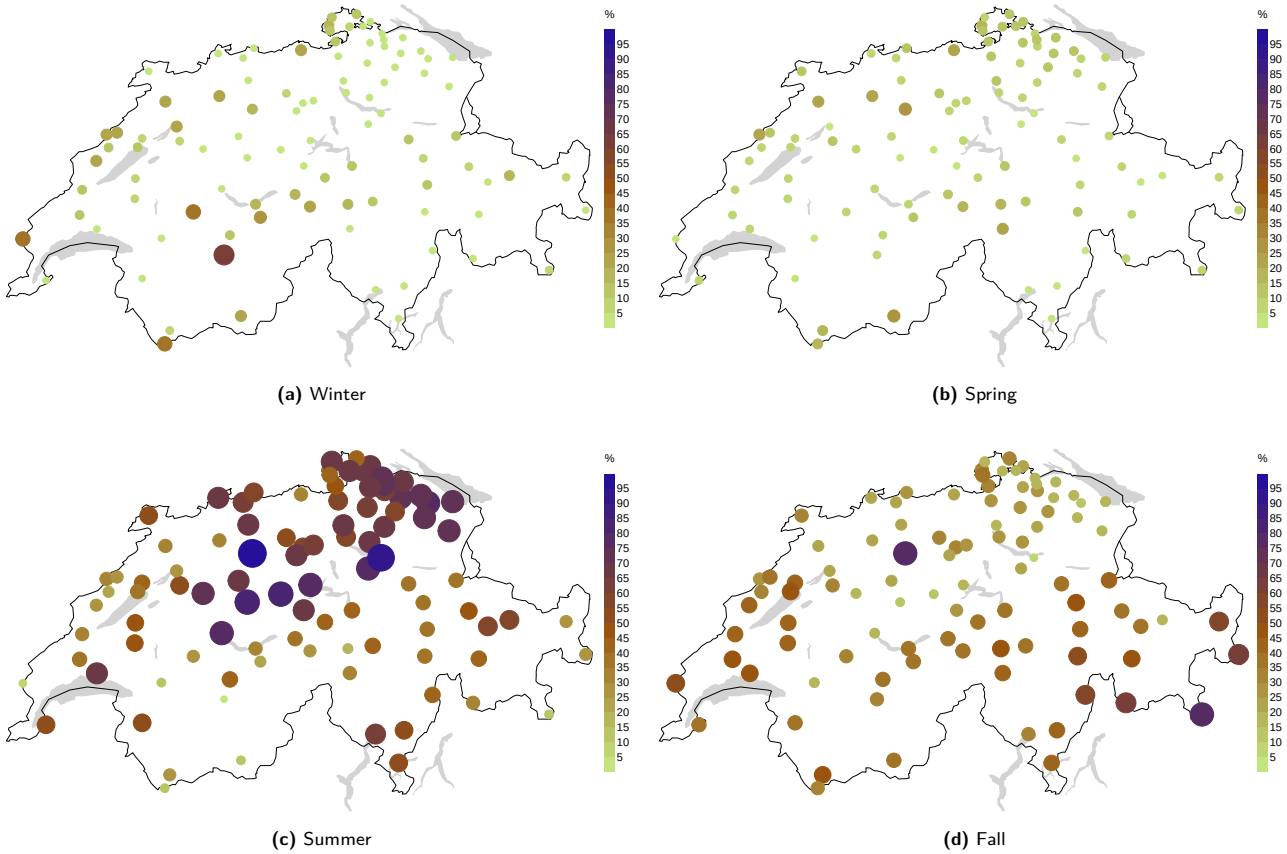

(a) Winter **(b)** Spring

(c) Summer **(d)** Fall

Fig. 4.11: Probability for a 100 year event to fall into a particular season in Winter (a), Spring (b), Summer (d), and Fall (c). The sum for each season's months are shown. The colours indicate the probability $p \in [0, 1]$. The size of the dots is proportional to the probability. Similar figures for all months can be found in the Appendix, Section F.2

4.3.2 Probabilities

Further insight in the climate of extreme precipitation can be obtained with the spatial analysis of the probability for a given event to occur in a certain month (s. Section F.2 in the Appendix) or season. The event chosen here is a yearly 100 year event, which, of course, differs from station to station. In Fig. 4.11 these values are plotted for all four seasons.

In Winter (s. Fig. 4.11a), the chance for the occurrence of a 100 year precipitation event is generally very low (on average: 8.6 %). For 51 stations it is below 5 % and for 20 of them even below 1 %. It is least likely to happen in Lachen ($p \approx 0.09\,\%$) and most likely in Leukerbad ($p \approx 61\,\%$).

In Spring (s. Fig. 4.11b), the picture is similar, but the probabilities are more uniformly distributed over Switzerland ($p_{\text{min}} = 1.4\,\%,\ p_{\text{max}} = 26\,\%$). On average, an event with a yearly return period of 100 years happens with a probability of 9.5 % in Spring.

In Summer (s. Fig. 4.11c), a spatial pattern comes to light. There are now only very few stations with small probabilities for the occurrence of a yearly 100 year event. On average, the chance is 51 % ($p_{\text{min}} = 2.4\,\%,\ p_{\text{max}} = 92\,\%$). Most stations with the highest probabilities are located in the northeastern part of Switzerland.

In Fall (s. Fig. 4.11d), compared to July, the chance of a yearly 100 year event is reduced to approximately one third ($p = 32\,\%$). The regional differences are now mostly smaller ($p_{\text{min}} = 7\,\%,\ p_{\text{max}} = 76\,\%$). The largest chances can be observed again in Southern Switzerland.

We can summarise as follows: especially in Winter and Spring, the annual extreme precipitation events occur only rarely, in all of Switzerland. No distinct spatial patterns can be observed. In summer and fall it seems

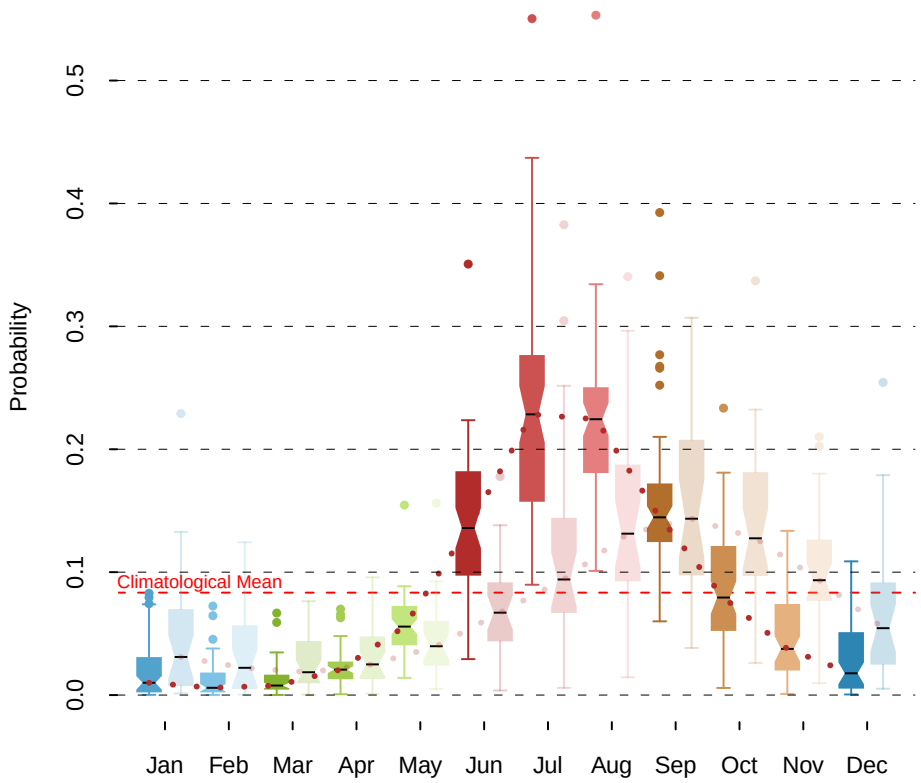

Fig. 4.12: Distribution for the probabilities of the occurrence of a 100 year event within the months of a year, separated in stations below (strong colours, first column each month) and above (pale colours, second column each month) 800 m a. s. l.The dotted lines connect each month's median, the horizontal dashed red line shows the probability in case of absent seasonality

that it might be worthwhile to investigate thoroughly whether the northeastern part of Northern Switzerland behaves differently from the rest of the country.

Taking into account all four seasons at once, it appears that stations in the Swiss Alps have a less pronounced seasonal cycle then the rest of Switzerland.

This can be shown with a boxplot (s. Fig. 4.12) of each month's probabilities, stratified by the stations' altitude. As a threshold we use a height of 800 m a. s. l.This threshold is motivated by the wish to have at least 30 stations in either group.

The monthly boxplots with the strong colours (the first column each month) show the distribution for the 66 stations situated below the threshold. We find, on average, very small values for winter and spring and rather high values for July and August. The seasonal cycle is pronounced.

The boxplot for the stations above 800 m a. s. l. (pale colours, second plots each month) show a slightly different behaviour. The smallest values also can be found in winter and especially in spring, the largest values in August, September, and October. The seasonal cycle is smoother for stations above 800 m a. s. l.

The boxplots also suggest that the phase of the seasonal cycle is shifted by about two months, such that extreme precipitation events at high altitudes have to be expected later in the year.

4.4 Summary of Results

As it turns out, modelling seasonal non-stationarities in extreme precipitation yields three major results:

It leads to a more plausible representation of the seasonal cycle in the return levels, and generally results in smaller confidence intervals than with the monthly S-GEV.

This is also true for yearly return levels derived from the seasonal NS-GEV. Except for Southern Switzerland we

obtain smaller confidence intervals. The new values for the yearly return levels have an impact on the expected frequency of heavy precipitation at most stations, even though, on average, the change is almost zero.

In addition, we find some evidence that long-term trends should be taken into account, since at almost half of the stations under consideration, we can see a (mostly upward) linear trend for return levels.

5 Discussion

In this section, we focus on effects due to the enhanced data sets. Then we examine how model selection affects the estimates of the generalised extreme value (GEV) parameters and the corresponding return levels, both on a monthly and a yearly basis. Due to their operational importance, the yearly return levels are examined once again in terms of their added value.

5.1 Impact of improved Database

So far, only the yearly maximum was used to estimate return levels, neglecting other extreme events of the same year. Thus we retrieve in total 110 events from the years 1901 to 2010. By introducing a seasonal cycle we gain the possibility to consider extreme events which occurred in an other month than the yearly maximum. This allows us to make use of 1320 events for our estimations.

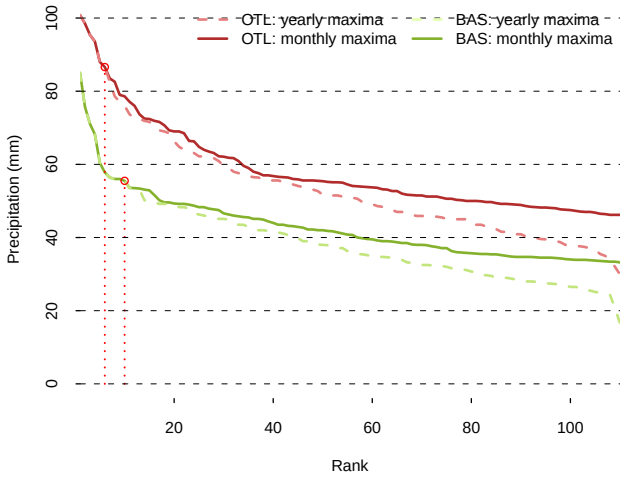

Fig. 5.1: Difference in rank distribution of yearly and monthly maxima at stations Basel/Binningen (green) and Locarno-Monti (red). The dashed lines show all values of the yearly dataset, the solid lines the 110 largest monthly maxima. The vertical red dotted lines mark the point at which both datasets are identical.

In Fig. 5.1 the difference in the ranked distribution between the two data series is illustrated for Basel/Binningen and Locarno-Monti. At Locarno-Monti, the dissimilarities start after the 7^{th} largest precipitation event, at Basel/Binningen after the 10^{th} one. The dashed line shows the 110 measurements of the yearly data, the solid line the 110 largest values of the monthly data.

When calculating on a yearly basis at Locarno-Monti, we miss already the 8^{th} highest precipitation events recorded within 110 years. Since the fitted GEV distribution depends largely on rare but extreme events, this might be an important information loss. At Basel/Binningen the first additional value usable for our new estimations corresponds to the 11^{th} largest precipitation event.

In summary, we can say that in most cases the use of monthly data does not add much information to the uppermost part of the GEV distribution, i. e. the tail of the distribution. On average, the first additional information is introduced with the 16^{th} element.

The monthly maxima yield a lot of additional information about more 'common' extreme events. As we will see below, this influences the best estimate of the yearly return levels derived from the seasonal analysis.

Still, the supplemental data is useless unless we employ a model capable to incorporate it reasonably.

5.2 Impact of Model Selection

We used some effort to devise multiple statistical models and to chose amongst them the most appropriate one for each station (s. Section 3.4). Indeed, as shown in Fig. 4.2, different stations require different models.

Depending on the model, a state of the art personal computer needs half an hour ($\mathcal{M}_{0,0}$) to ten hours ($\mathcal{M}_{2,2}$) to compute return levels and confidence intervals for one station only. This raises the question whether the individual models' results differ substantially or a simple and fast model would be adequate enough for all stations.

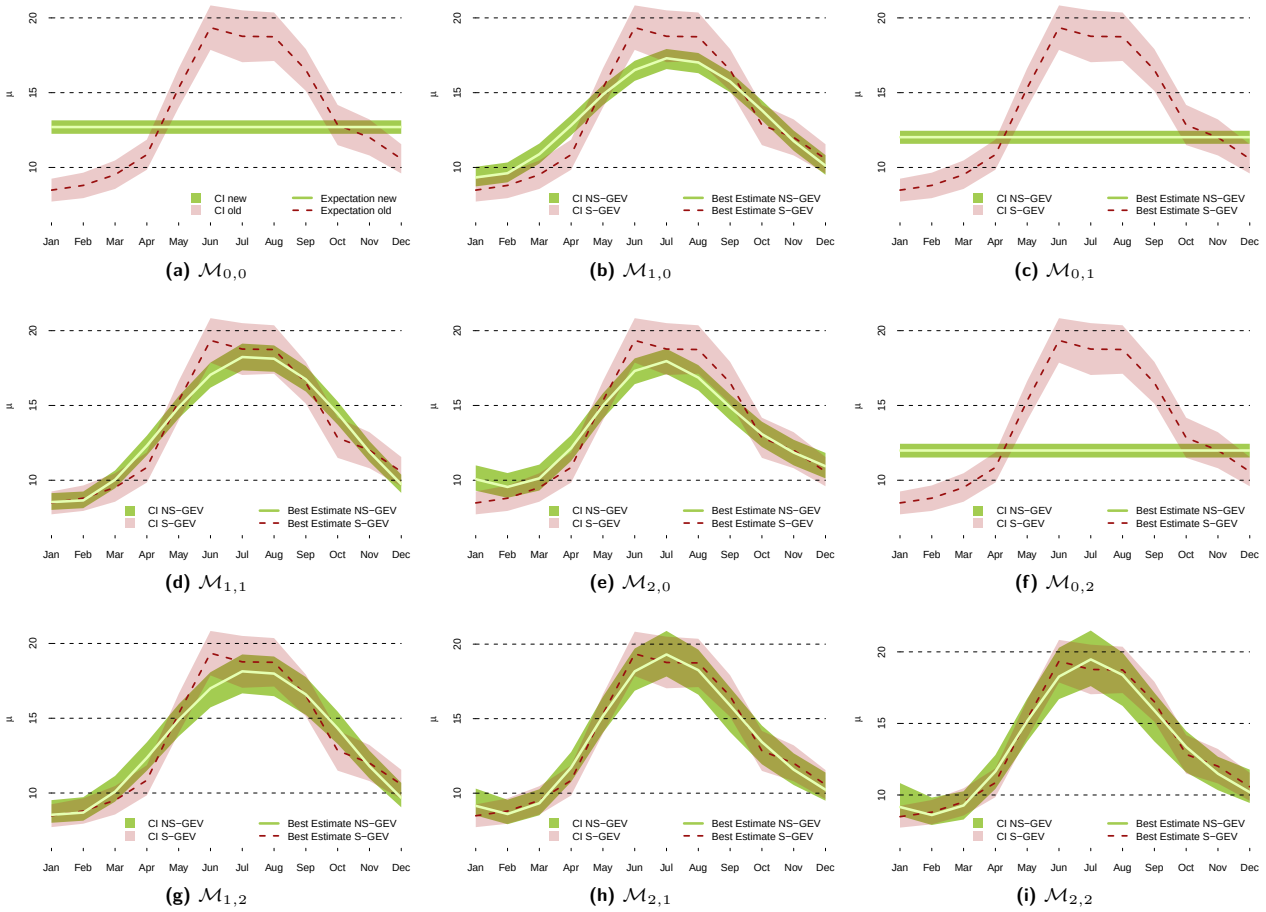

(a) $\mathcal{M}_{0,0}$ **(b)** $\mathcal{M}_{1,0}$ **(c)** $\mathcal{M}_{0,1}$

(d) $\mathcal{M}_{1,1}$ **(e)** $\mathcal{M}_{2,0}$ **(f)** $\mathcal{M}_{0,2}$

(g) $\mathcal{M}_{1,2}$ **(h)** $\mathcal{M}_{2,1}$ **(i)** $\mathcal{M}_{2,2}$

Fig. 5.2: Estimation of the monthly location parameter at station Basel/Binningen with the time-dependent models $\mathcal{M}_{0,0},\ldots,\mathcal{M}_{2,2}$ (green) and the monthly S-GEV (red). Note that the model selected was $\mathcal{M}_{2,1}$.

5.2.1 Parameter Estimation

The best model is the one which estimates the seasonal variability of the parameters μ, σ, and ξ best whilst remaining as simple as possible. We can visualise the first point plotting our estimates of the parameters computed with the time-dependent model with those evaluated with the monthly S-GEV.

The performance of the time-dependent models for the location parameter at Basel/Binningen is shown in Fig. 5.2. It illustrates that only the AIC_c's first and second model choice ($\mathcal{M}_{2,1}$ and $\mathcal{M}_{2,2}$; s. Tab. 4.1) represent the seasonal cycle of $\mu(t)$ in a satisfactory manner.

The corresponding figures for $\sigma(t)$ and $\xi(t)$ are shown in the Appendix (Fig. C.5 and Fig. C.6). Also the same figures for stations La Chaux-de-Fonds and Locarno-Monti, respectively, can be found in Sections C.1.1 and C.1.3.

5.2.2 Return Level Estimation

The influence of model selection can also be seen in the estimates of return levels and their confidence intervals (s. Fig. 5.3). The values presented in Tab. 5.1 illustrate this for Basel/Binningen: with $\mathcal{M}_{2,1}$ one of the more complex models is best (s. Tab. 4.1). The simpler models yield, when compared to the optimal model, poor results for the monthly return levels ($\Delta \in [-18\,\%,\ 41\,\%]$) and confidence intervals ($\Delta \in [-5\,\%,\ 18\,\%]$). Models of similar complexity often have similar and sometimes even nearly identical return levels but are dissimilar in confidence intervals. Altogether, these considerations support the automatic model selection and legitimate the larger computational demand since the differences between models in the monthly analyses are too large

to neglect.

This is not surprising, considering their poor representation of the parameters of the monthly S-GEV (s. Fig. 5.2). On the other hand, the yearly return levels derived from the seasonal analysis differ from those of the best model by rather modest amounts. As expected, the difference is larger for those models that model the seasonal cycle of only one of the two NS-GEV parameters (s. Tab. 3.2), and is surprisingly small for $\mathcal{M}_{1,1}$, no doubt because it is the simplest model that takes into account the seasonal variation of both μ and σ (s. Fig. 5.3d). This holds true at La Chaux-de-Fonds (s. Tab. G.1) and at Locarno-Monti (s. Tab. G.2) as well. The change in the confidence intervals, however, at the latter station is large and the return levels differ by $\Delta \in [-30\,\%,\ 46\,\%]$ for the monthly analyses. At La Chaux-de-Fonds, all models lead to similar results ($\Delta \leqslant |14\,\%|$), except for $\mathcal{M}_{0,0}$ ($\Delta \in [-54\,\%,\ 9\,\%]$). We think these rather small differences are due to the weak seasonal cycle.

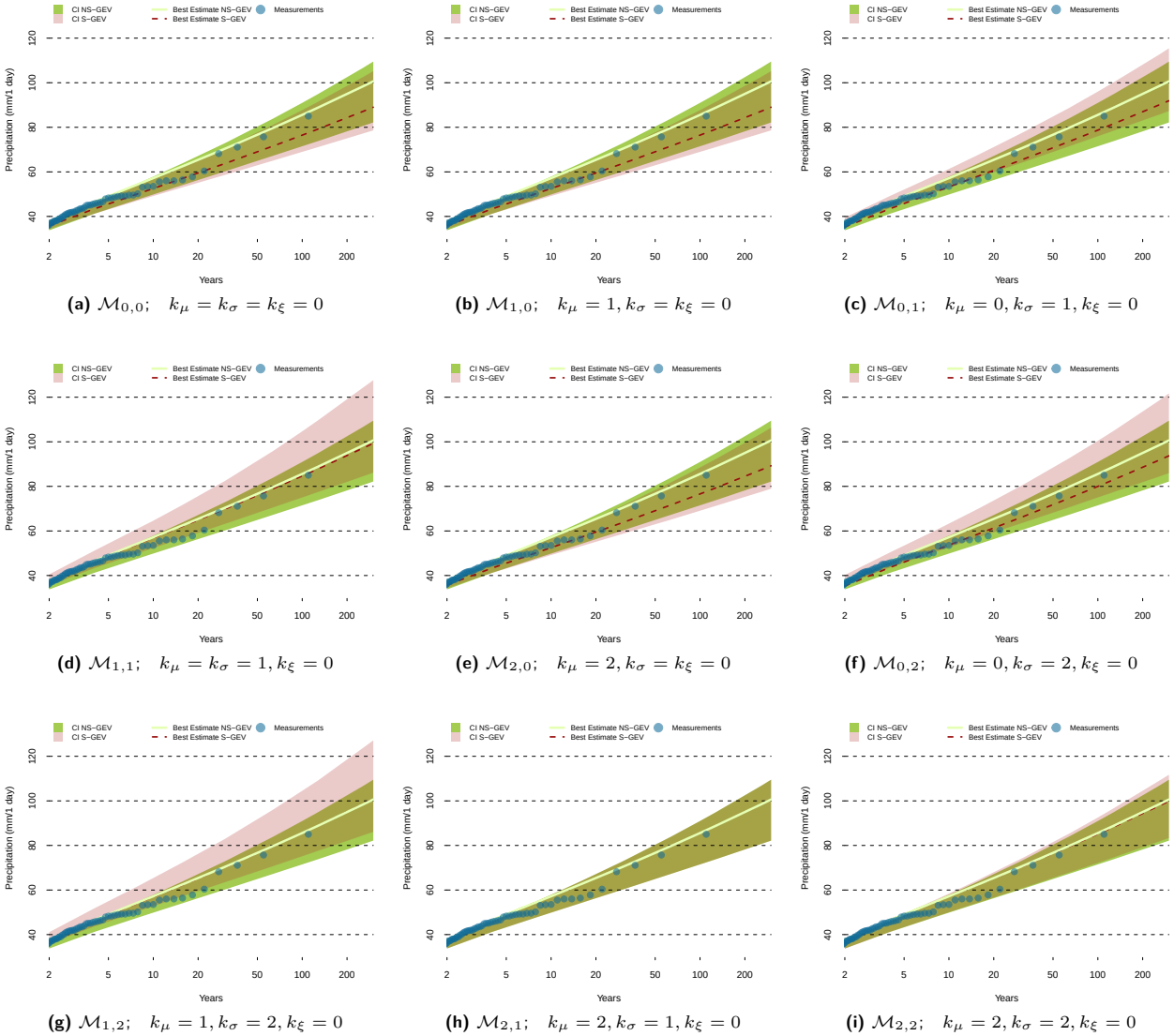

(a) $\mathcal{M}_{0,0}$; $k_\mu = k_\sigma = k_\xi = 0$ **(b)** $\mathcal{M}_{1,0}$; $k_\mu = 1, k_\sigma = k_\xi = 0$ **(c)** $\mathcal{M}_{0,1}$; $k_\mu = 0, k_\sigma = 1, k_\xi = 0$

(d) $\mathcal{M}_{1,1}$; $k_\mu = k_\sigma = 1, k_\xi = 0$ **(e)** $\mathcal{M}_{2,0}$; $k_\mu = 2, k_\sigma = k_\xi = 0$ **(f)** $\mathcal{M}_{0,2}$; $k_\mu = 0, k_\sigma = 2, k_\xi = 0$

(g) $\mathcal{M}_{1,2}$; $k_\mu = 1, k_\sigma = 2, k_\xi = 0$ **(h)** $\mathcal{M}_{2,1}$; $k_\mu = 2, k_\sigma = 1, k_\xi = 0$ **(i)** $\mathcal{M}_{2,2}$; $k_\mu = 2, k_\sigma = 2, k_\xi = 0$

Fig. 5.3: Basel/Binningen: Illustration of the model selection's impact on the yearly return levels and the confidence intervals derived from the time dependent NS-GEV. The green areas and the green line represent the 'best model's' best estimate and confidence interval respectively, the red line and area those for the model noted below the figure. Fig. (h) shows no deviation since it compares two times the 'best model'. The blue dots represent real observations.

Tab. 5.1: The influence of the model selection process on the yearly return levels (RLs) and their confidence intervals (CIs) at Basel/Binningen. The RLs and CIs for the best model are in green colours. The values for the other models are presented in relation to the best model. The first column denotes the model's name, the second indicates whether the results for the return level or the confidence interval are shown. In rows for the CI the first number shows the 2.5 %, the second one the 97.5 % quantile. Columns three to six show the results for return periods of 10, 30, 100 and 300 years and the last two columns show the RL for a 100_{feb} and a 100_{aug} event respectively.

Model		10 years	30 years	100 years	300 years	100_{feb}	100_{aug}
$\mathcal{M}_{0,0}$	RL	3 %	5 %	7 %	10 %	41 %	−18 %
	CI (2.5 %/97.5 %)	8 %/10 %	9 %/12 %	12 %/15 %	14 %/18 %		
$\mathcal{M}_{1,0}$	RL	−9 %	−10 %	−12 %	−13 %	28 %	−24 %
	CI (2.5 %/97.5 %)	−1 %/−2 %	−3 %/−3 %	−4 %/−4 %	−5 %/−4 %		
$\mathcal{M}_{0,1}$	RL	−7 %	−8 %	−9 %	−9 %	22 %	−15 %
	CI (2.5 %/97.5 %)	6 %/6 %	6 %/6 %	6 %/5 %	6 %/5 %		
$\mathcal{M}_{1,1}$	RL	−1 %	−1 %	−1 %	−1 %	0 %	0 %
	CI (2.5 %/97.5 %)	5 %/10 %	5 %/12 %	5 %/13 %	5 %/14 %		
$\mathcal{M}_{2,0}$	RL	−9 %	−10 %	−12 %	−13 %	28 %	−24 %
	CI (2.5 %/97.5 %)	−1 %/−1 %	−3 %/−2 %	−4 %/−3 %	−4 %/−3 %		
$\mathcal{M}_{0,2}$	RL	−7 %	−7 %	−7 %	−7 %	24 %	−8 %
	CI (2.5 %/97.5 %)	5 %/9 %	5 %/9 %	5 %/9 %	4 %/10 %		
$\mathcal{M}_{1,2}$	RL	0 %	0 %	0 %	0 %	1 %	−1 %
	CI (2.5 %/97.5 %)	6 %/11 %	5 %/12 %	5 %/13 %	5 %/14 %		
$\mathcal{M}_{2,1}$	*RL*	*57.2 mm*	*70.3 mm*	*85.6 mm*	*100.6 mm*	*33.8 mm*	*67.4 mm*
	CI (2.5 %/97.5 %)	*50 mm /58 mm*	*60 mm /73 mm*	*71 mm /91 mm*	*82 mm /110 mm*		
$\mathcal{M}_{2,2}$	RL	0 %	0 %	−1 %	−1 %	−1 %	0 %
	CI (2.5 %/97.5 %)	0 %/1 %	1 %/1 %	1 %/2 %	1 %/2 %		

5.2.3 Remarks on Model Selection

Our analyses show that even though it would be appealing to use simpler models which are more rapidly computed, model selection is important and must be done seriously. Otherwise GEV parameters are estimated poorly and results differ, e. g. at stations La Chaux-de-Fonds, Basel/Binningen, and Locarno-Monti, up to 54 % from the ones obtained by the best model.

There is one exception, concerning yearly best estimates: $\mathcal{M}_{1,1}$. The best estimates are close or even the same as the ones of the optimal model. The confidence intervals, on the other hand, differ often by more than 10 %. The gain in speed when using $\mathcal{M}_{1,1}$ instead of a more complex model, however, is extremely small if we are interested in best estimates only. If we are more concerned about confidence intervals we can save 20 % to 40 % of computational time, but at risk of loosing accuracy.

For rare stations with an almost negligible seasonality we find that all results are alike, independent of the model used—except for $\mathcal{M}_{0,0}$. The latter assumes the same GEV distribution for every month, and therefore does not model the non-stationarities at all.

5.3 Comparison with Previous Method

Hitherto, a stationary GEV was used to estimate the parameters and to calculate return levels and return periods, and is still currently used at MeteoSwiss (see for instance Appenzeller et al. (2006, p. 24 ff) and Schmutz et al. (2008, p. 15 ff)). We now apply this 'previous' method to the same time series, and compare with the seasonal NS-GEV analysis.

5.3.1 Yearly Return Levels

Note that it is not possible to test the performance with a Q-Q plot or a goodness-of-fit test, since the yearly best estimate and confidence intervals are derived numerically from the seasonal NS-GEV. Hence, there are no estimates of the GEV parameters available with which to construct the theoretical quantiles. On a monthly level, however, it is possible to use a Q-Q plot to assess the models' performance. The results are as expected: for many months the basic assumptions of extreme value theory (EVT) are met. On the other hand, in special cases such as October at La Chaux-de-Fonds, there are severe violations. The monthly Q-Q plots for the tree key stations can be found in the Appendix in Section C.2. Note that the calculation of the monthly empirical quantiles does not take into account the information buried in the seasonal cycle, while the GEV parameters determining the theoretical quantiles do.

Looking at the return level plots for all stations (s. Section D.1 in the Appendix) we can see that the best estimate is heavily influenced by the less extreme values. This finding is compatible with the remarks in Section 5.1. The best estimates often differ, but mostly remain within the NS-GEV's confidence intervals. We find many stations, such as for instance Basel/Binningen (s. Fig. 4.3b), where the best estimate and the corresponding confidence intervals, based on the seasonal analysis, are similar to results from the yearly S-GEV. There, the observations are mostly within the confidence intervals of both methods.

On the other hand, there are several stations, such as e. g. Bauma, where many observations are outside of the NS-GEV's confidence intervals (s. Fig. D.2e). At Zermatt (s. Fig. D.17a), the results obtained with the NS-GEV differ considerably from the ones of the yearly S-GEV, and seem incompatible with observations.

In all cases mentioned above, model selection is unambiguous and the applied algorithms are the same. It might be that neither of our proposed models are suitable to model the non-stationarities at stations such as Bauma and especially Zermatt. Indeed, the latter station has some unusual characteristics: The heaviest precipitation events occur mostly in spring or fall, and the seasonal cycle has thus two instead of one distinct maxima for extreme precipitation (not shown).

As it turns out, when looking at monthly instead of yearly maxima, the models are able to mimic the seasonal behaviour reasonably well (s. Fig. E.9a for Zermatt and Fig. E.1k for Bauma). It may be that the problem resides in the transformation from monthly to yearly return levels. We suspect Newton's Method to be the source of these inconsistencies.

5.3.2 Confidence Intervals

At a great number of stations, as shown in Fig. 4.5, the derived yearly return levels have smaller confidence intervals than their stationary counterparts. From the operational point of view, this is a gain, despite the increase in computational demand.

A few stations, such as Locarno-Monti, by contrast, have increased confidence intervals (red dotted stations in Fig. 4.5b), no doubt a consequence of the large uncertainty in the monthly NS-GEV parameters. As a rule of thumb, stations such as Locarno-Monti with a marked seasonality tend to have large confidence intervals, sometimes even larger than indicated by the yearly S-GEV, whereas stations with a mild seasonality benefit most from the new models in terms of the width of the confidence intervals.

Concluding, we might say that the results are somewhat surprising. The original intention was to model non-stationarities such that we do not violate one of the fundamental assumptions of EVT: stationarity. What we find now, however, is that our models often perform best, in terms of confidence intervals for yearly return levels, when the violation of stationarity is small, that is, when a weak seasonal cycle is observed.

5.3.3 Monthly Return Levels

One expectation of the present study is to gain the ability to make robust statements at a monthly resolution.

Yet a glance at Fig. 4.6 reveals that the results of the monthly S-GEV and of the NS-GEV differ significantly in some months. Comparison with fig. 4.1, however, shows that the monthly S-GEV return levels reflect the pattern of the shape parameter modulated by the monthly location and scale.

For example, the low value of the shape parameter in October at La Chaux-de-Fonds is due to the lack of heavy events in this specific month (s. Fig. 1.1a), and results in a particularly low return level estimate. Thus, the independent estimation for each month results in oscillations that may not have any climatologically plausible explanation.

Our initial apprehension that a block size of one month might be too small for the maxima to converge to a GEV distribution could not hold. We tested for this hypothesis by aggregating the same month of two consecutive years to one maximum by increasing the block length to two months. As a trade-off we lost 50 % of our years and had to work with a virtual time series of only 55 years. This enlarged the confidence intervals, but neither the best estimate, nor the confidence intervals, became less erratic (not shown).

One could argue that, despite our finding, it would be wise to aggregate two months of consecutive years into one to ensure a convergence of the maxima to a GEV distribution. Most likely, the effect would be small since in our seasonal NS-GEV, the estimates for a given month are estimated not only with the maxima of that particular month, but with those of the neighbouring months as well. This means that more information enters the evaluation of the GEV of a particular month than with the independent estimations. The seasonal evolution imposed in the form a truncated Fourier Series on the GEV parameters results in a smoother, more plausible behaviour than the monthly S-GEV October return level at La Chaux-de-Fonds.

6 Conclusions

The year 2010 will probably be remembered as a year of floods. Hundreds of people died in connection with extreme precipitation events in Brazil, China, Pakistan, Southern France, Guatemala, and many more places. In Switzerland the last large floods occurred in 2005 and 2007. They caused few casualties and enormous damage (2005: roughly CHF 3 billion Hilker et al. (2008)).

In the face of such devastating events, planning accurate infrastructure and adequate prevention measures is crucial, and requires quantitative knowledge of return periods and return levels. These are determined by means of the statistical tools of Extreme Value Theory, which assumes stationarity of the precipitation process. This requirement cannot be met of course, since precipitation in Switzerland exhibits a seasonal cycle. Yet, the method currently used operationally to calculate return levels and periods is based on this assumption.

The present thesis addresses this issue by modelling explicitly the seasonal non-stationarities of monthly maxima of daily precipitation. Its purpose is to evaluate their influence on return period estimates and shed some light on the seasonal behaviour of extreme precipitation. Non-stationarity is taken into account by introducing a time covariate in the parameters of the generalised extreme value (GEV) distribution. The location and scale parameter are modelled with a truncated Fourier Series, such that the time dependent GEV distribution follows the seasonal cycle in the form of a harmonic oscillation. The shape parameter is not allowed to vary with time: it is constant.

The number of terms of the Fourier Series is determined separately at each station by means of the Akaike Information Criterion, supported in the case of nested models by a Likelihood Ratio Test. The location and scale parameter are allowed to have a different number of Fourier Series terms. Yearly return level estimates are gained from the monthly GEV parameters of the non-stationary analysis with an iterative numerical procedure. Given the increased amount of data (twelvefold) due to the incorporation of monthly data, this estimate can generally be seen as providing more reliable estimates for yearly return levels and return periods.

The non-stationarities were modelled independently at 97 stations of the Swiss observational network for data sets of monthly maxima of daily precipitation. The stations were chosen according to their representativeness of precipitation variability in Switzerland, and the time series cover the period 1901 to 2010.

Results show that monthly return levels computed with the selected models adequately reproduce the GEV parameters' seasonality at most stations, both in amplitude and phase (s. Fig. 4.1). The yearly return levels derived from the non-stationary analysis differ from those estimated with the stationary analysis of yearly maxima, but are generally well within their confidence intervals. Still, for many stations the expected frequency of heavy precipitation must be revised. At station Basel/Binningen the August 2007 event, for instance, is no longer expected to occur on average every 93 years, but every 46 years. The sign of the change in frequency exhibits a spatial pattern. Indeed, in the northeastern part of Switzerland and the Central Alps, as well as in the Jura the estimates suggest that lower frequency values must be assigned to heavy precipitation events than hitherto evaluated. The opposite is true for southeastern Switzerland. (s. Fig. 4.4).

The derived analysis results at most locations in a reduction in return level uncertainty, except for a number of stations with a pronounced seasonal cycle in the southeastern part of Switzerland (s. Fig. 4.8). At about 10 % of stations, the yearly return levels derived from the Non-Stationary GEV (NS-GEV) appear implausible. Most of these are located in the southeastern part of Switzerland. This may be due to difficulties with the numerical algorithms, perhaps in conjunction with inadequate assumptions regarding the form of the seasonal cycle.

The seasonal analysis of extreme precipitation also shows that the selected models lead to reasonable estimates of the monthly return levels. Therefore, the NS-GEV allows us to explore the spatial and seasonal variation from a climatic perspective.

We find, for instance, that the probability for a 100-year event occurring in the winter and spring months is, on average, very low. The dominant seasons are summer and fall (s. Fig. 4.11). The results also indicate that the seasonal cycle in Northern Switzerland is ahead of the southern one. A similar dependence also can be found for stations above and below 800 m a. s. l., indicating that extreme events in the Alpine region tend to occur later in the year compared to the low lands (s. Fig. 4.12). Return levels also show a seasonal cycle with maxima occurring mostly in July and August. Overall, largest return levels are found in Ticino.

It must be noted that difficulties encountered in the computation of confidence intervals for the derived yearly return levels might have been alleviated, had a block-bootstrapping procedure been applied rather than the parameteric re-sampling. Instead of sampling artificial observations for a given month from the estimated GEV, this could be done by sampling with replacement from the monthly observed maxima. This would preserve the underlying seasonality and avoid sampling exaggerately large values. Future work should investigate this possibility. Also, given the length of the time series, it might be interesting to consider more sophisticated model than a linear trend or other covariates than time that might be relevant for decadal climate variability, for instance.

Further, a tentative experiment was performed with an additional linear long-term trend in the already selected models. It turned out that, at nearly half of the stations, the model selection process signalled a significant improvement if the effect of this long-term non-stationarity was included in the model (s. Fig. 4.8a). In all but three cases the trend was positive. The spatial distribution indicates positive trends especially in Northeastern Switzerland. Our results have a similar spatial pattern as results for Winter from Schmidli and Frei (2005, Figure 3), who looked into long term trends in heavy precipitation events.

These results indicate the necessity of a thorough analysis, introducing for instance independent trends for each season. This seems reasonable since trends in average rainfall are expected to depend on the seasons. (North et al., 2007, p. 35)

The significance of the additional linear time-dependent term in the model selection, however, does not imply a significant trend in the values of the return levels. In Schaffhausen, for instance, we found an increase in return levels of more than 10 mm per decade, even for a 10 year event (s. Fig. 4.9b). A precipitation event which in 1919 was considered to be a 300 year event can now be considered as a 100 year event. Yet, the estimates of the model with trend remain within the confidence intervals of our NS-GEV model without a long-term trend. This is the case for other stations as well. Again, this suggests that more detailed analyses are required to quantify possible trends in a more reliable fashion.

Finally, we dare say that we managed to exploit the information contained within the annual cycle to obtain more reliable estimates of return levels and return periods for most stations. Also, the availability of plausible monthly return levels should lead to further and new enquiries in the climatic aspects of heavy precipitation.

Acknowledgements

It is a pleasure to thank those who made this thesis possible. Especially I am indebted to Dr. Sophie Fukutome who dedicated a great deal of her time in advising and tutoring me. I greatly benefited from her scientific expertise and her knowledge. I enjoyed our collaboration and could benefit a lot.

Also I am very grateful to Dr. Mark Liniger who not only is a sensitive team leader but also helped with his concise remarks to improve this thesis.

Without the help of PD Dr. Christof Appenzeller, who gave me the opportunity to write this thesis at MeteoSwiss, this work could not have been written. I am also thankful to Christof for reviewing this work and providing pertinent remarks and ideas.

Thanks to Christoph Frei and his lecture at ETH I realised that statistics and climate studies can complement each other in an extremely interesting manner. It was his lecture which made me think about writing my master thesis about a statistical topic. Later at MeteoSwiss his generous help made it possible to solve several problems I encountered. Particularly the method to derive yearly return level estimates from the non-stationary monthly GEV was his idea.

It was delightful to work at MeteoSwiss with its excellent working atmosphere. All people where very helpful and I would like to thank them for their kindness and the interest they showed in my work.

Finally, I sincerely want to thank my personal environment which not only provided a lot of support but also many helpful remarks about the thesis.

References

Akaike, H. (1973), *Information theory and an extension of the maximum likelihood principle*, Akademiai Kiado, pp. 267–281.

Appenzeller, C., Bader, S., Duding, O., Eckert, P., Frei, C., Germann, U., Hächler, P., Keuerleber-Burk, D. K., Liniger, M., Rotach, M., Schubiger, F., Walser, A. and Zbinden, P. (2006), 'Starkniederschlagsereignis August 2005', *Technical Report MeteoSwiss* **211**, 63pp.

Bartholy, J. and Pongracz, R. (2007), 'Regional analysis of extreme temperature and precipitation indices for the Carpathian Basin from 1946 to 2001', *Global and Planetary Change* **57**(1-2), 83–95. Extreme Climatic Events.

Begert, M. (2008), 'Die Repräsentativität der Stationen im Swiss National Basic Climatological Network (Swiss NBCN)', *Technical Report MeteoSwiss* **217**, 40pp.

Begert, M., Seiz, G., Foppa, N., Schlegel, T., Appenzeller, C. and Müller, G. (2007), 'Die Überführung der klimatologischen Referenzstationen der Schweiz in das Swiss National Basic Climatological Network (Swiss NBCN)', *Technical Report MeteoSwiss* **215**, 43pp.

Begert, M., Seiz, G., Foppa, N., Schlegel, T., Musa, M., Baudraz, G. and Michael, M. (2003), 'Homogenisierung von Klimamessreihen der Schweiz und Bestimmung der Normwerte 1961-1990', *Scientific Report MeteoSwiss* **67**, 170pp.

Buishand, T. A. and Demaré, G. R. (1990), 'Estimation of the annual maximum distribution from samples of maxima in separate seasons', *Stochastic Hydrology and Hydraulics* **4**, 89–103.

Buonomo, E., Jones, R., Huntingford, C. and Hannaford, J. (2007), 'On the robustness of changes in extreme precipitation over Europe from two high resolution climate change simulations', *Quarterly Journal of the Royal Meteorological Society* **133**(622), 65–81.

Burnham, K. P. and Anderson, D. R. (2002), *Model selection and multimodel inference*, Springer.

Coles, S. (2001), *An Introduction to Statistical Modeling of Extreme Values*, London: Springer.

Coles, S. and Stephenson, A. (2009), *ismev: An Introduction to Statistical Modeling of Extreme Values*. Original S functions by Stuart Coles and R port and R documentation files by Alec Stephenson. R package version 1.34.
URL: *http://CRAN.R-project.org/package=ismev*

Cooke, M. L., Burgess, P. S., Jones, L. W., Morris, S. B., Olds, L., Renne, R. R. and White, G. F. (1950), 'Water Policy for the American People', Printed.
URL: *http://content.lib.utah.edu/u?/wwdl-doc,1984*

Davison, A. C. and Smith, R. L. (1990), 'Models for Exceedances over High Thresholds', *Journal of the Royal Statistical Society. Series B (Methodological)* **52**(3), pp. 393–442.

Fox, J. and Andersen, R. (2005), *Using the R Statistical Computing Environment to Teach Social Statistics Courses*, Department of Sociology, McMaster University.
URL: *http://www.unt.edu/rss/Teaching-with-R.pdf*

Frei, C. (2009), *Analysis of Climate and Weather Data*, Federal Office of Meteorology and Climatology. Lecture Notes.

Frei, C. (2010), *gevXgpd: Extreme Value Analysis*. R package version 1.3.5.

Fukutome, S., Liniger, M. and Frei, C. (2009), AN ALPINE CLIMATOLOGY OF EXTREME EVENTS, *in* 'Annalen der Meteorologie', number 44, Deutscher Wetterdienst, Deutscher Wetterdienst, Frankfurter Strasse 135, D-63067 Offenbach am Main, Germany. Oral presentation, 30th ICAM, Rastatt.
URL: *http://www.pa.op.dlr.de/icam2009/extabs/ICAM2009-AnnMeteo44-OralPresentations.pdf*

Gilleland, E., Katz, R. and Young, G. (2009), *extRemes: Extreme value toolkit*. R package version 1.60.
URL: *http://CRAN.R-project.org/package=extRemes*

Gumbel, E. J. (1958), *Statistics of extremes*, Columbia University Press, New York.

Gyarmati, P. (2004), Atmosphärische Zirkulationsmuster bei Starkniederschlägen im Wallis (1961–2000), Diplomarbeit, University of Berne.

Hilker, N., Badoux, A. and Hegg, C. (2008), 'Unwetterschäden in der Schweiz im Jahre 2007'.

Hubbard, D. W. (2007), *How to measure anything*, 2 edn, Wiley.

Katz, R. W., Brush, G. S. and Parlange, M. B. (2005), 'Statistics of extremes: modeling ecological disturbances', *Ecology* **86**(5), 1124–1134.

Katz, R. W., Parlange, M. B. and Naveau, P. (2002), 'Statistics of extremes in hydrology', *Advances in Water Resources* **25**, 1287–1304.

Katz, R. W., Parlange, M. B. and Tebaldi, C. (2003), 'Stochastic Modeling of the Effects of Large-Scale Circulation on Daily Weather in the Southeastern U.S.', *Climatic Change* **60**, 189–216.

Klein Tank, A. M. G. and Können, G. P. (2003), 'Trends in Indices of Daily Temperature and Precipitation Extremes in Europe, 1946–99', *Journal of Climate* **16**(22), 3665–3680.

Leadbetter, M. R., Lindgren, G. and Rootzen, H. (1983), *Extremes and related properties of random sequences and processes*, Vol. 31 of *Springer series in statistics*, Springer-Verlag, New York.

Maraun, D., Rust, H. W. and Osborn, T. J. (2009), 'The annual cycle of heavy precipitation across the United Kingdom: a model based on extreme value statistics', *Int. J. Climatol.* **29**(12), 1731–1744.

Menéndez, M., Méndez, F. J., Izaguirre, C., Luceño, A. and Losada, I. J. (2009), 'The influence of seasonality on estimating return values of significant wave height', *Coastal Engineering* **56**(3), 211–219.

MeteoSchweiz (2009), 'Manuelle Niederschlagsmessnetze', online.

MeteoSwiss (2010), 'SwissMetNet: Ein Messnetz für die Zukunft!', online.

Moore, R. J. (1987), Combined regional flood frequency analysis and regression on catchment charactersitics by maximum likelihood estimation, *in* V. P. Singh, ed., 'Regional Flood Frequency Analysis', Reidel, Dordrecht, pp. 119–131.

Mudersbach, C. and Juergen, J. (2011), An advanced statistical extreme value model for evaluating storm surge heights considering systematic records and sea level rise scenarios, *in* J. M. Smith and P. Lynett, eds, 'Proceedings of 32nd Conference on Coastal Engineering, Shanghai, China, 2010', Vol. 1, Coastal Engineering Research Council, North America.

Müller, G. (1980), 'Die beobachtungsnetze der schweizerischen meteorologischen anstalt', *Technical Report MeteoSwiss* **93**, 66pp.

North, N., Kljun, N., Kasser, F., Heldstab, J., Maibach, M., Reutimann, J. and Guyer, M. (2007), Klimaänderung in der Schweiz. Indikatoren zu Ursachen, Auswirkungen, Massnahmen, number 0728 *in* 'Umwelt-Zustand', Bundesamt für Umwelt (BAFU), p. 77.

Parey, S., Malek, F., Laurent, C. and Dacunha-Castelle, D. (2007), 'Trends and climate evolution: Statistical approach for very high temperatures in France', *Climatic Change* **81**, 331–352.

R Development Core Team (2009), *R: A Language and Environment for Statistical Computing*, R Foundation for Statistical Computing, Vienna, Austria. ISBN 3-900051-07-0.
URL: *http://www.R-project.org*

Rosenzweig, C., Iglesias, A., Yang, X., Epstein, P. R. and Chivian, E. (2001), 'Climate Change and Extreme Weather Events; Implications for Food Production, Plant Diseases, and Pests', *Global Change & Human Health* **2**, 90–104.

Rust, H. W., Maraun, D. and Osborn, T. J. (2009), 'Modelling seasonality in extreme precipitation', *The European Physical Journal – Special Topics* **174**(1), 99–111.

Schmidli, J. and Frei, C. (2005), 'Trends of heavy precipitation and wet and dry spells in Switzerland during the 20th century', *International Journal of Climatology* **25**(6), 753–771.

Schmutz, C., Arpagaus, M., Clementi, L., Frei, C., Fukutome, S., Germann, U., Liniger, M. and Schacher, F. (2008), 'Meteorologische ereignisanalyse des hochwassers 8. bis 9. august 2007', *Technical Report MeteoSwiss* **222**, 30pp.

Sebah, P. and Gourdon, X. (2001), 'Newton's method and high order iterations', online.

Sienz, F., Schneidereit, A., Blender, R., Fraedrich, K. and Lunkeit, F. (2010), 'Extreme value statistics for North Atlantic cyclones', *Tellus A* **62**(4), 347–360.

Trömel, S. and Schönwiese, C.-D. (2007), 'Probability change of extreme precipitation observed from 1901 to 2000 in Germany', *Theoretical and Applied Climatology* **87**, 29–39.

Zeller, J., Geiger, H. and Röthlisberger, G. (1991), Starkniederschläge des schweizerischen Alpen- und Alpenrandgebietes, Technical report, Eidgenössische Forschungsanstalt für Wald, Schnee und Landschaft WSL.

Zhang, X., Zwiers, F. W. and Li, G. (2004), 'Monte Carlo Experiments on the Detection of Trends in Extreme Values', *Journal of Climate* **17**(10), 1945–1952.

Appendix A Abbreviations

A.1 In General

AIC	Akaike's information criterion
AIC_c	second-order AIC
ΔAIC_c	Akaike difference
AIC_{min}	minimum AIC value
AIC_w	Akaike weights
ANETZ	Automatic Network
BAM	Bauma
BAS	Basel/Binningen
BM	block maxima
CDF	La Chaux-de-Fonds
CDF	cumulative density function
CI	confidence interval
EVT	extreme value theory
ENET	Complementary Network
i. i. d.	independent and identically distributed
GEV	generalised extreme value
GSB	Col du Grand St-Bernard
LAC	Lachen
LLR-test	log-likelihood ratio test
LEU	Leukerbad
ML	maximum-likelihood method
MLE	maximum-likelihood estimator
NIME	"Niederschlagsmesseinheit"
Swiss NBCN	Swiss National Basic Climatological Network
Swiss NBCN-P	Swiss National Basic Climatological Network for Precipitation
NS-GEV	Non-Stationary GEV
OTL	Locarno-Monti
PDF	probability density function
PWM	probability weighted moments
POT	peak over threshold
MeteoSwiss	Federal Office of Meteorology and Climatology
RL	return level
RP	return period
S-GEV	Stationary GEV
SHA	Schaffhausen
SMN	SwissMetNet
WMO	World Meteorological Organization

A.2 Mathematical

α	Level of *significance*
μ	*Location parameter* of a GEV
κ	Index of summation of the Fourier Series
ϕ	*Phase*
σ	*Scale parameter* of a GEV
θ	Vector $(\mu, \sigma, \xi)^T$
$\hat{\theta}$	Vector of maximum-likelihood estimators (MLEs) $(\hat{\mu}, \hat{\sigma}, \hat{\xi})^T$
ξ	*Shape parameter* of a GEV
ω	*Angular Frequency*
c_i	Centre of the i^{th} block
g	The probability density function of a GEV
j	$j = 0, \ldots, 0$, denoting each of the models, devised to account for the seasonal non-stationarities
k	Number of summands of the Fourier Series
ℓ	*Log-Likelihood*
m_t	independent realisations of a GEV distributed random variable
n	Sample *size*
p	probability
t	*time* in general
y	Return Period of y years
z	A given amount of precipitation
z_y	An amount of precipitation corresponding to a specific RP, hence a RL
$\widehat{E}$	The estimate of a statistical distribution; the best guess.
A	*Amplitude*
F	An unknown process which generated the data we are analysing.
G	The cumulative density function of a GEV
K	Number of parameters
$\mathcal{L}$	*Likelihood*
$\mathcal{M}$	*Statistical Model* to model non-stationarities
M_n	$\max\{X_1, \ldots, X_n\}$, maximum of n time units
S	An artificial *sample* generated for parametric resampling.
T	*Number of blocks* within a year, e. g. 12 in case of months.
X	*Random variable*, here heavy precipitation events
X_y	*RL*, of a y year event

Appendix B Considered Stations

B.1 All Stations

Abbr.	name	lat	lon	alt	1 hour	1 day	2 days	3 days	4 days	5 days	10 days
ABE	Aarberg	47.04	7.28	490 m ü. M.		✓	✓	✓	✓	✓	✓
AES	Aesch, LU	47.25	8.25	511 m ü. M.		✓	✓	✓	✓	✓	✓
AFT	Affeltrangen	47.53	9.02	479 m ü. M.		✓	✓	✓	✓	✓	✓
AIE	Affoltern im Emmental	47.06	7.74	755 m ü. M.		✓	✓	✓	✓	✓	✓
AIR	Airolo	46.53	8.6	1139 m ü. M.		✓	✓	✓	✓	✓	✓
ALT	Altdorf	46.89	8.62	438 m ü. M.	✓	✓	✓	✓	✓	✓	✓
APP	Appenzell	47.33	9.39	780 m ü. M.		✓	✓	✓	✓	✓	✓
ARB	Arbon	47.5	9.43	400 m ü. M.		✓	✓	✓	✓	✓	✓
ARI	Arisdorf	47.51	7.78	430 m ü. M.		✓	✓	✓	✓	✓	✓
ARO	Arosa	46.78	9.67	1840 m ü. M.		✓	✓	✓	✓	✓	✓
BAM	Bauma	47.37	8.89	655 m ü. M.		✓	✓	✓	✓	✓	✓
BAS	Basel / Binningen	47.54	7.58	316 m ü. M.	✓	✓	✓	✓	✓	✓	✓
BER	Bern / Zollikofen	46.99	7.46	553 m ü. M.	✓	✓	✓	✓	✓	✓	✓
BEX	Bex	46.24	7	402 m ü. M.		✓	✓	✓	✓	✓	✓
BEY	Bellelay	47.26	7.17	930 m ü. M.		✓	✓	✓	✓	✓	✓
BIL	Biel/Bienne	47.12	7.26	433 m ü. M.		✓	✓	✓	✓	✓	✓
BIZ	Bischofszell	47.5	9.23	470 m ü. M.	✓	✓	✓	✓	✓	✓	✓
BLZ	Bellinzona	46.19	9.01	225 m ü. M.		✓	✓	✓	✓	✓	✓
BMU	Beromünster	47.21	8.19	658 m ü. M.		✓	✓	✓	✓	✓	✓
BNE	Les Brenets	47.07	6.71	907 m ü. M.		✓	✓	✓	✓	✓	✓
BOT	Boltigen	46.63	7.39	855 m ü. M.		✓	✓	✓	✓	✓	✓
BRP	Brusio-Piazzo	46.26	10.12	830 m ü. M.		✓	✓	✓	✓	✓	✓
BSP	Bourg-St-Pierre	45.95	7.21	1664 m ü. M.		✓	✓	✓	✓	✓	✓
BUC	Buch, SH	47.72	8.78	425 m ü. M.		✓	✓	✓	✓	✓	✓
BUE	Bülach	47.52	8.53	402 m ü. M.		✓	✓	✓	✓	✓	✓
BZN	Beznau	47.56	8.24	327 m ü. M.		✓	✓	✓	✓	✓	✓
CDF	La Chaux-de-Fonds	47.08	6.79	1018 m ü. M.	✓	✓	✓	✓	✓	✓	✓
CHD	Château-d'Oex	46.48	7.14	985 m ü. M.		✓	✓	✓	✓	✓	✓
CHM	Chaumont	47.05	6.99	1073 m ü. M.		✓	✓	✓	✓	✓	✓
CHU	Chur	46.87	9.53	556 m ü. M.	✓	✓	✓	✓	✓	✓	✓
COS	Cossonay	46.61	6.51	570 m ü. M.		✓	✓	✓	✓	✓	✓
COU	Couvet	46.92	6.63	741 m ü. M.		✓	✓	✓	✓	✓	✓
CUE	La Cure	46.46	6.07	1152 m ü. M.		✓	✓	✓	✓	✓	✓
DAV	Davos	46.81	9.84	1594 m ü. M.	✓	✓	✓	✓	✓	✓	✓
DIE	Diessenhofen	47.69	8.73	405 m ü. M.		✓	✓	✓	✓	✓	✓
EIN	Einsiedeln	47.13	8.75	910 m ü. M.		✓	✓	✓	✓	✓	✓
EKO	Eschlikon	47.45	8.97	580 m ü. M.		✓	✓	✓	✓	✓	✓
ELM	Elm	46.92	9.18	965 m ü. M.		✓	✓	✓	✓	✓	✓
ENG	Engelberg	46.82	8.41	1036 m ü. M.	✓	✓	✓	✓	✓	✓	✓

Tab. B.1: All stations we considered are listed here. Additionally, their location, elevation, and the availability of their time series is noted.

Abbr.	name	lat	lon	alt	1 hour	1 day	2 days	3 days	4 days	5 days	10 days
ENT	Entlebuch	46.98	8.07	808 m ü. M.		✓	✓	✓	✓	✓	✓
EPT	Eptingen	47.39	7.82	565 m ü. M.		✓	✓	✓	✓	✓	✓
ESZ	Eschenz	47.65	8.88	417 m ü. M.		✓	✓	✓	✓	✓	✓
FLW	Flawil	47.41	9.2	572 m ü. M.		✓	✓	✓	✓	✓	✓
FRF	Frauenfeld	47.57	8.89	393 m ü. M.		✓	✓	✓	✓	✓	✓
GIN	Grüningen	47.28	8.77	495 m ü. M.		✓	✓	✓	✓	✓	✓
GLA	Glarus	47.03	9.07	517 m ü. M.	✓	✓	✓	✓	✓	✓	✓
GOS	Göschenen	46.67	8.59	1099 m ü. M.		✓	✓	✓	✓	✓	✓
GSB	Col du Grand St-Bernard	45.87	7.17	2472 m ü. M.	✓	✓	✓	✓	✓	✓	✓
GTT	Guttannen	46.66	8.29	1055 m ü. M.		✓	✓	✓	✓	✓	✓
HLL	Hallau	47.7	8.46	432 m ü. M.		✓	✓	✓	✓	✓	✓
HTW	Herbetswil	47.3	7.59	524 m ü. M.		✓	✓	✓	✓	✓	✓
ILH	Illhart	47.62	9.04	540 m ü. M.		✓	✓	✓	✓	✓	✓
ILZ	Ilanz	46.77	9.2	705 m ü. M.		✓	✓	✓	✓	✓	✓
INT	Interlaken	46.67	7.87	577 m ü. M.	✓	✓	✓	✓	✓	✓	✓
JUS	Jussy	46.23	6.26	465 m ü. M.		✓	✓	✓	✓	✓	✓
KAL	Kalchrain	47.61	8.89	580 m ü. M.		✓	✓	✓	✓	✓	✓
KAS	Kandersteg	46.5	7.67	1176 m ü. M.		✓	✓	✓	✓	✓	✓
KUE	Küsnacht, ZH	47.31	8.59	412 m ü. M.		✓	✓	✓	✓	✓	✓
LAC	Lachen	47.19	8.86	426 m ü. M.		✓	✓	✓	✓	✓	✓
LAG	Langnau i.E.	46.94	7.81	755 m ü. M.		✓	✓	✓	✓	✓	✓
LEU	Leukerbad	46.38	7.63	1390 m ü. M.		✓	✓	✓	✓	✓	✓
LOH	Lohn, SH	47.76	8.68	584 m ü. M.		✓	✓	✓	✓	✓	✓
LSN	Lausanne	46.53	6.64	601 m ü. M.		✓	✓	✓	✓	✓	✓
LTB	Lauterbrunnen	46.6	7.91	818 m ü. M.		✓	✓	✓	✓	✓	✓
LUG	Lugano	46	8.96	273 m ü. M.	✓	✓	✓	✓	✓	✓	✓
LUZ	Luzern	47.04	8.3	454 m ü. M.	✓	✓	✓	✓	✓	✓	✓
MER	Meiringen	46.73	8.18	595 m ü. M.		✓	✓	✓	✓	✓	✓
MES	Mesocco	46.39	9.23	800 m ü. M.		✓	✓	✓	✓	✓	✓
MMO	Mormont	47.44	7.04	540 m ü. M.		✓	✓	✓	✓	✓	✓
MOH	Möhlin	47.57	7.86	341 m ü. M.		✓	✓	✓	✓	✓	✓
MUR	Muri, AG	47.27	8.33	574 m ü. M.		✓	✓	✓	✓	✓	✓
NEU	Neuchâtel	47	6.95	485 m ü. M.	✓	✓	✓	✓	✓	✓	✓
NIE	Niederneunforn	47.6	8.78	440 m ü. M.		✓	✓	✓	✓	✓	✓
OTL	Locarno / Monti	46.17	8.79	367 m ü. M.	✓	✓	✓	✓	✓	✓	✓
PAV	Payerne-Ville	46.82	6.94	450 m ü. M.		✓	✓	✓	✓	✓	✓
PDM	Les Ponts-de-Martel	47	6.73	1052 m ü. M.		✓	✓	✓	✓	✓	✓
ROM	Romont	46.7	6.93	688 m ü. M.		✓	✓	✓	✓	✓	✓
SAR	Sargans	47.05	9.44	487 m ü. M.		✓	✓	✓	✓	✓	✓
SCH	Schleitheim	47.74	8.48	499 m ü. M.		✓	✓	✓	✓	✓	✓
SCU	Scuol	46.79	10.28	1304 m ü. M.	✓	✓	✓	✓	✓	✓	✓
SED	Sedrun	46.68	8.78	1400 m ü. M.		✓	✓	✓	✓	✓	✓
SHA	Schaffhausen	47.69	8.62	438 m ü. M.	✓	✓	✓	✓	✓	✓	✓

Tab. B.1: All stations we considered are listed here. Additionally, their location, elevation, and the availability of their time series is noted.

Abbr.	name	lat	lon	alt	1 hour	1 day	2 days	3 days	4 days	5 days	10 days
SMA	Zürich / Fluntern	47.38	8.57	556 m ü. M.	✓	✓	✓	✓	✓	✓	✓
SMM	Sta. Maria, Val Müstair	46.6	10.42	1390 m ü. M.		✓	✓	✓	✓	✓	✓
SOG	Soglio	46.34	9.54	1093 m ü. M.		✓	✓	✓	✓	✓	✓
SRN	Sarnen	46.89	8.25	475 m ü. M.		✓	✓	✓	✓	✓	✓
STU	St. Urban	47.22	7.85	491 m ü. M.		✓	✓	✓	✓	✓	✓
SUG	Sulgen	47.54	9.18	445 m ü. M.		✓	✓	✓	✓	✓	✓
SVG	Savognin	46.59	9.6	1172 m ü. M.		✓	✓	✓	✓	✓	✓
THU	Thun	46.76	7.61	560 m ü. M.		✓	✓	✓	✓	✓	✓
UNK	Unterkulm	47.31	8.12	470 m ü. M.		✓	✓	✓	✓	✓	✓
VAR	Valeyres-sous-Rances	46.75	6.53	512 m ü. M.		✓	✓	✓	✓	✓	✓
VLS	Vals	46.62	9.18	1253 m ü. M.		✓	✓	✓	✓	✓	✓
WBR	Wil bei Rafz	47.6	8.51	406 m ü. M.		✓	✓	✓	✓	✓	✓
WCH	Wilchingen	47.67	8.46	420 m ü. M.		✓	✓	✓	✓	✓	✓
WIN	Winterthur-Seen	47.48	8.76	510 m ü. M.		✓	✓	✓	✓	✓	✓
ZER	Zermatt	46.03	7.75	1638 m ü. M.	✓	✓	✓	✓	✓	✓	✓

Tab. B.1: All stations we considered are listed here. Additionally, their location, elevation, and the availability of their time series is noted.

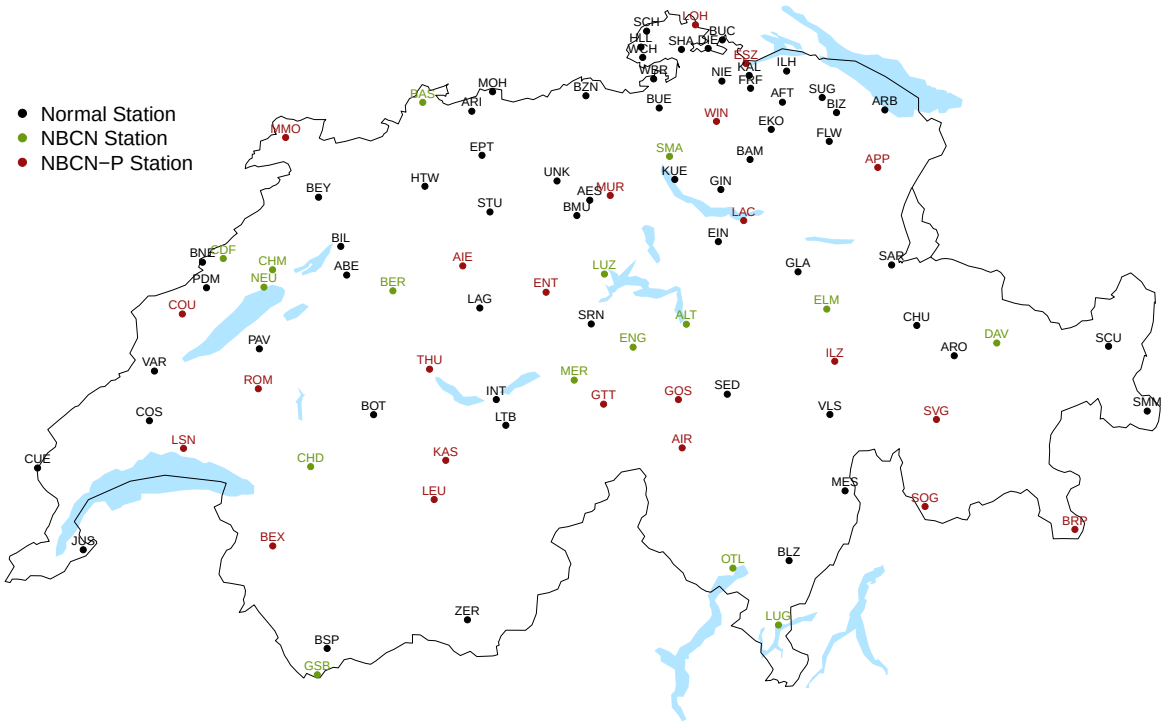

Fig. B.1: These are the 97 stations we investigate. Green coloured points depict Swiss NBCN stations, red ones stations of the Swiss NBCN-P.

Appendix C Additional Figures: Model Selection

C.1 Influence of Model Selection at stations CDF, BAS and OTL

C.1.1 CDF

Location parameter – μ

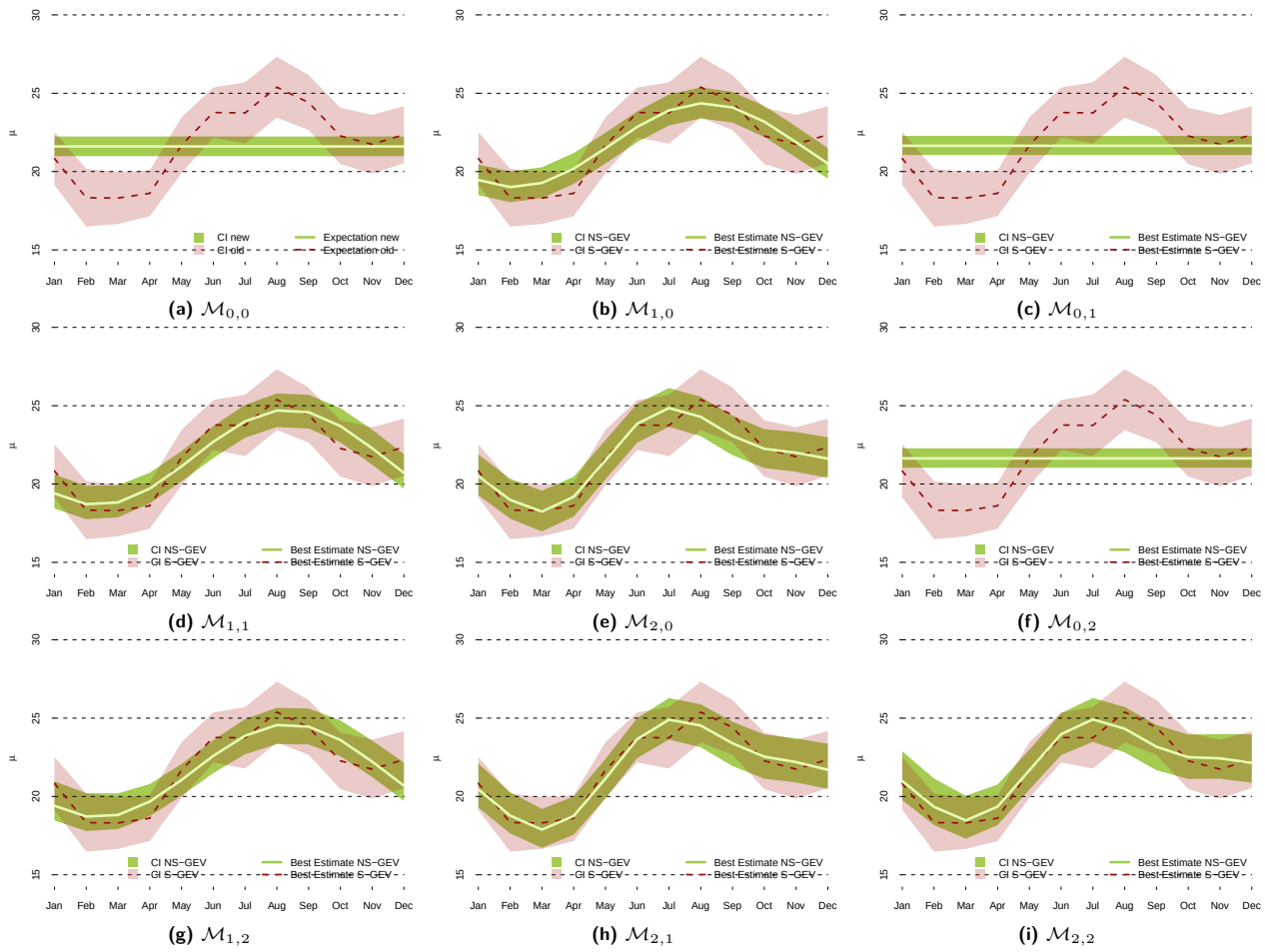

(a) $\mathcal{M}_{0,0}$ **(b)** $\mathcal{M}_{1,0}$ **(c)** $\mathcal{M}_{0,1}$

(d) $\mathcal{M}_{1,1}$ **(e)** $\mathcal{M}_{2,0}$ **(f)** $\mathcal{M}_{0,2}$

(g) $\mathcal{M}_{1,2}$ **(h)** $\mathcal{M}_{2,1}$ **(i)** $\mathcal{M}_{2,2}$

Fig. C.1: Estimation of the monthly location parameter at station La Chaux-de-Fonds with the time-dependent models $\mathcal{M}_{0,0},\ldots,\mathcal{M}_{2,2}$ (green) and the monthly S-GEV (red). Note that the model selected was $\mathcal{M}_{2,1}$.

Scale parameter – σ

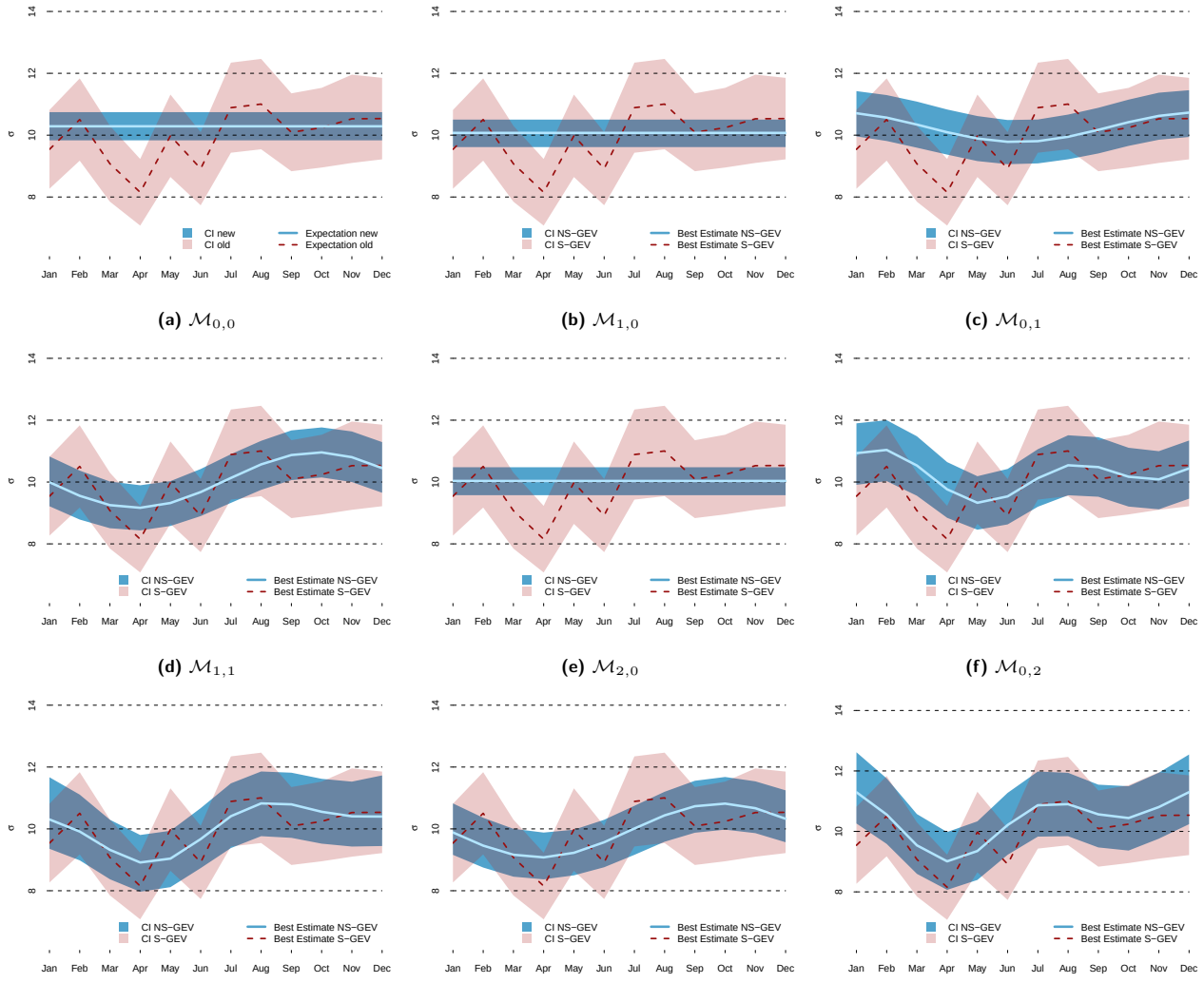

(a) $\mathcal{M}_{0,0}$ **(b)** $\mathcal{M}_{1,0}$ **(c)** $\mathcal{M}_{0,1}$

(d) $\mathcal{M}_{1,1}$ **(e)** $\mathcal{M}_{2,0}$ **(f)** $\mathcal{M}_{0,2}$

(g) $\mathcal{M}_{1,2}$ **(h)** $\mathcal{M}_{2,1}$ **(i)** $\mathcal{M}_{2,2}$

Fig. C.2: Estimation of the monthly location parameter at station La Chaux-de-Fonds with the time-dependent models $\mathcal{M}_{0,0},\ldots,\mathcal{M}_{2,2}$ (green) and the monthly S-GEV (red). Note that the model selected was $\mathcal{M}_{2,1}$.

Shape parameter – ξ

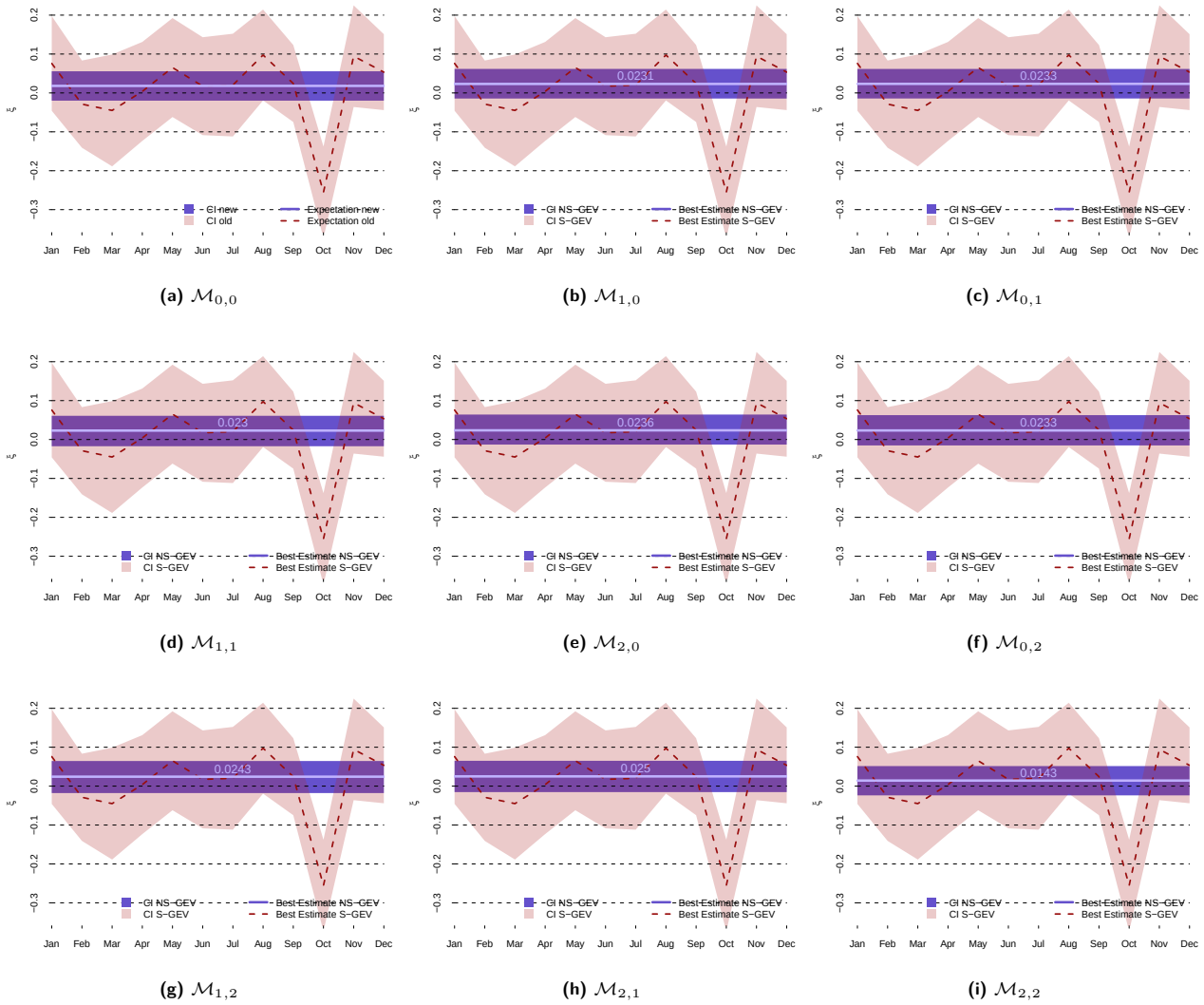

(a) $\mathcal{M}_{0,0}$ **(b)** $\mathcal{M}_{1,0}$ **(c)** $\mathcal{M}_{0,1}$

(d) $\mathcal{M}_{1,1}$ **(e)** $\mathcal{M}_{2,0}$ **(f)** $\mathcal{M}_{0,2}$

(g) $\mathcal{M}_{1,2}$ **(h)** $\mathcal{M}_{2,1}$ **(i)** $\mathcal{M}_{2,2}$

Fig. C.3: Estimation of the monthly location parameter at station La Chaux-de-Fonds with the time-dependent models $\mathcal{M}_{0,0},\ldots,\mathcal{M}_{2,2}$ (green) and the monthly S-GEV (red). Note that the model selected was $\mathcal{M}_{2,1}$.

Return Level Plots

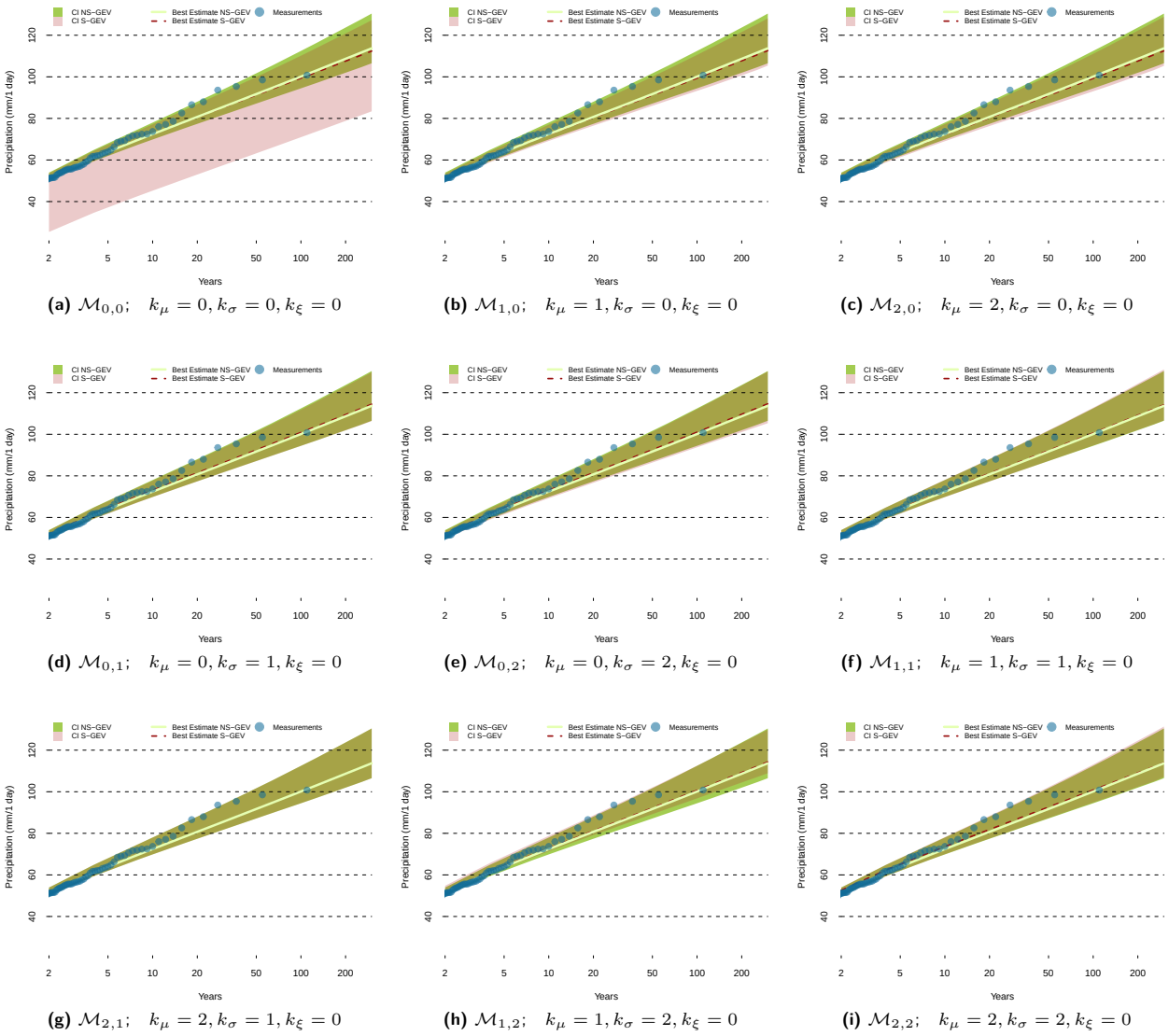

(a) $\mathcal{M}_{0,0}$; $k_\mu = 0, k_\sigma = 0, k_\xi = 0$ **(b)** $\mathcal{M}_{1,0}$; $k_\mu = 1, k_\sigma = 0, k_\xi = 0$ **(c)** $\mathcal{M}_{2,0}$; $k_\mu = 2, k_\sigma = 0, k_\xi = 0$

(d) $\mathcal{M}_{0,1}$; $k_\mu = 0, k_\sigma = 1, k_\xi = 0$ **(e)** $\mathcal{M}_{0,2}$; $k_\mu = 0, k_\sigma = 2, k_\xi = 0$ **(f)** $\mathcal{M}_{1,1}$; $k_\mu = 1, k_\sigma = 1, k_\xi = 0$

(g) $\mathcal{M}_{2,1}$; $k_\mu = 2, k_\sigma = 1, k_\xi = 0$ **(h)** $\mathcal{M}_{1,2}$; $k_\mu = 1, k_\sigma = 2, k_\xi = 0$ **(i)** $\mathcal{M}_{2,2}$; $k_\mu = 2, k_\sigma = 2, k_\xi = 0$

Fig. C.4: La Chaux-de-Fonds: Illustration of the model selection's impact on the yearly return levels and the confidence intervals derived from the time dependent NS-GEV. The green areas and the green line represent the 'best model's' best estimate and confidence interval respectively, the red line and area those for the model noted below the figure. Fig. (h) shows no deviation since it compares two times the 'best model'. The blue dots represent real observations.

C.1.2 BAS

Scale parameter – σ

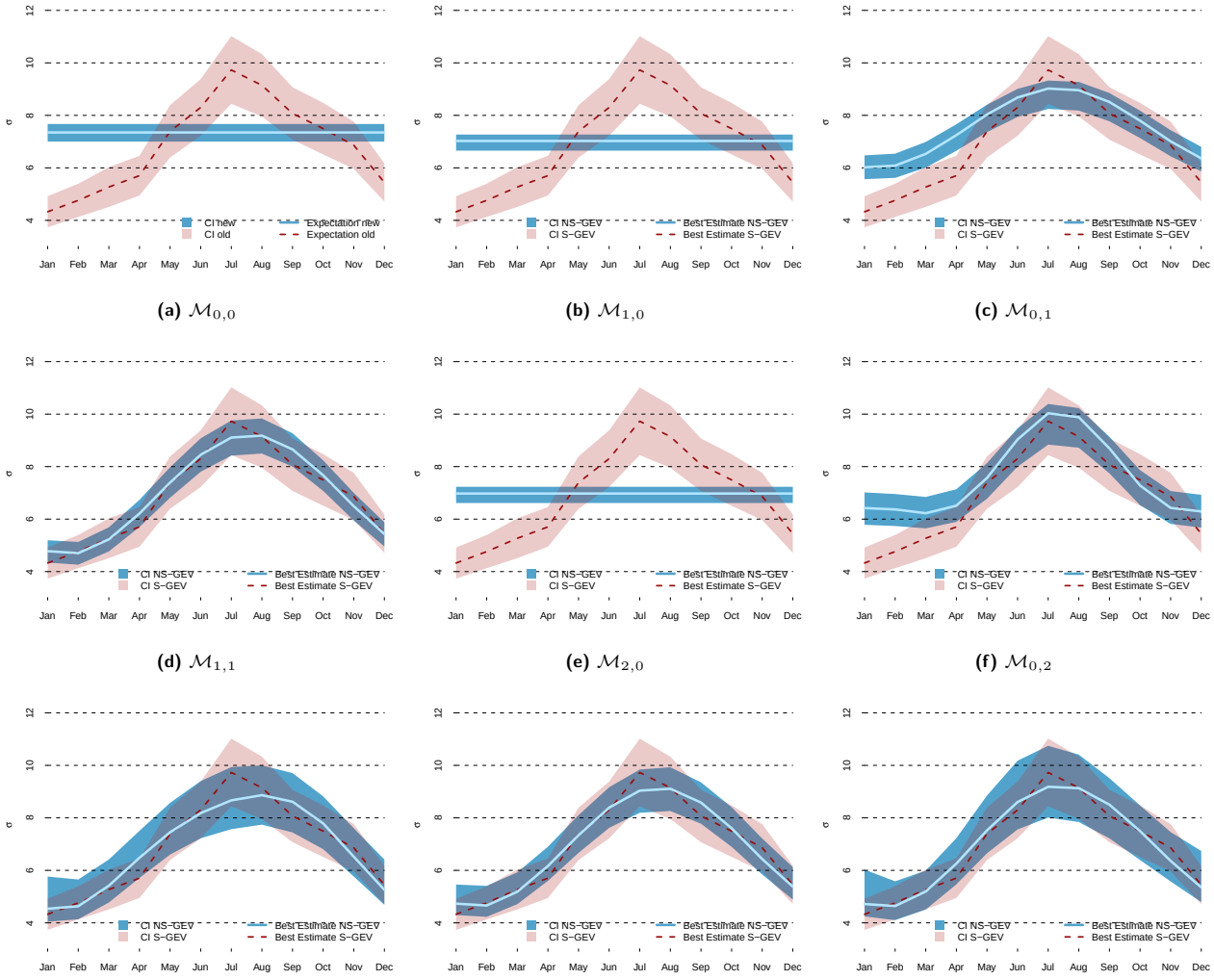

(a) $\mathcal{M}_{0,0}$ **(b)** $\mathcal{M}_{1,0}$ **(c)** $\mathcal{M}_{0,1}$

(d) $\mathcal{M}_{1,1}$ **(e)** $\mathcal{M}_{2,0}$ **(f)** $\mathcal{M}_{0,2}$

(g) $\mathcal{M}_{1,2}$ **(h)** $\mathcal{M}_{2,1}$ **(i)** $\mathcal{M}_{2,2}$

Fig. C.5: Estimation of the monthly location parameter at station Basel/Binningen with the time-dependent models $\mathcal{M}_{0,0},\ldots,\mathcal{M}_{2,2}$ (green) and the monthly S-GEV (red). Note that the model selected was $\mathcal{M}_{2,1}$.

Shape parameter – ξ

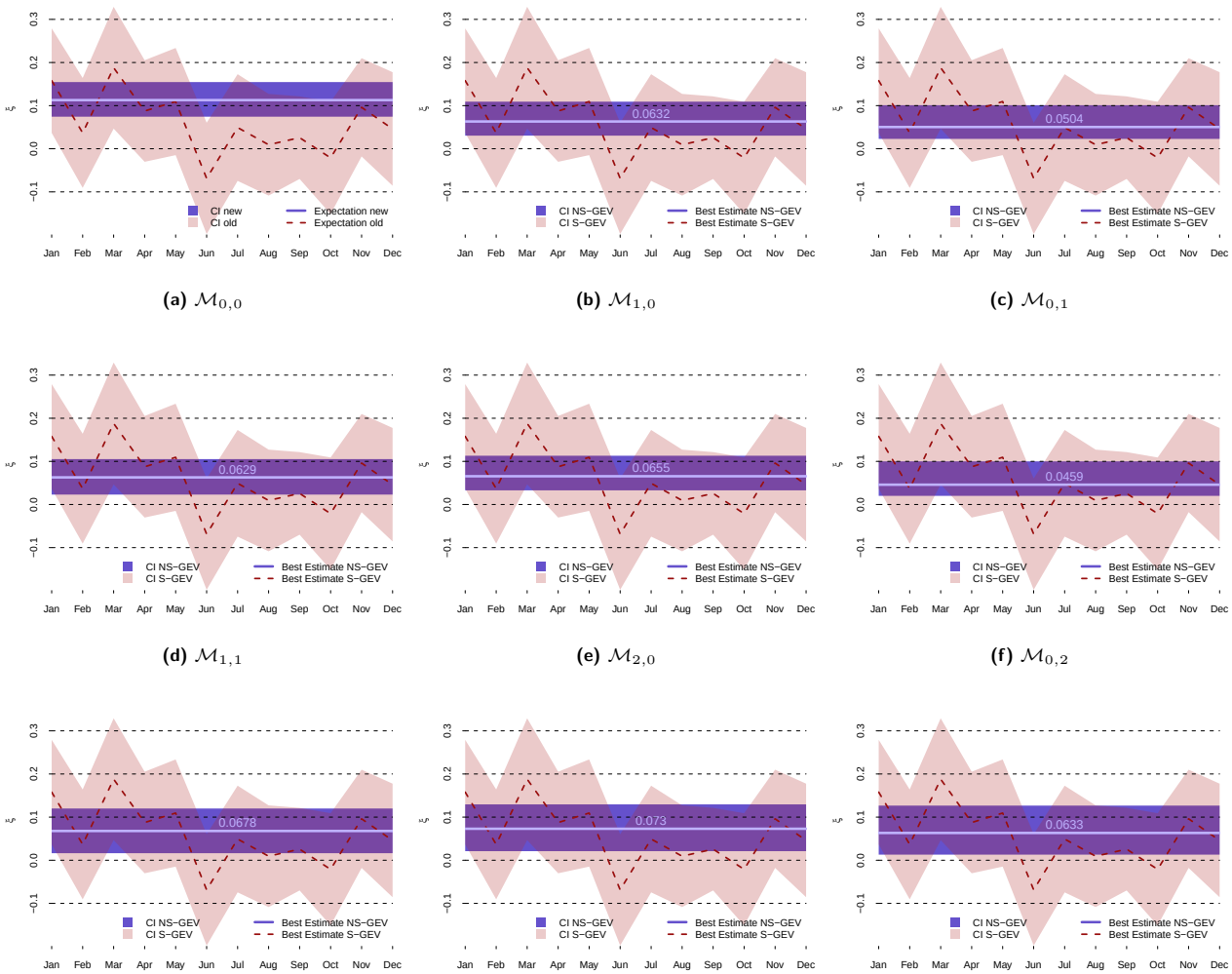

(a) $\mathcal{M}_{0,0}$ **(b)** $\mathcal{M}_{1,0}$ **(c)** $\mathcal{M}_{0,1}$

(d) $\mathcal{M}_{1,1}$ **(e)** $\mathcal{M}_{2,0}$ **(f)** $\mathcal{M}_{0,2}$

(g) $\mathcal{M}_{1,2}$ **(h)** $\mathcal{M}_{2,1}$ **(i)** $\mathcal{M}_{2,2}$

Fig. C.6: Estimation of the monthly location parameter at station Basel/Binningen with the time-dependent models $\mathcal{M}_{0,0},\ldots,\mathcal{M}_{2,2}$ (green) and the monthly S-GEV (red). Note that the model selected was $\mathcal{M}_{2,1}$.

C.1.3 OTL

Location parameter – μ

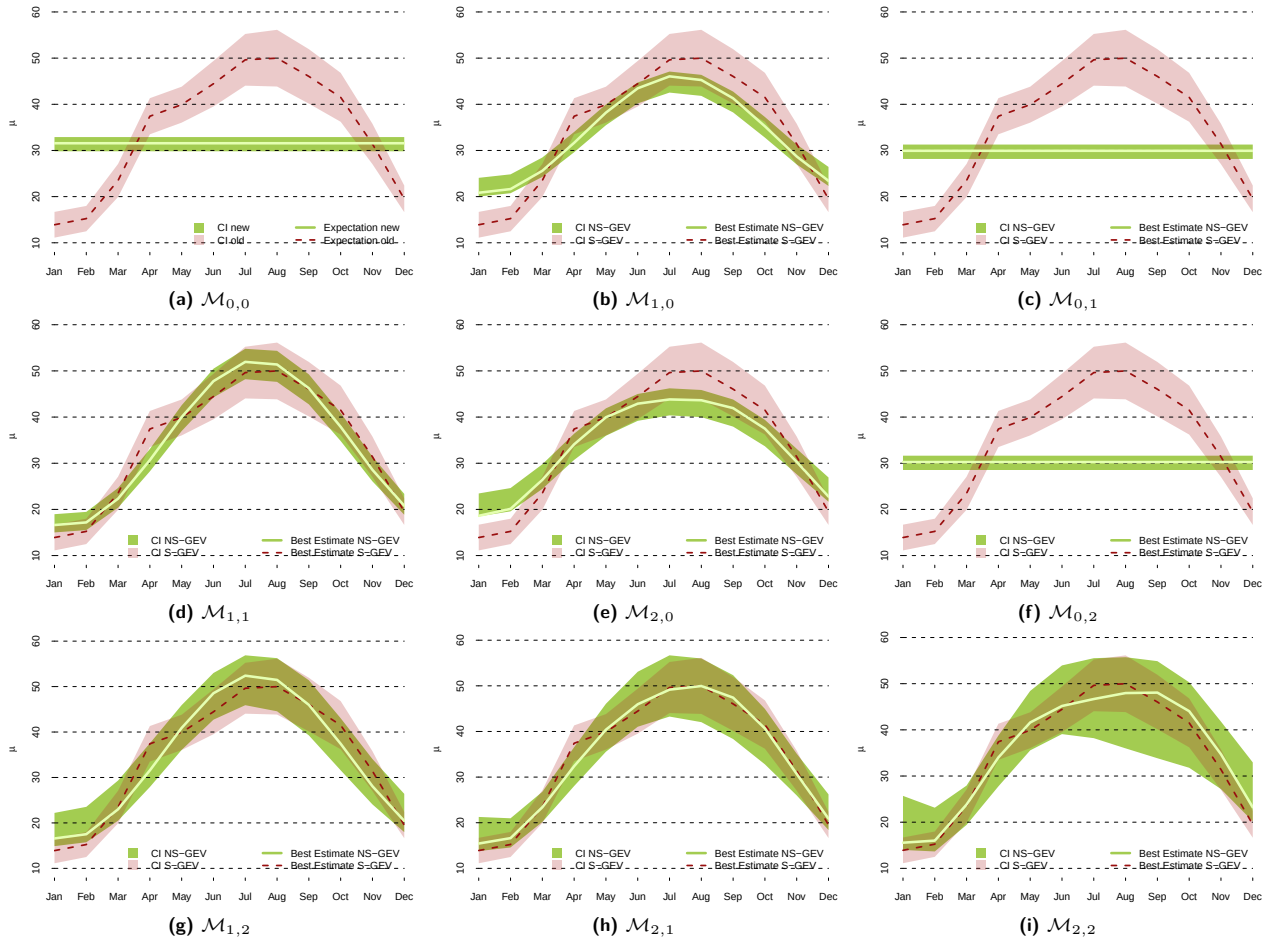

(a) $\mathcal{M}_{0,0}$ (b) $\mathcal{M}_{1,0}$ (c) $\mathcal{M}_{0,1}$

(d) $\mathcal{M}_{1,1}$ (e) $\mathcal{M}_{2,0}$ (f) $\mathcal{M}_{0,2}$

(g) $\mathcal{M}_{1,2}$ (h) $\mathcal{M}_{2,1}$ (i) $\mathcal{M}_{2,2}$

Fig. C.7: Estimation of the monthly location parameter at station Locarno-Monti with the time-dependent models $\mathcal{M}_{0,0},\ldots,\mathcal{M}_{2,2}$ (green) and the monthly S-GEV (red). Note that the model selected was $\mathcal{M}_{1,2}$.

Scale parameter – σ

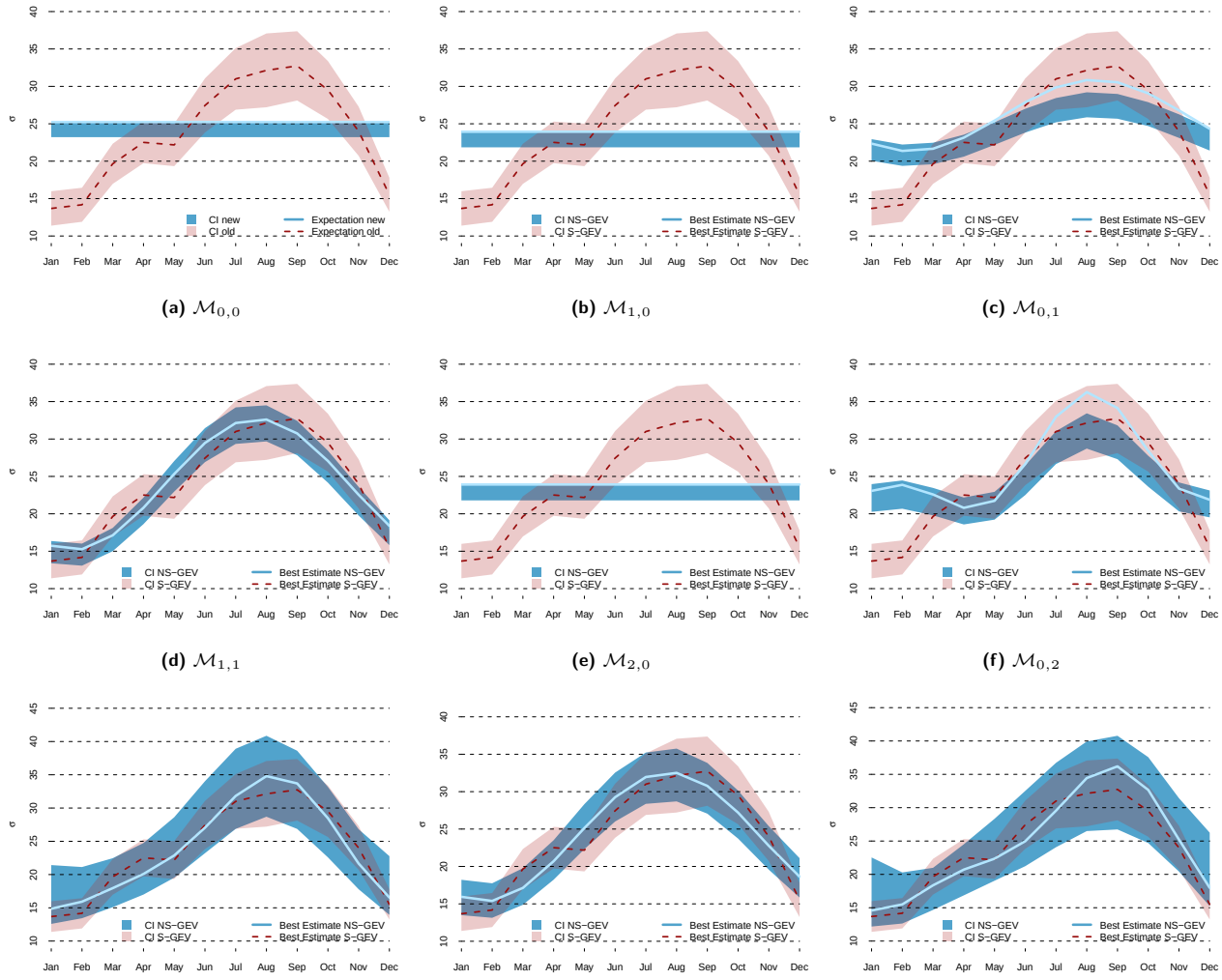

(a) $\mathcal{M}_{0,0}$ **(b)** $\mathcal{M}_{1,0}$ **(c)** $\mathcal{M}_{0,1}$

(d) $\mathcal{M}_{1,1}$ **(e)** $\mathcal{M}_{2,0}$ **(f)** $\mathcal{M}_{0,2}$

(g) $\mathcal{M}_{1,2}$ **(h)** $\mathcal{M}_{2,1}$ **(i)** $\mathcal{M}_{2,2}$

Fig. C.8: Estimation of the monthly location parameter at station Locarno-Monti with the time-dependent models $\mathcal{M}_{0,0},\ldots,\mathcal{M}_{2,2}$ (green) and the monthly S-GEV (red). Note that the model selected was $\mathcal{M}_{1,2}$.

Shape parameter – ξ

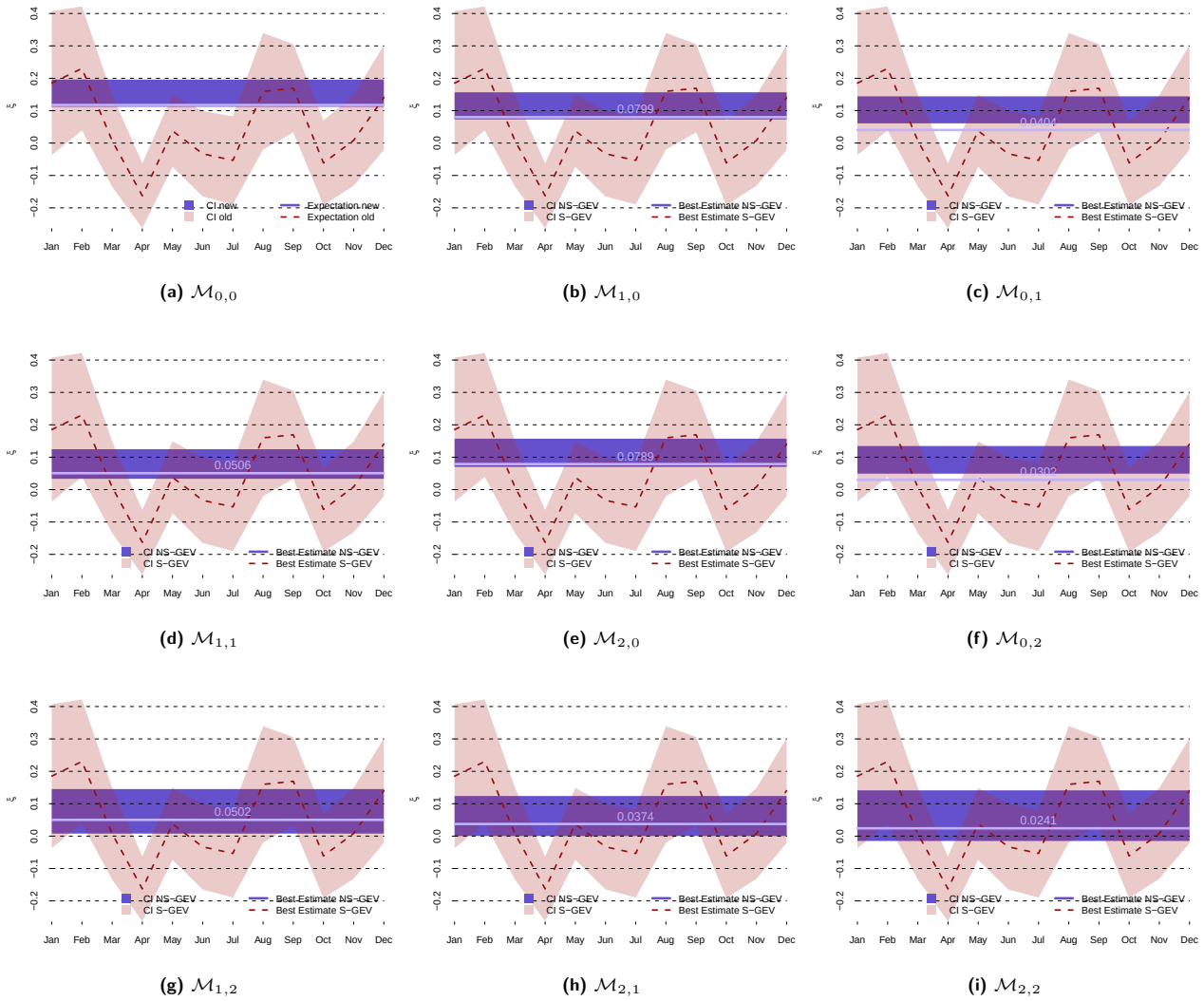

(a) $\mathcal{M}_{0,0}$ **(b)** $\mathcal{M}_{1,0}$ **(c)** $\mathcal{M}_{0,1}$

(d) $\mathcal{M}_{1,1}$ **(e)** $\mathcal{M}_{2,0}$ **(f)** $\mathcal{M}_{0,2}$

(g) $\mathcal{M}_{1,2}$ **(h)** $\mathcal{M}_{2,1}$ **(i)** $\mathcal{M}_{2,2}$

Fig. C.9: Estimation of the monthly location parameter at station Locarno-Monti with the time-dependent models $\mathcal{M}_{0,0},\ldots,\mathcal{M}_{2,2}$ (green) and the monthly S-GEV (red). Note that the model selected was $\mathcal{M}_{1,2}$.

Return Level Plots

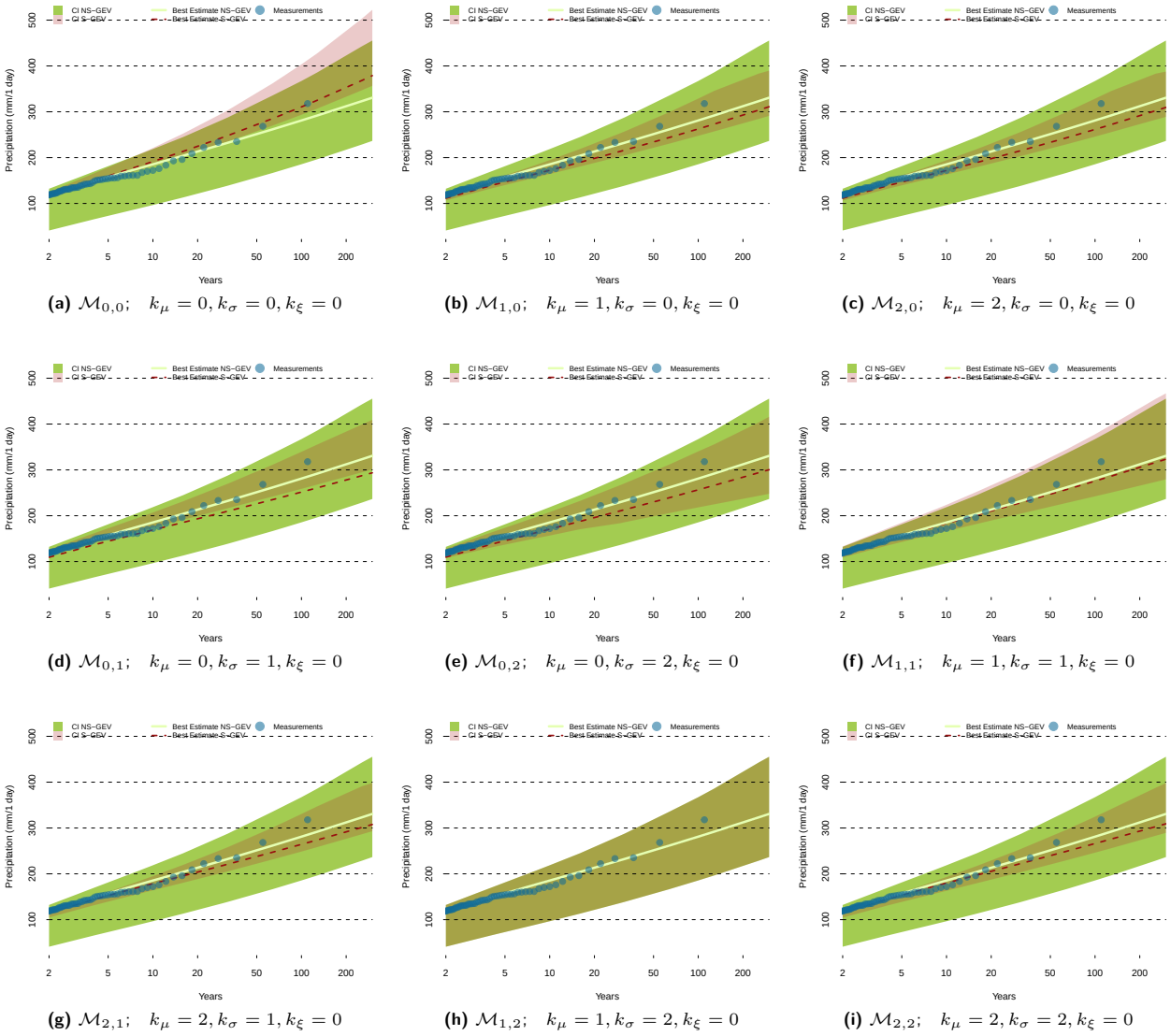

(a) $\mathcal{M}_{0,0}$; $k_\mu = 0, k_\sigma = 0, k_\xi = 0$ **(b)** $\mathcal{M}_{1,0}$; $k_\mu = 1, k_\sigma = 0, k_\xi = 0$ **(c)** $\mathcal{M}_{2,0}$; $k_\mu = 2, k_\sigma = 0, k_\xi = 0$

(d) $\mathcal{M}_{0,1}$; $k_\mu = 0, k_\sigma = 1, k_\xi = 0$ **(e)** $\mathcal{M}_{0,2}$; $k_\mu = 0, k_\sigma = 2, k_\xi = 0$ **(f)** $\mathcal{M}_{1,1}$; $k_\mu = 1, k_\sigma = 1, k_\xi = 0$

(g) $\mathcal{M}_{2,1}$; $k_\mu = 2, k_\sigma = 1, k_\xi = 0$ **(h)** $\mathcal{M}_{1,2}$; $k_\mu = 1, k_\sigma = 2, k_\xi = 0$ **(i)** $\mathcal{M}_{2,2}$; $k_\mu = 2, k_\sigma = 2, k_\xi = 0$

Fig. C.10: Locarno-Monti: Illustration of the model selection's impact on the yearly return levels and the confidence intervals derived from the time dependent NS-GEV. The green areas and the green line represent the 'best model's' best estimate and confidence interval respectively, the red line and area those for the model noted below the figure. Fig. (h) shows no deviation since it compares two times the 'best model'. The blue dots represent real observations.

C.2 Q-Q Plots

C.2.1 La Chaux-de-Fonds

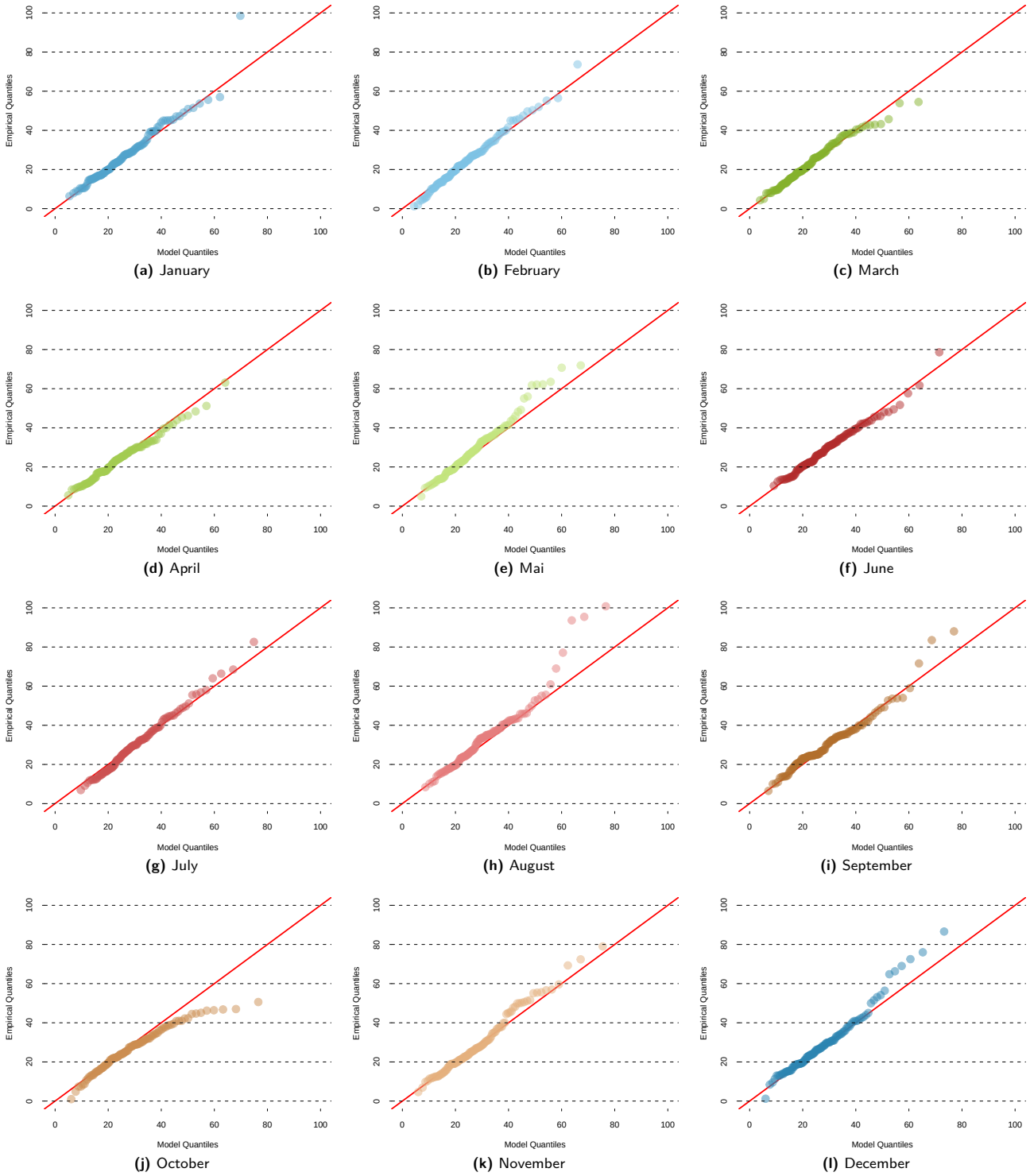

(a) January **(b)** February **(c)** March

(d) April **(e)** Mai **(f)** June

(g) July **(h)** August **(i)** September

(j) October **(k)** November **(l)** December

Fig. C.11: Monthly Q-Q Plots for the optimal model at La Chaux-de-Fonds

C.2.2 Basel/Binningen

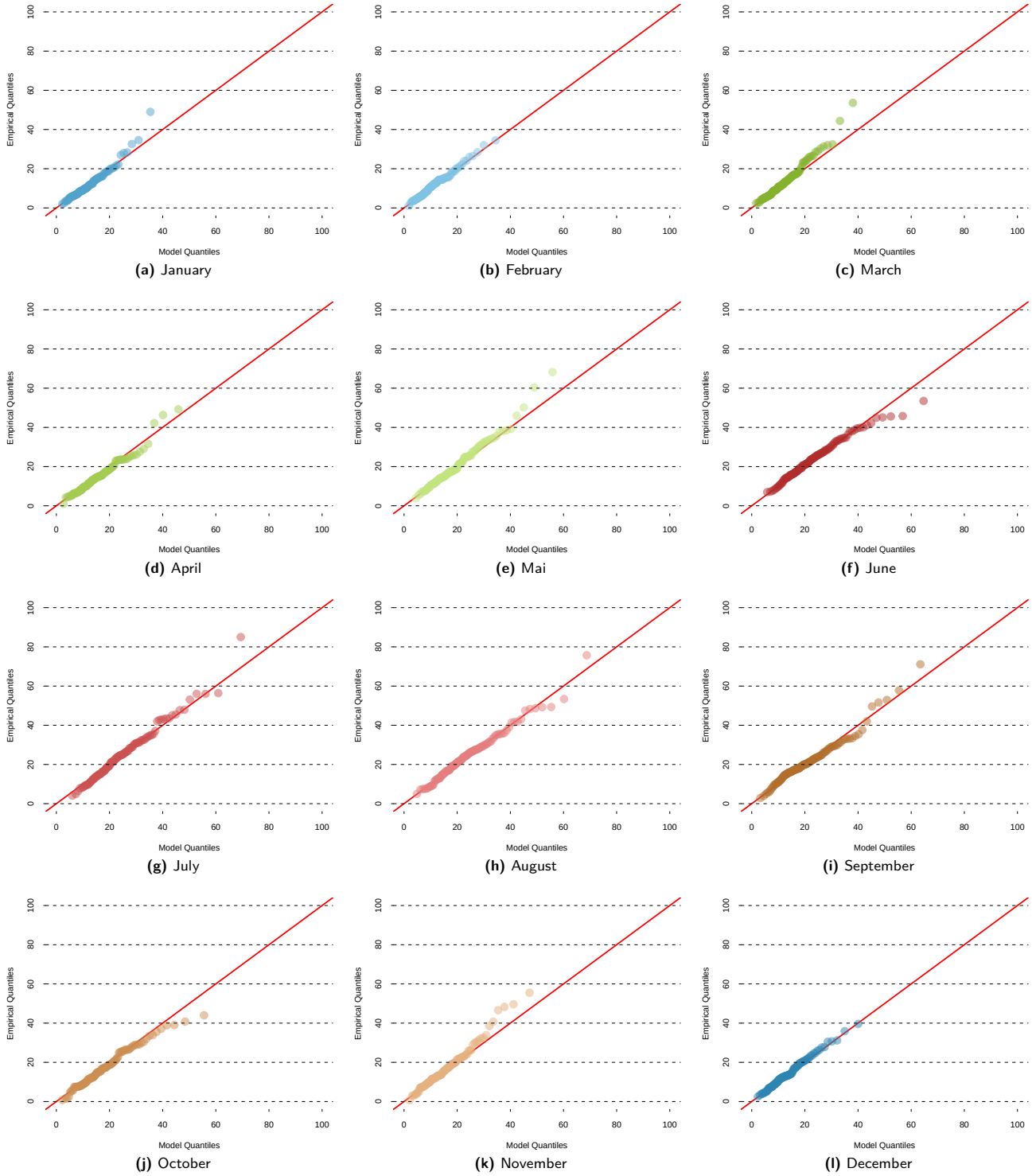

(a) January (b) February (c) March

(d) April (e) Mai (f) June

(g) July (h) August (i) September

(j) October (k) November (l) December

Fig. C.12: Monthly Q-Q Plots for the optimal model at Basel/Binningen

C.2.3 Locarno-Monti

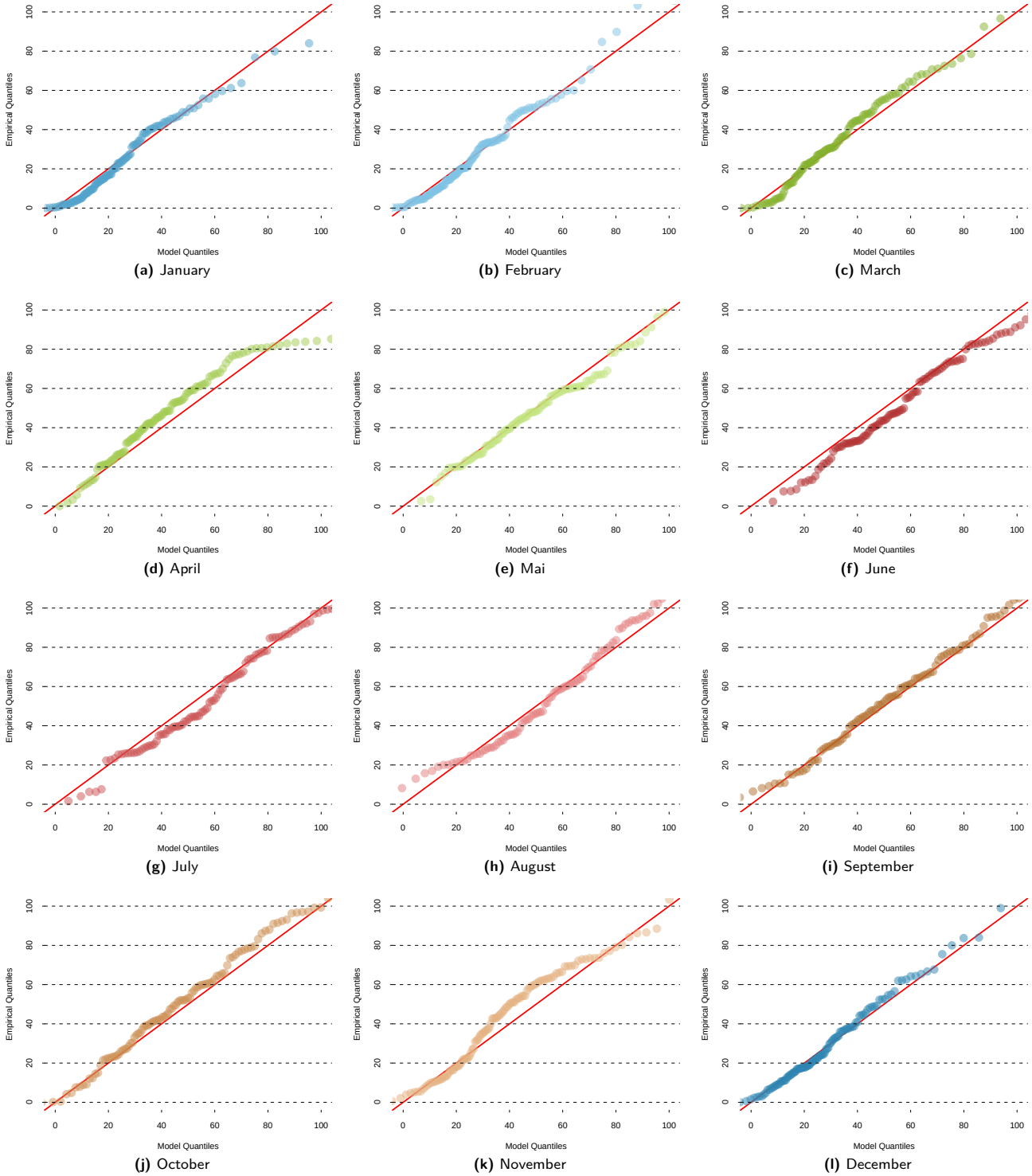

(a) January (b) February (c) March

(d) April (e) Mai (f) June

(g) July (h) August (i) September

(j) October (k) November (l) December

Fig. C.13: Monthly Q-Q Plots for the optimal model at Locarno-Monti

Appendix D Additional Figures: Estimate of Yearly Return Levels

D.1 Daily maxima: Return Level Plots for all Stations

D.1.1 Stations ABE to ALT

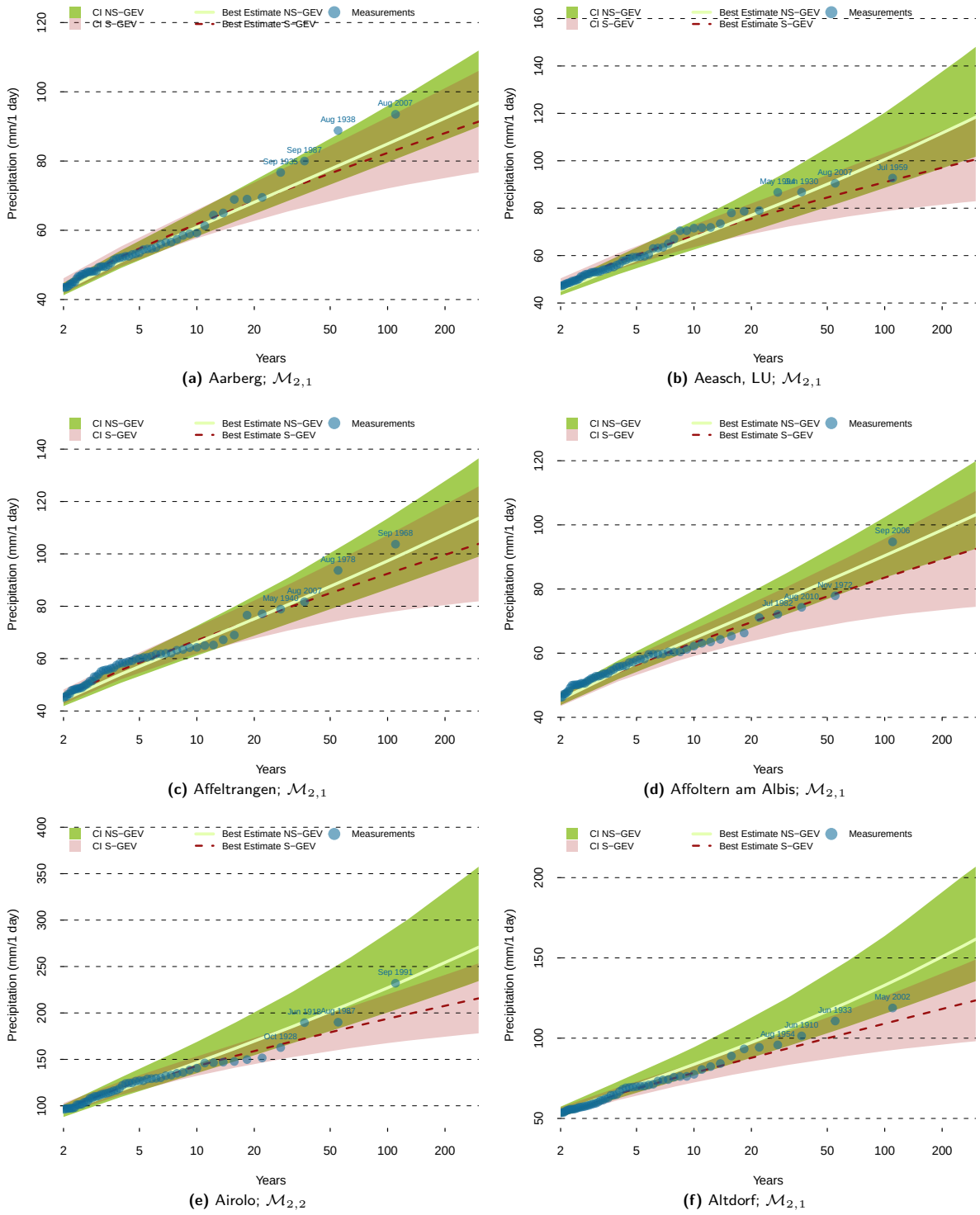

(a) Aarberg; $\mathcal{M}_{2,1}$ **(b)** Aeasch, LU; $\mathcal{M}_{2,1}$

(c) Affeltrangen; $\mathcal{M}_{2,1}$ **(d)** Affoltern am Albis; $\mathcal{M}_{2,1}$

(e) Airolo; $\mathcal{M}_{2,2}$ **(f)** Altdorf; $\mathcal{M}_{2,1}$

Fig. D.1: Return levels of the yearly S-GEV (red) and the NS-GEV (green) model. The areas mark the confidence interval's spread, the lines the best estimates. Blue dots indicate the heaviest yearly precipitation events observed.

D.1.2 Stations APP to BAS

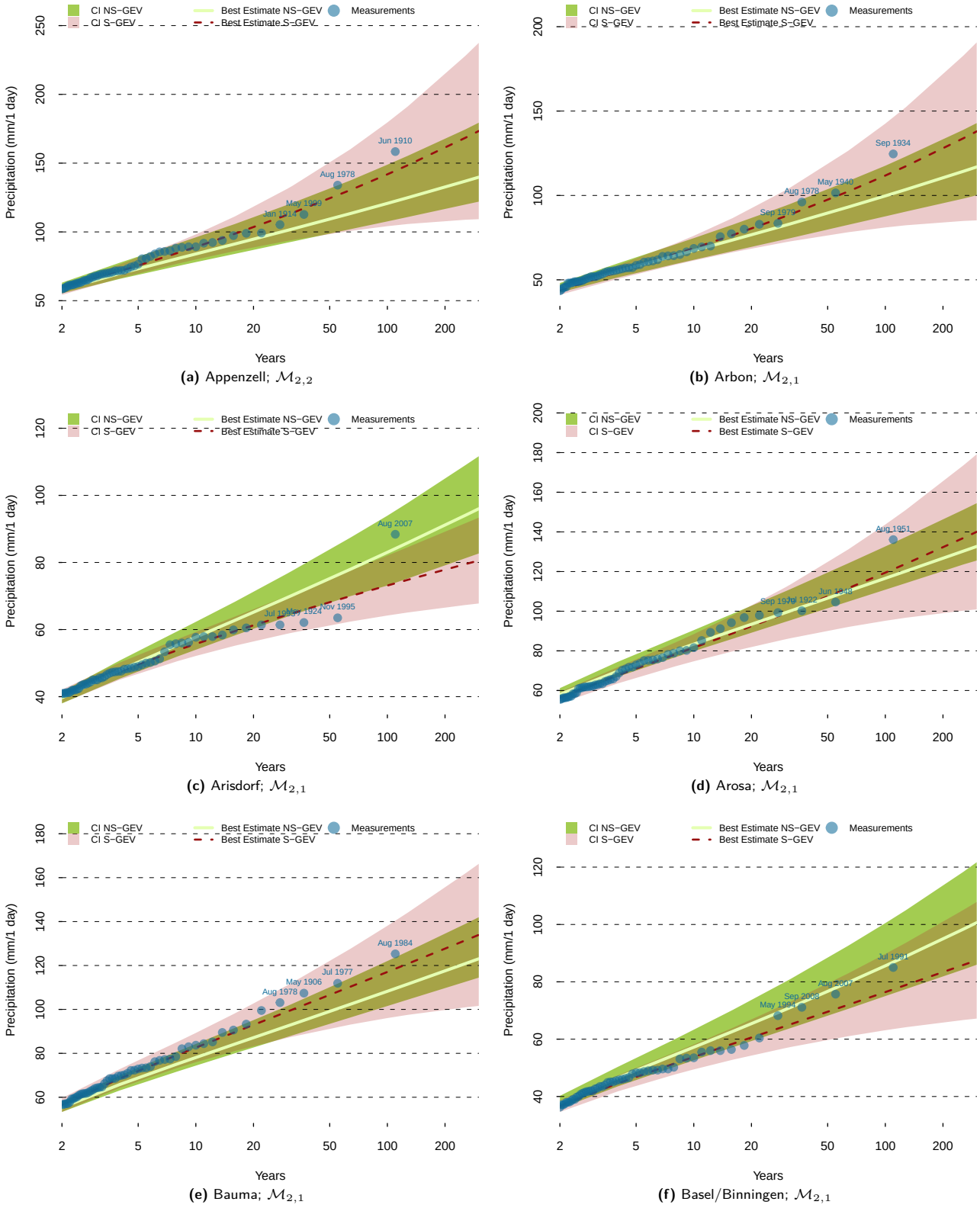

(a) Appenzell; $\mathcal{M}_{2,2}$ (b) Arbon; $\mathcal{M}_{2,1}$

(c) Arisdorf; $\mathcal{M}_{2,1}$ (d) Arosa; $\mathcal{M}_{2,1}$

(e) Bauma; $\mathcal{M}_{2,1}$ (f) Basel/Binningen; $\mathcal{M}_{2,1}$

Fig. D.2: Return levels of the yearly S-GEV (red) and the NS-GEV (green) model. The areas mark the confidence interval's spread, the lines the best estimates. Blue dots indicate the heaviest yearly precipitation events observed.

D.1.3 Stations BER to BLZ

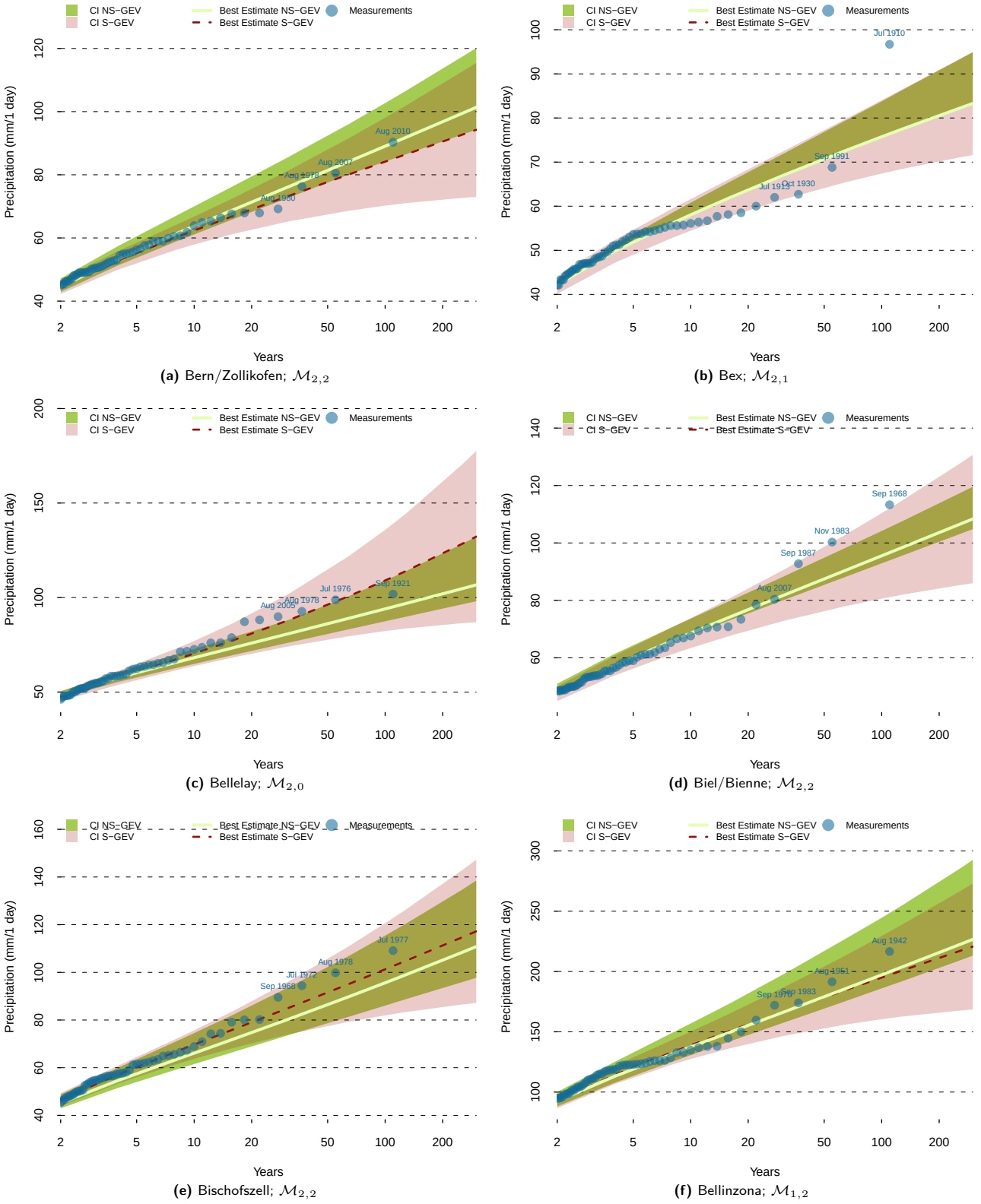

(a) Bern/Zollikofen; $\mathcal{M}_{2,2}$

(b) Bex; $\mathcal{M}_{2,1}$

(c) Bellelay; $\mathcal{M}_{2,0}$

(d) Biel/Bienne; $\mathcal{M}_{2,2}$

(e) Bischofszell; $\mathcal{M}_{2,2}$

(f) Bellinzona; $\mathcal{M}_{1,2}$

Fig. D.3: Return levels of the yearly S-GEV (red) and the NS-GEV (green) model. The areas mark the confidence interval's spread, the lines the best estimates. Blue dots indicate the heaviest yearly precipitation events observed.

D.1.4 Stations BMU to BUC

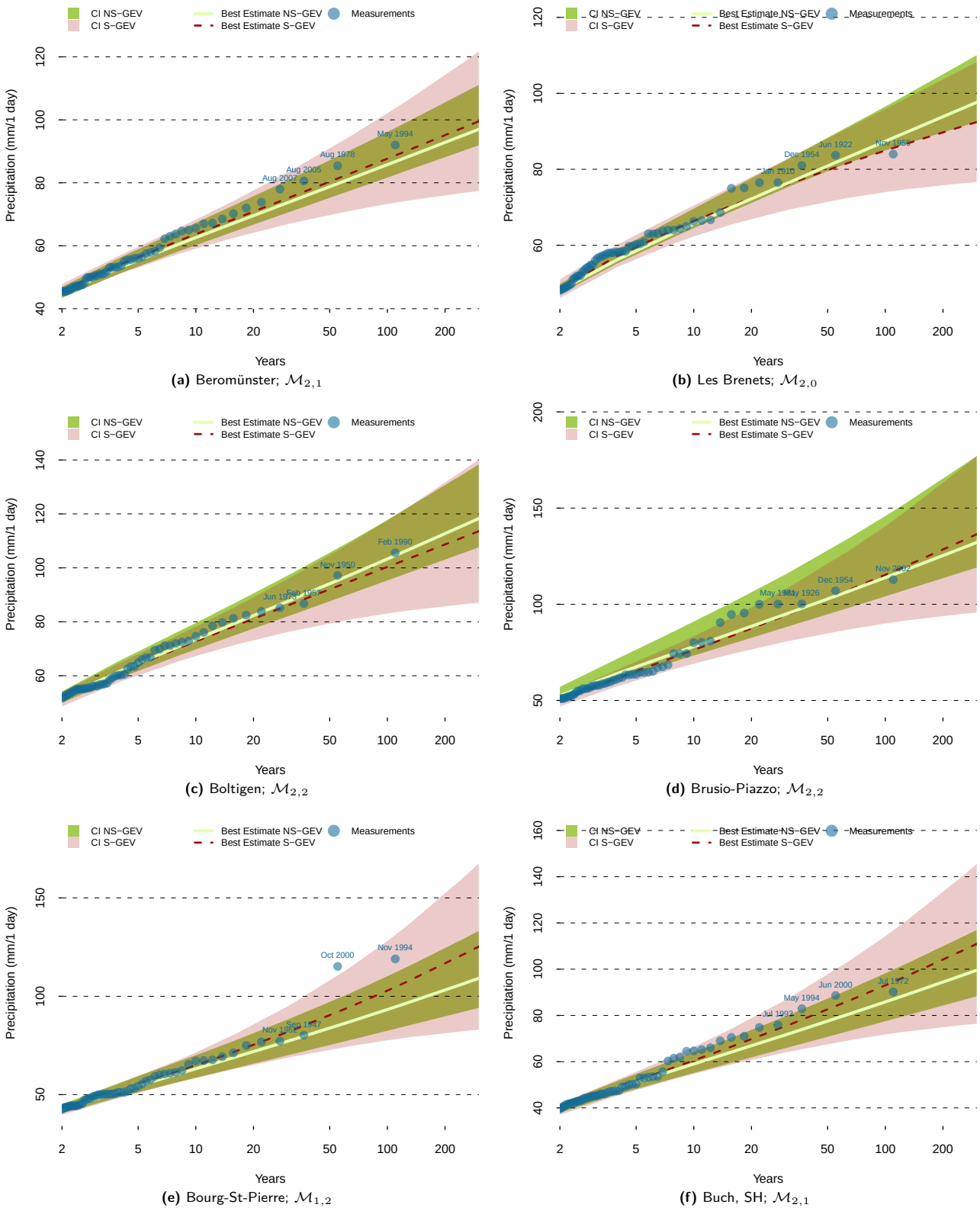

(a) Beromünster; $\mathcal{M}_{2,1}$ **(b)** Les Brenets; $\mathcal{M}_{2,0}$

(c) Boltigen; $\mathcal{M}_{2,2}$ **(d)** Brusio-Piazzo; $\mathcal{M}_{2,2}$

(e) Bourg-St-Pierre; $\mathcal{M}_{1,2}$ **(f)** Buch, SH; $\mathcal{M}_{2,1}$

Fig. D.4: Return levels of the yearly S-GEV (red) and the NS-GEV (green) model. The areas mark the confidence interval's spread, the lines the best estimates. Blue dots indicate the heaviest yearly precipitation events observed.

D.1.5 Stations BUE to CHU

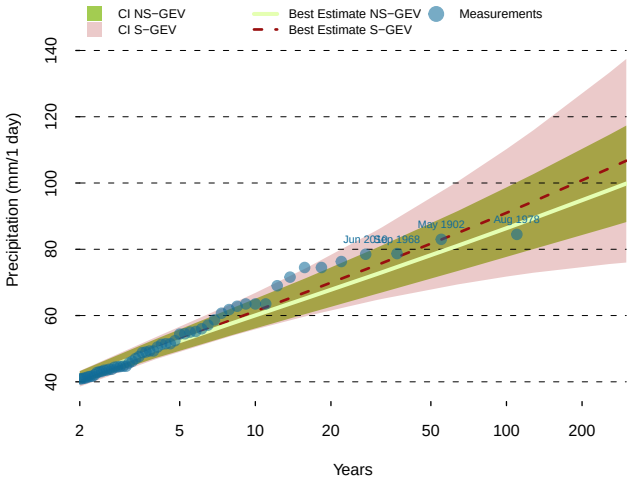

(a) Bülach; $\mathcal{M}_{2,1}$

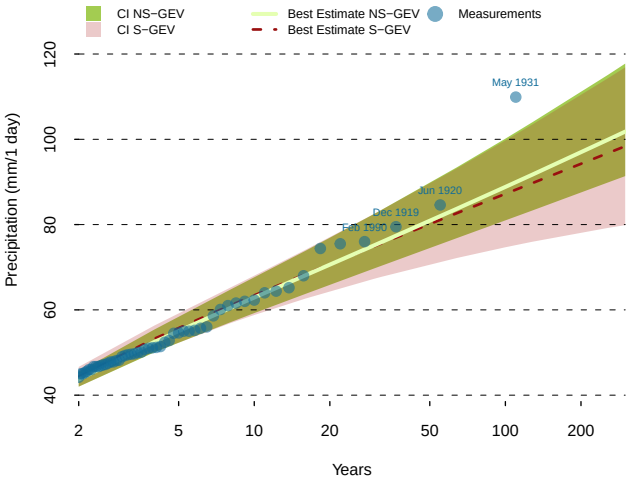

(b) Beznau; $\mathcal{M}_{2,0}$

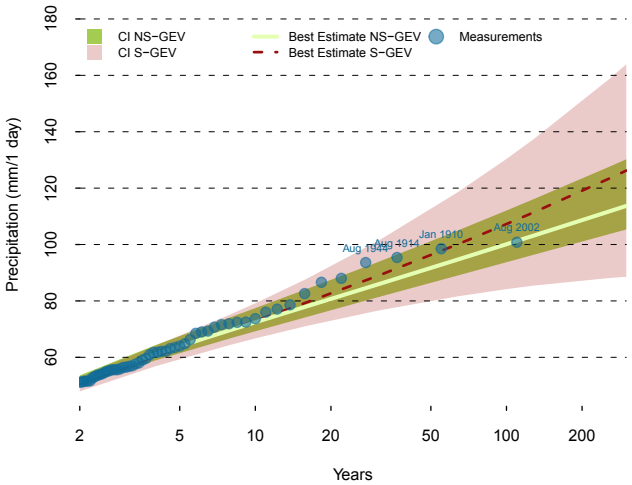

(c) La Chaux-de-Fonds; $\mathcal{M}_{2,1}$

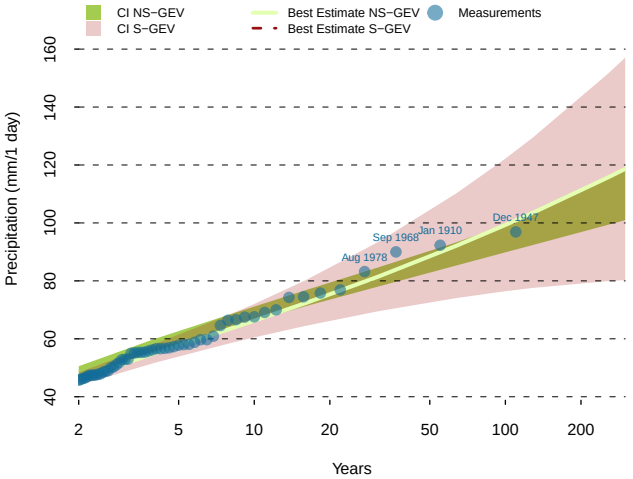

(d) Château-d'Oex; $\mathcal{M}_{2,1}$

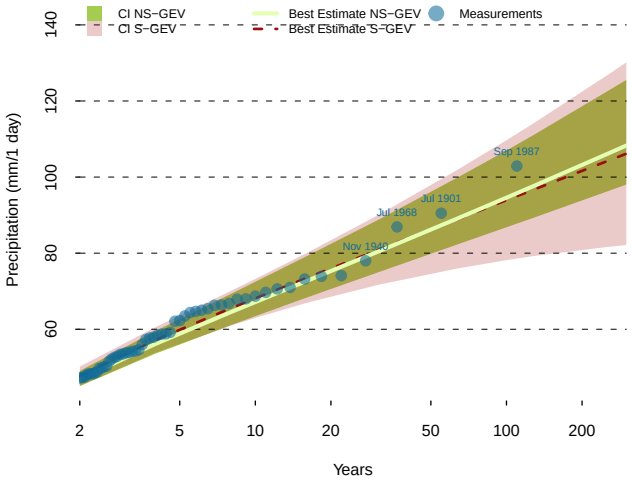

(e) Chaumont; $\mathcal{M}_{2,1}$

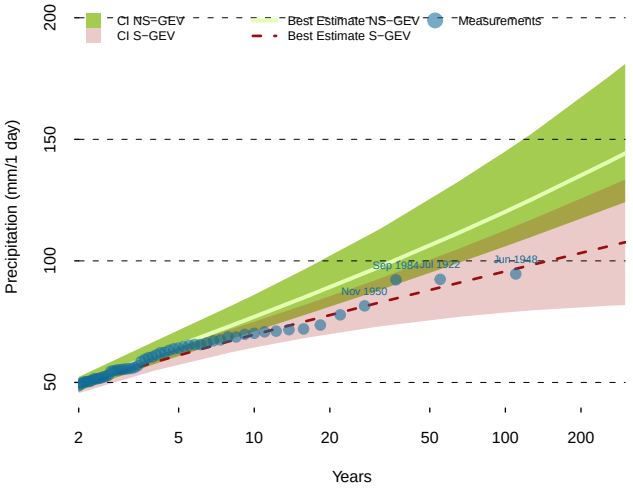

(f) Chur; $\mathcal{M}_{2,1}$

Fig. D.5: Return levels of the yearly S-GEV (red) and the NS-GEV (green) model. The areas mark the confidence interval's spread, the lines the best estimates. Blue dots indicate the heaviest yearly precipitation events observed.

D.1.6 Stations COS to EIN

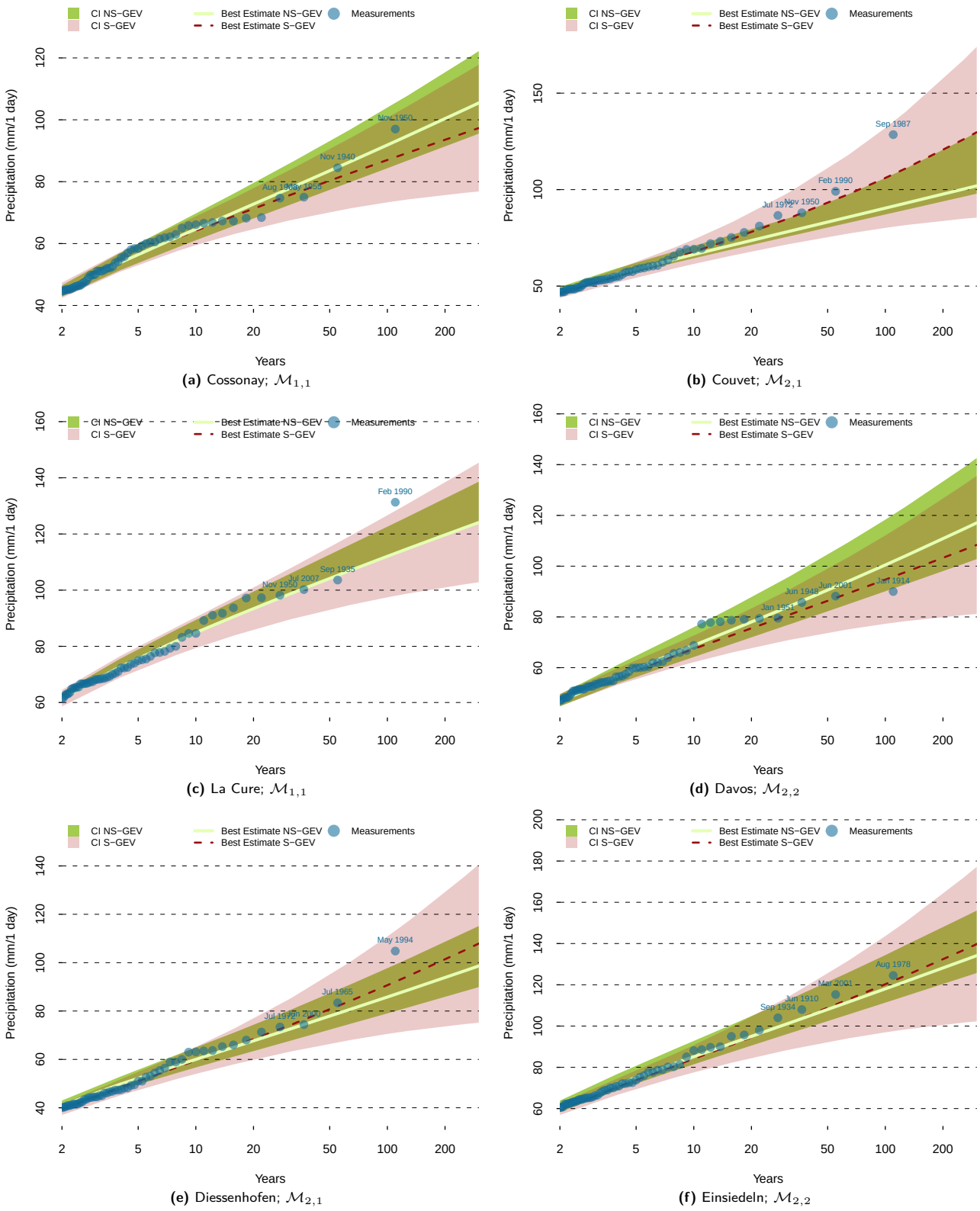

(a) Cossonay; $\mathcal{M}_{1,1}$ **(b)** Couvet; $\mathcal{M}_{2,1}$

(c) La Cure; $\mathcal{M}_{1,1}$ **(d)** Davos; $\mathcal{M}_{2,2}$

(e) Diessenhofen; $\mathcal{M}_{2,1}$ **(f)** Einsiedeln; $\mathcal{M}_{2,2}$

Fig. D.6: Return levels of the yearly S-GEV (red) and the NS-GEV (green) model. The areas mark the confidence interval's spread, the lines the best estimates. Blue dots indicate the heaviest yearly precipitation events observed.

D.1.7 Stations EKO to ESZ

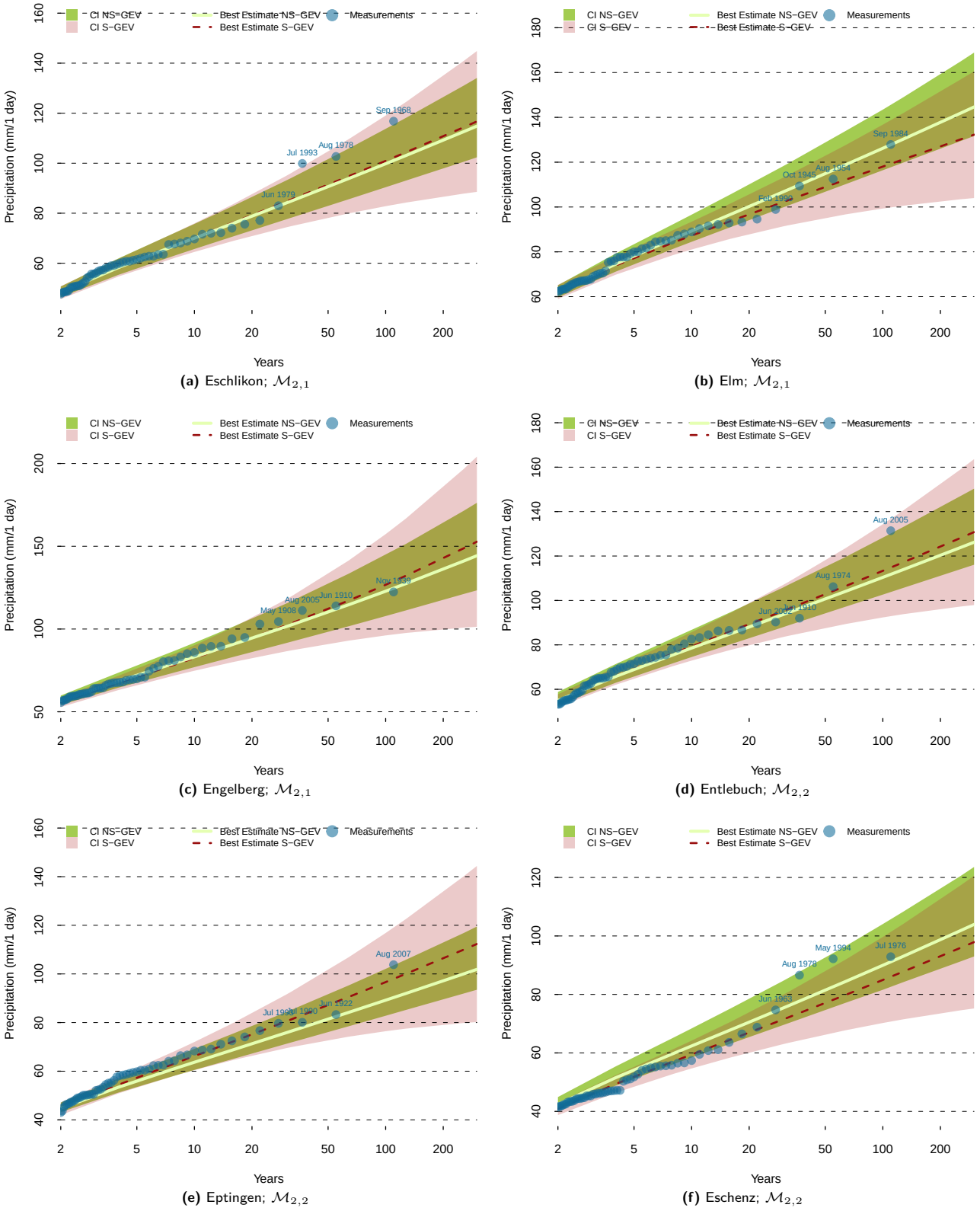

(a) Eschlikon; $\mathcal{M}_{2,1}$ **(b)** Elm; $\mathcal{M}_{2,1}$

(c) Engelberg; $\mathcal{M}_{2,1}$ **(d)** Entlebuch; $\mathcal{M}_{2,2}$

(e) Eptingen; $\mathcal{M}_{2,2}$ **(f)** Eschenz; $\mathcal{M}_{2,2}$

Fig. D.7: Return levels of the yearly S-GEV (red) and the NS-GEV (green) model. The areas mark the confidence interval's spread, the lines the best estimates. Blue dots indicate the heaviest yearly precipitation events observed.

D.1.8 Stations FLW to GSB

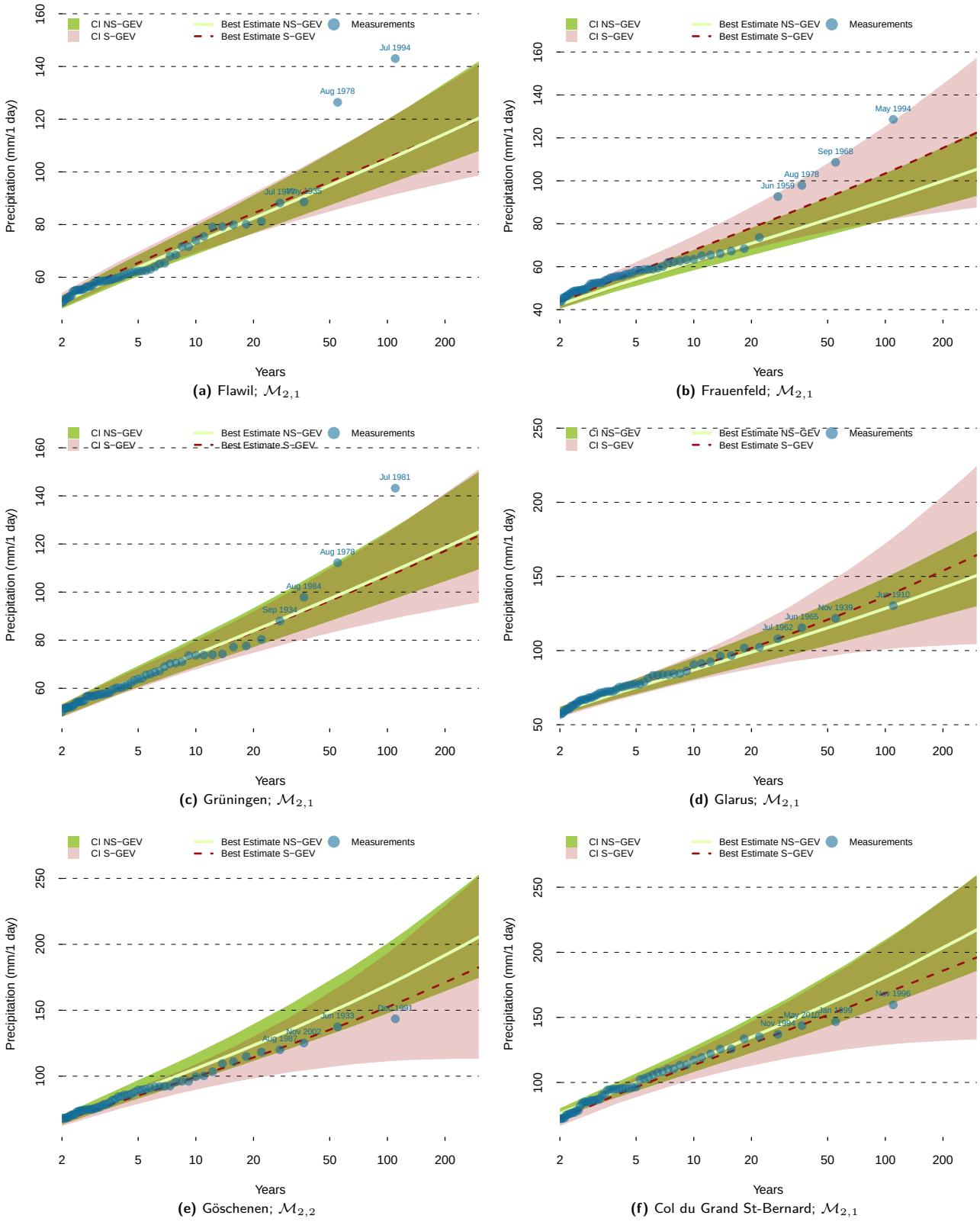

(a) Flawil; $\mathcal{M}_{2,1}$ **(b)** Frauenfeld; $\mathcal{M}_{2,1}$

(c) Grüningen; $\mathcal{M}_{2,1}$ **(d)** Glarus; $\mathcal{M}_{2,1}$

(e) Göschenen; $\mathcal{M}_{2,2}$ **(f)** Col du Grand St-Bernard; $\mathcal{M}_{2,1}$

Fig. D.8: Return levels of the yearly S-GEV (red) and the NS-GEV (green) model. The areas mark the confidence interval's spread, the lines the best estimates. Blue dots indicate the heaviest yearly precipitation events observed.

D.1.9 Stations GTT to INT

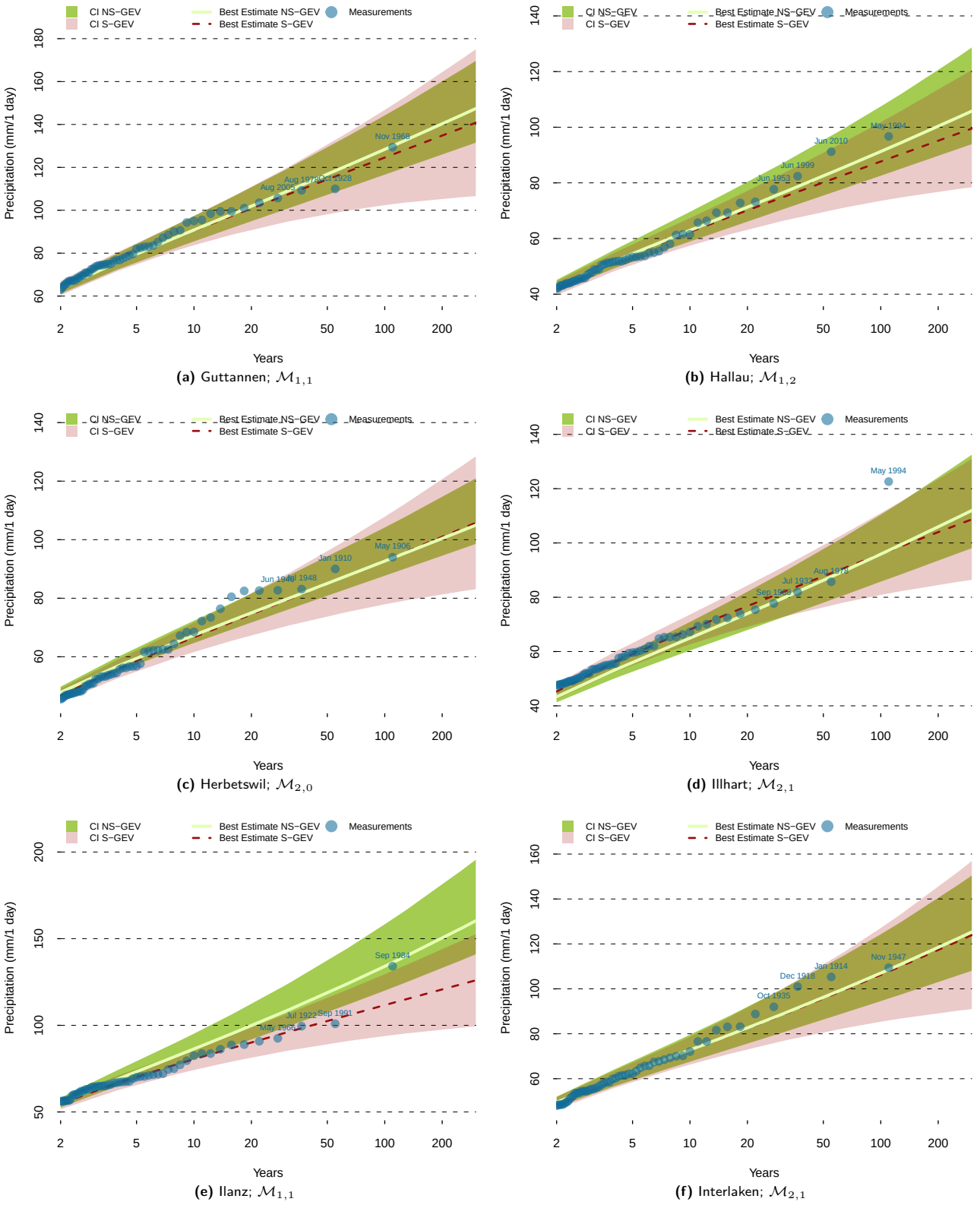

(a) Guttannen; $\mathcal{M}_{1,1}$ **(b)** Hallau; $\mathcal{M}_{1,2}$

(c) Herbetswil; $\mathcal{M}_{2,0}$ **(d)** Illhart; $\mathcal{M}_{2,1}$

(e) Ilanz; $\mathcal{M}_{1,1}$ **(f)** Interlaken; $\mathcal{M}_{2,1}$

Fig. D.9: Return levels of the yearly S-GEV (red) and the NS-GEV (green) model. The areas mark the confidence interval's spread, the lines the best estimates. Blue dots indicate the heaviest yearly precipitation events observed.

D.1.10 Stations JUS to LAG

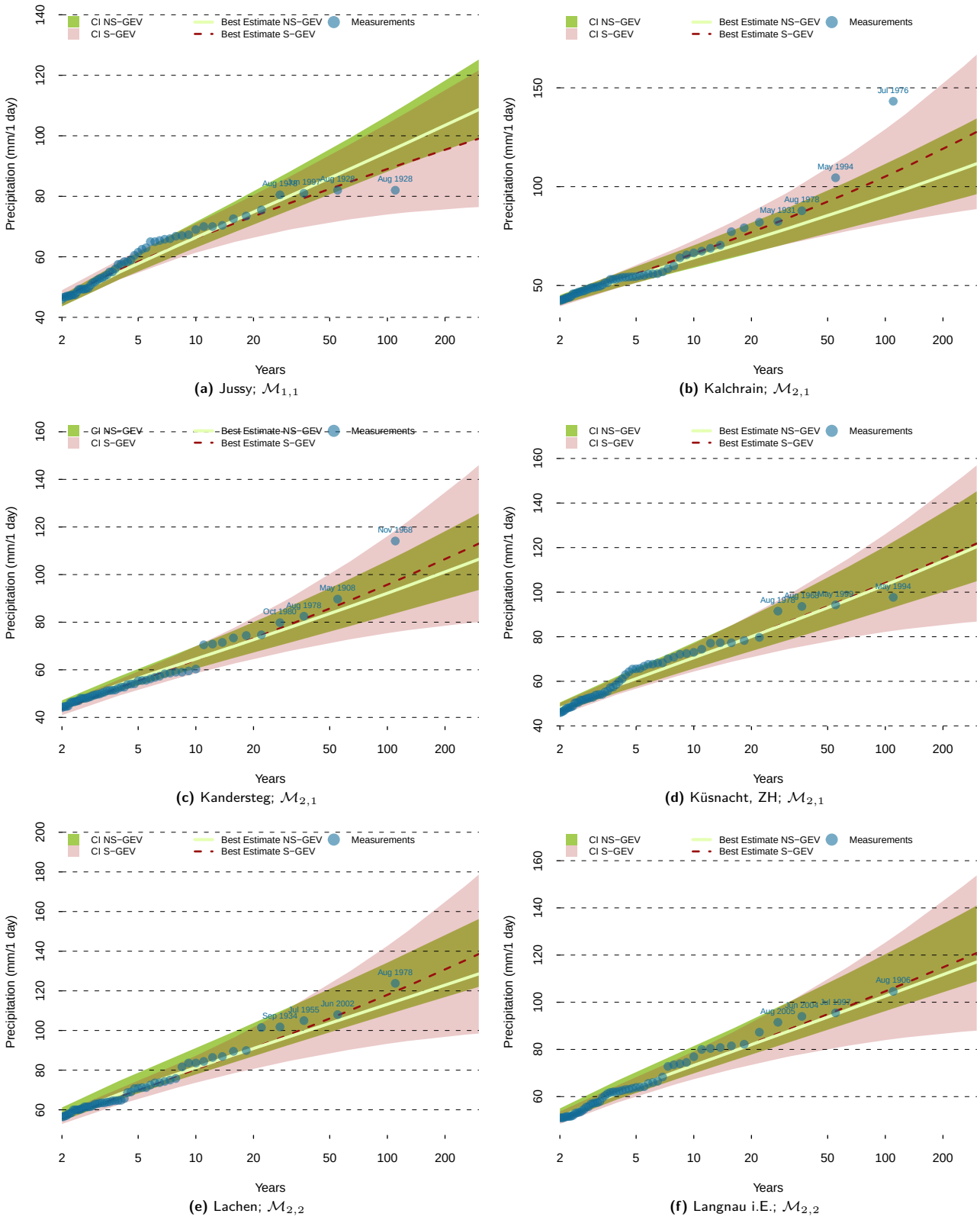

(a) Jussy; $\mathcal{M}_{1,1}$ (b) Kalchrain; $\mathcal{M}_{2,1}$

(c) Kandersteg; $\mathcal{M}_{2,1}$ (d) Küsnacht, ZH; $\mathcal{M}_{2,1}$

(e) Lachen; $\mathcal{M}_{2,2}$ (f) Langnau i.E.; $\mathcal{M}_{2,2}$

Fig. D.10: Return levels of the yearly S-GEV (red) and the NS-GEV (green) model. The areas mark the confidence interval's spread, the lines the best estimates. Blue dots indicate the heaviest yearly precipitation events observed.

D.1.11 Stations LEU to LUZ

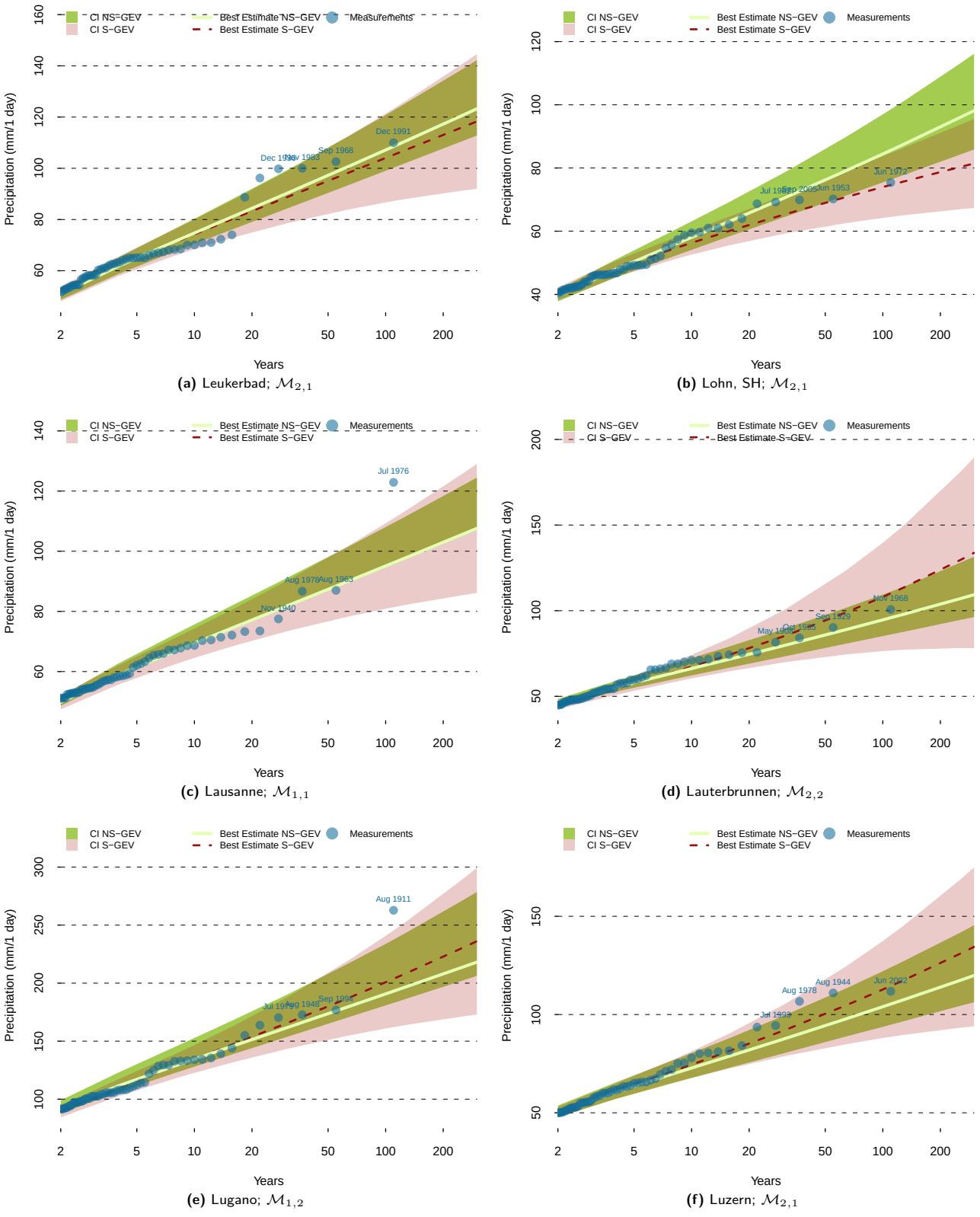

(a) Leukerbad; $\mathcal{M}_{2,1}$ **(b)** Lohn, SH; $\mathcal{M}_{2,1}$

(c) Lausanne; $\mathcal{M}_{1,1}$ **(d)** Lauterbrunnen; $\mathcal{M}_{2,2}$

(e) Lugano; $\mathcal{M}_{1,2}$ **(f)** Luzern; $\mathcal{M}_{2,1}$

Fig. D.11: Return levels of the yearly S-GEV (red) and the NS-GEV (green) model. The areas mark the confidence interval's spread, the lines the best estimates. Blue dots indicate the heaviest yearly precipitation events observed.

D.1.12 Stations MER to NEU

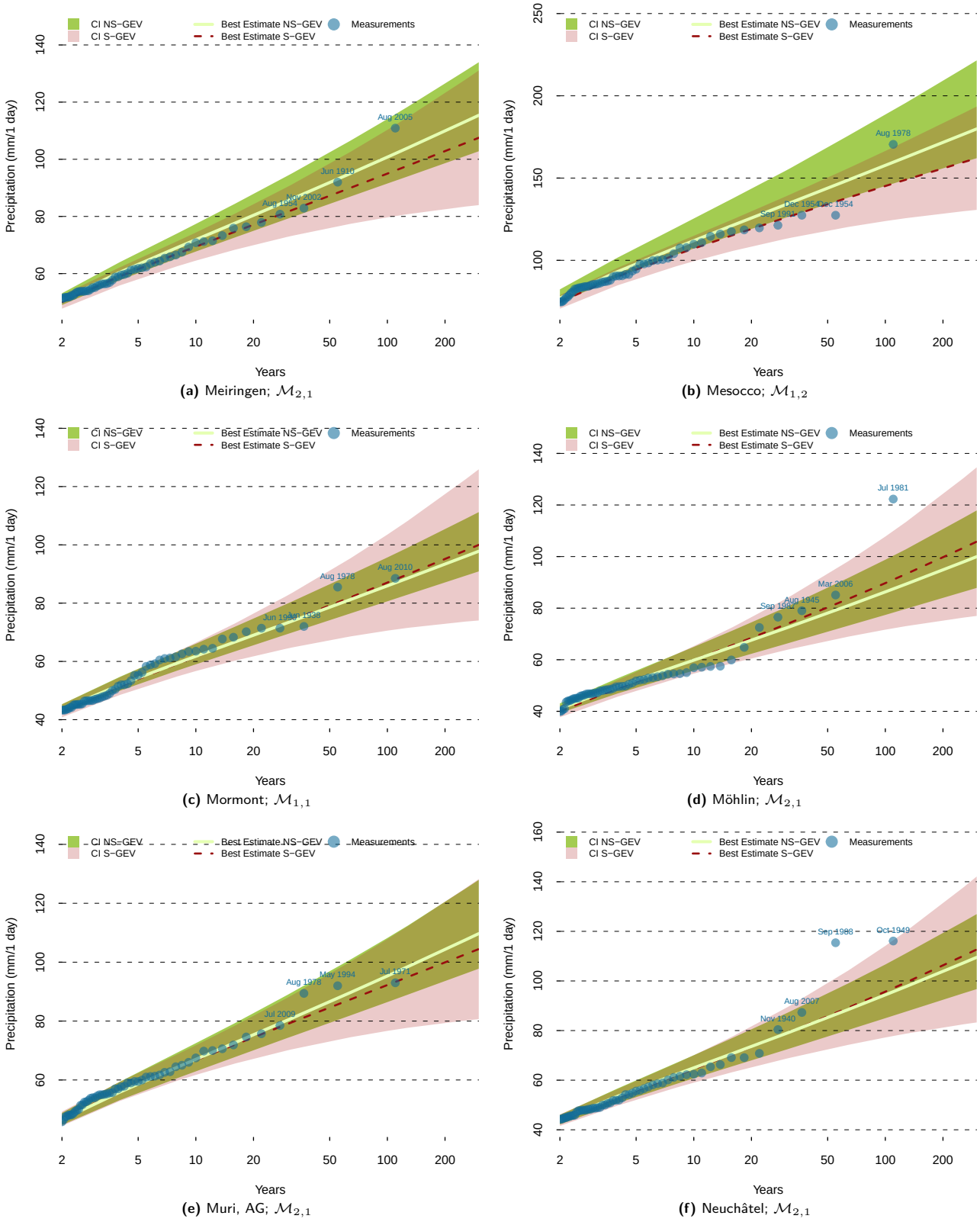

(a) Meiringen; $\mathcal{M}_{2,1}$ **(b)** Mesocco; $\mathcal{M}_{1,2}$

(c) Mormont; $\mathcal{M}_{1,1}$ **(d)** Möhlin; $\mathcal{M}_{2,1}$

(e) Muri, AG; $\mathcal{M}_{2,1}$ **(f)** Neuchâtel; $\mathcal{M}_{2,1}$

Fig. D.12: Return levels of the yearly S-GEV (red) and the NS-GEV (green) model. The areas mark the confidence interval's spread, the lines the best estimates. Blue dots indicate the heaviest yearly precipitation events observed.

D.1.13 Stations NIE to SAR

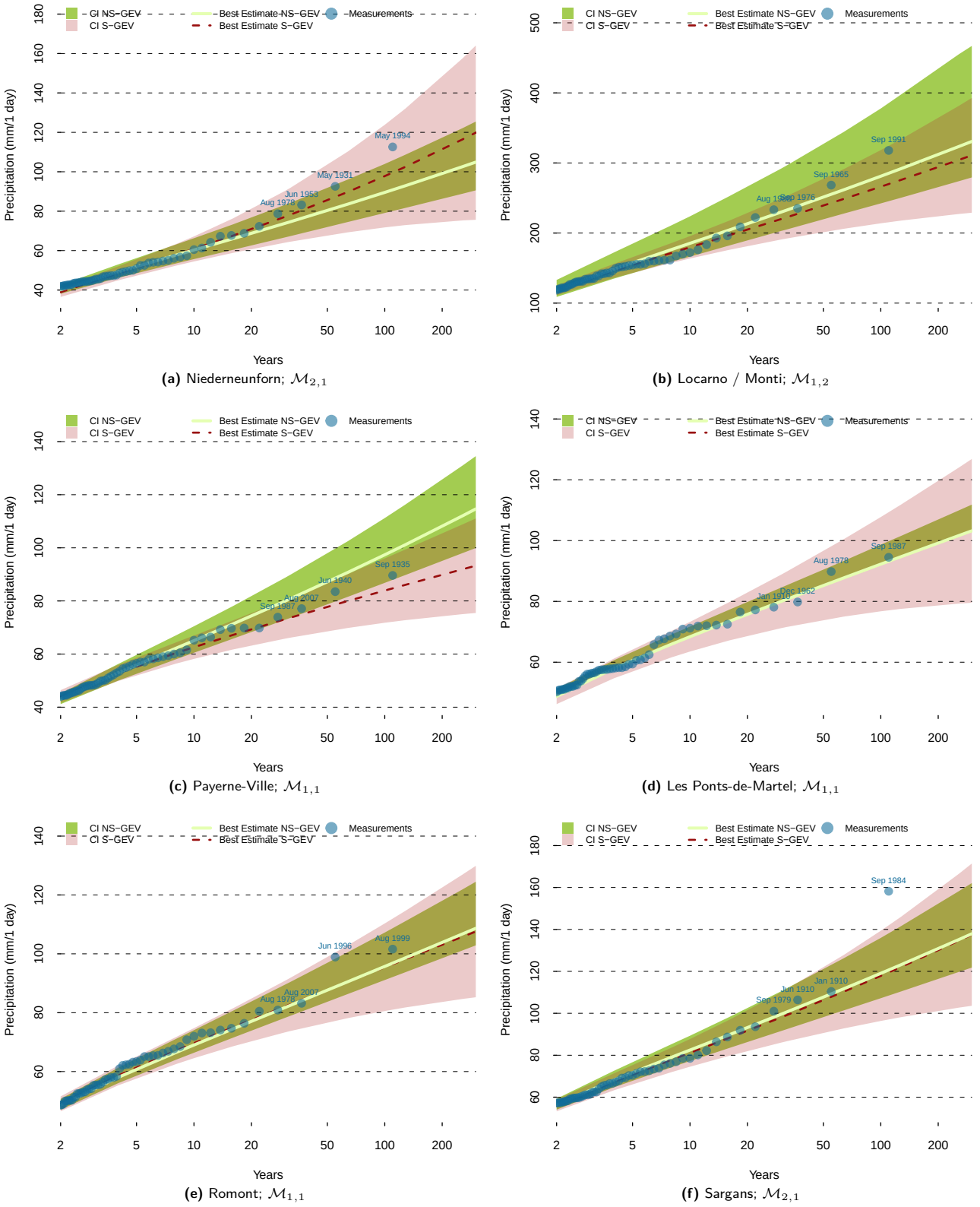

(a) Niederneunforn; $\mathcal{M}_{2,1}$ **(b)** Locarno / Monti; $\mathcal{M}_{1,2}$

(c) Payerne-Ville; $\mathcal{M}_{1,1}$ **(d)** Les Ponts-de-Martel; $\mathcal{M}_{1,1}$

(e) Romont; $\mathcal{M}_{1,1}$ **(f)** Sargans; $\mathcal{M}_{2,1}$

Fig. D.13: Return levels of the yearly S-GEV (red) and the NS-GEV (green) model. The areas mark the confidence interval's spread, the lines the best estimates. Blue dots indicate the heaviest yearly precipitation events observed.

D.1.14 Stations SCH to SMM

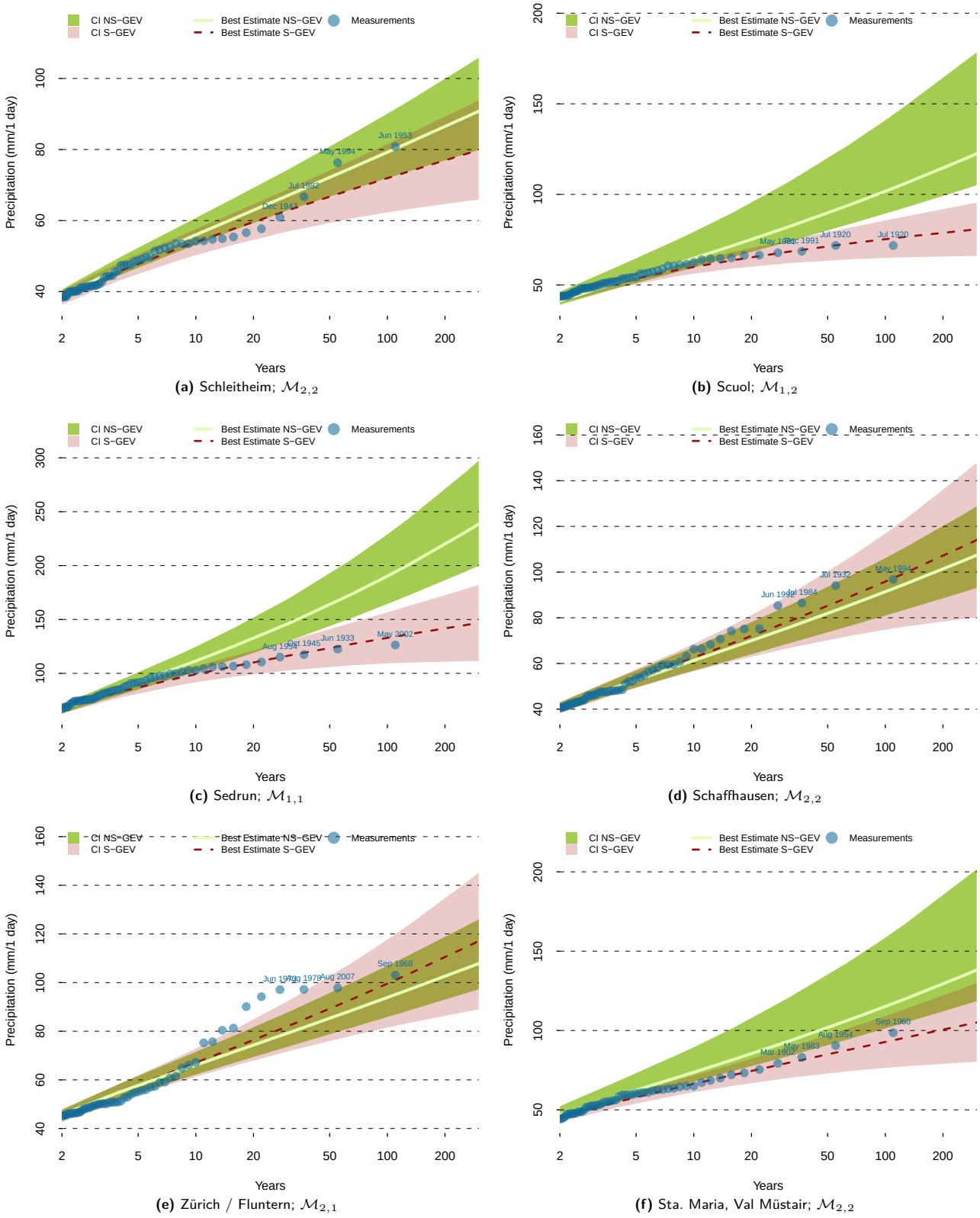

(a) Schleitheim; $\mathcal{M}_{2,2}$ **(b)** Scuol; $\mathcal{M}_{1,2}$

(c) Sedrun; $\mathcal{M}_{1,1}$ **(d)** Schaffhausen; $\mathcal{M}_{2,2}$

(e) Zürich / Fluntern; $\mathcal{M}_{2,1}$ **(f)** Sta. Maria, Val Müstair; $\mathcal{M}_{2,2}$

Fig. D.14: Return levels of the yearly S-GEV (red) and the NS-GEV (green) model. The areas mark the confidence interval's spread, the lines the best estimates. Blue dots indicate the heaviest yearly precipitation events observed.

D.1.15 Stations SOG to THU

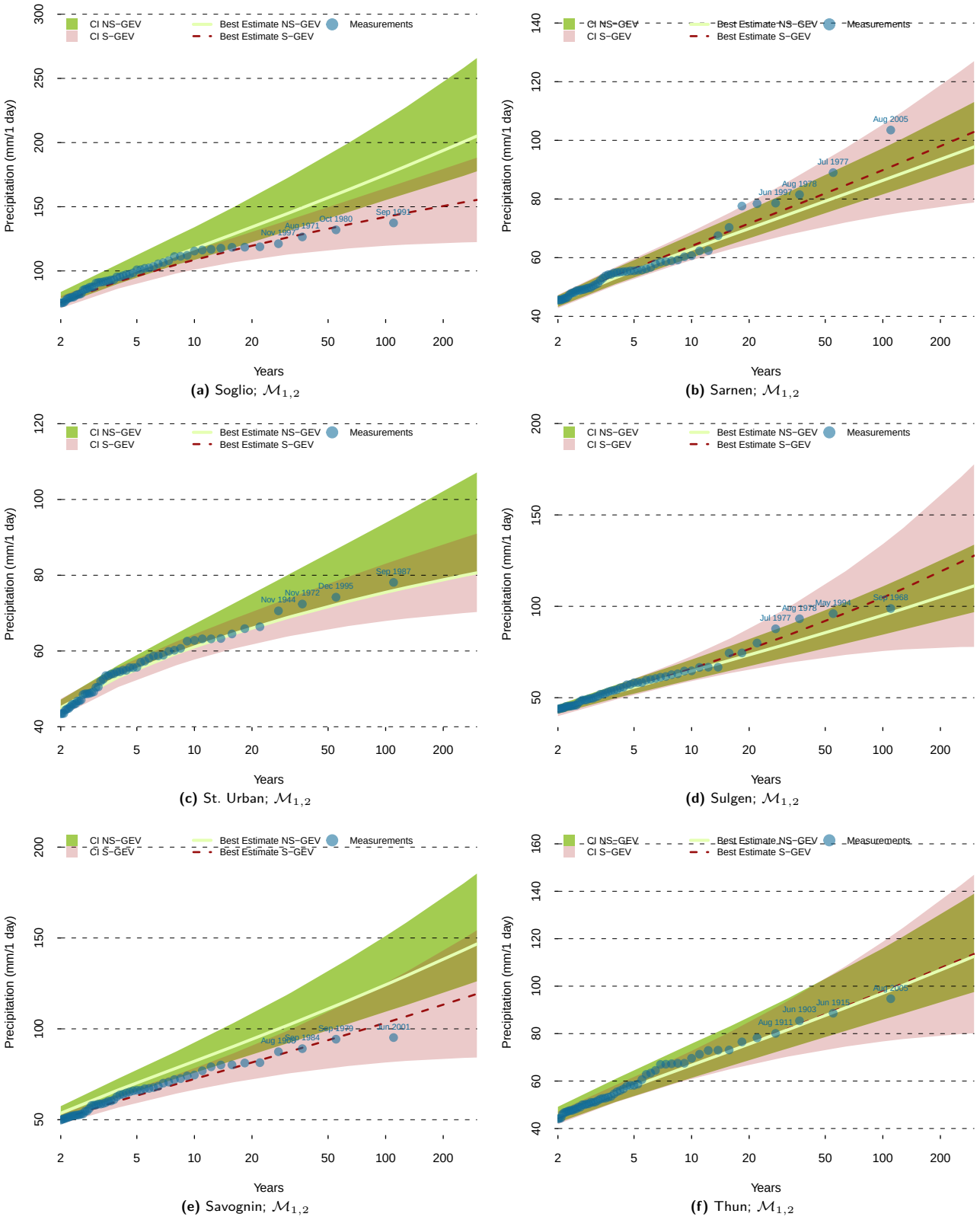

(a) Soglio; $\mathcal{M}_{1,2}$ **(b)** Sarnen; $\mathcal{M}_{1,2}$

(c) St. Urban; $\mathcal{M}_{1,2}$ **(d)** Sulgen; $\mathcal{M}_{1,2}$

(e) Savognin; $\mathcal{M}_{1,2}$ **(f)** Thun; $\mathcal{M}_{1,2}$

Fig. D.15: Return levels of the yearly S-GEV (red) and the NS-GEV (green) model. The areas mark the confidence interval's spread, the lines the best estimates. Blue dots indicate the heaviest yearly precipitation events observed.

D.1.16 Stations UNK to WIN

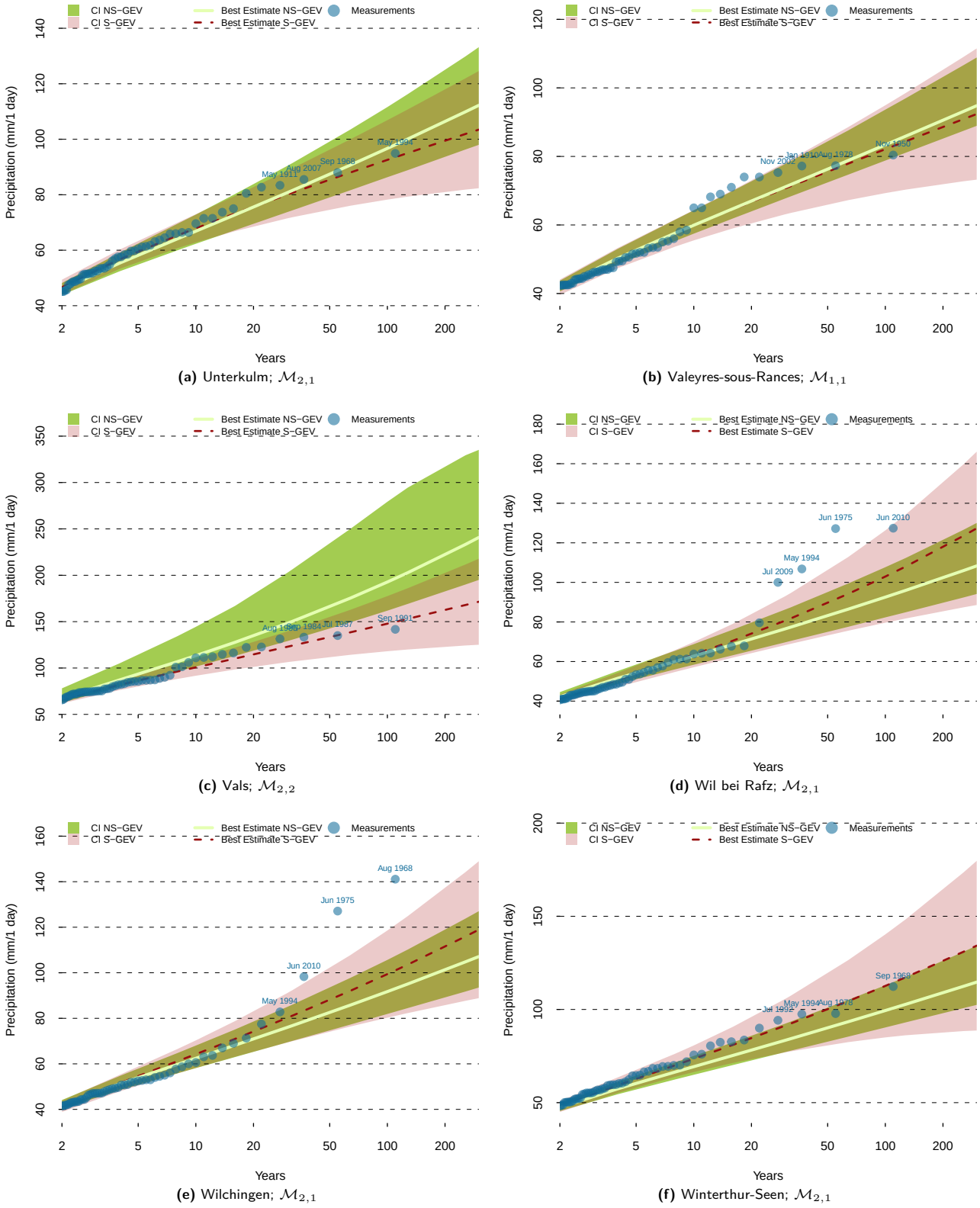

(a) Unterkulm; $\mathcal{M}_{2,1}$ **(b)** Valeyres-sous-Rances; $\mathcal{M}_{1,1}$

(c) Vals; $\mathcal{M}_{2,2}$ **(d)** Wil bei Rafz; $\mathcal{M}_{2,1}$

(e) Wilchingen; $\mathcal{M}_{2,1}$ **(f)** Winterthur-Seen; $\mathcal{M}_{2,1}$

Fig. D.16: Return levels of the yearly S-GEV (red) and the NS-GEV (green) model. The areas mark the confidence interval's spread, the lines the best estimates. Blue dots indicate the heaviest yearly precipitation events observed.

D.1.17 Stations ZER

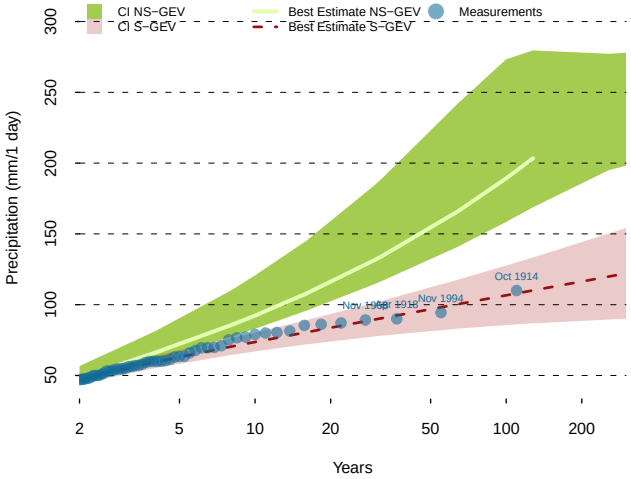

(a) Zermatt; $\mathcal{M}_{2,2}$

Fig. D.17: This plot compares return levels of the yearly S-GEV (red) and the NS-GEV (green) model. The areas mark the confidence interval's spread, the lines the best estimates. Blue dots indicate the heaviest precipitation events within the observations.

D.2 Results for Different Time Scales in CDF, BAS and OTL

D.2.1 1 hour maxima

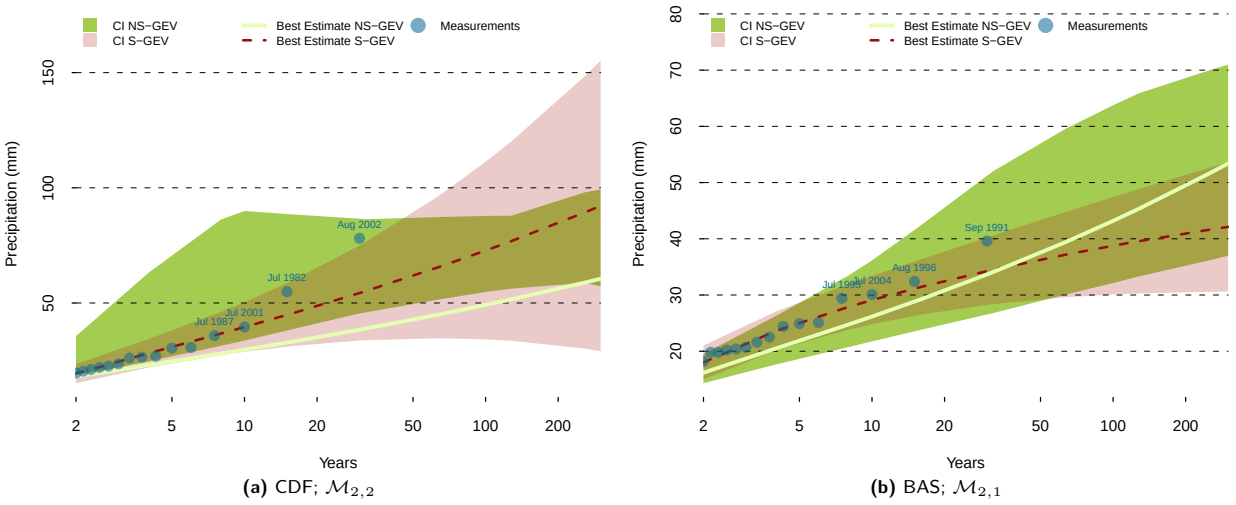

(a) CDF; $\mathcal{M}_{2,2}$ **(b)** BAS; $\mathcal{M}_{2,1}$

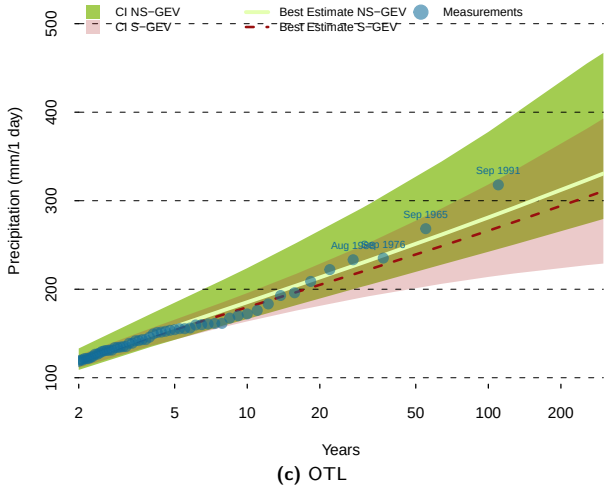

(c) OTL

Fig. D.18: Return levels of the yearly S-GEV (red) and the NS-GEV (green) model for the stations La Chaux-de-Fonds (a), Basel/Binningen (b) and Locarno-Monti (c). The areas mark the confidence interval's spread, the lines the best estimates. Blue dots indicate the heaviest yearly precipitation events observed.

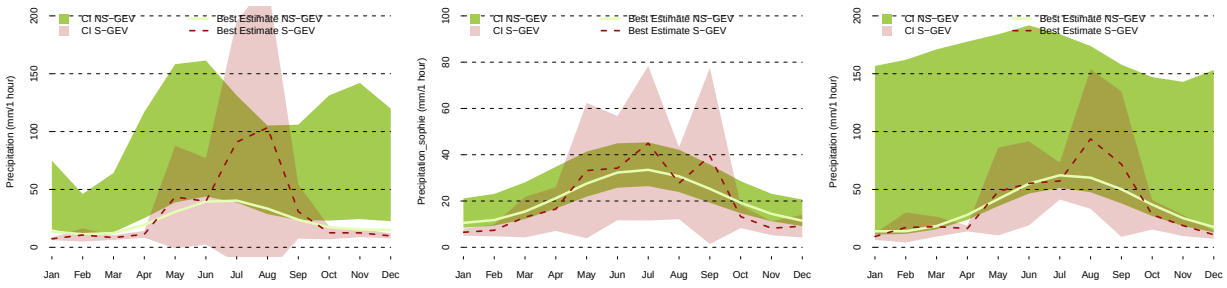

(a) CDF; $\mathcal{M}_{2,2}$ **(b)** BAS; $\mathcal{M}_{2,1}$ **(c)** OTL

Fig. D.19: Return levels for a monthly return period of 100 years. The seasonal values, modeled with the 'best' model, are shown with green colours, the independently estimated (S-GEV) in red. The coloured areas mark the confidence intervals, the lines the best estimates.

D.2.2 2 day maxima

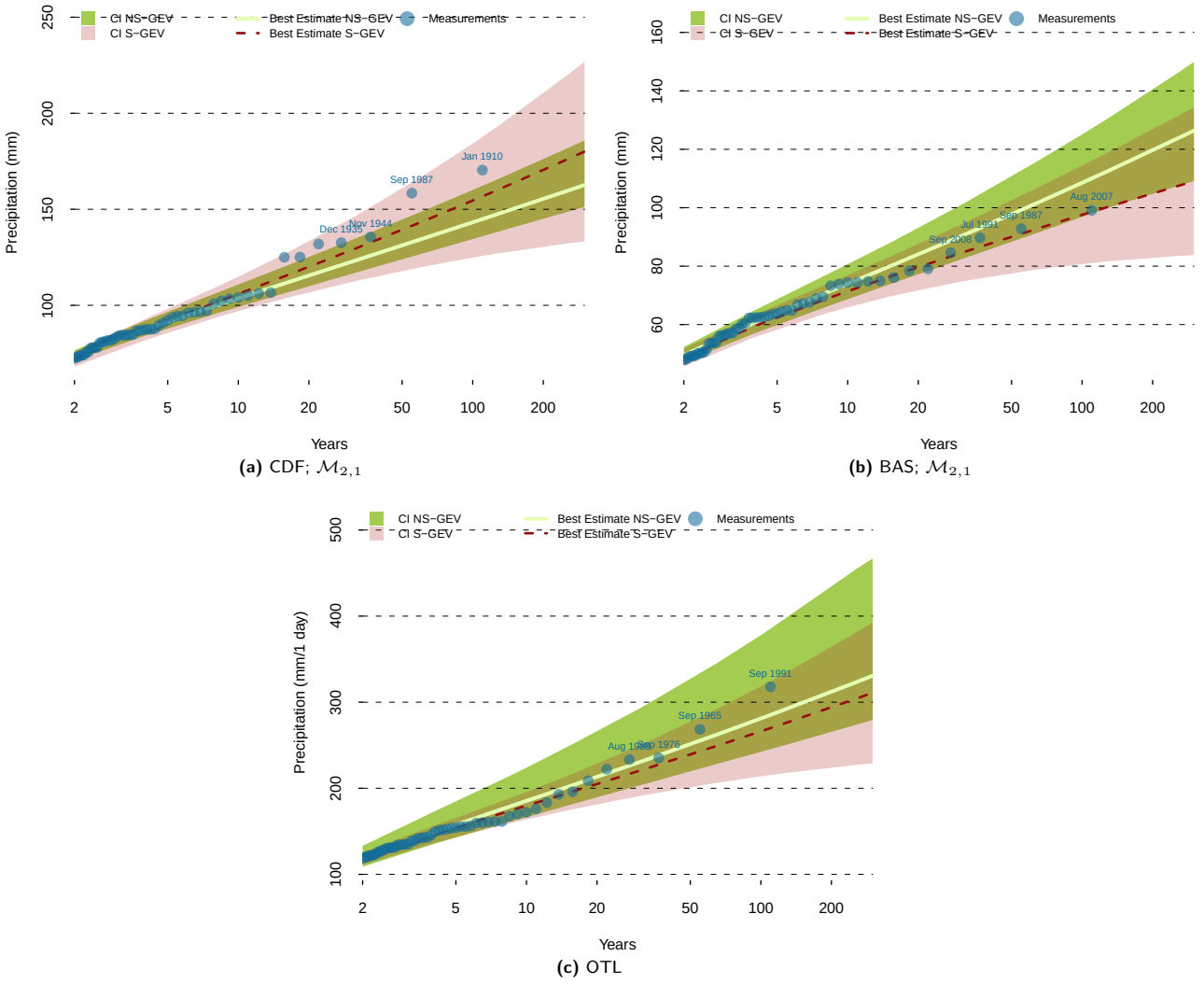

(a) CDF; $\mathcal{M}_{2,1}$ **(b)** BAS; $\mathcal{M}_{2,1}$

(c) OTL

Fig. D.20: Return levels of the yearly S-GEV (red) and the NS-GEV (green) model for the stations La Chaux-de-Fonds (a), Basel/Binningen (b) and Locarno-Monti (c). The areas mark the confidence interval's spread, the lines the best estimates. Blue dots indicate the heaviest yearly precipitation events observed.

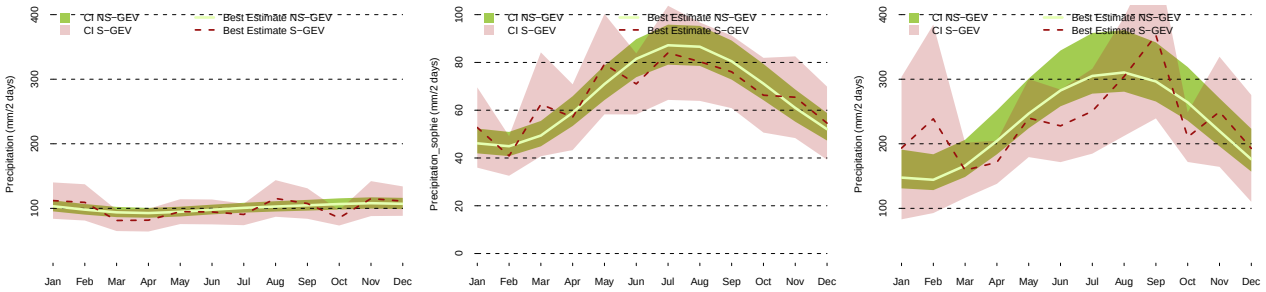

(a) CDF; $\mathcal{M}_{2,2}$ **(b)** BAS; $\mathcal{M}_{2,1}$ **(c)** OTL

Fig. D.21: Return levels for a monthly return period of 100 years. The seasonal values, modeled with the 'best' model, are shown with green colours, the independently estimated (S-GEV) in red. The coloured areas mark the confidence intervals, the lines the best estimates.

D.2.3 3 day maxima

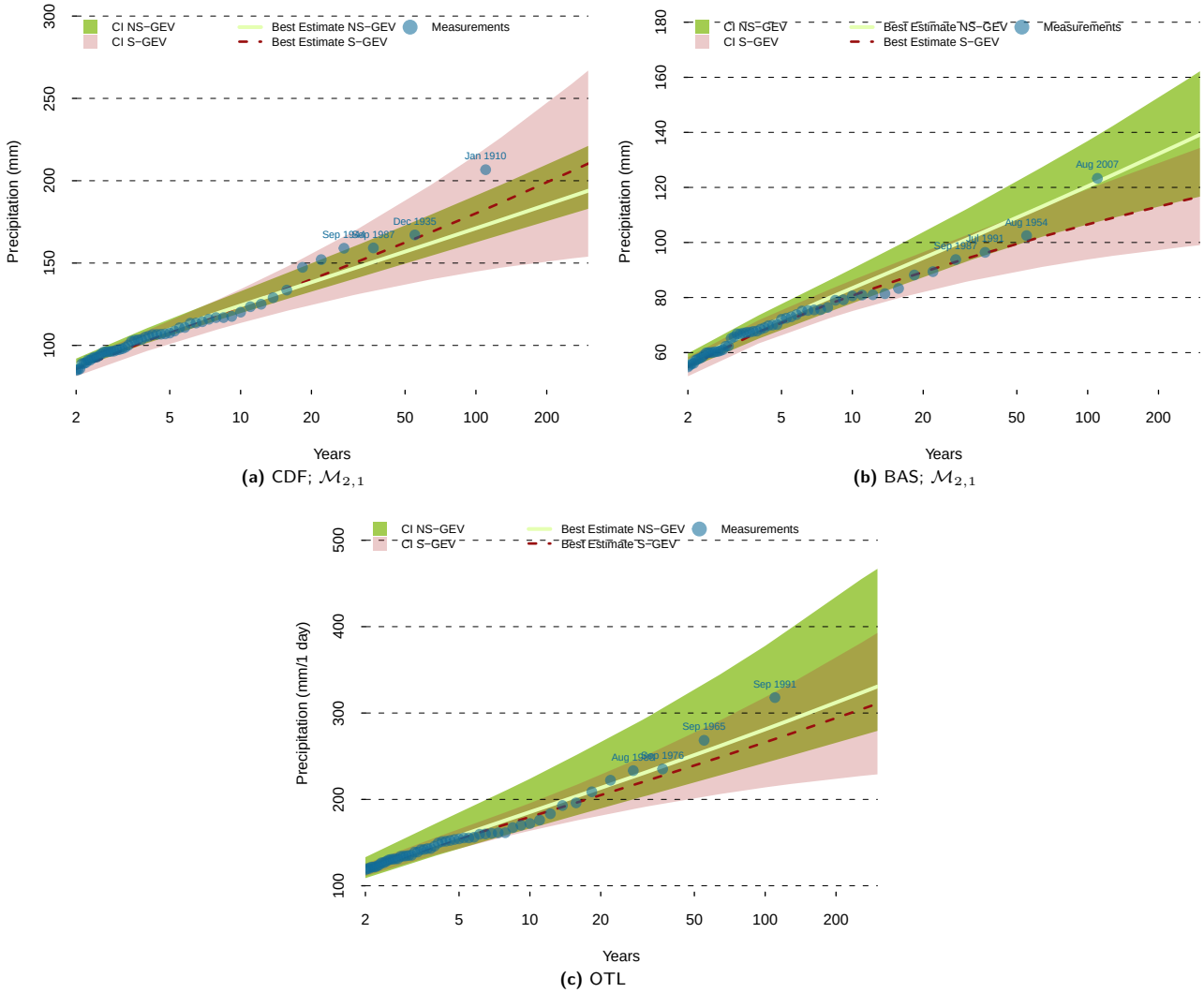

(a) CDF; $\mathcal{M}_{2,1}$ **(b)** BAS; $\mathcal{M}_{2,1}$ **(c)** OTL

Fig. D.22: Return levels of the yearly S-GEV (red) and the NS-GEV (green) model for the stations La Chaux-de-Fonds (a), Basel/Binningen (b) and Locarno-Monti (c). The areas mark the confidence interval's spread, the lines the best estimates. Blue dots indicate the heaviest yearly precipitation events observed.

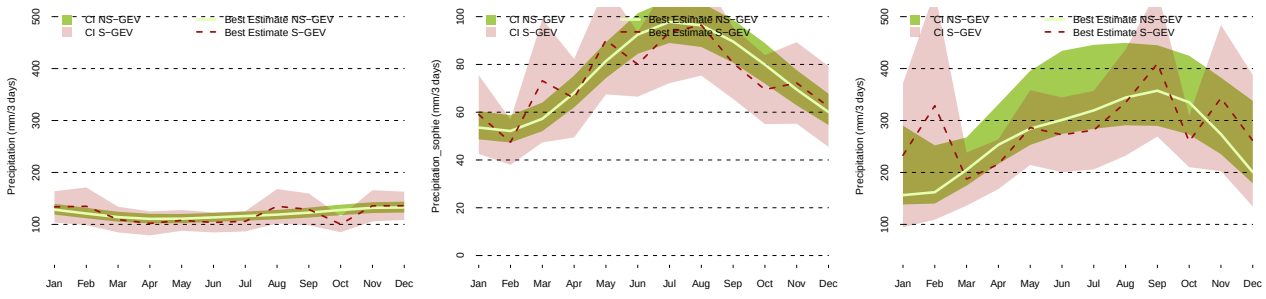

(a) CDF; $\mathcal{M}_{2,2}$ **(b)** BAS; $\mathcal{M}_{2,1}$ **(c)** OTL

Fig. D.23: Return levels for a monthly return period of 100 years. The seasonal values, modeled with the 'best' model, are shown with green colours, the independently estimated (S-GEV) in red. The coloured areas mark the confidence intervals, the lines the best estimates.

D.2.4 4 day maxima

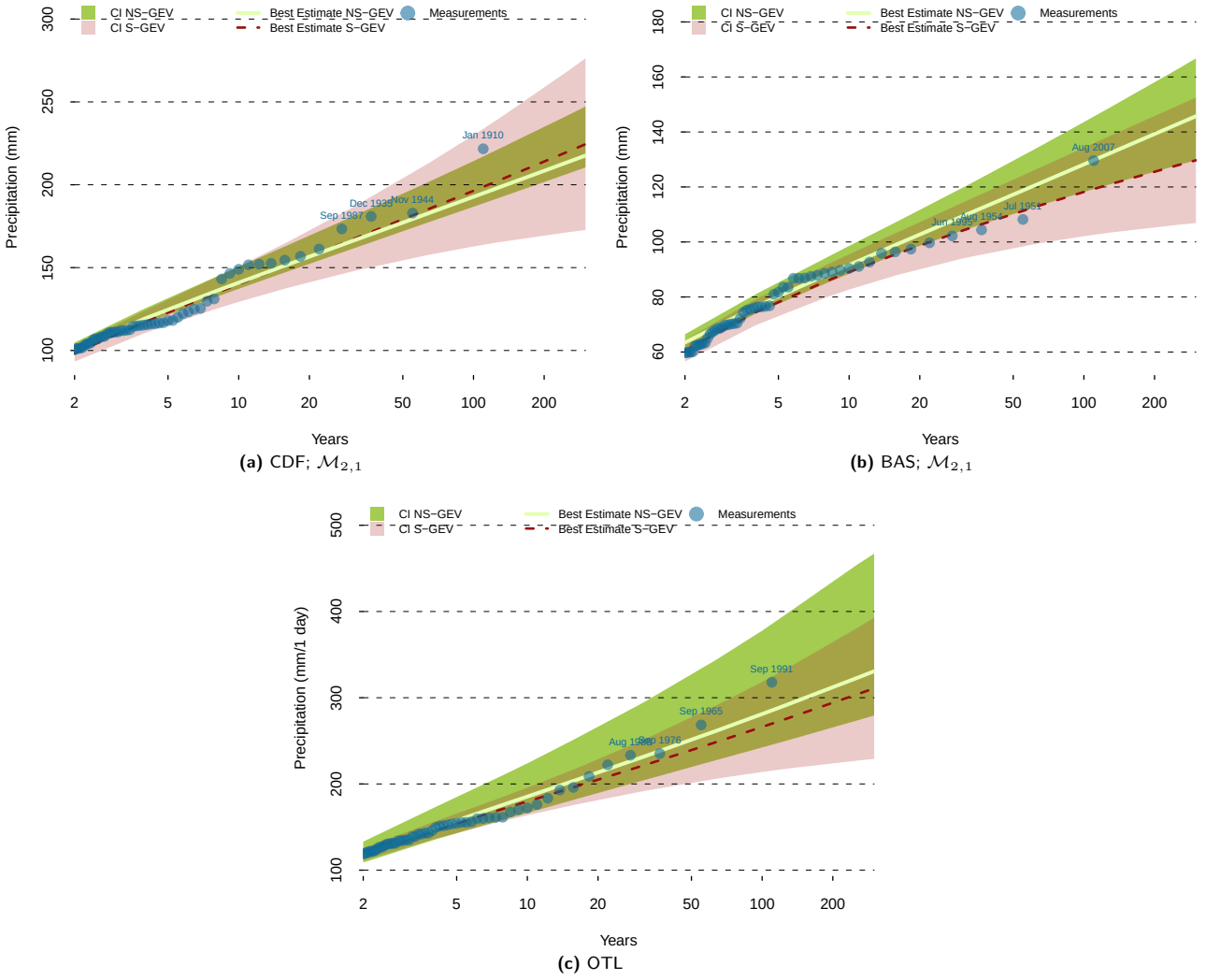

(a) CDF; $\mathcal{M}_{2,1}$ **(b)** BAS; $\mathcal{M}_{2,1}$ **(c)** OTL

Fig. D.24: Return levels of the yearly S-GEV (red) and the NS-GEV (green) model for the stations La Chaux-de-Fonds (a), Basel/Binningen (b) and Locarno-Monti (c). The areas mark the confidence interval's spread, the lines the best estimates. Blue dots indicate the heaviest yearly precipitation events observed.

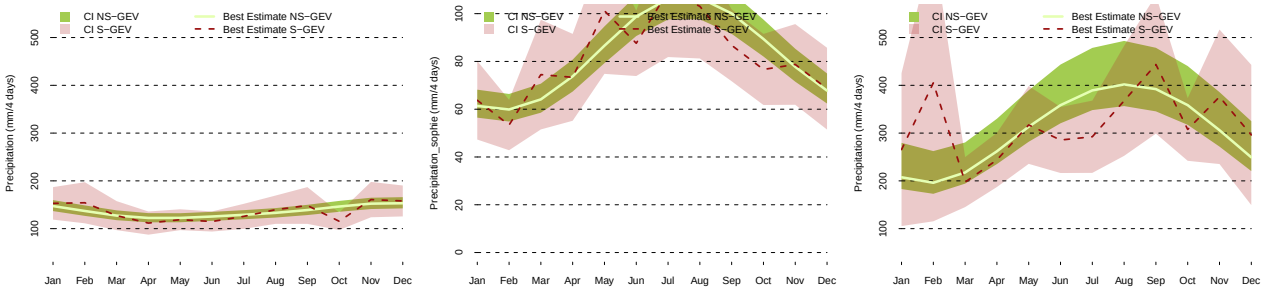

(a) CDF; $\mathcal{M}_{2,2}$ **(b)** BAS; $\mathcal{M}_{2,1}$ **(c)** OTL

Fig. D.25: Return levels for a monthly return period of 100 years. The seasonal values, modeled with the 'best' model, are shown with green colours, the independently estimated (S-GEV) in red. The coloured areas mark the confidence intervals, the lines the best estimates.

D.2.5 5 day maxima

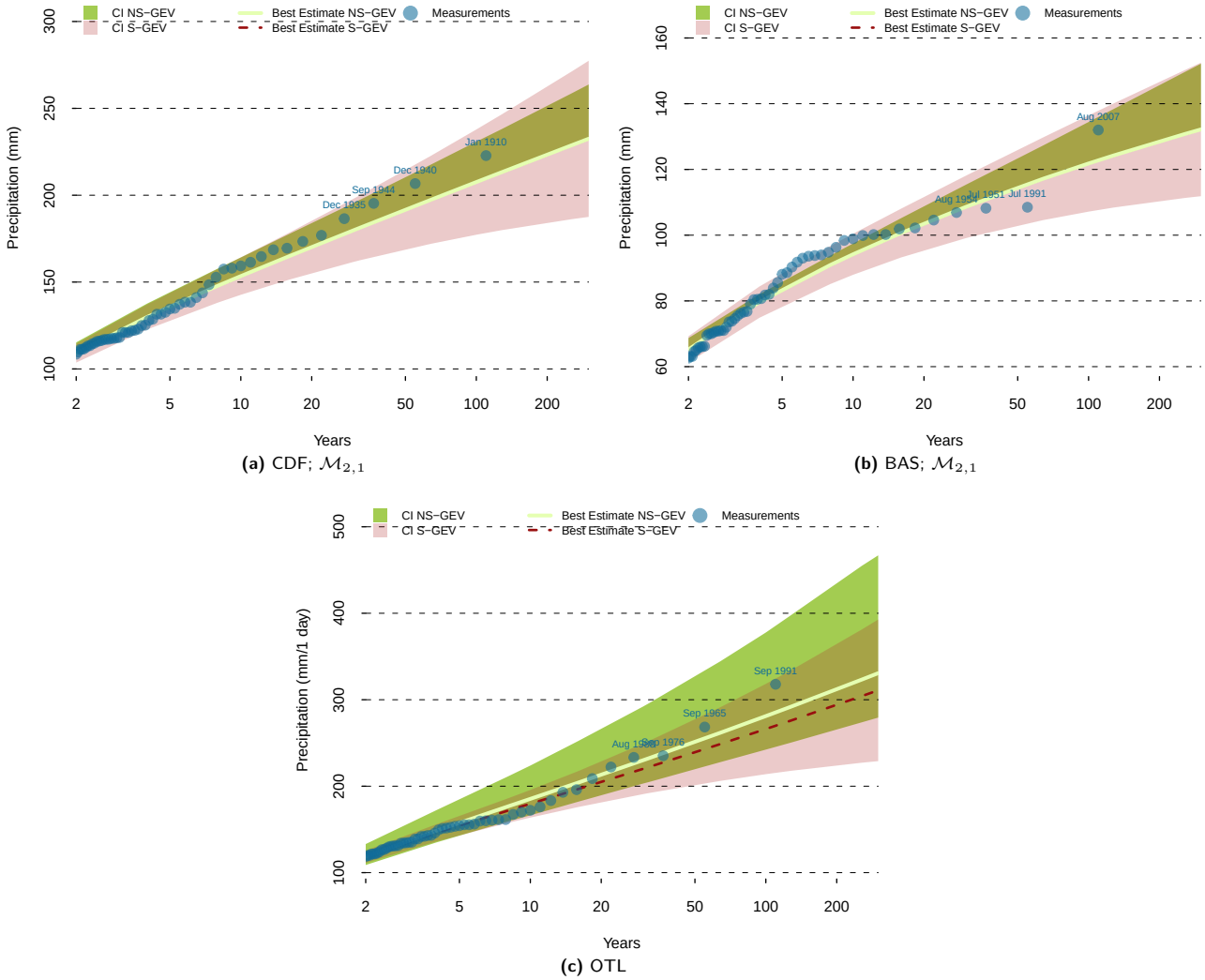

(a) CDF; $\mathcal{M}_{2,1}$ **(b)** BAS; $\mathcal{M}_{2,1}$ **(c)** OTL

Fig. D.26: Return levels of the yearly S-GEV (red) and the NS-GEV (green) model for the stations La Chaux-de-Fonds (a), Basel/Binningen (b) and Locarno-Monti (c). The areas mark the confidence interval's spread, the lines the best estimates. Blue dots indicate the heaviest yearly precipitation events observed.

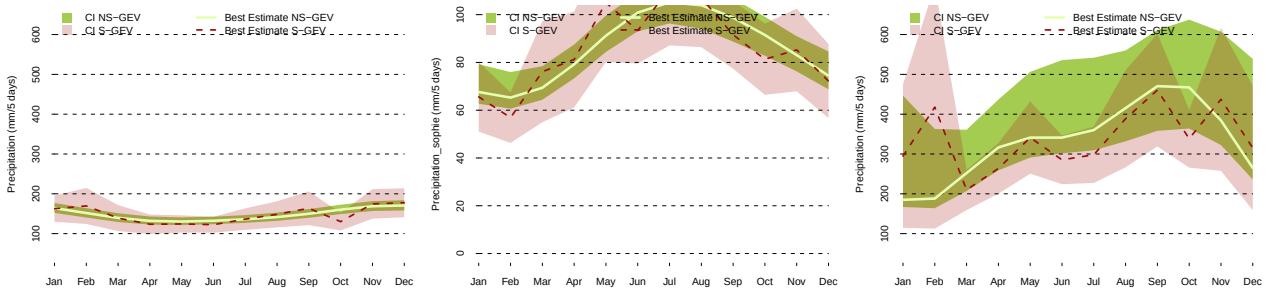

(a) CDF; $\mathcal{M}_{2,2}$ **(b)** BAS; $\mathcal{M}_{2,1}$ **(c)** OTL

Fig. D.27: Return levels for a monthly return period of 100 years. The seasonal values, modeled with the 'best' model, are shown with green colours, the independently estimated (S-GEV) in red. The coloured areas mark the confidence intervals, the lines the best estimates.

D.2.6 10 day maxima

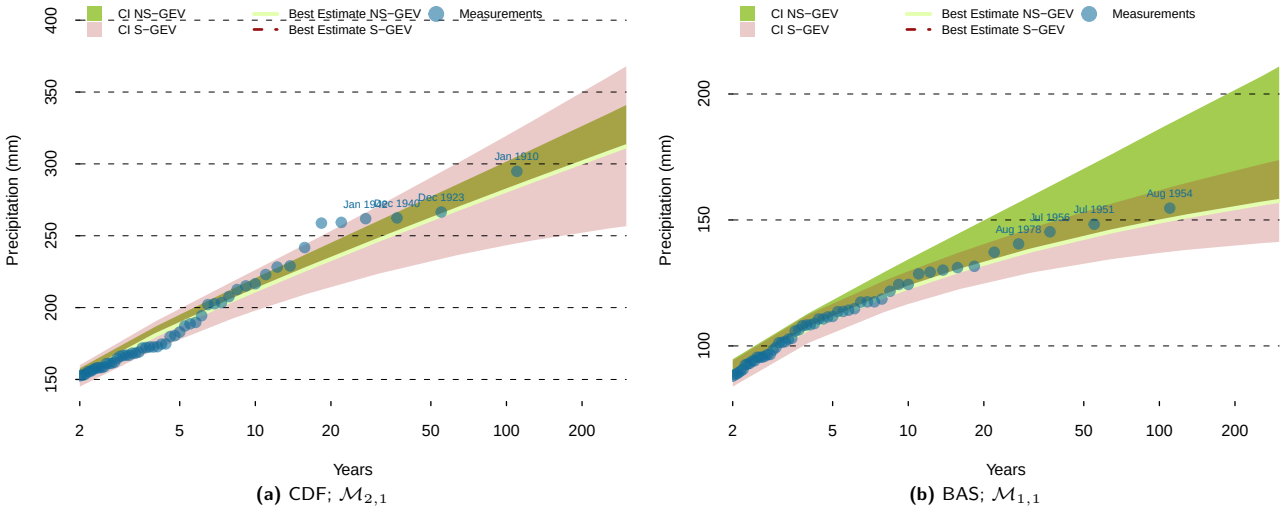

(a) CDF; $\mathcal{M}_{2,1}$ **(b)** BAS; $\mathcal{M}_{1,1}$

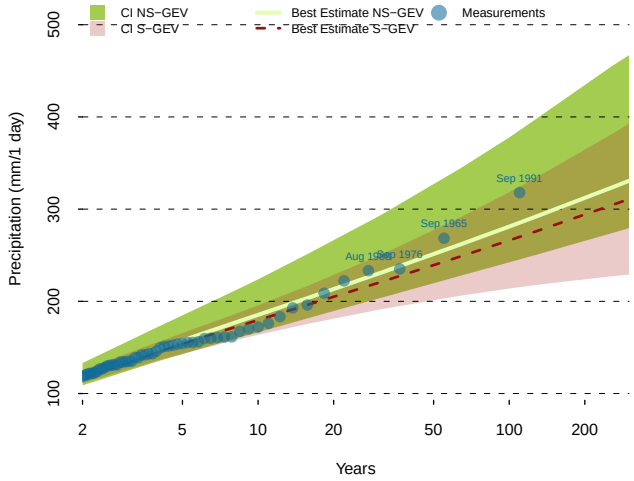

(c) OTL

Fig. D.28: Return levels of the yearly S-GEV (red) and the NS-GEV (green) model for the stations La Chaux-de-Fonds (a), Basel/Binningen (b) and Locarno-Monti (c). The areas mark the confidence interval's spread, the lines the best estimates. Blue dots indicate the heaviest yearly precipitation events observed.

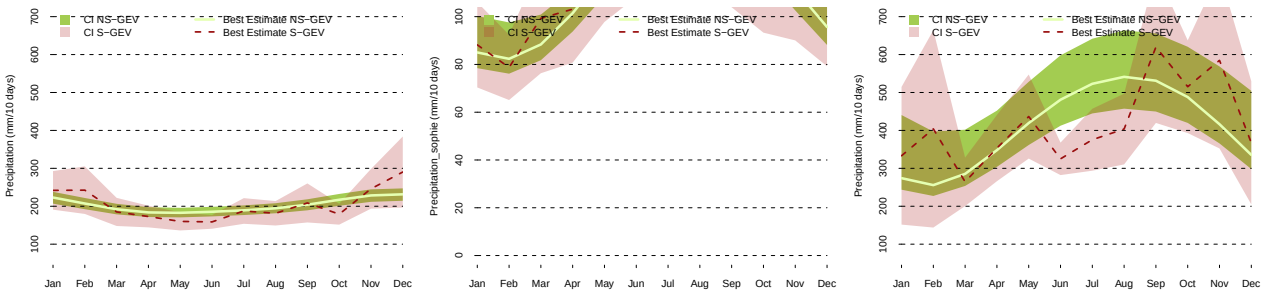

(a) CDF; $\mathcal{M}_{2,2}$ **(b)** BAS; $\mathcal{M}_{2,1}$ **(c)** OTL

Fig. D.29: Return levels for a monthly return period of 100 years. The seasonal values, modeled with the 'best' model, are shown with green colours, the independently estimated (S-GEV) in red. The coloured areas mark the confidence intervals, the lines the best estimates.

Appendix E Additional Figures: Estimate of Monthly Return Levels

E.1 Stations ABE to BAS

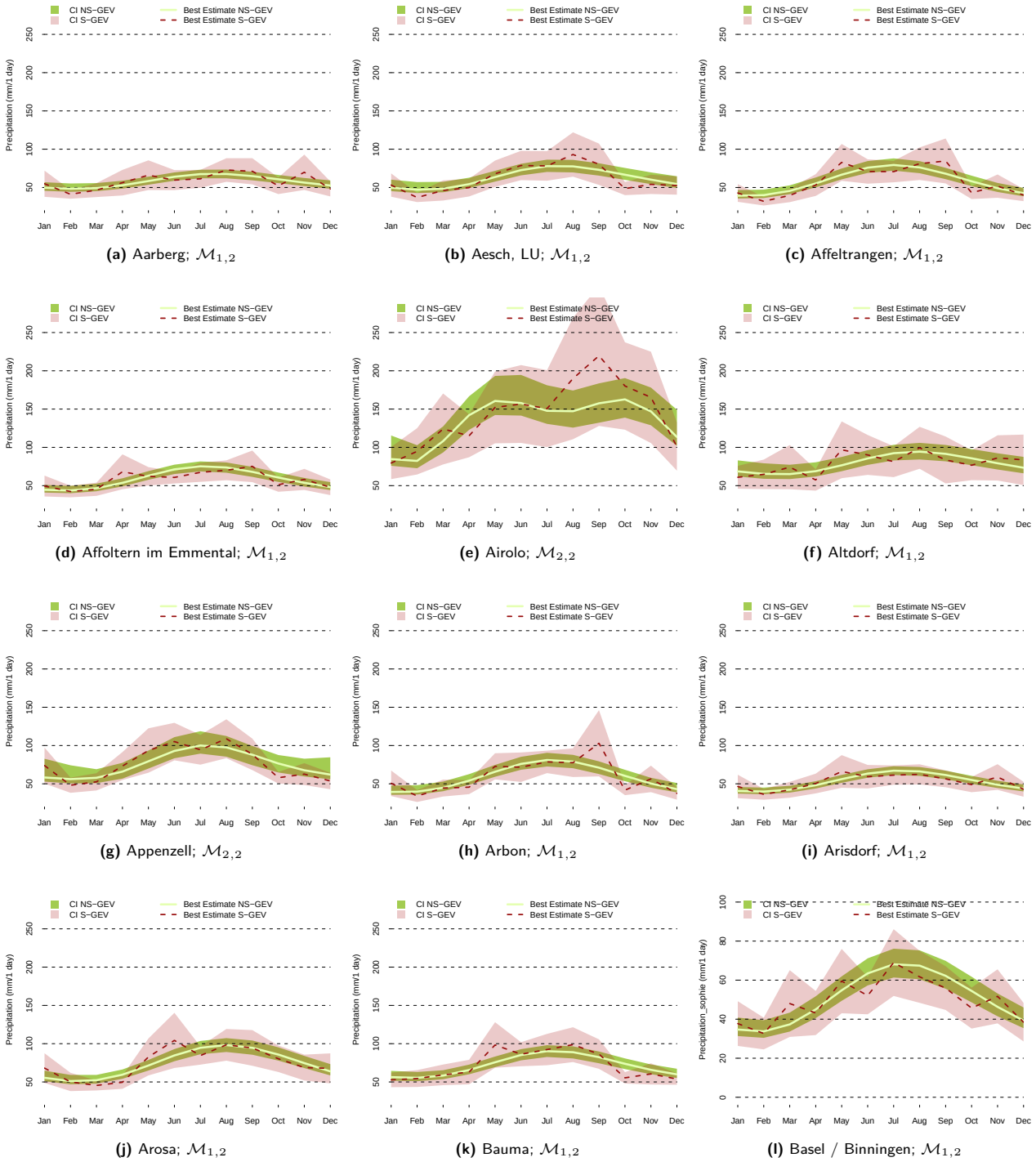

(a) Aarberg; $\mathcal{M}_{1,2}$ **(b)** Aesch, LU; $\mathcal{M}_{1,2}$ **(c)** Affeltrangen; $\mathcal{M}_{1,2}$

(d) Affoltern im Emmental; $\mathcal{M}_{1,2}$ **(e)** Airolo; $\mathcal{M}_{2,2}$ **(f)** Altdorf; $\mathcal{M}_{1,2}$

(g) Appenzell; $\mathcal{M}_{2,2}$ **(h)** Arbon; $\mathcal{M}_{1,2}$ **(i)** Arisdorf; $\mathcal{M}_{1,2}$

(j) Arosa; $\mathcal{M}_{1,2}$ **(k)** Bauma; $\mathcal{M}_{1,2}$ **(l)** Basel / Binningen; $\mathcal{M}_{1,2}$

Fig. E.1: Return levels for a monthly return period of 100 years. The seasonal values, modeled with the 'best' model, are shown with green colours, the independently estimated (S-GEV) in red. The coloured areas mark the confidence intervals, the lines the best estimates.

E.2 Stations BER to BUC

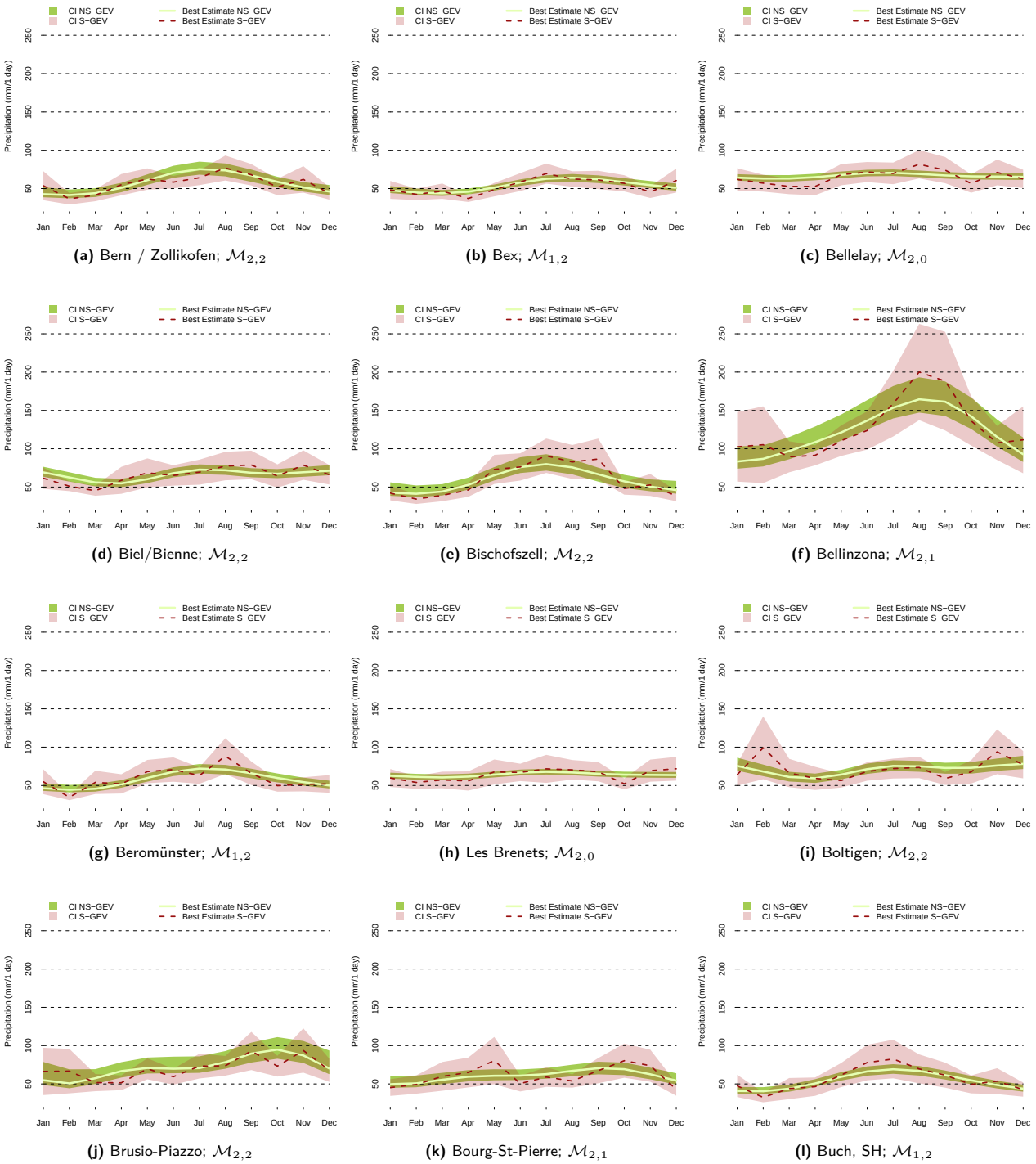

(a) Bern / Zollikofen; $\mathcal{M}_{2,2}$ **(b)** Bex; $\mathcal{M}_{1,2}$ **(c)** Bellelay; $\mathcal{M}_{2,0}$

(d) Biel/Bienne; $\mathcal{M}_{2,2}$ **(e)** Bischofszell; $\mathcal{M}_{2,2}$ **(f)** Bellinzona; $\mathcal{M}_{2,1}$

(g) Beromünster; $\mathcal{M}_{1,2}$ **(h)** Les Brenets; $\mathcal{M}_{2,0}$ **(i)** Boltigen; $\mathcal{M}_{2,2}$

(j) Brusio-Piazzo; $\mathcal{M}_{2,2}$ **(k)** Bourg-St-Pierre; $\mathcal{M}_{2,1}$ **(l)** Buch, SH; $\mathcal{M}_{1,2}$

Fig. E.2: Return levels for a monthly return period of 100 years. The seasonal values, modeled with the 'best' model, are shown with green colours, the independently estimated (S-GEV) in red. The coloured areas mark the confidence intervals, the lines the best estimates.

E.3 Stations BUE to EIN

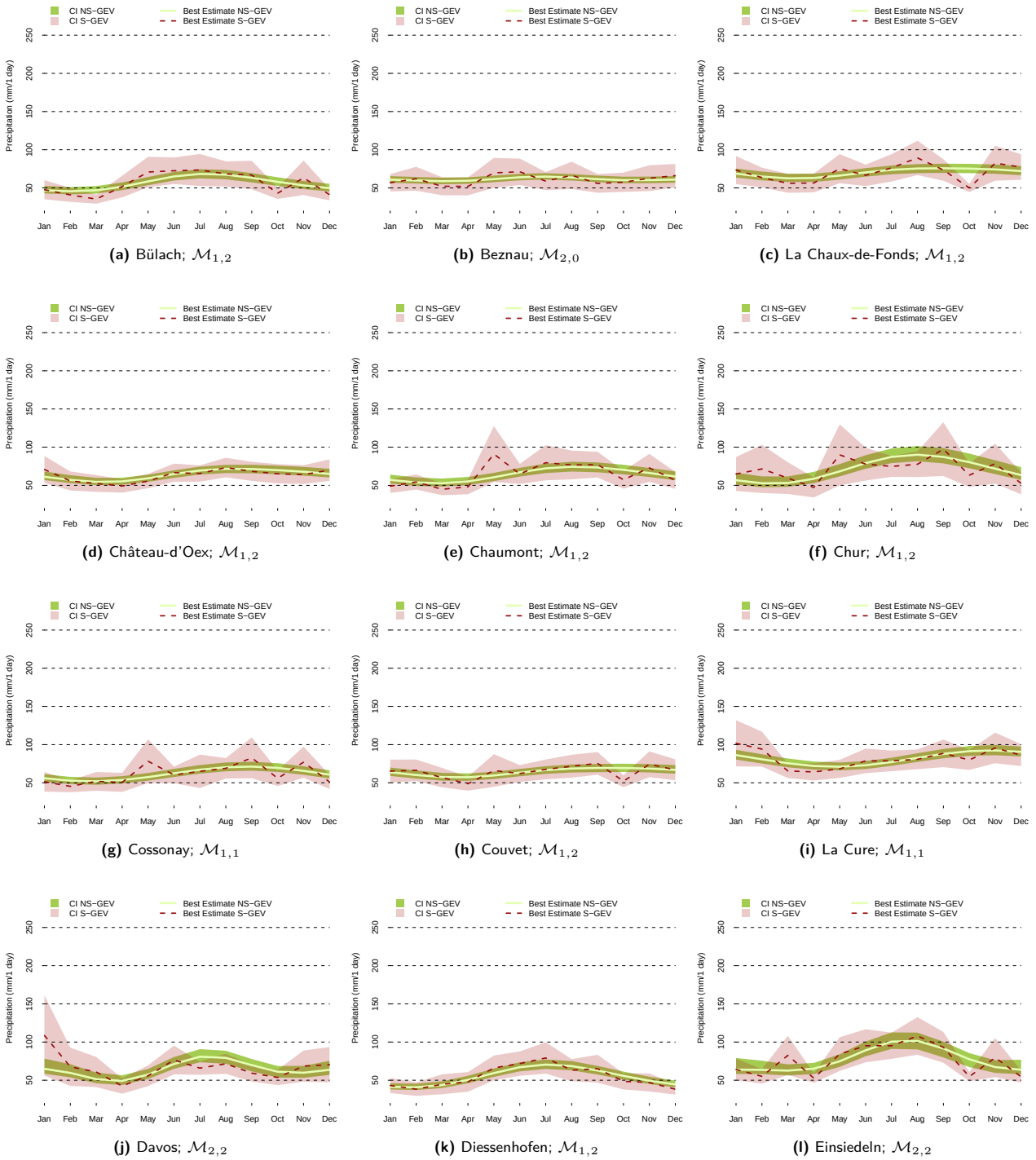

(a) Bülach; $\mathcal{M}_{1,2}$ **(b)** Beznau; $\mathcal{M}_{2,0}$ **(c)** La Chaux-de-Fonds; $\mathcal{M}_{1,2}$

(d) Château-d'Oex; $\mathcal{M}_{1,2}$ **(e)** Chaumont; $\mathcal{M}_{1,2}$ **(f)** Chur; $\mathcal{M}_{1,2}$

(g) Cossonay; $\mathcal{M}_{1,1}$ **(h)** Couvet; $\mathcal{M}_{1,2}$ **(i)** La Cure; $\mathcal{M}_{1,1}$

(j) Davos; $\mathcal{M}_{2,2}$ **(k)** Diessenhofen; $\mathcal{M}_{1,2}$ **(l)** Einsiedeln; $\mathcal{M}_{2,2}$

Fig. E.3: Return levels for a monthly return period of 100 years. The seasonal values, modeled with the 'best' model, are shown with green colours, the independently estimated (S-GEV) in red. The coloured areas mark the confidence intervals, the lines the best estimates.

E.4 Stations EKO to GSB

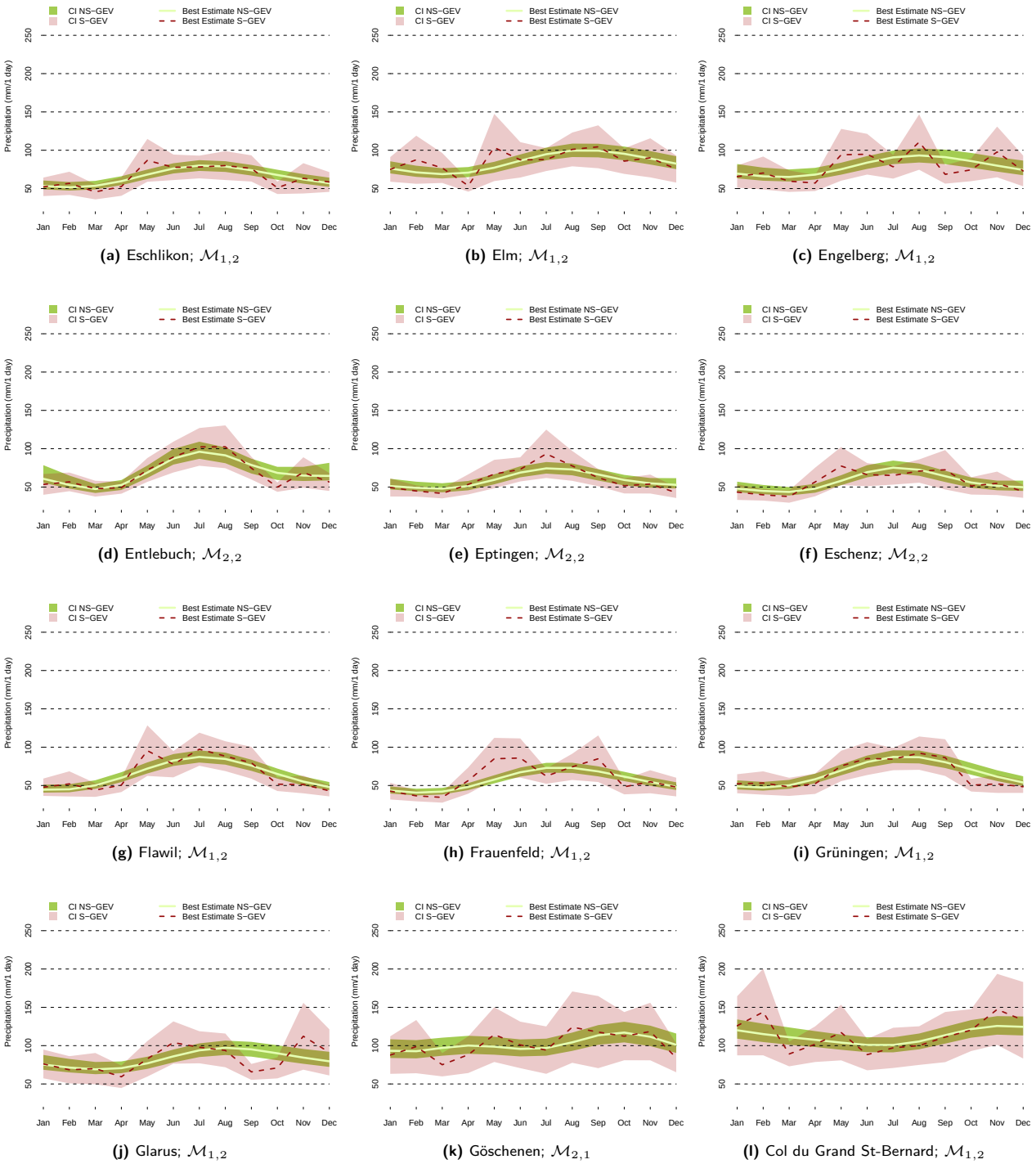

(a) Eschlikon; $\mathcal{M}_{1,2}$ **(b)** Elm; $\mathcal{M}_{1,2}$ **(c)** Engelberg; $\mathcal{M}_{1,2}$

(d) Entlebuch; $\mathcal{M}_{2,2}$ **(e)** Eptingen; $\mathcal{M}_{2,2}$ **(f)** Eschenz; $\mathcal{M}_{2,2}$

(g) Flawil; $\mathcal{M}_{1,2}$ **(h)** Frauenfeld; $\mathcal{M}_{1,2}$ **(i)** Grüningen; $\mathcal{M}_{1,2}$

(j) Glarus; $\mathcal{M}_{1,2}$ **(k)** Göschenen; $\mathcal{M}_{2,1}$ **(l)** Col du Grand St-Bernard; $\mathcal{M}_{1,2}$

Fig. E.4: Return levels for a monthly return period of 100 years. The seasonal values, modeled with the 'best' model, are shown with green colours, the independently estimated (S-GEV) in red. The coloured areas mark the confidence intervals, the lines the best estimates.

E.5 Stations GTT to LAG

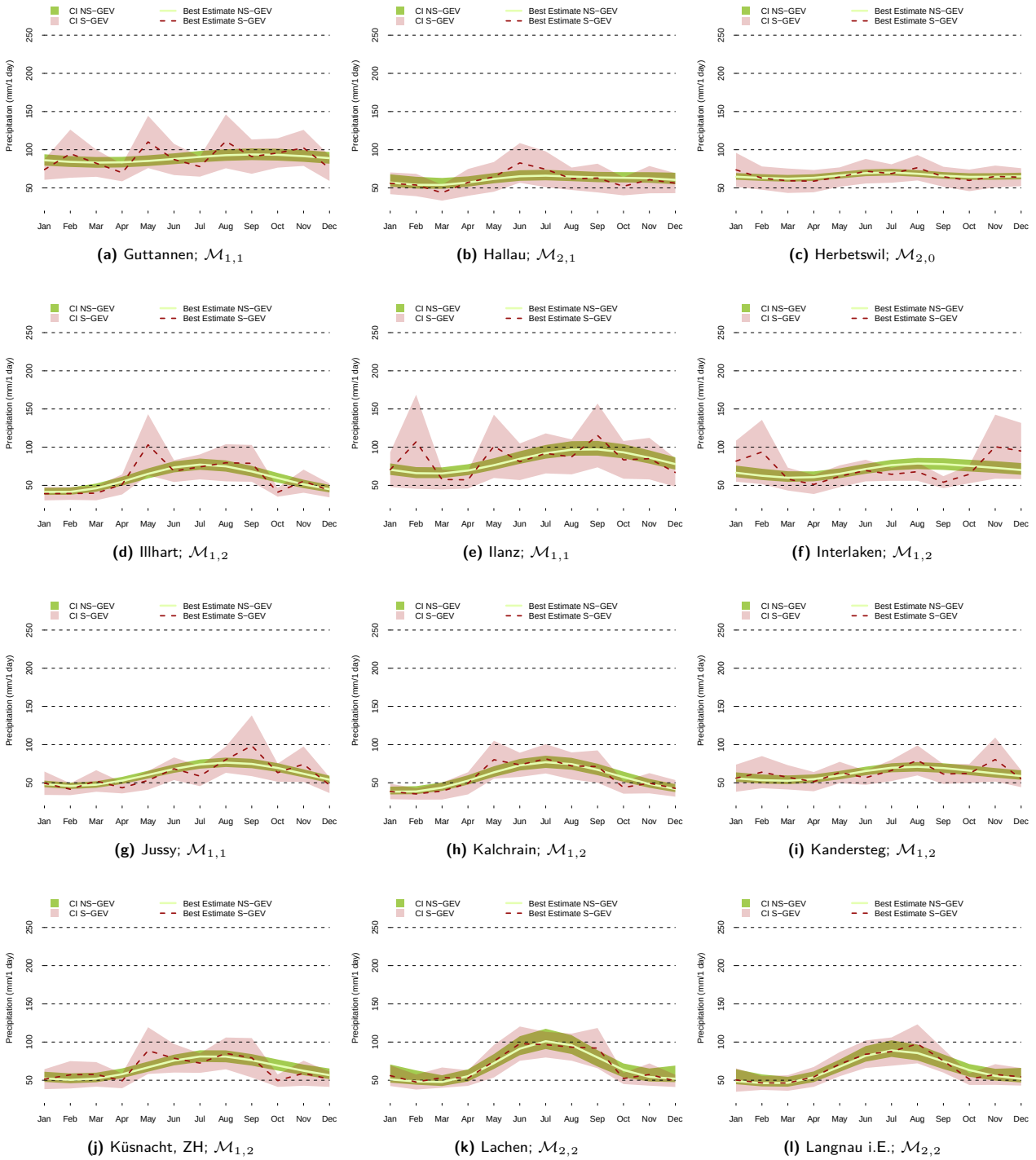

(a) Guttannen; $\mathcal{M}_{1,1}$ **(b)** Hallau; $\mathcal{M}_{2,1}$ **(c)** Herbetswil; $\mathcal{M}_{2,0}$

(d) Illhart; $\mathcal{M}_{1,2}$ **(e)** Ilanz; $\mathcal{M}_{1,1}$ **(f)** Interlaken; $\mathcal{M}_{1,2}$

(g) Jussy; $\mathcal{M}_{1,1}$ **(h)** Kalchrain; $\mathcal{M}_{1,2}$ **(i)** Kandersteg; $\mathcal{M}_{1,2}$

(j) Küsnacht, ZH; $\mathcal{M}_{1,2}$ **(k)** Lachen; $\mathcal{M}_{2,2}$ **(l)** Langnau i.E.; $\mathcal{M}_{2,2}$

Fig. E.5: Return levels for a monthly return period of 100 years. The seasonal values, modeled with the 'best' model, are shown with green colours, the independently estimated (S-GEV) in red. The coloured areas mark the confidence intervals, the lines the best estimates.

E.6 Stations LEU to NEU

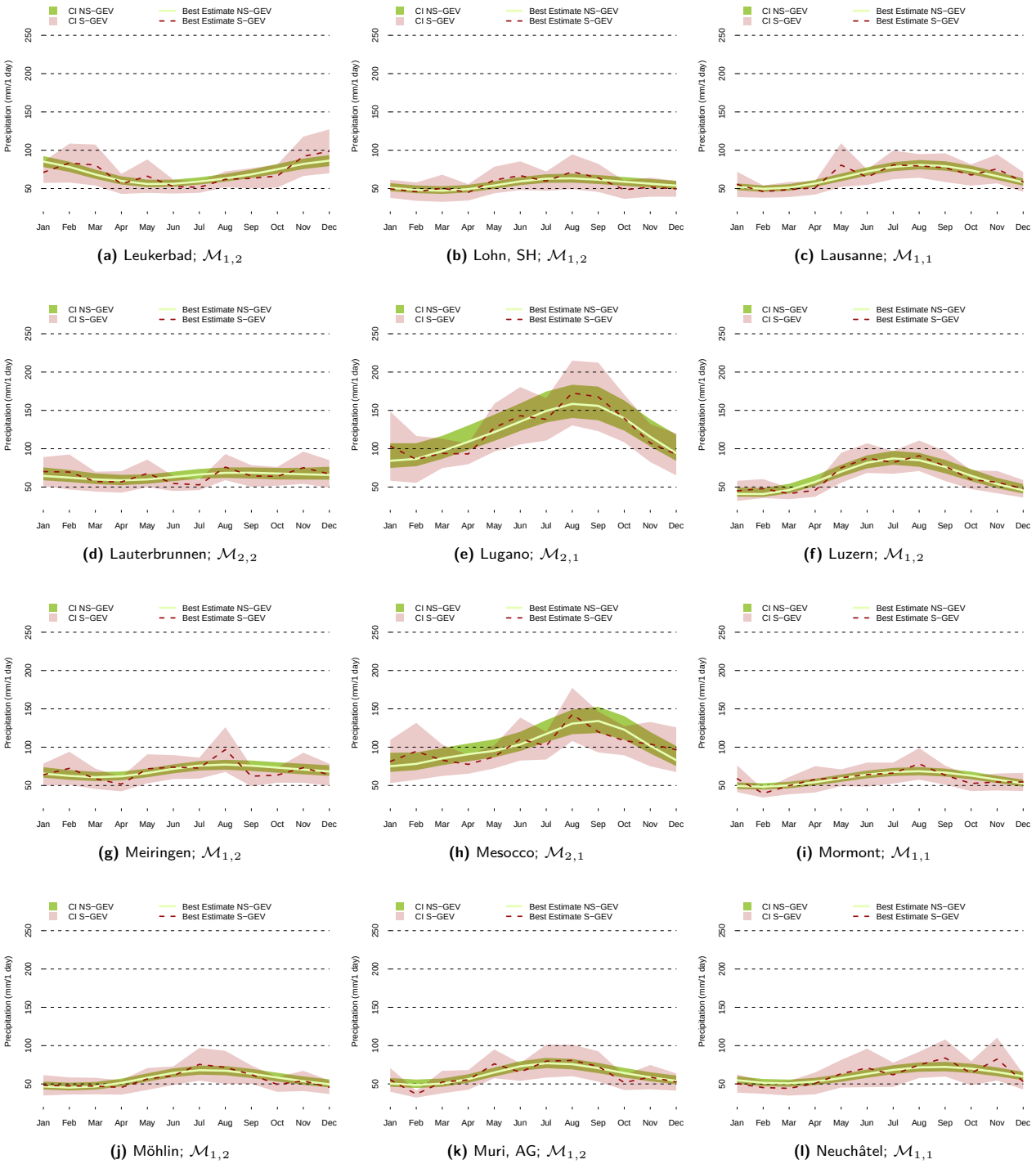

(a) Leukerbad; $\mathcal{M}_{1,2}$ **(b)** Lohn, SH; $\mathcal{M}_{1,2}$ **(c)** Lausanne; $\mathcal{M}_{1,1}$

(d) Lauterbrunnen; $\mathcal{M}_{2,2}$ **(e)** Lugano; $\mathcal{M}_{2,1}$ **(f)** Luzern; $\mathcal{M}_{1,2}$

(g) Meiringen; $\mathcal{M}_{1,2}$ **(h)** Mesocco; $\mathcal{M}_{2,1}$ **(i)** Mormont; $\mathcal{M}_{1,1}$

(j) Möhlin; $\mathcal{M}_{1,2}$ **(k)** Muri, AG; $\mathcal{M}_{1,2}$ **(l)** Neuchâtel; $\mathcal{M}_{1,1}$

Fig. E.6: Return levels for a monthly return period of 100 years. The seasonal values, modeled with the 'best' model, are shown with green colours, the independently estimated (S-GEV) in red. The coloured areas mark the confidence intervals, the lines the best estimates.

E.7 Stations NIE to SMM

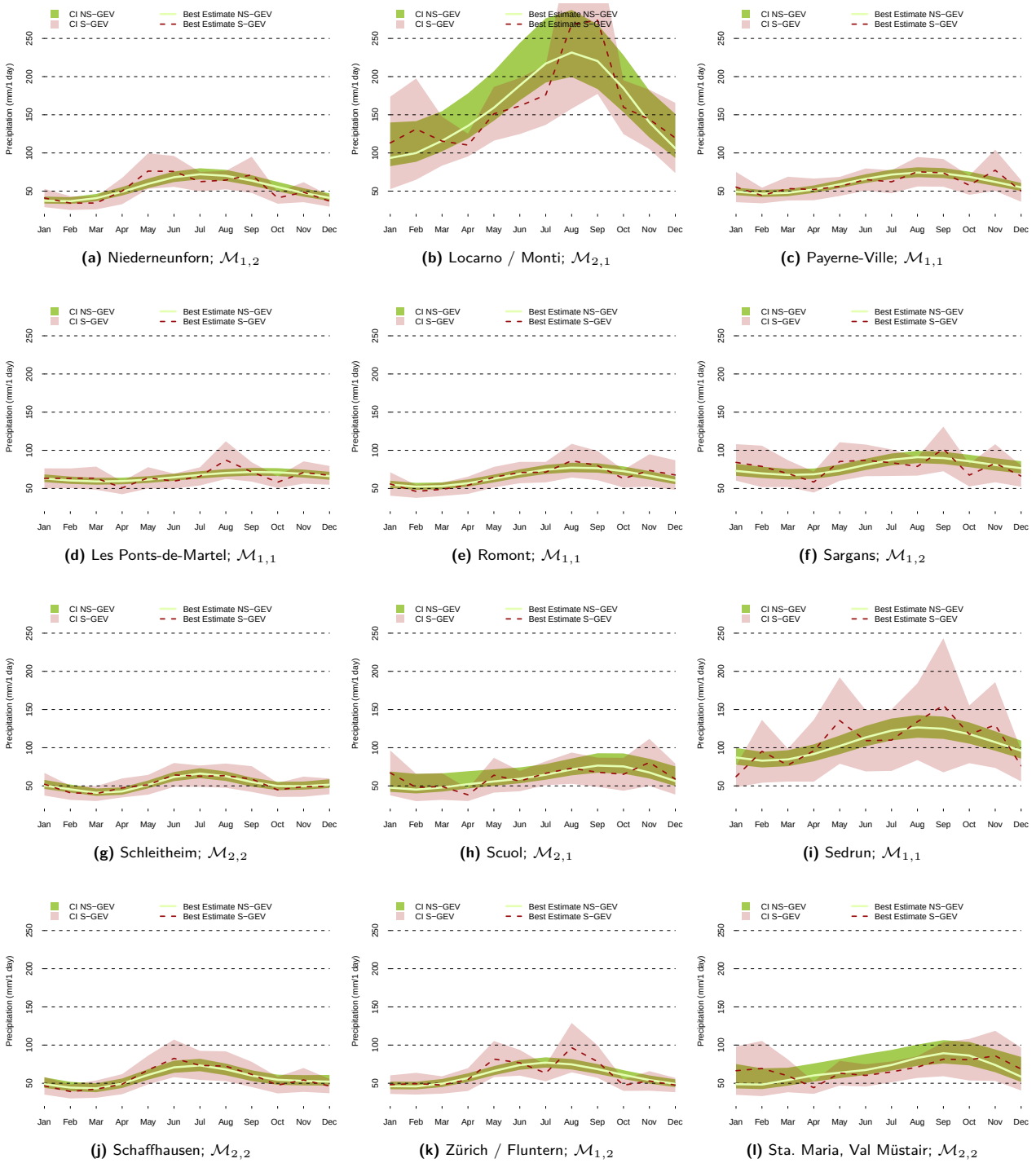

(a) Niederneunforn; $\mathcal{M}_{1,2}$ **(b)** Locarno / Monti; $\mathcal{M}_{2,1}$ **(c)** Payerne-Ville; $\mathcal{M}_{1,1}$

(d) Les Ponts-de-Martel; $\mathcal{M}_{1,1}$ **(e)** Romont; $\mathcal{M}_{1,1}$ **(f)** Sargans; $\mathcal{M}_{1,2}$

(g) Schleitheim; $\mathcal{M}_{2,2}$ **(h)** Scuol; $\mathcal{M}_{2,1}$ **(i)** Sedrun; $\mathcal{M}_{1,1}$

(j) Schaffhausen; $\mathcal{M}_{2,2}$ **(k)** Zürich / Fluntern; $\mathcal{M}_{1,2}$ **(l)** Sta. Maria, Val Müstair; $\mathcal{M}_{2,2}$

Fig. E.7: Return levels for a monthly return period of 100 years. The seasonal values, modeled with the 'best' model, are shown with green colours, the independently estimated (S-GEV) in red. The coloured areas mark the confidence intervals, the lines the best estimates.

E.8 Stations SOG to WIN

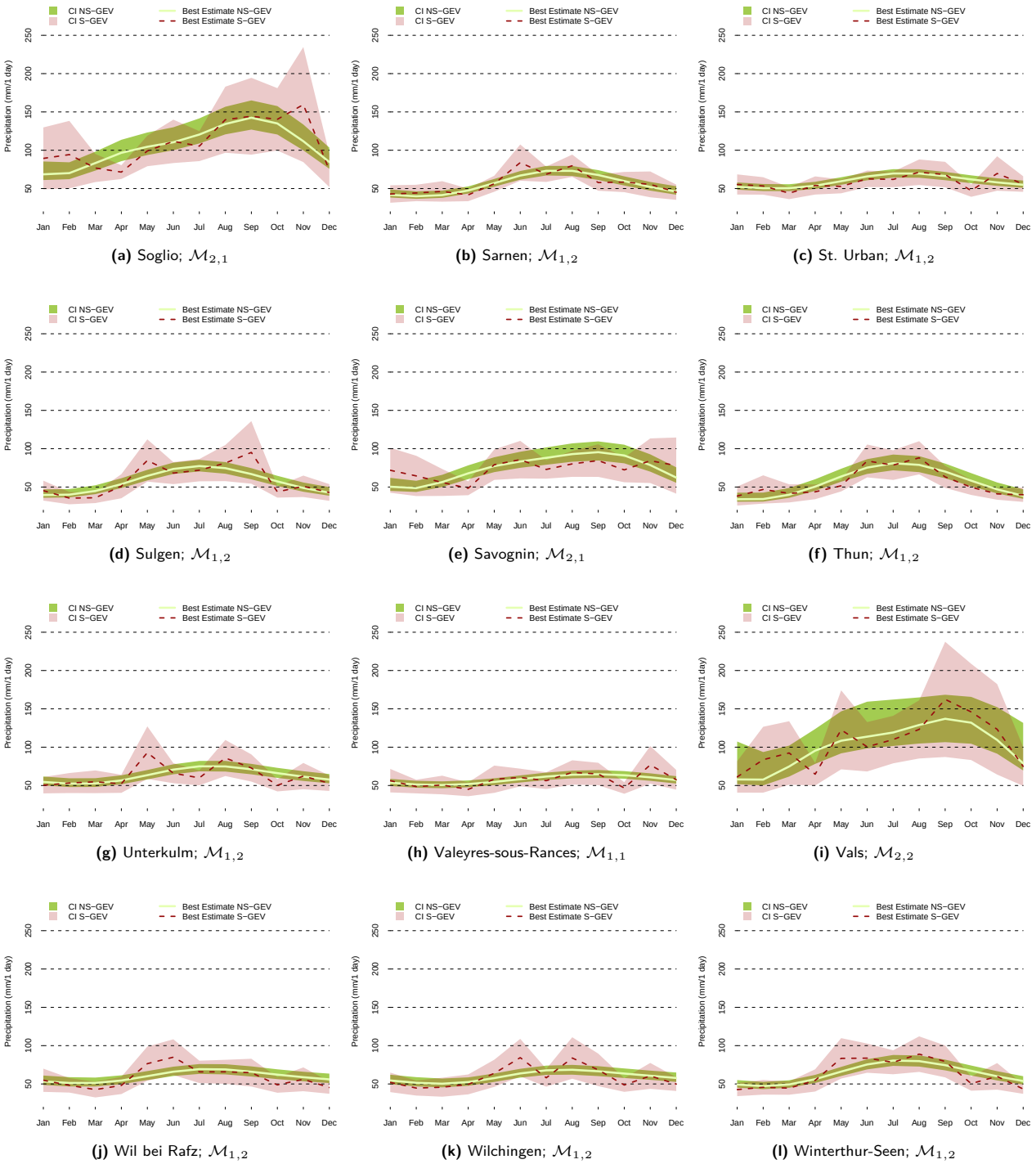

(a) Soglio; $\mathcal{M}_{2,1}$ **(b)** Sarnen; $\mathcal{M}_{1,2}$ **(c)** St. Urban; $\mathcal{M}_{1,2}$

(d) Sulgen; $\mathcal{M}_{1,2}$ **(e)** Savognin; $\mathcal{M}_{2,1}$ **(f)** Thun; $\mathcal{M}_{1,2}$

(g) Unterkulm; $\mathcal{M}_{1,2}$ **(h)** Valeyres-sous-Rances; $\mathcal{M}_{1,1}$ **(i)** Vals; $\mathcal{M}_{2,2}$

(j) Wil bei Rafz; $\mathcal{M}_{1,2}$ **(k)** Wilchingen; $\mathcal{M}_{1,2}$ **(l)** Winterthur-Seen; $\mathcal{M}_{1,2}$

Fig. E.8: Return levels for a monthly return period of 100 years. The seasonal values, modeled with the 'best' model, are shown with green colours, the independently estimated (S-GEV) in red. The coloured areas mark the confidence intervals, the lines the best estimates.

E.9 Station ZER

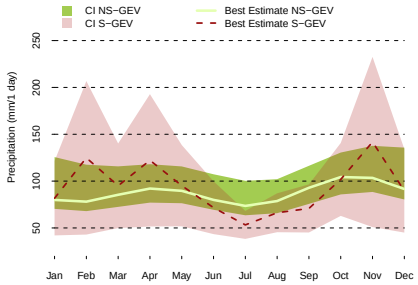

(a) Zermatt; $\mathcal{M}_{2,2}$

Fig. E.9: Return levels for a monthly return period of 100 years. The seasonal values, modeled with the 'best' model, are shown with green colours, the independently estimated (S-GEV) in red. The coloured areas mark the confidence intervals, the lines the best estimates.

Appendix F Additional Figures: Spatial Distribution of Extremes

F.1 Monthly RLs for a monthly RP of 100 Years

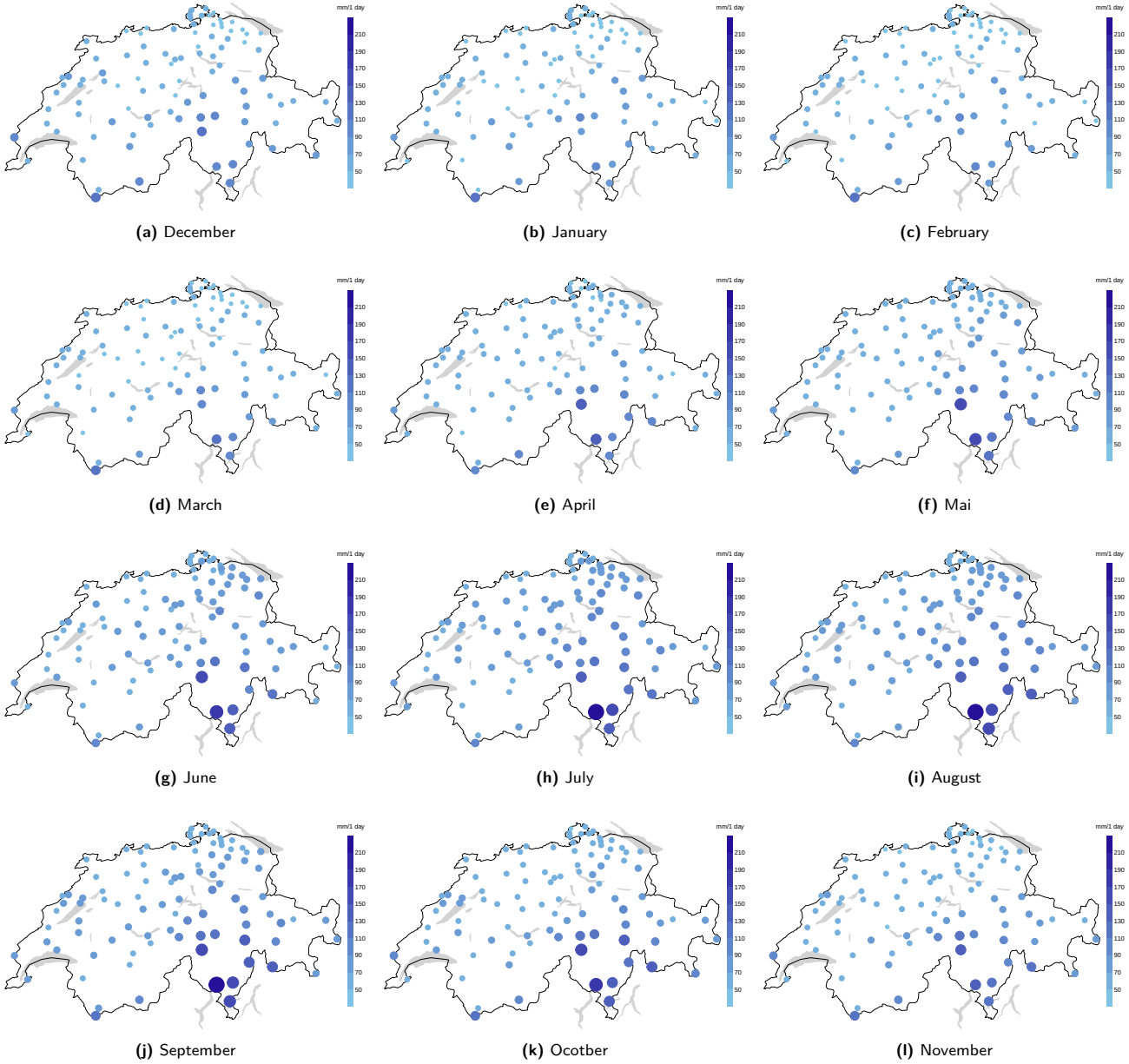

(a) December **(b)** January **(c)** February

(d) March **(e)** April **(f)** Mai

(g) June **(h)** July **(i)** August

(j) September **(k)** Ocotber **(l)** November

Fig. F.1: Best estimates of return levels for monthly 100 year events. The colours indicate the precipitation amount within 1 day in mm. The size of the dots is proportional to the return level.

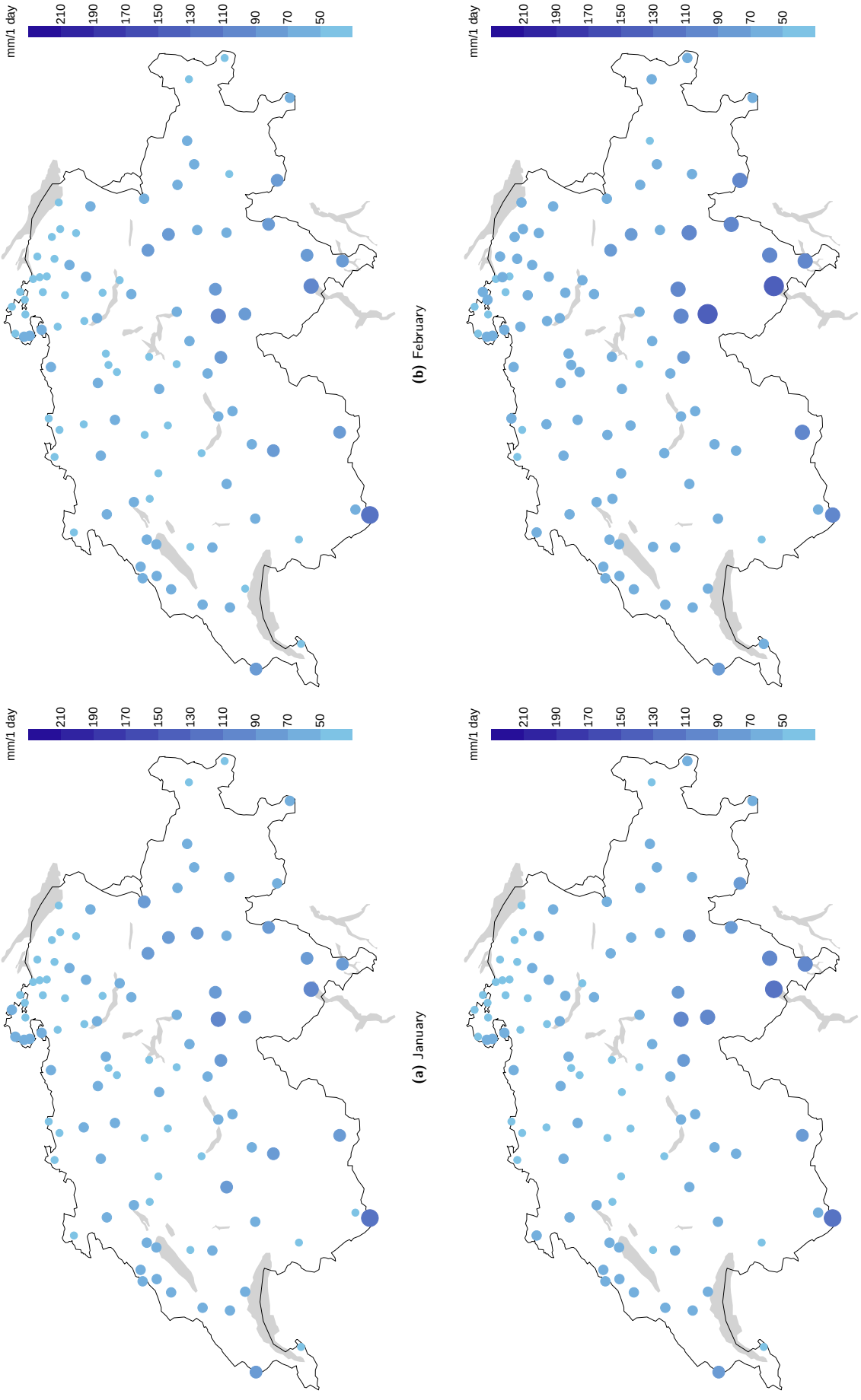

Fig. F.2: Best estimates of return levels for monthly 100 year events. The colours indicate the precipitation amount within 1 day in mm. The size of the dots is proportional to the return level.

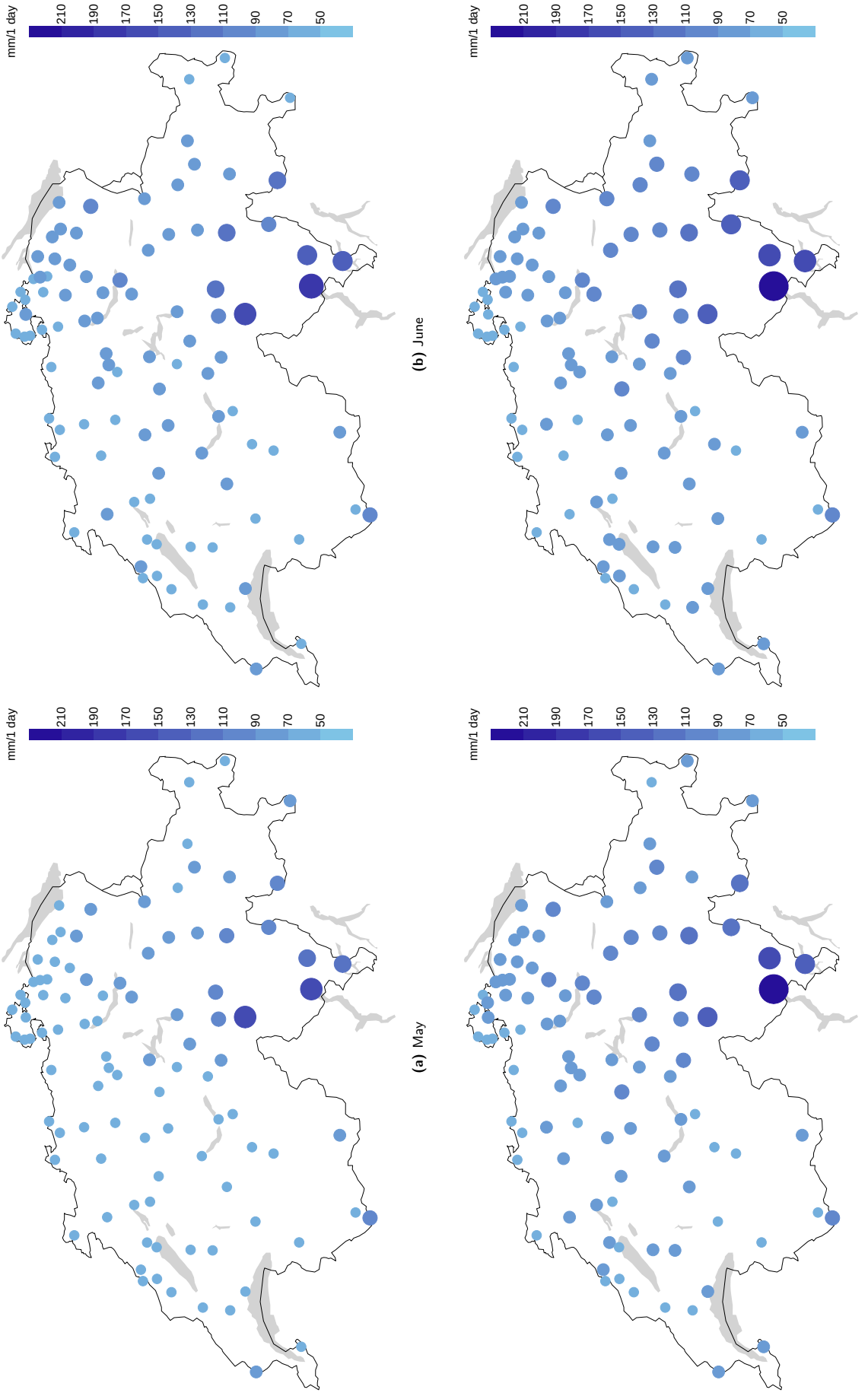

Fig. F.3: Best estimates of return levels for monthly 100 year events. The colours indicate the precipitation amount within 1 day in mm. The size of the dots is proportional to the return level.

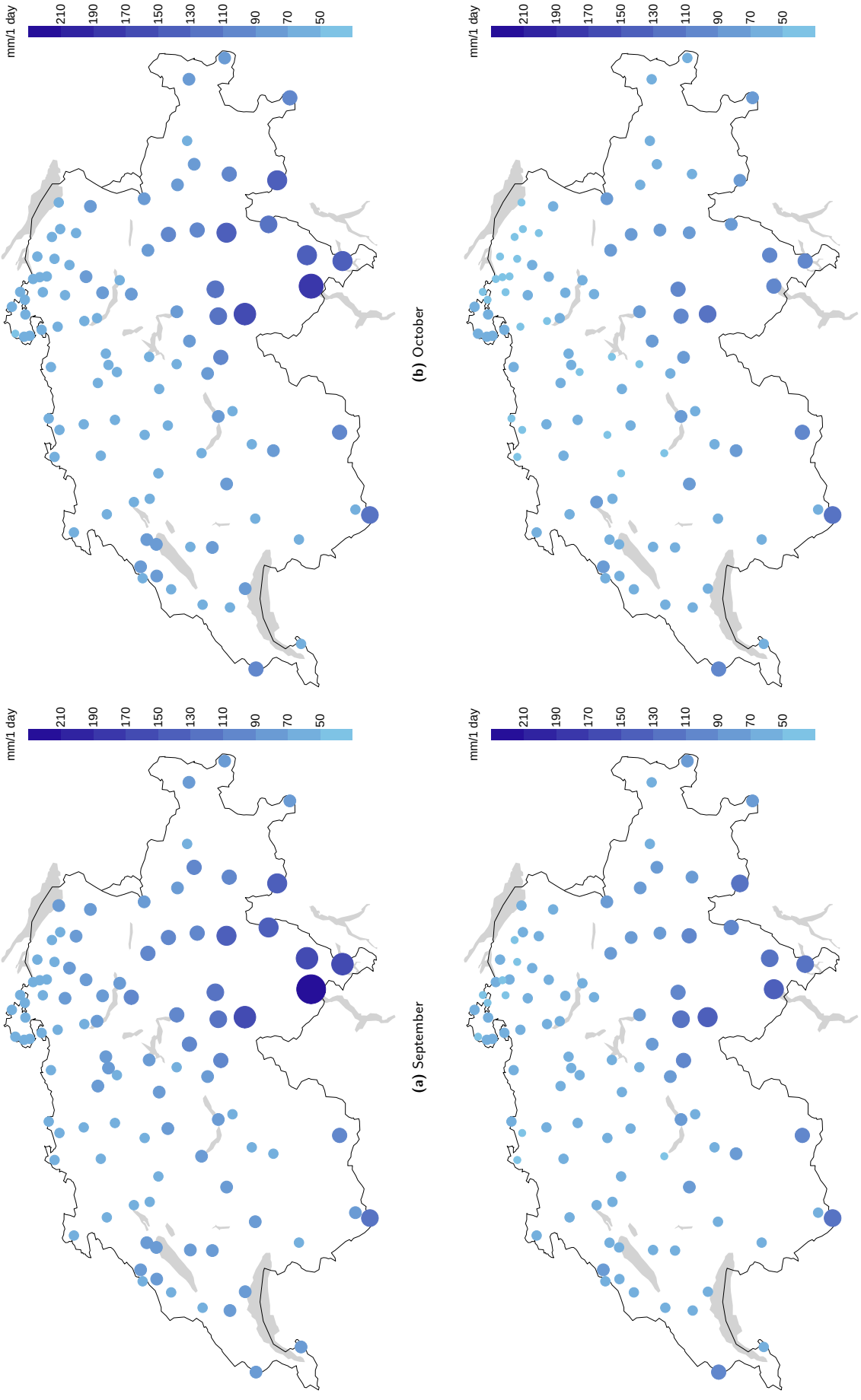

Fig. F.4: Best estimates of return levels for monthly 100 year events. The colours indicate the precipitation amount within 1 day in mm. The size of the dots is proportional to the return level.

F.2 Monthly Probabilities for a RP of 100 Years

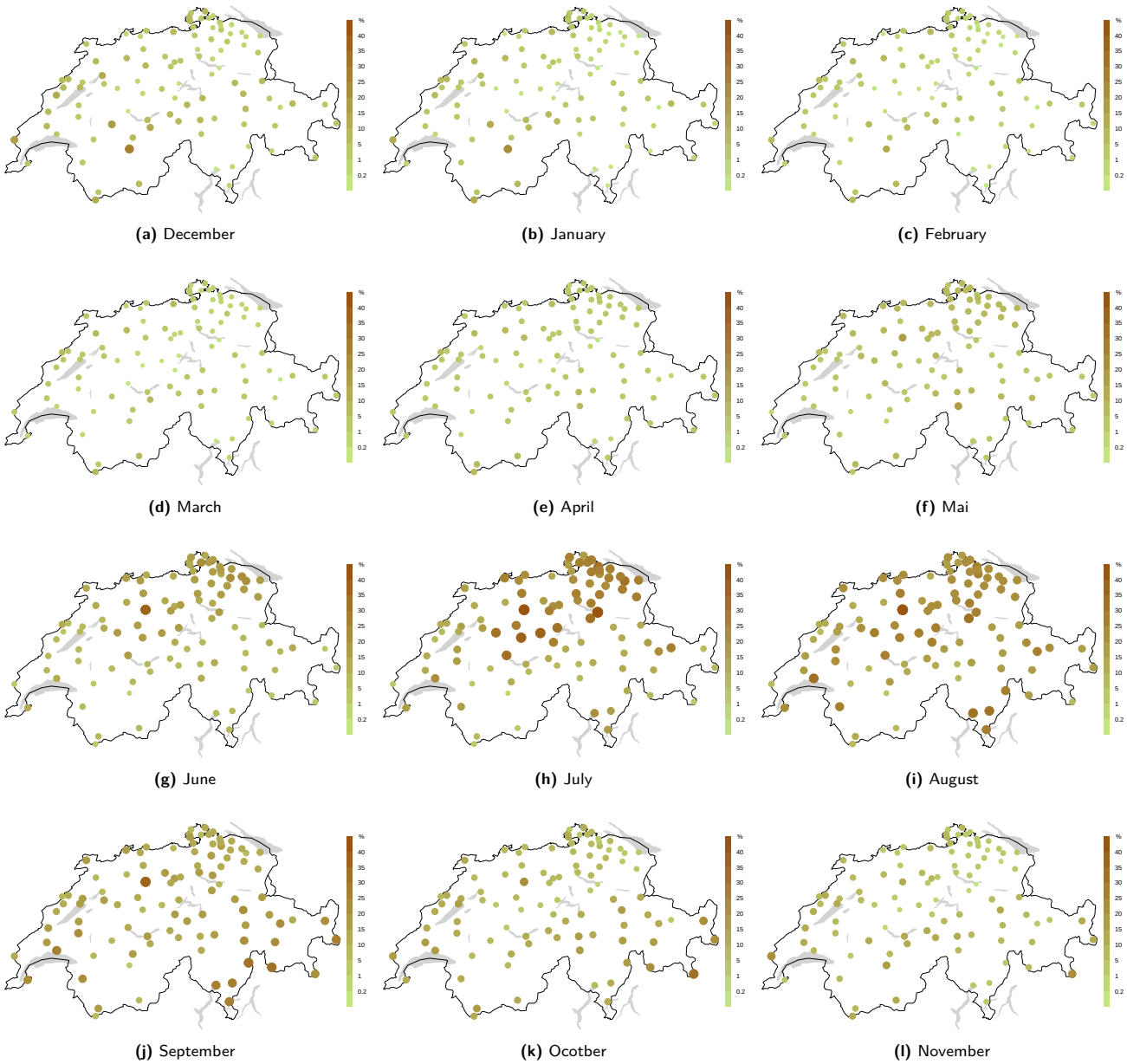

(a) December **(b)** January **(c)** February

(d) March **(e)** April **(f)** Mai

(g) June **(h)** July **(i)** August

(j) September **(k)** Ocotber **(l)** November

Fig. F.5: Probability for a 100 year event to fall into a particular month. The colours and the bullets size indicate the probability $p \in [0, 1]$. The size of the dots is proportional to the probability.

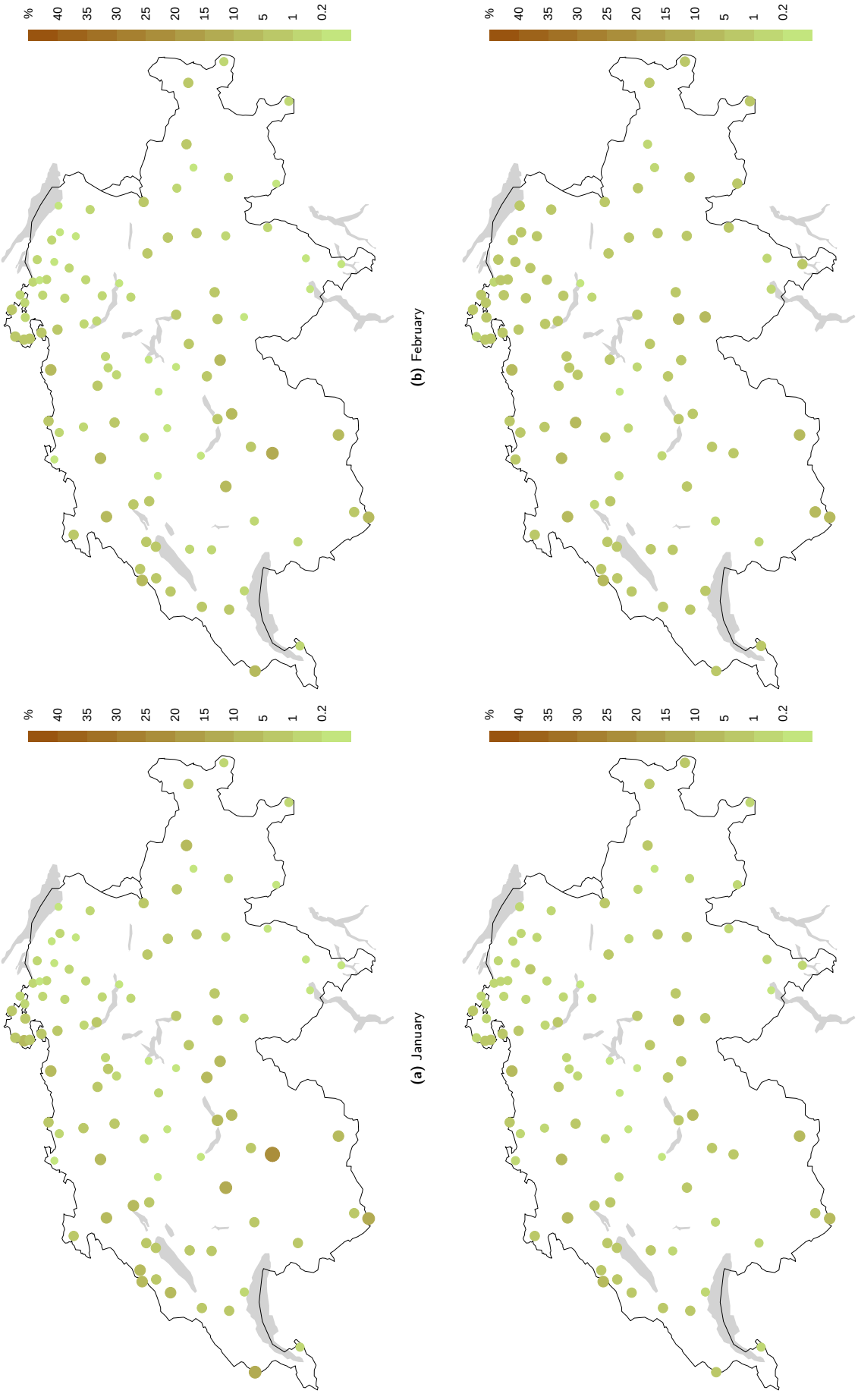

Fig. F.6: Probability for a 100 year event to fall into a particular month. The colours and the bullets size indicate the probability $p \in [0, 1]$. The size of the dots is proportional to the probability.

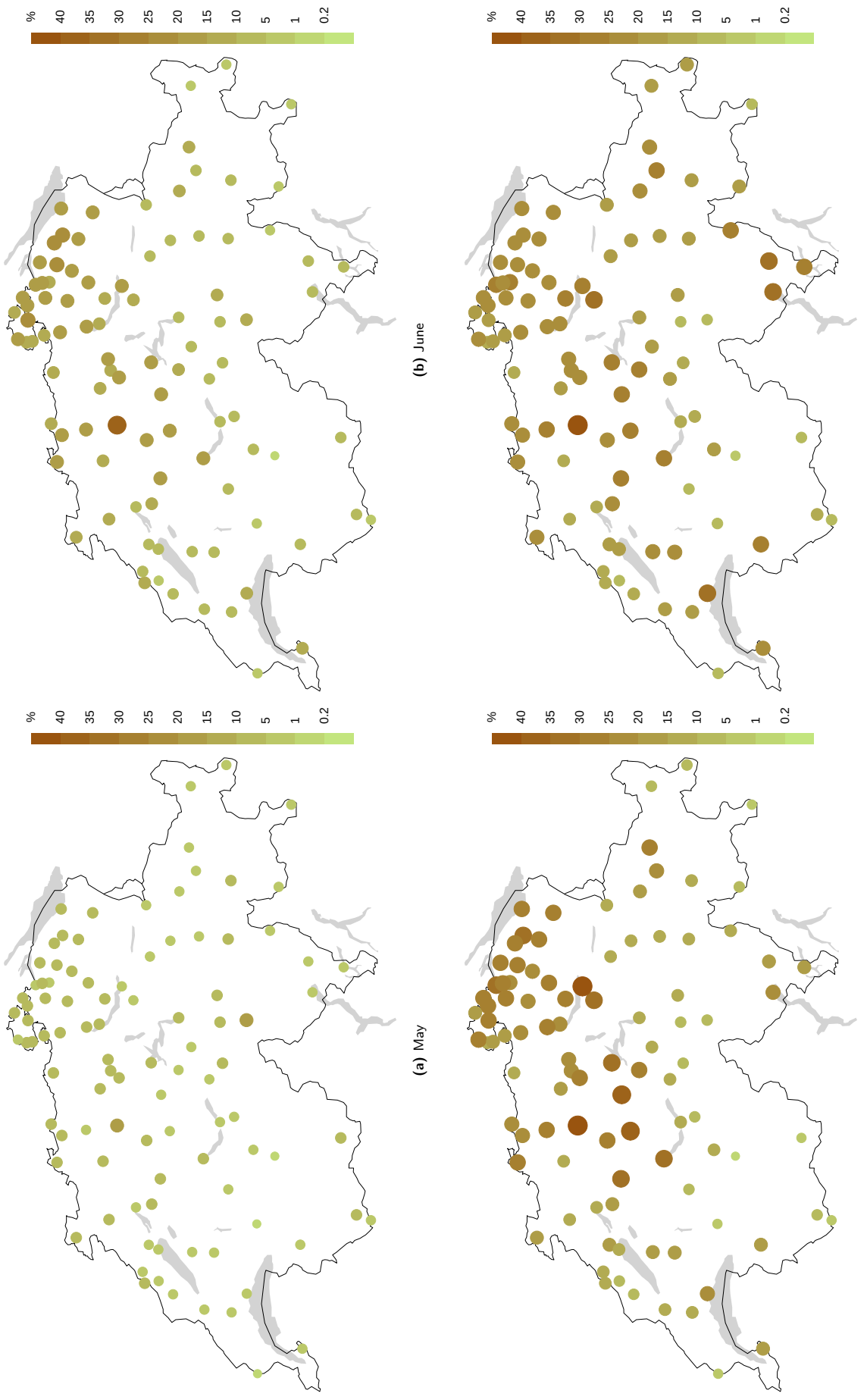

Fig. F.7: Probability for a 100 year event to fall into a particular month. The colours and the bullets size indicate the probability $p \in [0, 1]$. The size of the dots is proportional to the probability.

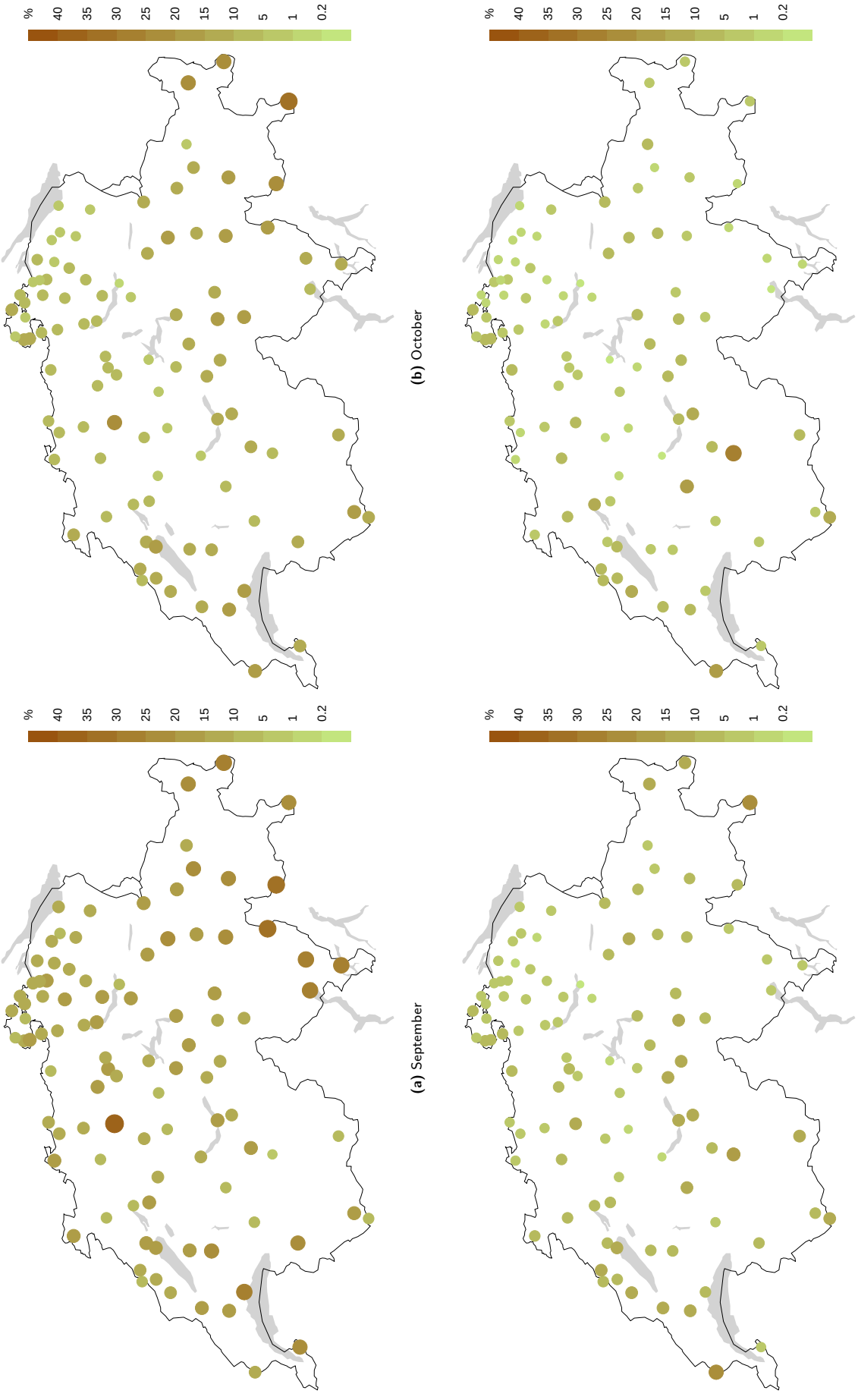

Fig. F.8: Probability for a 100 year event to fall into a particular month. The colours and the bullets size indicate the probability $p \in [0, 1]$. The size of the dots is proportional to the probability.

Appendix G Additional Tables

G.1 Comparison of all statistical models at CDF

Tab. G.1: The influence of the model selection process on the yearly return levels (RLs) and their confidence intervals (CIs) at La Chaux-de-Fonds. The RLs and CIs for the best model are in green colours. The values for the other models are presented in relation to the best model. The first column denotes the model's name, the second indicates whether the results for the return level or the confidence interval are shown. In rows for the CI the first number shows the 2.5 %, the second one the 97.5 % quantile. Columns three to six show the results for return periods of 10, 30, 100 and 300 years and the last two columns show the RL for a 100_{feb} and a 100_{aug} event respectively.

Model		10 years	30 years	100 years	300 years	100_{feb}	100_{aug}
$\mathcal{M}_{0,0}$	RL	0 %	0 %	−1 %	−1 %	9 %	−6 %
	CI (2.5 %/97.5 %)	−54 %/−1 %	−42 %/−2 %	−33 %/−2 %	−28 %/−2 %		
$\mathcal{M}_{1,0}$	RL	0 %	0 %	−1 %	−1 %	4 %	−3 %
	CI (2.5 %/97.5 %)	−1 %/−1 %	−1 %/−2 %	−1 %/−2 %	−1 %/−2 %		
$\mathcal{M}_{0,1}$	RL	1 %	1 %	1 %	1 %	11 %	−8 %
	CI (2.5 %/97.5 %)	0 %/0 %	0 %/0 %	0 %/−1 %	0 %/0 %		
$\mathcal{M}_{1,1}$	RL	1 %	1 %	0 %	0 %	0 %	1 %
	CI (2.5 %/97.5 %)	0 %/0 %	0 %/0 %	0 %/0 %	0 %/1 %		
$\mathcal{M}_{2,0}$	RL	0 %	−1 %	−1 %	−1 %	4 %	−3 %
	CI (2.5 %/97.5 %)	−1 %/−1 %	−1 %/−1 %	−2 %/−1 %	−1 %/−1 %		
$\mathcal{M}_{0,2}$	RL	1 %	1 %	1 %	1 %	14 %	−4 %
	CI (2.5 %/97.5 %)	−1 %/−1 %	−1 %/−1 %	−1 %/0 %	−1 %/0 %		
$\mathcal{M}_{1,2}$	RL	1 %	1 %	1 %	1 %	3 %	2 %
	CI (2.5 %/97.5 %)	2 %/1 %	2 %/1 %	2 %/0 %	2 %/0 %		
$\mathcal{M}_{2,1}$	*RL*	*72.4 mm*	*85.6 mm*	*100.1 mm*	*113.7 mm*	*64.9 mm*	*75.4 mm*
	CI (2.5 %/97.5 %)	*70 mm /78 mm*	*82 mm /94 mm*	*94 mm /112 mm*	*107 mm /130 mm*		
$\mathcal{M}_{2,2}$	RL	2 %	1 %	1 %	0 %	7 %	1 %
	CI (2.5 %/97.5 %)	0 %/0 %	0 %/0 %	0 %/1 %	1 %/1 %		

G.2 Comparison of all statistical models at OTL

Tab. G.2: The influence of the model selection process on the yearly return levels (RLs) and their confidence intervals (CIs) at Locarno-Monti. The RLs and CIs for the best model are in green colours. The values for the other models are presented in relation to the best model. The first column denotes the model's name, the second indicates whether the results for the return level or the confidence interval are shown. In rows for the CI the first number shows the 2.5 %, the second one the 97.5 % quantile. Columns three to six show the results for return periods of 10, 30, 100 and 300 years and the last two columns show the RL for a 100_{feb} and a 100_{aug} event respectively.

Model		10 years	30 years	100 years	300 years	100_{feb}	100_{aug}
$\mathcal{M}_{0,0}$	RL	3 %	6 %	10 %	13 %	46 %	−25 %
	CI (2.5 %/97.5 %)	47 %/1 %	41 %/5 %	37 %/9 %	34 %/13 %		
$\mathcal{M}_{1,0}$	RL	−7 %	−7 %	−7 %	−6 %	35 %	−30 %
	CI (2.5 %/97.5 %)	41 %/−12 %	33 %/−12 %	25 %/−12 %	19 %/−17 %		
$\mathcal{M}_{0,1}$	RL	−10 %	−11 %	−12 %	−13 %	28 %	−25 %
	CI (2.5 %/97.5 %)	45 %/−6 %	36 %/−7 %	28 %/−8 %	21 %/−11 %		
$\mathcal{M}_{1,1}$	RL	−1 %	−2 %	−2 %	−2 %	−4 %	−5 %
	CI (2.5 %/97.5 %)	42 %/2 %	33 %/3 %	23 %/3 %	15 %/2 %		
$\mathcal{M}_{2,0}$	RL	−8 %	−8 %	−7 %	−7 %	35 %	−31 %
	CI (2.5 %/97.5 %)	41 %/−12 %	32 %/−12 %	25 %/−12 %	18 %/−17 %		
$\mathcal{M}_{0,2}$	RL	−9 %	−9 %	−10 %	−10 %	33 %	−11 %
	CI (2.5 %/97.5 %)	38 %/−5 %	26 %/−6 %	15 %/−8 %	5 %/−9 %		
$\mathcal{M}_{1,2}$	*RL*	*185.4 mm*	*229.9 mm*	*281.1 mm*	*330.7 mm*	*99.9 mm*	*231.5 mm*
	CI (2.5 %/97.5 %)	*97 mm /219 mm*	*136 mm /284 mm*	*186 mm /367 mm*	*237 mm /455 mm*		
$\mathcal{M}_{2,1}$	RL	−4 %	−5 %	−6 %	−7 %	−6 %	−9 %
	CI (2.5 %/97.5 %)	41 %/−12 %	33 %/−11 %	25 %/−11 %	19 %/−14 %		
$\mathcal{M}_{2,2}$	RL	−3 %	−4 %	−6 %	−7 %	−9 %	−7 %
	CI (2.5 %/97.5 %)	41 %/−13 %	32 %/−13 %	25 %/−13 %	18 %/−14 %		

MeteoSchweiz
Krähbühlstrasse 58
CH-8044 Zürich

T +41 44 256 91 11
www.meteoschweiz.ch

MeteoSchweiz
Flugwetterzentrale
CH-8060 Zürich-Flughafen

T +41 43 816 20 10
www.meteoswiss.ch

MeteoSvizzera
Via ai Monti 146
CH-6605 Locarno Monti

T +41 91 756 23 11
www.meteosvizzera.ch

MétéoSuisse
7bis, av. de la Paix
CH-1211 Genève 2

T +41 22 716 28 28
www.meteosuisse.ch

MétéoSuisse
Chemin de l'Aérologie
CH-1530 Payerne

T +41 26 662 62 11
www.meteosuisse.ch